THE DEVELOPMENT OF

ELECTROANALYTICAL TECHNIQUES

A Thesis Submitted for the Degree of

Doctor of Philosophy

in

The University of Oxford

by

Peter Wood

Lincoln College

March 1979

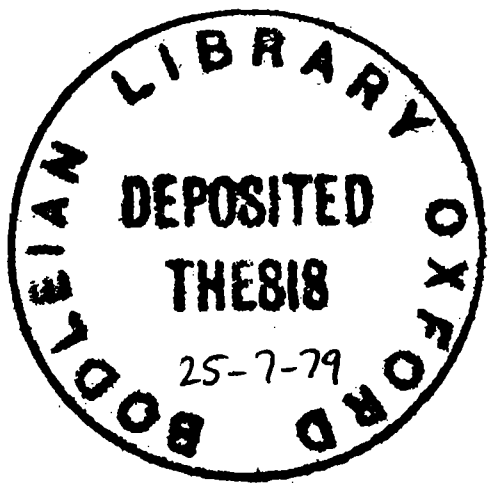

Physical Chemistry Laboratory

Oxford.

THE DEVELOPMENT OF ELECTROANALYTICAL TECHNIQUES

Abstract of a Thesis Submitted for the Degree of Doctor of Philosophy in the University of Oxford, by Peter Wood, Lincoln College, Hilary Term 1979.

This thesis describes the development of an electroanalytical technique for the estimation of compounds of biochemical interest. The technique involves titration with hypobromite using double electrode systems - the rotating ring disc electrode (RRDE) and the flow-through tubular double electrode (TDE). Hypobromite is continuously electrogenerated at the upstream disc (generator) electrode and is transported by convection and diffusion to the downstream ring (detector) electrode where it is detected amperometrically. The presence of a reactive substrate in solution decreases the amount of titrant which reaches the ring, and from measurements of the generating and detecting currents the bulk concentration of substrate may be estimated.

At pH 9.2 the amine group of amino acids reacts with two hypobromite molecules and some side chains (e.g. cystinyl, tyrosinyl, tryptophanyl) will also react. The reactivity of these side chains permits the titration of proteins. The titration response may be described theoretically which enables the calculation of the number of hypobromite molecules which react with one protein molecule (~500 for haemoglobin). With this chemical amplification the detection limit of the technique is $\sim 10^{-8}$ g ml^{-1} for proteins and $\sim 10^{-8}$ M for amino acids.

An electronic circuit has been developed which enables the detector electrode to control the rate at which titrant is generated. This autotitrator produces a generator current which is proportional to substrate concentration, and with the TDE should enable the continuous estimation of proteins as they are eluted from a chromatographic column.

Proteins have been titrated at pH 9.2 and pH 5; the ratio of a protein's titration responses reflects its amino acid composition and, when combined with the extinction coefficient, enables the identification of proteins. Patent applications for this method of identification and for the autotitration technique have been submitted.

ACKNOWLEDGEMENTS

I would like to thank

Professor W.J. Albery - for his supervision of this work.

Pharmacia Fine Chemicals AB, Uppsala, Sweden - for their financial support.

Herr Lars-Göran Andrén, Dr Bengt Falk and Dr Michael L.Hitchman - for many interesting and fruitful discussions during the progress of this work.

The staff of the P.C.L. workshops - for construction of equipment.

Carol - for her patience during, and assistance with, the production of this thesis.

CONTENTS

CHAPTER I. INTRODUCTION

The aim of this work has been to develop an electroanalytical technique for the estimation of compounds of biochemical interest in aqueous solution, and to use this technique as the basis of a detection system for liquid chromatography of proteins.

This introductory chapter is divided into three sections: in the first section electroanalytical techniques are reviewed, with examples of how they have been applied to protein or related analyses; in the second section a qualitative description of the electrode systems used in this work is presented (a quantitative description is given in Chapter II); finally the expected properties of a liquid chromatography - electrochemical detection system are indicated, and compared with presently available systems.

1. ELECTROANALYTICAL TECHNIQUES

"Electroanalytical chemistry comprises methods of chemical analysis based on the phenomena associated with the reactions at electrodes in contact with electrolyte solutions and with the passage of electricity (i.e. transport of ions) through electrolyte solutions" (Lingane). The passage of electricity through an electrolyte solution is dependent on the conductance of that solution, but as conductometric techniques are not used in the work presented in this thesis they will not be discussed. The techniques actually used in this work rely on the phenomena associated with the reactions at electrodes in contact with electrolyte solutions, these phenomena being the current flowing through the electrode in question, and the potential difference across that electrode - solution interface. It is also possible to evaluate the total charge which has passed through an electrode and these three quantities can be easily

measured with good precision and accuracy.

a) Oxidation/Reduction of Electroactive Substances

In this set of electroanalytical techniques electron transfer occurs between an electrode and the substance being analysed, and the techniques may be subdivided according to the quantities measured. In coulometry a current is measured over a period of time and the current-time integral (i.e. total charge passed) is evaluated. The second method (voltammetry) involves the measurement of instantaneous current and potential values.

The coulometric technique relies upon the electron transfer reaction having 100% current efficiency and knowledge of the number of electrons transferred per molecule of electroactive substance. Reaction is allowed to proceed to completion, and the consumption of all of the electroactive substance may be determined in two ways. One way is to pass a constant current and detect the end point by means of a chemical indicator or physical measurement (e.g. a shift in electrode potential). A second method of end point detection is to control the working electrode potential, thus isolating the desired electrode reaction so that the current will drop to zero when electrolysis is complete. Coulometry is applicable in principal to all types of reducible or oxidisable substances, organic as well as inorganic, and the sensitivity is typically 10^{-6} M. It is, however, unlikely to be a suitable technique for the determination of proteins - several electron transfer steps may proceed due to the occurrence of several electroactive sites on each molecule and/or further reactions of the oxidised (or reduced) protein. These reaction products may polymerise and be adsorbed on the electrode surface, inhibiting further electron transfer.

The remainder of this section reviews the study of current-potential relations, which is known generally as voltammetry. The current observed at a given potential depends upon the rate of the electrode reaction (which is potential dependent) and also depends upon the rate of transport of the electroactive substance from the bulk of the solution to the

electrode surface (figure I.1). Two transport processes operate at a stationary electrode in a stationary solution. The first is diffusion down a concentration gradient, which is a consequence of depletion of the electroactive substance by electrolysis. The second transport process is migration under the applied electric field, but when excess supporting electrolyte is added then migration is negligible. If the potential applied to the working electrode-solution interface is such that the rate constant for electron transfer is greater than the transport rate constant then the rate of reaction, and observed limiting current i_L, will be diffusion controlled; in this case the concentration, c, of the electroactive substance at the electrode surface (z = 0) is zero, since it reacts as soon as it arrives at the electrode (figures I.1 and I.2). The half-wave potential, $E_{1/2}$, is characteristic of the electrode reaction under consideration (1). The diffusion-limited current is given by Fick's First Law

$$i = nFAj = nFAD\left(\frac{\partial c}{\partial z}\right)_{z=o} = nFAD\frac{(c_\infty - c_o)}{Z_D}$$

$$i_L = nFADc_\infty / Z_D \qquad (I.1)$$

where Z_D describes the thickness of the diffusion layer, the region of solution in which concentration gradients occur. The number of electrons transferred per molecule of electroactive substance is n, F is the Faraday constant, A is the area of the electrode, D is the diffusion coefficient of the electroactive species and c_∞ the bulk concentration of this species.

For semi-infinite linear diffusion (a stationary electrode in a stationary solution) the transport equation for a plane electrode is Fick's Second Law.

$$\frac{\partial c}{\partial t} = D\frac{\partial^2 c}{\partial z^2} \qquad (I.2)$$

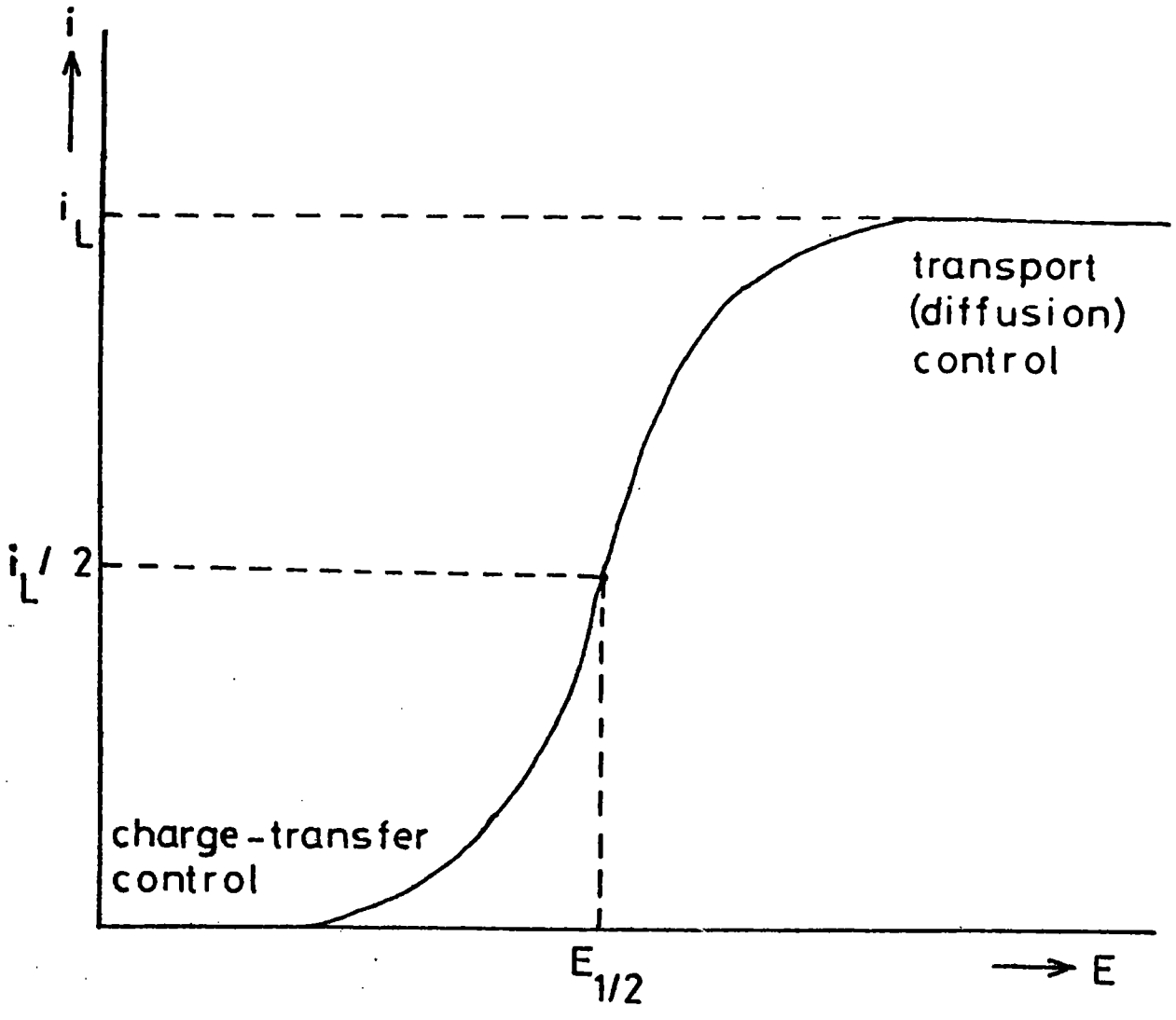

Figure 1.1. Schematic voltammogram

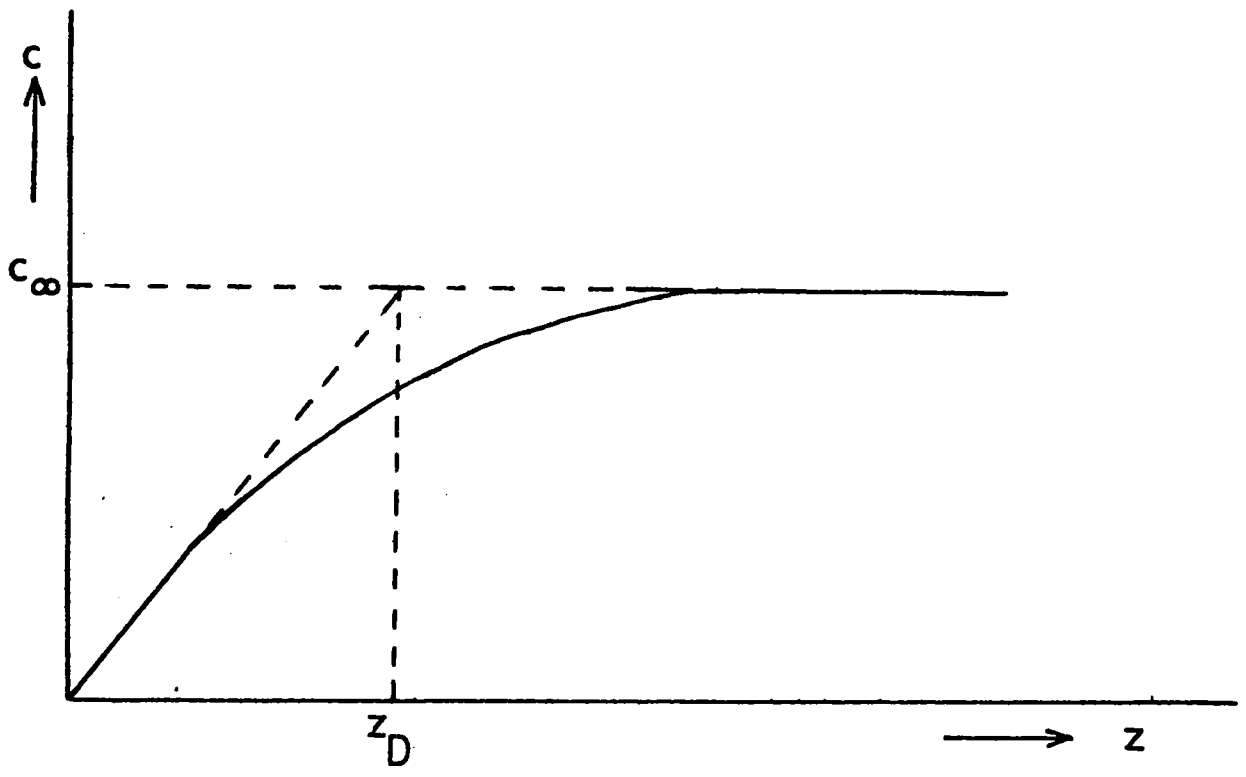

Figure 1.2. Schematic concentration profile near electrode surface, for case of limiting current.

the boundary conditions being

$$\begin{array}{lll} Z = 0, & t = 0 & c = c_\infty \\ Z = 0, & t > 0 & c = 0 \\ Z \to \infty, & t \geqslant 0 & c = c_\infty \end{array} \qquad \text{(I.3)}$$

Using Laplace transforms (Appendix 1) equation I.2 can be solved to give the concentration c(z,t), and from this the concentration gradient can be obtained; the limiting current is given by the expression

$$i_L\ (t) = nFA \frac{D^{1/2}}{\pi^{1/2} t^{1/2}} c_\infty \qquad \text{(I.4)}$$

The current decreases with $t^{1/2}$ since prolonged electrolysis causes the diffusion layer ($Z_D = \pi^{1/2}\ D^{1/2}\ t^{1/2}$) to increase in thickness. This depletion also results in density gradients, so that the effects of natural convection (which were omitted from equation I.2) will increase with time, resulting in deviations from equation I.4. However for short periods of electrolysis the agreement between theory and experiment is good, and the linear relationship between i_L (t) and c_∞ forms the basis of some electroanalytical techniques - pulse voltammetry (2,3), differential pulse voltammetry (4) and differential double pulse voltammetry (5).

The above techniques require control of the electrode potential and of the time at which the current is measured. Instrumentation is simpler if a time-independent current can be obtained - this is virtually achieved using the dropping mercury electrode (DME), in which the current is measured at a growing drop which is periodically replaced by a new drop. Hence the electrode surface is continually renewed, and each new drop starts its life looking at an undepleted solution. Equation (I.4) can be extended to include the time-dependent area of the electrode, and the effect of this drop growing into the solution, to give

$$i_L\ (t) \propto D^{1/2}\ t^{1/6} c_\infty \qquad \text{(I.5)}$$

(Equation I.4 applies to a plane electrode so the time of electrolysis must be such that the thickness of the diffusion layer is much less than

the radius of the drop). The technique is termed polarography and, with damping of the measured current, time-independent polarograms of the form of figure I.1 can be obtained.

An alternative method of obtaining time-independent currents is to limit the thickness of the diffusion layer, and this can be achieved using forced convection - rotation or vibration of the electrode in solution, or forced flow of the solution over the electrode surface. Rotating disc and tubular electrodes are used in this work, and once again voltammograms of the form of figure I.1 can be recorded.

There appears to be no simple oxidation or reduction of proteins so that, like coulometry, these techniques have not been applied to the direct determination of proteins. In amino-acids oxidation of the NH_2 group is feasible and this has been used in high performance liquid chromatography (HPLC) for electrochemical detection (LCEC) (6). The electrode used was a glassy carbon wall jet electrode detector (WJED), which is a forced convection electrode in which the solution, in the form of a jet, flows over the working electrode surface. The WJED and similar LCEC systems have been applied to the determination of catecholamines, phenols, steroids, ascorbic acid and uric acid; detection systems are commercially available, an undergraduate teaching experiment has been described (7) and a review has been recently published (8). The detection limit of these systems is typically 1ng, with 5 µl injected sample volume (= 10^{-6} M on injection, assuming MW = 200).

Although proteins are not directly reduced cathodic waves can be obtained with solutions of proteins using a mercury electrode. These are catalytic waves corresponding to the evolution of hydrogen; the reduction is effected at a decreased overvoltage due to catalytically active groups in protein molecules. In buffered solutions (pH 6 - 10) the height of the "prenatrium" wave is determined by the concentration of protein in solution (9). A second type of catalytic wave is observed when the

supporting electrolyte contains cobalt or nickel salts as well as buffer ions. After the wave corresponding to the reduction of the metal ion a double wave is observed, the height of which is related to the concentration of protein in solution. This second technique is the Brdicka reaction (10), and involves a complex of cobalt (or nickel) ions with protein molecules which contain thiol or disulphide groups. Drake (11) has described the use of the prenatrium wave at a DME for automatic recording in the chromatography of proteins. The detection limit was 0.001% (10 μg ml^{-1}) and the most suitable range 0.005 - 0.1%. The application of the Brdicka reaction to the analysis of proteins has been reviewed by Muller (12).

The lower limit of D.C. voltammetry is generally 10^{-6}M; however the use of fast pulse techniques, while requiring more complex instrumentation, extends this limit to 10^{-8} - 10^{-9}M. This is because thinner diffusion layers, and therefore higher currents, are obtained. In addition when a differential pulse technique is used the current due to double-layer charging can be subtracted allowing smaller Faradaic currents to be extracted from the total current. Palacek and Pechan (13) applied differential pulse polarography to the Brdicka reaction, and detected protein at 0.05 μg ml^{-1} ($\sim 10^{-9}$M). Although protein determination is possible by catalytic wave techniques, there are associated problems - the restriction to only sulphur-containing proteins and the necessity of using mercury electrodes. Furthermore (from the point of view of automation) in using the more sensitive differential techniques it is necessary to record a current peak waveform, the height of which is proportional to concentration, rather than the steady single current value obtained with D.C. techniques.

b) Potentiometry

Potentiometry is a form of voltammetry in which the current passing through an electrode is maintained at a constant value while the potential of that electrode is monitored. The technique demands a well defined reaction at local equilibrium. The current is usually chosen to be zero, and the Nernst equation then gives the concentration dependence of the electrode potential.

$$E = E^{\ominus} + \frac{RT}{nF} \ln \frac{c_o}{c_R} \qquad (I.6)$$

where c_o is the concentration of an oxidised species and c_R the concentration of the corresponding reduced species. These concentrations are the bulk concentrations since, with zero current, there are no concentration gradients; $E^{\ominus}$ is the standard electrode potential of the redox couple ($c_o = c_R$ = unit activity $\simeq$ unit concentration). Toribara and Koval (14) have reported that a silver wire immersed in a solution of a thiol or thiol containing protein exhibits a potential related to thiol (hence protein) concentration.

$$E = E^{\ominus} + 0.059 \log [RSH] \qquad (I.7)$$

The lower limit of detection for potentiometric electrodes is generally 10^{-6}M, but the logarithmic response results in poor sensitivity. This, together with problems of interfering ions and gradual poisoning, means that direct potentiometry is unsuitable for protein determination.

c) Reaction with Electroactive Titrant

The reaction of proteins at electrodes is unsuitable for use in direct voltammetric or potentiometric monitoring. However proteins will react with chemical reagents, and some of these reagents (or reaction products) are themselves electroactive, so that electrometric monitoring of the

rate or end-point of such a reaction will enable monitoring of protein concentrations.

Harrap and Gruen (15) have titrated denatured proteins with silver nitrate to determine the number of disulphide groups; they used a Ag_2S specific ion indicator for potentiometric end-point detection. Other workers have used Hg (II) as a titrant (16, 17). Ag (I) and Hg (II) titrations can also be followed amperometrically (18). This is a voltammetric technique, at a fixed electrode potential, and involves measuring the diffusion limited current due to reduction of the titrant. This current is proportional to the concentration of titrant surviving in solution and will therefore rise rapidly after the end-point of the titration.

Amine groups will react with hypobromite, and analytical use has been made of the oxidation of ammonia by hypobromite for 70 years. Artman and Skrabal (19) and, independently, Rupp and Rossler (20) showed that ammonia and urea can be titrated with hypobromite. Kolthoff, Stricks and Morren (21) investigated voltammograms for hypobromite solutions at the rotating platinum electrode, and inferred that it should be possible to carry out amperometric titrations with hypobromite. The authors applied the titration to the determination of nitrogen in glutathione, bovine plasma albumin and human serum after Kjeldahl digestion - the ammonia produced could be determined at concentrations between 6×10^{-4} and 4×10^{-5}M with an accuracy and precision better than 2%. The overall reaction of hypobromite with ammonia, in alkaline solution, is

$$3\ OBr^- + 2NH_3 \longrightarrow N_2 + 3Br^- + 3H_2O$$

Velghe and Claeys (22, 23) have used hypobromite solution with amperometric end-point detection in the determinations of diethylamine (5×10^{-4} - 5×10^{-2}M) and amphetamine sulphate (5 - 25mg, in tablets). The same workers have also reported (24) the bromination of 10^{-2}M solutions of glycine and lysine, two moles of hypobromite per $-NH_2$ group being used.

Norkus and Shimkyavichyute (25) have suggested a procedure for the direct potentiometric titration of various amines in a bicarbonate medium with 0.1M NaOBr, and determined twelve amino acids in a sample range 7 - 90mg with an accuracy of $\leqslant 5\%$. Abramov (26) has determined methionine by amperometric titration, using 0.1M $KBrO_3$ in the presence of HCl and HBr. In this acidic medium bromine is generated, which reacts with the sulphur.

In the above amperometric titrations, using Ag(I) and hypobromite standard solutions as titrants, the measured currents arise from the following electrode reactions

$$Ag\ (I) + e^- \longrightarrow Ag(0)$$

$$OBr^- + 2H^+ + 2e^- \longrightarrow Br^- + H_2O$$

However the reverse electrochemical reactions can be accomplished simply by altering the potential of the working electrode; the reactive titrants may therefore be electrochemically generated, this being the basis of coulometric titrations. This method of addition of a reagent has some important advantages over the usual method of addition as a standard solution - some reagents which are difficult to store and use (e.g. bromine) may be easily added electrolytically. Furthermore the ease with which small quantities of electricity can be measured permits the coulometric titration of microgram quantities in ordinary volumes with good precision and accuracy.

The use of electrogenerated bromine in analysis is well established, and it was one of the first titrants used by Szebelledy and Somogyi (27) in their original studies of coulometric titrations. Krivis, Supp and Gazda (28) and Christian, Knoblock and Purdy (29) have published papers describing procedures for coulometric titration of ammonia with hypobromite using direct amperometric end-point detection. In continuation of this work Christian and coworkers have determined protein nitrogen by direct titration of Kjeldahl digests (30), and urea nitrogen in blood and urine (31), ammonia being formed from urease hydrolysis of the urea. In this latter study it was observed that native protein

in serum samples resulted in abnormally high titration blanks, suggesting that the protein reacted with the generated hypobromite. This observation resulted in Christian describing the coulometric titration of proteins with electrogenerated hypobromite (32); the detectable limit of this technique is ~80 μg of protein in a cell of 30ml volume (~3 μg ml^{-1}).

The studies by Christian are the basis of the work presented in this thesis, this method of protein determination having evolved from investigations of the bromination of amine groups at pH8 - 10. Proteins are composed of amino acids, but the amino groups are consumed in the formation of peptide bonds leaving only side chains and terminal amino groups to react with hypobromite. Christian attempted to determine what reaction or reactions occur between proteins and hypobromite, and suggested that phenylhydroxy, disulphide and thiol groups, in addition to the amine group, would contribute to the titration. The bromination of amino acid side chains is supported by the results of several East European workers (33 - 35); they have reported the coulometric titration (with bromine) of methionine,tryptophan and cysteine, in acidic media using both amperometric and potentiometric end-point detection. Also Belliveau (36) has proposed that bromine vapour be used to develop thin layer chromatography plates carrying sulphur containing compounds (including the amino acids cysteine, cystine and methionine): the sulphur is oxidised and an acid is formed, the position of which can be detected using a pH sensitive flourogenic spray reagent. In addition to these studies of bromination, techniques of iodinating proteins are well developed (37), these techniques being used for radiolabelling (with ^{125}I and ^{131}I) and for studies of the activity of functional groups (38).

The potentiometric, amperometric and coulometric titrations described above all take considerable time to perform - Christian's

coulometric titration of proteins takes 35 - 200 seconds. This is because the techniques require titration to an end-point, i.e. complete reaction between protein and titrant (c.f. coulometry). However titrations can be performed very quickly using double electrode flow systems (RRDE, TDE) in which the titrant is generated at one electrode and transported by diffusion and convection to the second electrode where it is detected. The titration reaction occurs between the two electrodes in the diffusion layer; therefore only a small fraction of the active bulk species is titrated (c.f. polarography) and the titration is fast ($<$ 1s). These electrode systems are described in the next section, and the mathematical theory presented in the next chapter.

In this laboratory Cook (39) studied the bromination of ammonia using the rotating ring disc electrode (RRDE), and constructed a tubular double electrode (TDE) apparatus with the intention of applying it to the flow through analysis of ammonia in solution. Therefore it was decided to study the reaction of proteins with hypobromite using the RRDE, and further develop the TDE diffusion layer technique to enable continuous analysis of proteins eluted from chromatographic columns. Since the commencement of this work Rauwel and Thevenot (40) have described the bromination of sulphur containing compounds (including cystine, methionineand ovalbumin) using the RRDE; the titrations were performed at pH 0.3 and 6.7, and the authors appear to be unaware of the work of Christian and others on the bromination of proteins and amine groups. Since publication Christian's protein determination has been cited only twice (apart from reviews); one citation is by Christian himself (41), and Broome (42) has determined albumin and haemoglobin by coulometric titration after separation by countercurrent electrophoresis.

2. FORCED CONVECTION ELECTRODES

In the previous section (I.1.a) it was explained that electrolysis under conditions of semi-infinite diffusion results in time-dependent diffusion layers and currents. It was also indicated that the use of forced convection, to limit the thickness of the diffusion layer, can result in time-independent currents. Nernst (43) assumed a stationary thin layer of solution to be in contact with the electrode; within this layer it was postulated that diffusion alone controlled the transport of substances to the electrode, the concentration gradient being linear. This concept however is an oversimplification, and the theory provides no information as to the variation of the diffusion layer thickness with hydrodynamic parameters such as solution velocity and flow rate. A theoretical description of the diffusion layer may be obtained by solving the convection-diffusion mass transport equation

$$\frac{\partial c}{\partial t} = D \nabla^2 c - \underline{v} . \nabla c. \qquad (I.8)$$

In order to be able to solve the general equation (I.8) explicitly, one must first know the functional dependence of the fluid velocity vector, $\underline{v}$, upon the coordinates of the system. This necessitates the prior solution of the fluid flow equations (the Navier-Stokes equation, which describes the effect of forces on the fluid, and the equation of continuity, which expresses the fact that matter is conserved) with the appropriate boundary conditions.

The solution of hydrodynamic equations of motion is beyond the scope of this work; detailed solutions of the appropriate convective-diffusion equations are presented in chapter II. In this section a qualitative description of forced convection electrodes used in this work is given (rotating and tubular electrodes); the wall jet electrode is also described, as this system has been used in voltammetric liquid chromatography detectors.

a) The Rotating Disc Electrode (RDE)

The RDE consists of a disc of metal (e.g. platinum) surrounded by a coplanar, circular mantle of a non-conducting material (usually Teflon or Araldite); the disc is connected to a stainless steel shaft through which electrical contact is made and by which the electrode is rotated in solution.

The rotating disc system is one of the few cases for which an explicit solution of the stationary (time-independent) form of the Navier-Stokes equation is possible; von Karman (44) obtained an approximate solution, and this was improved by Cochran (45). The rotation of the electrode effects stirring of the solution; the liquid at the disc surface is stationary relative to the disc; further from the disc liquid is thrown out centrifugally and is replaced from below (figure I.3). A hydrodynamic boundary layer can be defined, and can be physically pictured as the approximate thickness of the liquid layer dragged by the rotating disc. The thickness of this layer, δ_o, can be given approximately by

$$\delta_o \simeq 3 \left(\frac{\nu}{\omega}\right)^{1/2} \qquad (I.9)$$

where ν = kinematic viscosity (viscosity/density)

ω = rotation speed

and it is in this layer that velocity gradients are greatest and the effect of the liquid viscosity is evident; the thickness is typically 0.1 - 1 mm.

Cochran's solution for v_z, the velocity of fluid perpendicular to the disc (see figure I.4) is

$$v_z = -(\nu\omega)^{1/2}(0.510z_1^2 - 0.333z_1^3 + 0.103z_1^4 \ldots) \qquad (I.10)$$

in terms of the dimensionless variable z_1,

$$z_1 = z(\omega/\nu)^{1/2}; \qquad (I.11)$$

the negative sign in equation I.10 arises since fluid flow is towards the disc. Levich (46) used the first term in Cochran's solution to solve the

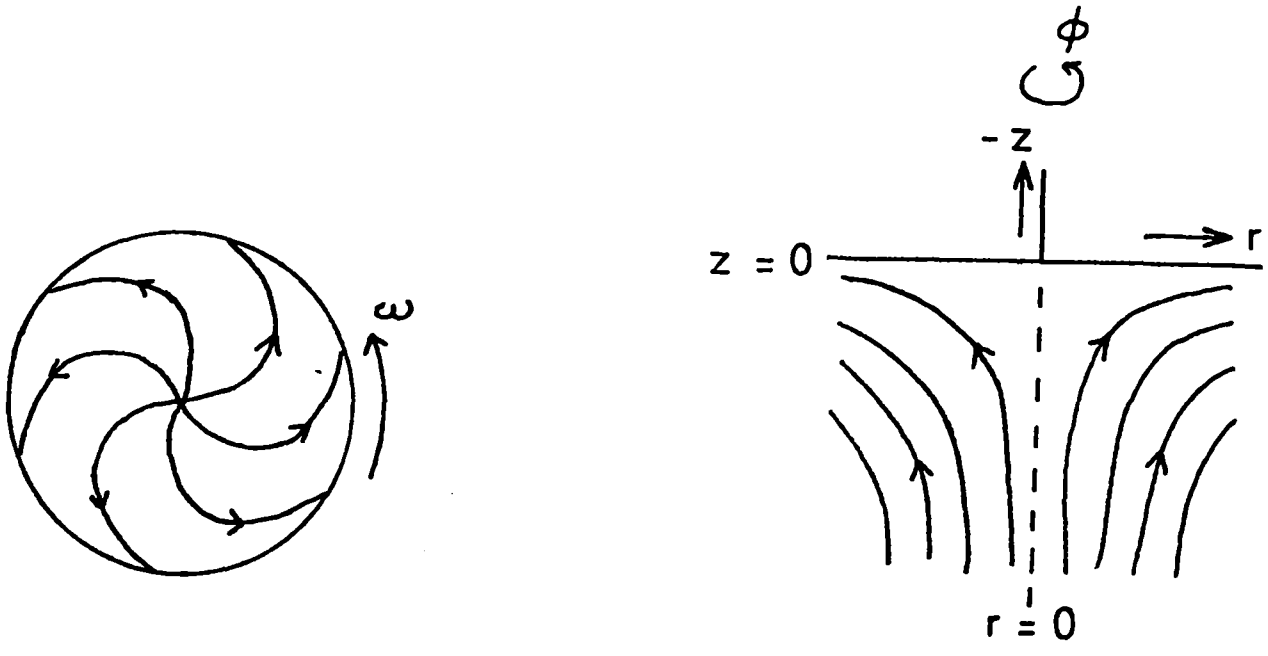

streamlines near the disc surface

streamlines below the disc surface

Figure 1.3.

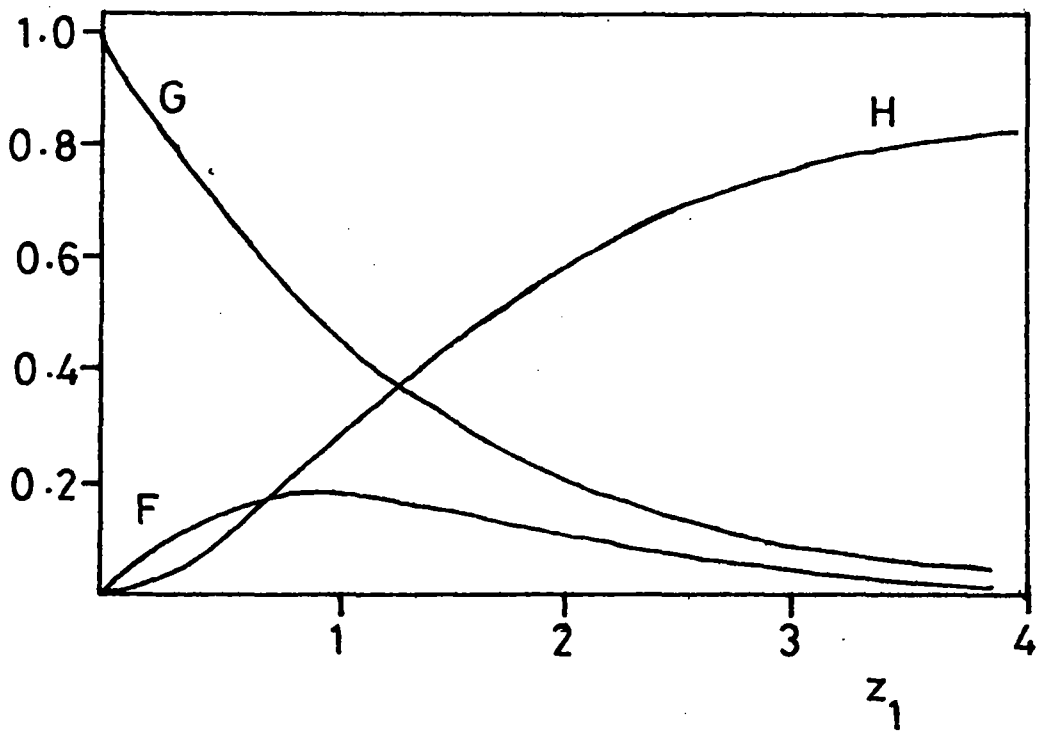

$$v_r = r\omega F(z_1)$$

$$v_\phi = r\omega G(z_1)$$

$$v_z = -(\nu\omega)^{1/2} H(z_1)$$

Figure 1.4. Flow functions at the RDE

convective-diffusion transport equation, and the thickness of the diffusion layer is given by

$$\delta = z_D = 1.6\, D^{1/3}\, \omega^{-1/2}\, \nu^{1/6} \qquad (I.12)$$

assuming a high Schmidt number ($Sc = \nu/D \simeq 10^3$ for aqueous solutions). Typical values of z_D are 5 - 50 μm, and the transport boundary layer thickness is independent of r, the radial coordinate: the RDE is a uniformly accessible surface. Equation I.12 can be rearranged:

$$Z_D = 1.6 \left(\frac{D}{\nu}\right)^{1/3} \left(\frac{\nu}{\omega}\right)^{1/2} \qquad (I.13)$$

which illustrates how the Schmidt number relates the thickness of the diffusion layer to that of the hydrodynamic (viscosity) boundary layer. The flow functions (figure I.4) show that, contrary to the Nernst hypothesis, there is some convection in the diffusion layer (at $z < 0.1z_1$).

The diffusion layer thickness, and therefore the flux to the disc, can be widely and easily varied by altering the rotation speed; the limiting current at an RDE is given by

$$i_L = 0.62nF\pi\, r^2 D^{2/3}\, \omega^{1/2}\, \nu^{-1/6} c_\infty \quad . \qquad (I.14)$$

This linear relationship between i_L and c_∞, the bulk concentration of the electroactive species, is the basis of the analytical utility of the RDE; knowledge of this concentration enables the determination of diffusion coefficients.

A review of the RDE and its applications to kinetics and analysis has been published by Riddiford (47); Levich's book (48) also presents detailed solutions of the hydrodynamic equations and of the convective - diffusion equation. The applications and developments of the RDE in this group have been reviewed by Albery (49).

b) The Tubular Electrode (TE)

An alternative electrode system, achieving forced convection, is the tubular electrode; in this the electrode is stationary and electrolyte is flowed through it under non-turbulent conditions. The TE referred to

here has a circular cross-section (figure I.5); those electrodes having rectangular cross-section are usually termed channel electrodes. Blaedel (50) developed a tubular electrode for practical voltammetric measurements by sealing a seamless platinum tube into glass to give a smooth glass-platinum inner wall. The method of construction of tubular electrodes used in this work is described in chapter III.

The flow in a tube is characterised by two regions - the inlet region and the Poiseuille flow region (figure I.6). In the inlet region, the viscous fluid entering the tube is subject to the retarding action of the walls. Because of this frictional action a boundary layer forms at the walls and gradually thickens as the distance, x, from the entry point increases; the initially flat velocity profile assumes a Poiseuille profile when the boundary layer thickness is equal to the radius of the tube. The boundary layer thickness at a flat plate is given by (48)

$$\delta_o = 5.2 \ (\nu x/v_o)^{1/2} \qquad (I.15)$$

where v_o is the flow velocity and the constant 5.2 is the result of a numerical computation. Although the TE is not a flat plate, equation I.15 can be used to estimate the entry length h (figure I.6) since, at this value of x, $\delta_o = R$

$$h = v_o R^2/(5.2)^2 \nu = Re.\ R/(5.2)^2 \qquad (I.16)$$

where $Re = v_o R/\nu$ is the dimensionless Reynolds number for the TE; Levich gives (48)

$$h \sim 0.1\ R.\ Re \qquad (I.17)$$

Beyond this point the formation of the Poiseuille profile is completed. The flow thereafter is in the axial direction with a parabolic velocity profile given by

$$v_x = v_o\ (1 - r^2/R^2) \qquad (I.18)$$

where $v_o = R^2\ \Delta P/4\mu\ L$ is the maximum velocity at the axis of the tube ($r = 0$) and ΔP is the pressure drop over the distance L.

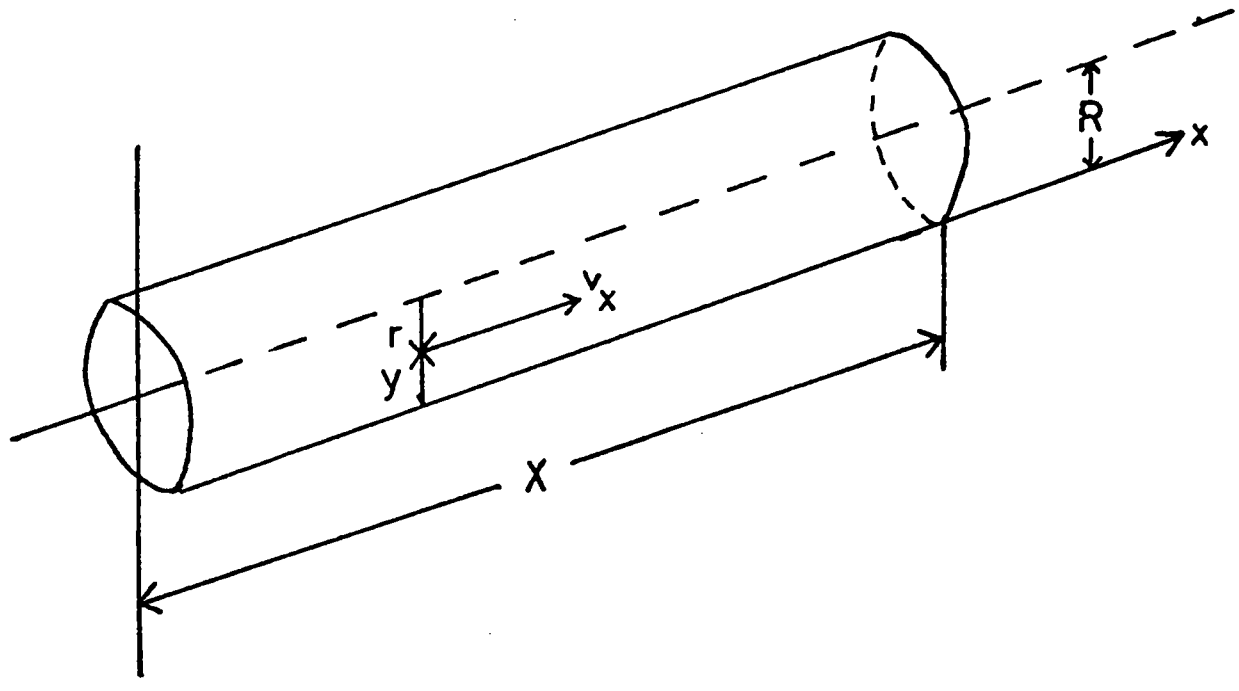

Figure I.5. Coordinates and tube parameters

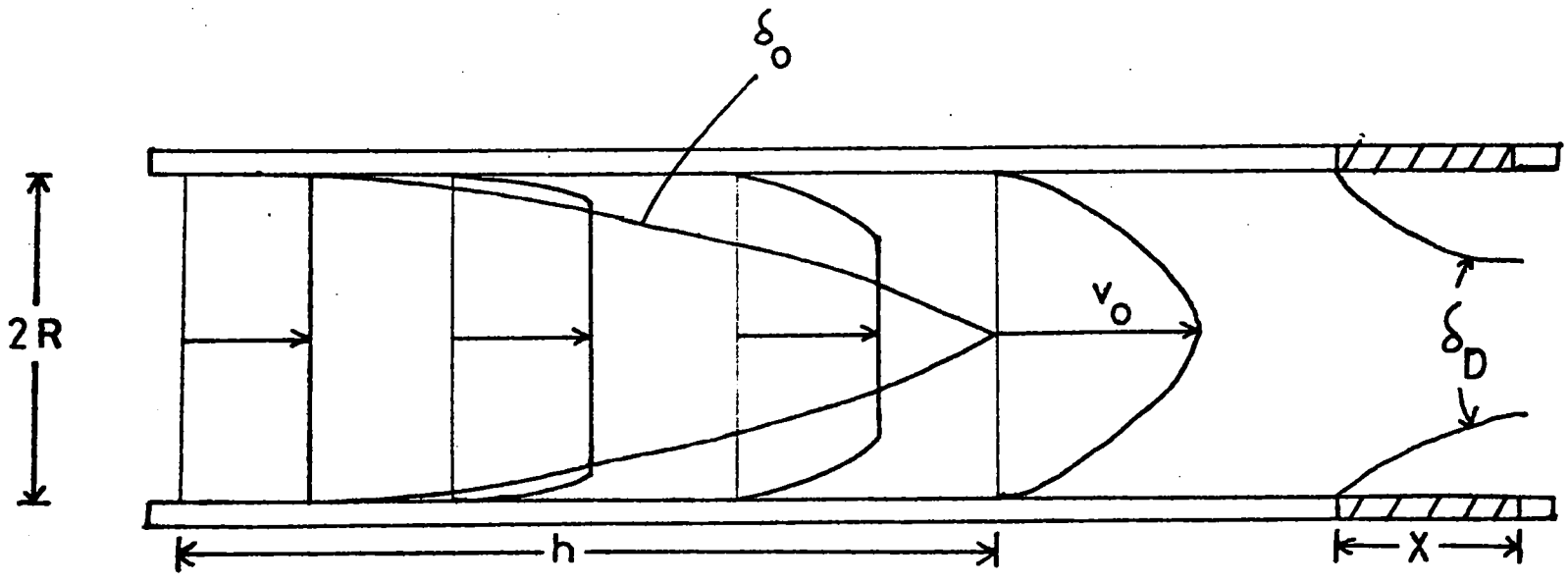

Figure I.6. Establishment of a Poiseuille profile and diffusion layer in a tube for laminar flow

This expression for v_x can be used in the solution of the convective-diffusion equation (48). The diffusion layer thickness (see figure I.6) is given by

$$\delta_D = 1.5 \left(\frac{D}{\nu}\right)^{1/3} \left(\frac{\nu}{v_o R}\right)^{1/3} (R^2 x)^{1/3}$$

$$= 1.5 \; Sc^{-1/3} \; Re^{-1/3} \; (R^2 x)^{1/3} \qquad (I.19)$$

and integration of the flux along the length of the electrode gives the limiting current as

$$i_L = 5.31 \times 10^5 n D^{2/3} X^{2/3} V_f^{1/3} c_\infty \qquad (I.20)$$

where V_f = volume flow rate = $v_o \; \pi R^2/2$

X = length of electrode.

The TE, unlike the RDE, is not a uniformly accessible surface, and $i_L \propto X^{2/3}$ since the diffusion layer thickness increases with $x^{1/3}$; this is because the downstream portion of the electrode is in contact with solution which has already reacted at the upstream portion. The limiting current, when expressed in terms of the volume flow rate (which is the experimentally measurable hydrodynamic parameter), is seen to be independent of the radius of the tube. Decreasing the tube radius would result in a higher flow velocity and (equation I.19) a thinner diffusion layer; therefore the limiting flux to the electrode would be greater, but this is offset by the decreased circumference of the electrode. One other point about equation (I.20) is that it does not contain the kinematic viscosity (c.f. equation I.14); this is because the theory has assumed fully developed laminar flow (the parabolic velocity profile) in which case the hydrodynamic (viscosity) boundary layer extends to the centre of the tube.

The TE has not been used as much as the RDE because of its non-uniform accessibility which results in any theoretical treatment being more difficult. However $i_L \propto c_\infty$, and its flow-through nature together with its low volume ($< 100\,\mu l$) make the TE extremely attractive for continuous voltammetric analysis. Blaedel (50) found i_L to be proportional to $V_f^{0.335}$, in good agreement with theory. He observed the onset of turbulence at Re =

200 - 300, which is far below the critical value of 2000 - 3000; this was due to rough edges at the metal-glass seals. The Reynolds number is a dimensionless number which directly reflects the experimental variables; it is comprised of a characteristic velocity, a characteristic length and the kinematic viscosity. For a TE

$$Re = v_o R/\nu \qquad (I.21)$$

or, in terms of the volume flow rate

$$Re = \frac{2V_f}{\pi R \nu} \qquad (I.22)$$

c) The Wall-Jet Electrode Detector (WJED)

The term wall-jet applies to the phenomena when a jet of fluid strikes a wall perpendicularly and then spreads radially over the surface of the wall, and a WJED is illustrated in figure I.7. The fluid flow has been described by Glauert (51) and is depicted in figure I.8, along with the diffusion layer. Yamada and Matsuda (52) used Glauert's results to derive the expression for the limiting current:

$$i_L = 1.60\ nFD^{2/3}\nu^{-5/12}V_f^{3/4}a^{-1/2}R^{3/4} \qquad (I.23)$$

where a = nozzle diameter

R = radius of electrode

This electrode system is not uniformly accessible, showing an $R^{3/4}$ dependence for the same reason as the TE $X^{2/3}$ dependence. The dependence on nozzle diameter is to be expected and once again the kinematic viscosity affects the limiting current. The WJED possesses a high flow rate dependence ($\propto V_f^{3/4}$); small cell columes ($\sim 5\ \mu l$) are possible and in a single pass some 10 - 15% of an electroactive substance may be electrolysed which results in high sensitivity. In this electrode forced convection is a far more efficient process than in the TE ($i_L \propto V_f^{1/3}$), but this also means that the measured currents are affected more by fluctuations in flow rate. The design of the electrode allows easy maintenance of the working electrode surface, which is a desirable quality for a continuous monitor.

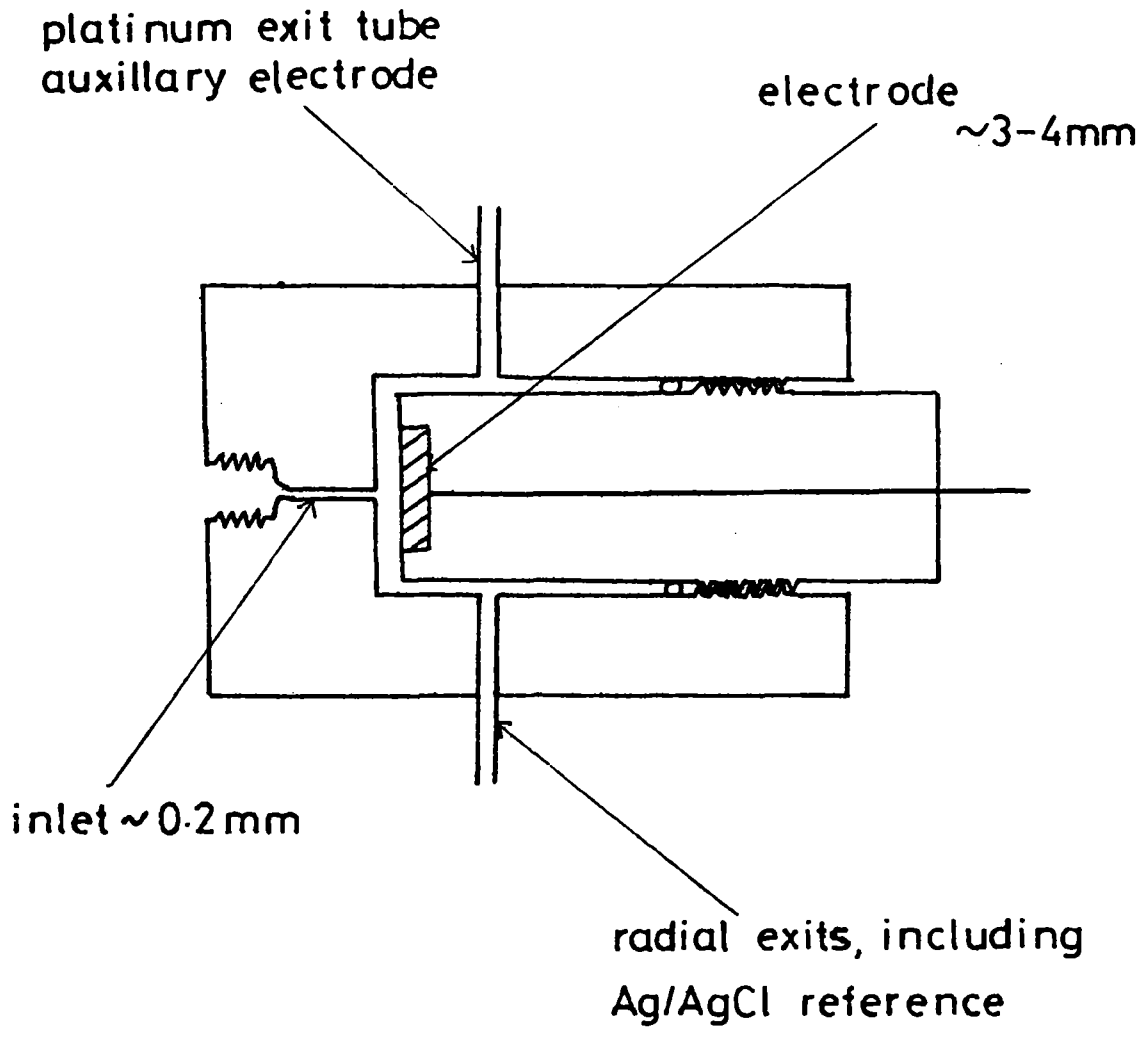

Figure 1.7. Wall Jet Electrode

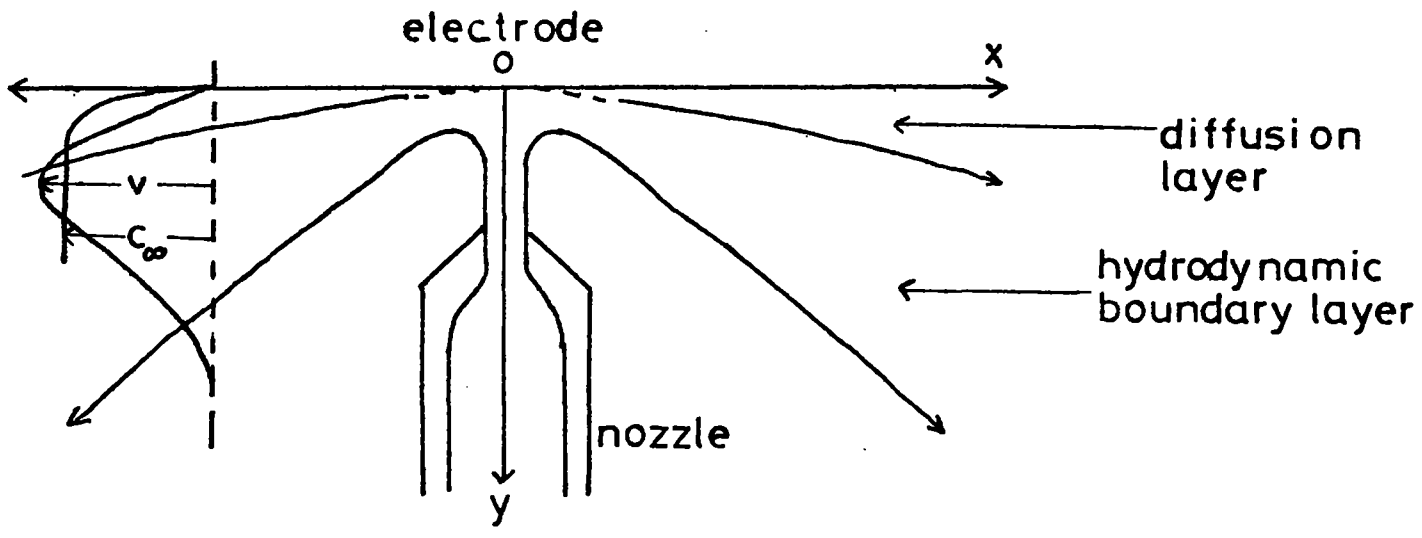

Figure 1.8. Schematic representation of the velocity and concentration distribution in the WJED

The WJED and similar systems have been used in HPLC detection (8) and anodic stripping voltammetry (53) in addition to hydrodynamic voltammetry (52).

d) The Rotating Ring Disc Electrode (RRDE)

This electrode is similar to the RDE (the fluid flow is identical) but has a concentric ring of metal separated from the central disc by an annulus of non-conducting material (figure I.9). The ring electrode permits electrochemical detection of the products of the disc electrode reaction.

In a simple RRDE experiment species are generated at the disc and detected, as a limiting current, at the ring:

Disc $\quad C \pm ne \rightarrow B$

Ring $\quad B \pm ne \rightarrow C.$

A schematic concentration profile is shown in figure I.10; in the bulk of the solution the concentration of B,b, is zero since this species is being generated at the disc; also at the ring electrode surface b=0 since B is being detected as a limiting current. The intermediate B is transported away from the disc: some escapes into the bulk of the solution; some crosses the gap and reacts at the ring and this fraction, termed the collection efficiency, is defined by the current ratio

$$N_o = -i_R/i_D \qquad (I.24)$$

The negative sign appears because of the opposite reactions occuring at disc and ring.

N_o was first calculated approximately by Ivanov and Levich (54) and later exactly by Albery and Bruckenstein (55,56) who found that

$$N_o = 1-F(\alpha/\beta) + \beta^{2/3}[1-F(\alpha)] - (1+\alpha+\beta)^{2/3}[1-F\{(\alpha/\beta)(1+\alpha+\beta)\}] \qquad (I.25)$$

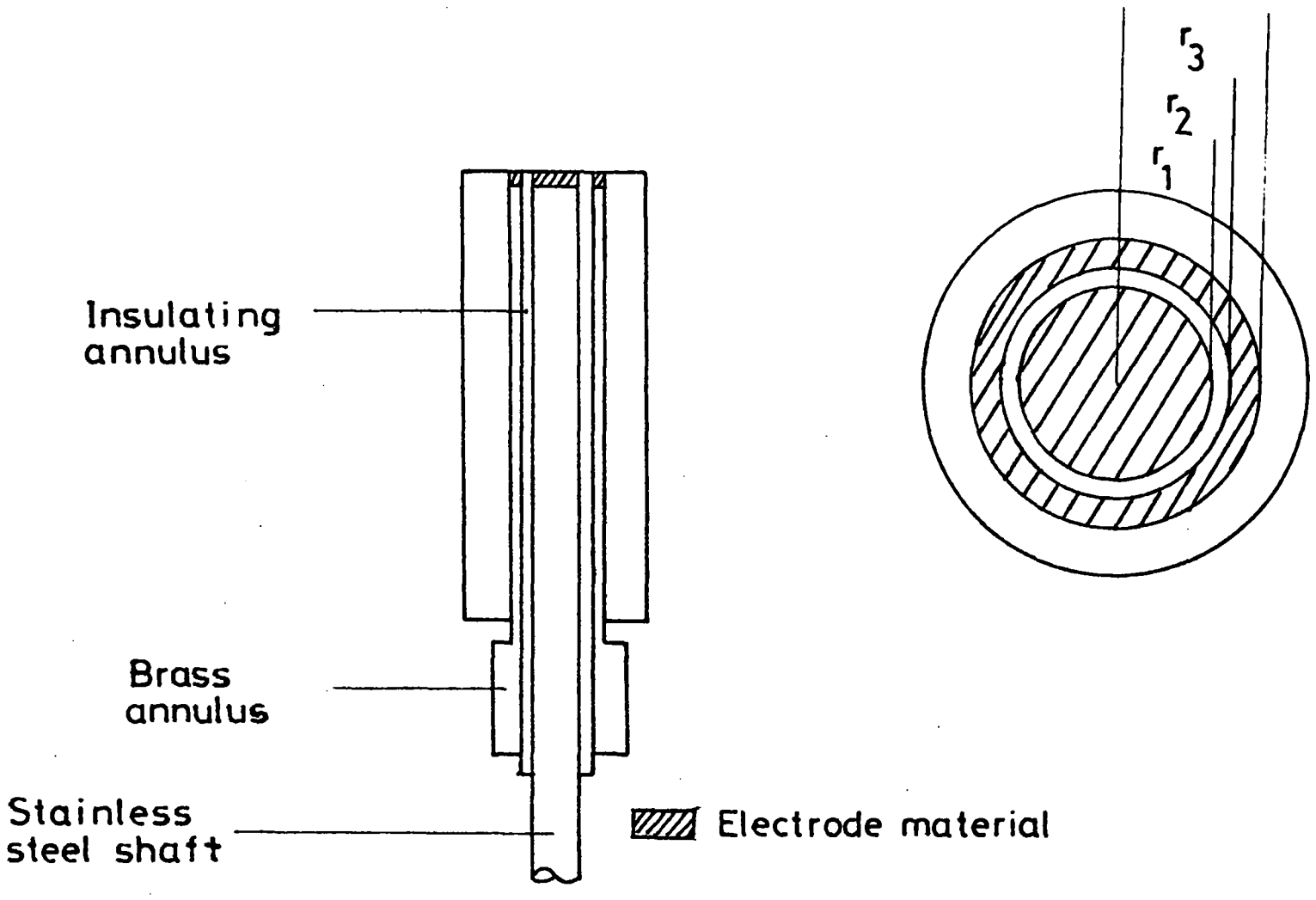

Figure I.9. The ring-disc electrode

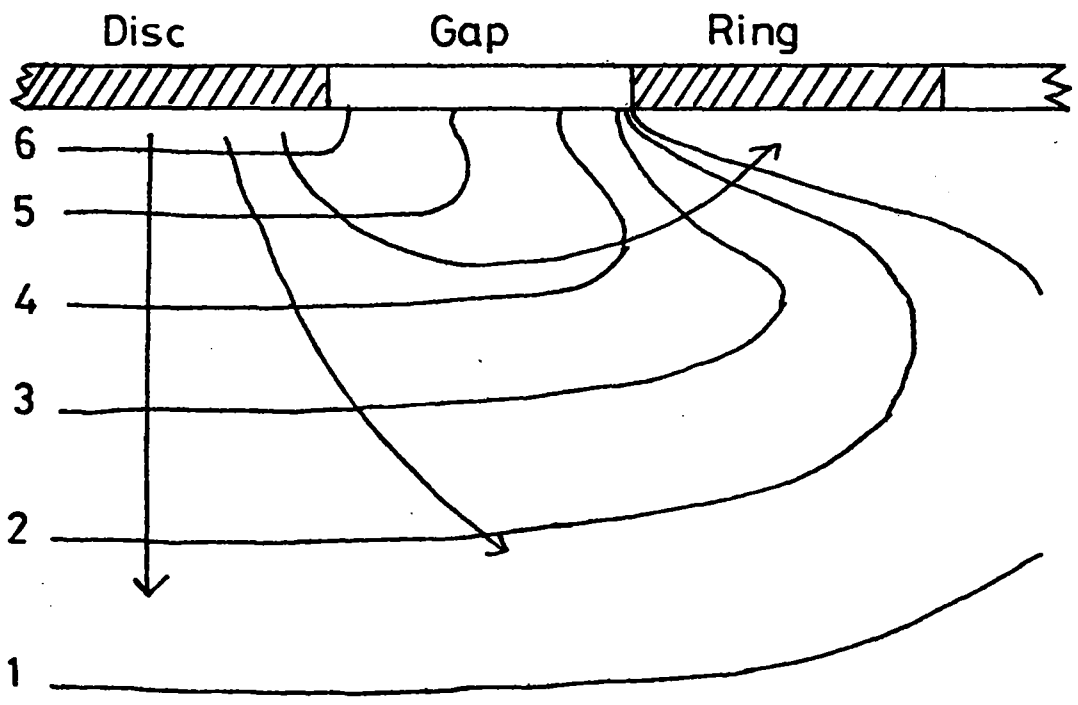

Figure I.10. Schematic concentration profile at RRDE

where the function F is given by

$$F(x) = \frac{3^{1/2}}{4\pi} \ln \left\{ \frac{(1 + x^{1/3})^3}{1 + x} \right\} + \frac{3}{2\pi} \arctan \left\{ \frac{(2x^{1/3} - 1)}{3^{1/2}} \right\} + \frac{1}{4} \qquad \text{(I.26)}$$

and α and β are functions of the geometry of the electrode

$$\alpha = (r_2/r_1)^3 - 1$$

$$\beta = (r_3/r_1)^3 - (r_2/r_1)^3 \qquad \text{(I.27)}$$

The constant $\beta^{2/3}$ is in fact the proportionality constant relating a limiting current at the ring electrode to that at the disc electrode:

$$i_{R,L} = \beta^{2/3} \cdot i_{D,L} \qquad \text{(I.28)}$$

The theoretical expression for N_o is obtained by solution of the convective- diffusion equation in the zones of the disc, gap and ring, this solution requiring the use of Laplace transformations. Transport of B from the disc to the ring is effected by diffusion normal to the electrode and by radial convection (radial diffusion is a negligible transport process). N_o is predicted to be purely a function of electrode geometry (i.e. independent of rotation speed) and good agreement between theory and experiment has been found (56,57); N_o is typically 0.10-0.25, and may be evaluated using a Texas SR52 programmable calculator (221 steps).

In the diffusion layer titration technique (58) a reagent (A) is added to the solution to react with and remove the intermediate (B) during its journey to the ring. With the disc electrode passing no current there is a uniform concentration of C(the electroactive species) and A(the added reagent) throughout the solution. When a small current is passed through the disc (in the correct direction) the intermediate B is generated at the disc surface; this immediately reacts with A so that b = 0 everywhere in solution (this argument is for a very fast reaction in the steady state). However this reaction has depleted the concentration of A in the diffusion layer; this is illustrated in figure I.11. As the disc current is further

increased the concentration of A at the electrode surface, a_o, decreases and at a disc current which is given the symbol M, $a_o = 0$. The transport of A to the electrode surface, where it reacts with B, is diffusion limited and

$$M = 0.62 n_B F A D^{2/3} \omega^{1/2} \nu^{-1/6} a_\infty \qquad (I.29)$$

At this point the flux of B (controlled by the disc current) is equal in magnitude to the flux of A (controlled by the pumping action of the rotating disc), and the behaviour of A is analogous to that of an electroactive substance undergoing charge transfer at a disc electrode.

When the disc current is increased above M then the flux of B is greater than the flux of A. In the case of a very fast reaction between A and B there will be, in solution, a region dominated by A and a region dominated by B, the two being distinctly separated at the reaction boundary where a=b=0. No B will be detected until the disc current is such that the B-dominated region reaches the inside edge of the ring (figure I.12); this is usually at $i_D/M = 1.5\text{-}2.0$. As the disc current is further increased the B-dominated region moves across the ring and the ring current increases; the ring current becomes a linear function of the disc current when the ring electrode lies entirely in the B-dominated region ($i_D/M > 2.5 - 3.0$):

$$i_R = N_o |i_D| - M\beta^{2/3} \qquad (I.30)$$

The second term in this equation, since it includes $\beta^{2/3}$, represents a limiting current at the ring electrode (see equation I.28); therefore the above equation can be interpreted as

$$i_R = N_o |i_D| - M\beta^{2/3} \qquad (I.31)$$

flux of B to ring in presence of A = flux of B to ring in absence of A − limiting flux of A to ring

The result (figure I.12) is a displacement of the linear portion of the titration curve away from the N_o line; extrapolation of this linear portion to $i_R = 0$ gives

$$i_D = M\beta^{2/3}/N_o$$

$$= \text{constant} \times n_B D^{2/3} \omega^{1/2} a_\infty \qquad (I.32)$$

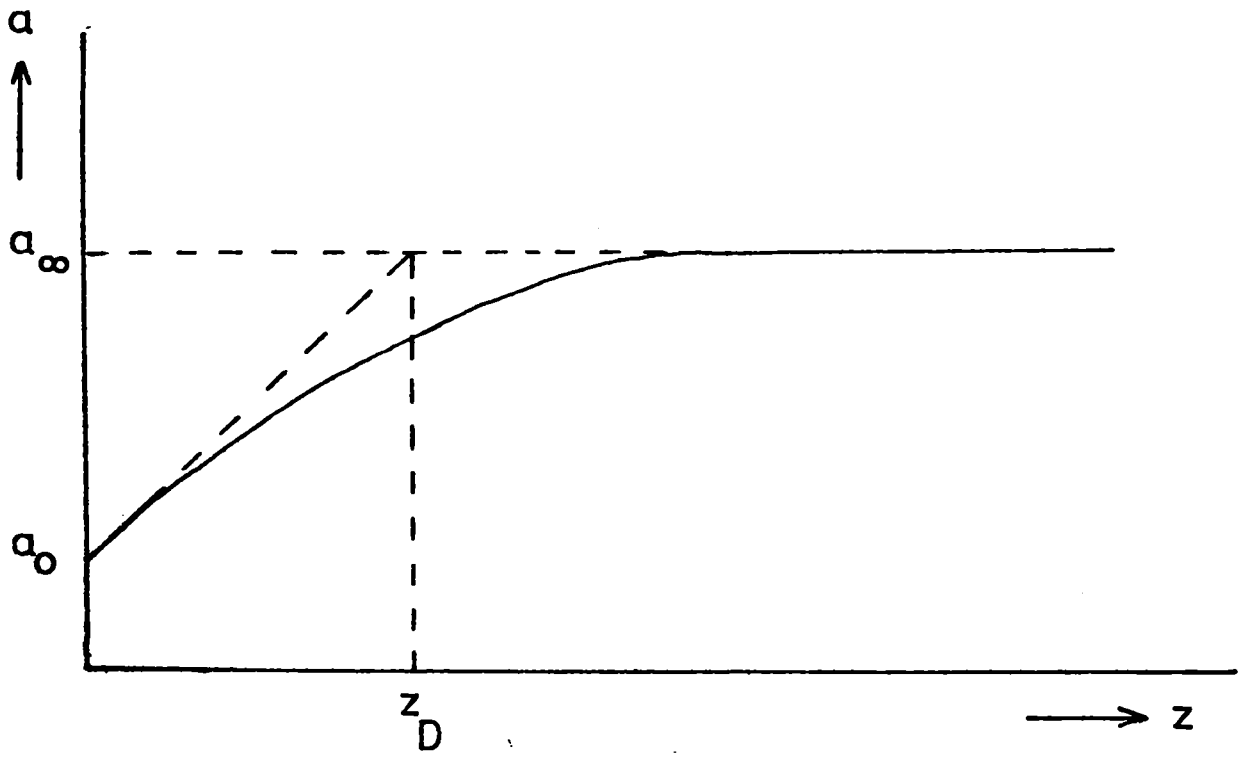

Figure I.11. Variation of concentration of A with z

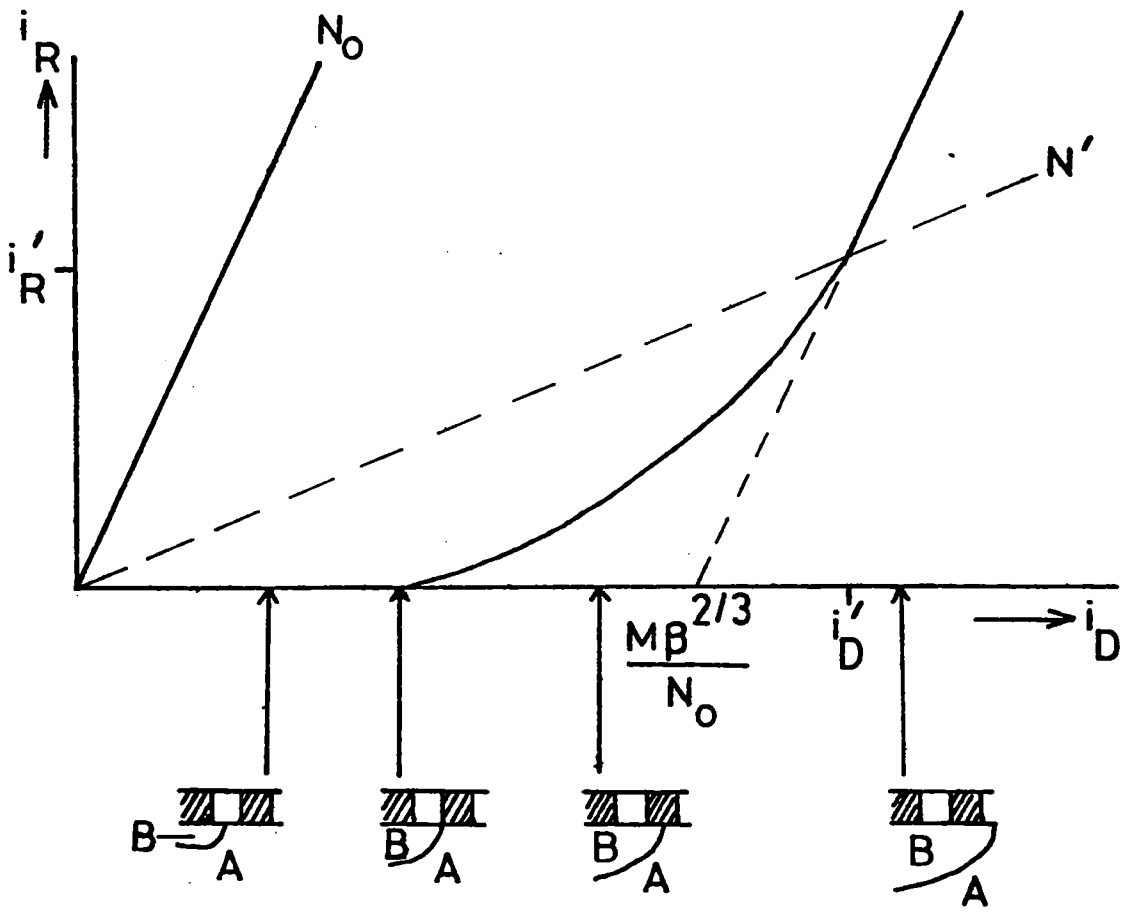

Figure 1.12. Ring disc electrode titration curve

This illustrates the analytical capability of the diffusion layer titration method: the displacement varies linearly with a_∞, the bulk concentration of the reagent A. There is also a rotation speed dependence, $\omega^{1/2}$: increasing the rotation speed increases the flux of A resulting in a larger displacement. The technique has been applied to the determination of As (III) (by titration with electrogenerated bromine) at concentrations as low as 10^{-7}M (58). The non-linear region of the theoretical titration curve can be described by values of i_D/M (a normalised disc current) and N' ($= i_R'/i_D'$) at different values of β_J, a dimensionless parameter which describes the radial position of the reaction boundary on the ring. These sets of three parameters (58) can again be determined using a Texas SR52 programmable calculator.

The above discussion of titration curves has assumed an infinitely fast reaction, in which case the solution regions dominated by A and B are distinctly separated by the reaction boundary at which $a = b = 0$ (figure I.13). When the reaction is not infinitely fast (having a second order rate constant k_2) then some A will be present in the B-dominated region, and vice versa; the reaction boundary, at r_J, is the point at which a=b. This situation results in ring current- disc current plots which are basically similar to the ideal titration curve, but which exhibit deviations in the region corresponding to the ring electrode not being completely in the B-dominated region.

The theory for the ideal titration curve yields values of i_D/M and N' for the case when $\beta_J = 1$ (reaction boundary at outside of ring, $r = r_3$) and this point can be identified on a second-order titration curve. The point on this $i_R - i_D$ plot corresponding to the reaction boundary being at the inside edge of the ring ($r = r_2$, $\beta_J = 0$) can be ascertained using

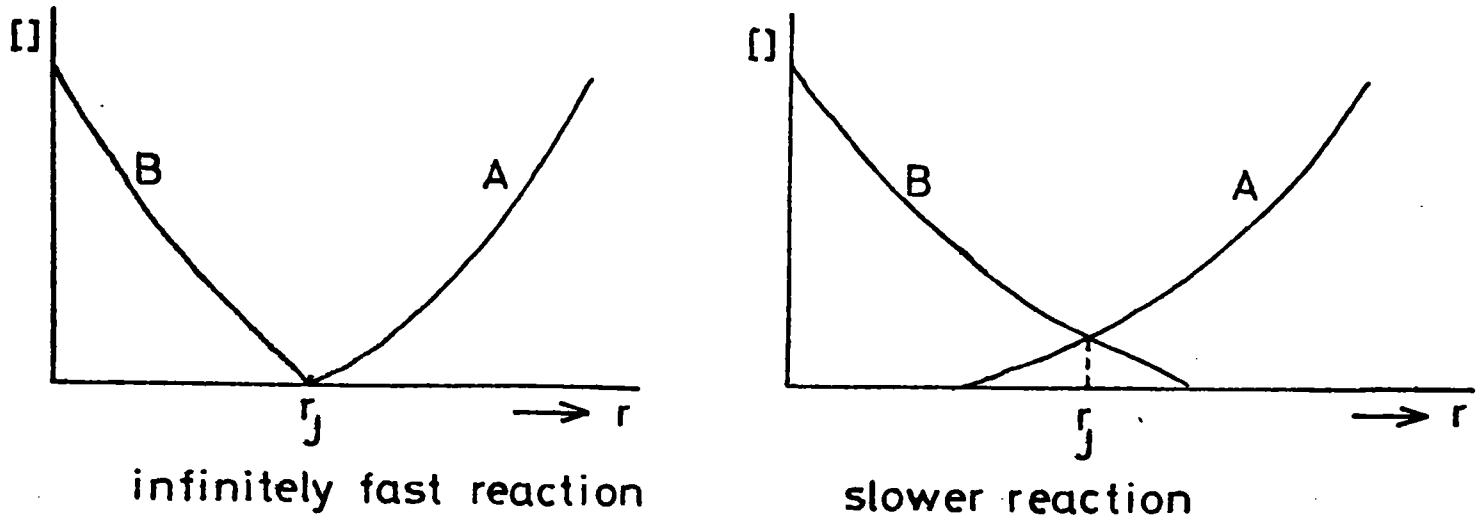

Figure 1.13. Schematic concentration profiles at RRDE for diffusion layer titrations.

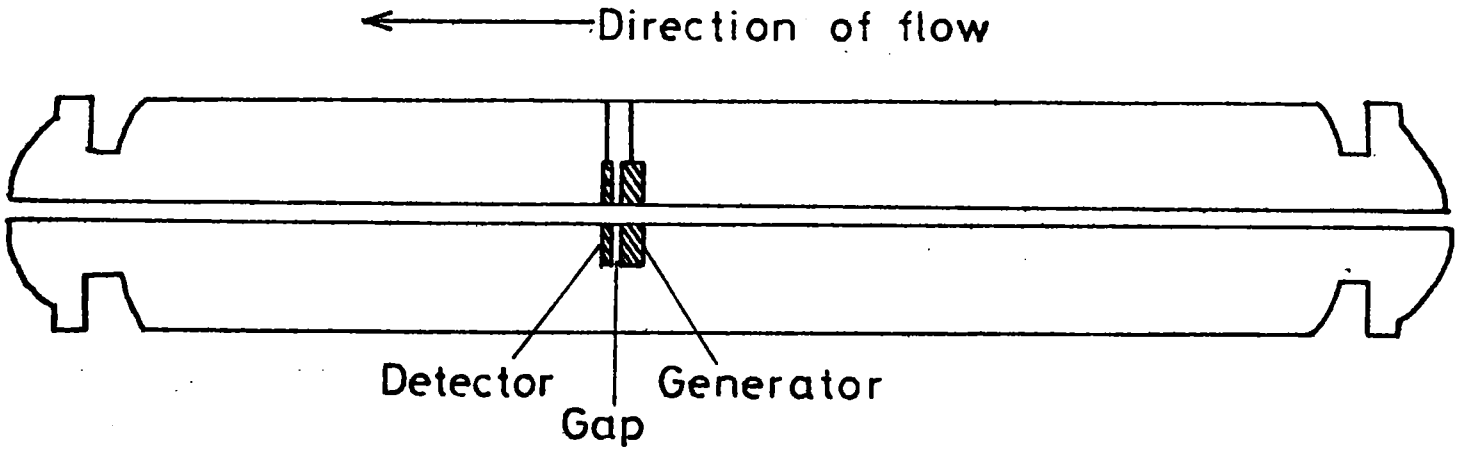

Figure 1.14. The tubular double electrode

the appropriate theoretical value of i_D/M. While an ideal titration curve would show zero ring current here, the second order curve exhibits a finite ring current $i_{R,\varkappa}$ due to penetration of B past the reaction boundary. An approximate analytical solution of the transport equations (59,60) predicts that

$$i_{R,\varkappa} = 0.21\pi\, r_1^2\, nFD\, \omega^{3/2} \nu^{-1/2} k_2^{-1} \qquad (I.33)$$

and results for the bromination of allyl alcohol, a reaction of known rate constant, were in good agreement with the theory. Equation I.33 does not contain the bulk concentration of A; as a_∞ is increased the concentration $a_J = b_J$ at the reaction boundary will also increase, but the extent of penetration of B past this boundary is reduced, and the two effects cancel.

Some additional applications of the RRDE have been described by Albery and Hitchman (61).

e) The Tubular Double Electrode (TDE)

This is the flow through analogue of the RRDE (see figure I.14) and consists of two tubular electrodes mounted very close together in the walls of a smooth tube. The first electrode (analogous to the disc) is termed the generator electrode and the second, downstream electrode is termed the detector.

The design and application of the channel double electrode has been described (62,63); this electrode is of rectangular cross-section, with two insulated electrodes mounted flush in one wall of a smooth channel, whose width is very large compared to its depth. The large width is necessary to minimise the edge effects from which this configuration suffers; these effects disappear when the edges are joined together in the circular cross-sectional TDE. In this laboratory Cook (39) developed a TDE with which he performed diffusion layer titrations of As (III) using electrogenerated bromine, and Schieffer and Blaedel (64) have used the TDE in anodic stripping voltammetry with collection.

Applications of the TDE are precisely those of the RRDE; the theoretical treatments for both types of electrode are very similar and remarks made for one are invariably true of the other. Once again it is the analytical application that deserves particular mention since this system permits diffusion layer titrations to be carried out in flowing systems. The equation describing the TDE titration curve is

$$i_{det} = Ni_{gen} - M\lambda^{2/3} \qquad (I.34)$$

which can be interpreted in the same way as equation I.31, recognising that $\lambda^{2/3}$ is the TDE analogue of the RRDE's $\beta^{2/3}$, and that M will have a different form (equation I.20).

The aim of this work has been to develop a technique, using the TDE, to perform diffusion layer titrations in a flowing system; solutions of the transport equations for the TDE for the particular cases of the collection efficiency and titration curves are presented in chapter II.

3. CHROMATOGRAPHIC DETECTORS

The characteristics of an ideal liquid chromatography (LC) detector have been specified by Snyder and Kirkland (65); the detector should:

Have high sensitivity and predictable response.

Respond to all solutes, or else have predictable specificity.

Be unaffected by changes in temperature and carrier flow.

Respond independently of the mobile phase.

Not contribute to extra-column band broadening.

Be reliable and convenient to use.

Have a response which increases linearly with the amount of solute.

Be non-destructive of the solute.

Provide qualitative information on the detected peak.

The specification of some real (non-ideal) detectors used in HPLC are presented in table I.1.

Table I.1. Properties of Selected HPLC Detectors (65)

Type of Detector	Analytical Property	Sensitivity to favourable sample ($g\ ml^{-1}$)	Linear Dynamic Range	Cell Volume (μl)	Response to Flow rate	Temperature Dependence
UV	Absorbance (A)	5×10^{-10}	5×10^{4}	10	None	Small
Refractometric	Refractive Index (n)	5×10^{-7}	10^{4}	2-10	None	Appreciable
Conductimetric	Conductivity ($\mu\Omega^{-1}$)	10^{-8}	2×10^{4}	0.5-2	None	$2\%\ K^{-1}$
Fluorometric	Flourescence	10^{-9}-10^{-10}	$\sim 10^{3}$	7	None	Small
IR	Absorbance(A)	10^{-6}	10^{4}	15	None	Small
Voltammetric	Current(A)	10^{-9}	10^{4}	5	$V_f^{3/4}$	$\sim 1.5\%K^{-1}$
TDE Titrations	Current(A)	?	?	10-80	$V_f^{1/3}$	$\sim 1.5\%K^{-1}$

The aim of this work has been to develop a detector for, primarily, the gel filtration chromatography (GFC) of proteins. The technique of GFC mainly uses the ultra violet detector; this is a selective detector, responding to a solute property (its concentration). The most commonly used wavelengths are 254 and 280 nm, and in proteins the tryptophanyl and tyrosinyl aromatic residues will absorb radiation of this wavelength. However some proteins, peptides and amino acids which do not contain these chromophores cannot be detected. It is then necessary to use the refractometric detector; this is a general detector, responding to the bulk refractive index. A differential refractometer monitors the difference in refractive index between a reference mobile phase and the mobile phase containing the sample as it elutes from the column. While this second detector responds to all solutes it is very sensitive to temperature changes.

The proposed tubular double electrode diffusion layer titration detector will be a selective detector, responding to the solute concentration. However the mechanism and extent of its response will differ from that of the UV detector. Some of its specifications have been inserted in table I.1, these having been estimated using information and experience available at the commencement of this work. The sensitivity and linear dynamic range of the technique must be determined experimentally, and so must the aspects of noise, stability and response time. However the response time must be fairly rapid to enable good resolution of peaks (30s or less for GPC, even less for HPLC). TDE's of 80 μl volume have been constructed, and halving of the diameter (to 0.5mm) and length will produce a detector of 10 μl cell volume. The equations for the displacement of the TDE titration curve (I.20, I.34) indicate that the detector response will be flow-rate dependent. Furthermore the temperature dependence of the diffusion coefficient ($\sim$2% K^{-1}) which appears in these equations will affect the response of the detector. The addition of bromide ions is necessary (to enable electrogeneration of hypobromite) and the use of a titration reaction

means that the detector will not be non-destructive. However the extent of destruction will be small ($\sim$0.1%) since titration occurs only in the diffusion layer.

CHAPTER II. THEORY

In this chapter detailed solutions of the transport equations for the tubular double electrode (TDE) are presented, for the particular cases of the collection efficiency and diffusion layer titration curves. These results have not been published and are an extension of the corresponding RRDE solutions, which have been discussed in section I.2.d. and are readily available in the literature (55 - 61). However the RRDE titration curve theory has been extended, to cover titrants and substrates with different diffusion coefficients and this new theory is presented in the third section of this chapter.

Generally the TDE is used in such a way that a species, C, present in the bulk of the solution, is oxidised or reduced at the generator electrode to an intermediate, B. This is then transported to the detector electrode, by a combination of diffusion and convection, and the potential of the detector is adjusted so that all intermediate reaching it is electrolysed (i.e. a limiting current is observed). The generalised reaction scheme is

$$C \pm ne \longrightarrow B \quad \text{at generator}$$
$$B \pm (+A) \longrightarrow \text{solution (reaction products)}$$
$$B \pm ne \longrightarrow C \quad \text{at detector}$$

Fluxes of electroactive species at the generator and detector electrodes give rise to currents, i_{gen} and i_{det} respectively, which can be readily plotted on the X and Y axes of an X - Y chart recorder.

1. THE TUBULAR DOUBLE ELECTRODE - COLLECTION EFFICIENCY

The theoretical description of the TDE is more difficult than that of its analogue, the RRDE. This is because the tubular generator electrode, unlike the rotating disc electrode, is not a uniformly accessible surface: at the disc of an RRDE there is a uniform surface

concentration, and a uniform flux. At the generator of a TDE it is therefore necessary to make an assumption for the boundary condition.

A theoretical treatment of the TDE was achieved by Braun (63) for the particular case of a channel electrode, which has a rectangular cross-section. Braun calculated the collection efficiency, under the assumption that a limiting flux of electroactive species exists at the generator electrode, by employing the same general approach as used by Albery and Bruckenstein (56) to solve the corresponding RRDE problem. Braun's expression for N_o, the collection efficiency, is

$$N_o = 1 + \lambda^{2/3}[1 - F(\vartheta)] - (1 + \vartheta + \lambda)^{2/3}[1 - F(\vartheta/\lambda)(1 + \vartheta + \lambda)] - F(\vartheta/\lambda) \qquad (II.I)$$

where ϑ is the ratio of gap thickness to generator electrode thickness and λ is the ratio of detector to generator electrode thickness; the function F(x) is given by equation I.26, and equation II.1 is identical to I.25 if ϑ is replaced by α , and λ is replaced by β .

Albery derived a relationship for the collection efficiency of a TDE, under the assumption of a uniform flux (as opposed to Braun's assumption of a limiting flux); the approach was again the same as that used in the derivation of the RRDE collection efficiency. This approach involves solving the convective-diffusion equation for the intermediate B in the zone of the generator electrode using a Laplace transformation, which provides a boundary condition for the solution of the transport equation in the zone of the gap. A second Laplace transformation solves this equation to provide once more a boundary condition for the Laplace transform-aided solution of the equation in the detector electrode zone. The result is a triple Laplace transform which was inverted (39) to give

$$N_o = 1 - (1 + \vartheta + \lambda)F\left(\frac{1 + \vartheta}{\lambda}\right) + (\vartheta + \lambda)F\left(\frac{\vartheta}{\lambda}\right) + \frac{3^{3/2}\,\lambda^{2/3}}{2\pi}\left[(1 + \vartheta)^{1/3} - \vartheta^{1/3}\right] \qquad (II.2)$$

where $\vartheta = l_2/l_1$, $\lambda = l_3/l_1$ and F (x) is given by equation I.26.

The two expressions for the collection efficiency differ because of the different conditions assumed at the generator electrode. The Braun condition of a limiting flux corresponds to the concentration of C being zero at the generator surface; this can be generalised to a uniform surface concentration, and this boundary condition is correct when the electrolysis of C is a reversible reaction. When the reaction of C at the generator electrode is electrochemically irreversible (1) then the surface concentration of A will not be uniform, and Albery's boundary condition of a uniform flux must be used. In this work bromide is oxidised to hypobromite at the generator electrode and this is a reversible reaction; therefore in this and the following section the TDE collection efficiency will be treated in terms of N_{Braun} rather than N_{Albery}.

The method of solution presented in this thesis uses a new simpler approach, which avoids the horrors of a triple Laplace transform, by using the single Laplace transforms of three quantities. This approach has previously been used to solve the convective - diffusion equation for the downstream distribution of products electrogenerated at a tube electrode (67); it is used in this section to calculate the collection efficiency of the TDE, and in the following section to calculate the theoretical titration curve.

The coordinate system used is illustrated in figure II.1. The time-independent convective-diffusion equation for the transport of the electrogenerated intermediate B is

$$v_o \left[1 - (r/r_o)^2 \right] \frac{\partial b}{\partial x} = D\left(\frac{\partial^2 b}{\partial r^2} + \frac{1}{r}\frac{\partial b}{\partial r}\right) \qquad \text{(II.3)}$$

in which the left hand side describes axial convection, and the right hand side represents radial diffusion. The term describing axial diffusion (down the tube) may be neglected because convection is much more efficient than diffusion. The axial coordinate, x, can be normalised with respect to

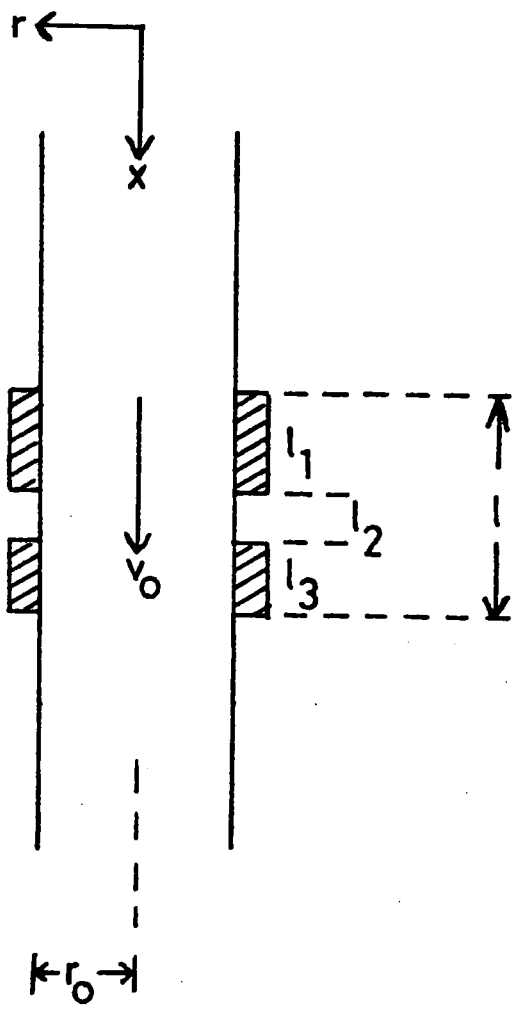

Figure II.1. TDE coordinates

the length, 1 (figure II.1), over which the experiment takes place and over which it is required to describe the concentration profile:

$$\chi = x/1 \qquad \text{(II.4)}$$

It is assumed that the effect of the electrodes on the concentration profile is confined close to the tube wall so that

$$1 - (r/r_o)^2 \simeq 2\,(r_o - r)\,/r_o = 2\xi \qquad \text{(II.5)}$$

where

$$r/r_o = 1 - \xi \qquad \text{(II.6)}$$

This enables equation II.3 to be rewritten as

$$\frac{2v_o r_o^2}{1D}\,\xi\,\frac{\partial b}{\partial \chi} = \frac{\partial^2 b}{\partial \xi^2} - \left(\frac{1}{1-\xi}\right)\frac{\partial b}{\partial \xi} \qquad \text{(II.7)}$$

Now let

$$\rho = \left(\frac{2v_o r_o^2}{1D}\right)^{1/3}\xi = \left(\frac{v_o r_o^2}{41D}\right)^{1/3}\left[1 - \left(\frac{r}{r_o}\right)^2\right] \qquad \text{(II.8)}$$

so that II.7 becomes

$$\rho\,\frac{\partial b}{\partial \chi} = \frac{\partial^2 b}{\partial \rho^2} - \frac{1}{1-\xi}\,\frac{\partial b}{\partial \rho}\left(\frac{1D}{2v_o r_o^2}\right)^{1/3} \qquad \text{(II.9)}$$

This last substitution (II.8) is an important point, since in nearly all experiments $(1D/2v_o r_o^2)^{1/3} \ll 1$. The dimensionless ratio inside the brackets describes the time taken for B to be swept down the tube $(1/v_o)$ compared to the time taken for B to diffuse across the tube (r_o^2/D). For reasonable values of 1 convection down the tube is much more efficient than diffusion across the tube, which justifies the assumption (equation II.5) that species are concentrated on the outside of the tube. When this condition holds then, for $\chi \sim 1$ $(x \sim 1)$ and $\rho \sim 1$, $\xi \sim (1D/2v_o r_o^2)^{1/3} \ll 1$, which enables equation II.9 to be reduced to a simpler form:

$$\rho\,\frac{\partial b}{\partial \chi} = \frac{\partial^2 b}{\partial \rho^2}\,. \qquad \text{(II.10)}$$

This is identical to the equation for a channel electrode (63), i.e. the approximations made have removed the circular nature of the TDE.

At this point Braun assumed a limiting flux at the generator electrode, and used the triple Laplace transformation technique. The method of solution presented here is to normalise b, firstly to fit the boundary condition at the generator electrode, and secondly to produce a function u. This function u is split into different contributions (u_n) whenever the boundary condition for u changes at the wall of the tube; this is illustrated in figure II.2; each u_n is associated with a χ_n, and $u_n = 0$ for $\chi_n \leqslant 0$. For $\chi_n > 0$ u_n must be solved, and the function u is the sum of all u_n's:

$$u = \sum_{1}^{n} u_n$$

The boundary condition for u_n on the wall of the tube is calculated from the boundary condition for the function u

$$u_n = u - \sum_{1}^{n-1} u_n$$

Since the form of u is a linear combination equation II.10 may be used as the differential equation for each u_n:

$$\rho \frac{\partial u_n}{\partial \chi_n} = \frac{\partial^2 u_n}{\partial \rho^2} \qquad \text{(II.11)}$$

Three boundary conditions are necessary for the solution of this equation, and two of these are common to the solution in all regions of the electrode:

$$\begin{aligned} u_n &\rightarrow 0 \quad \text{as} \quad \rho \rightarrow \infty \\ u_n &= 0 \quad \text{at} \quad \chi_n = 0. \end{aligned} \qquad \text{(II.12)}$$

The first condition expresses the fact that the concentration of intermediate is zero in the bulk of the solution, since it is being generated at the tube wall (the generator electrode), and the second boundary condition states that each $u_n \rightarrow 0$ as its $\chi_n \rightarrow 0$. The third boundary condition is specific to each region of the electrode. A Laplace transformation (see Appendix 1) of Equation II.11 with respect to χ_n gives

$$\rho s_n \bar{u}_n = \frac{\partial^2 \bar{u}_n}{\partial \rho^2} \qquad \text{(II.13)}$$

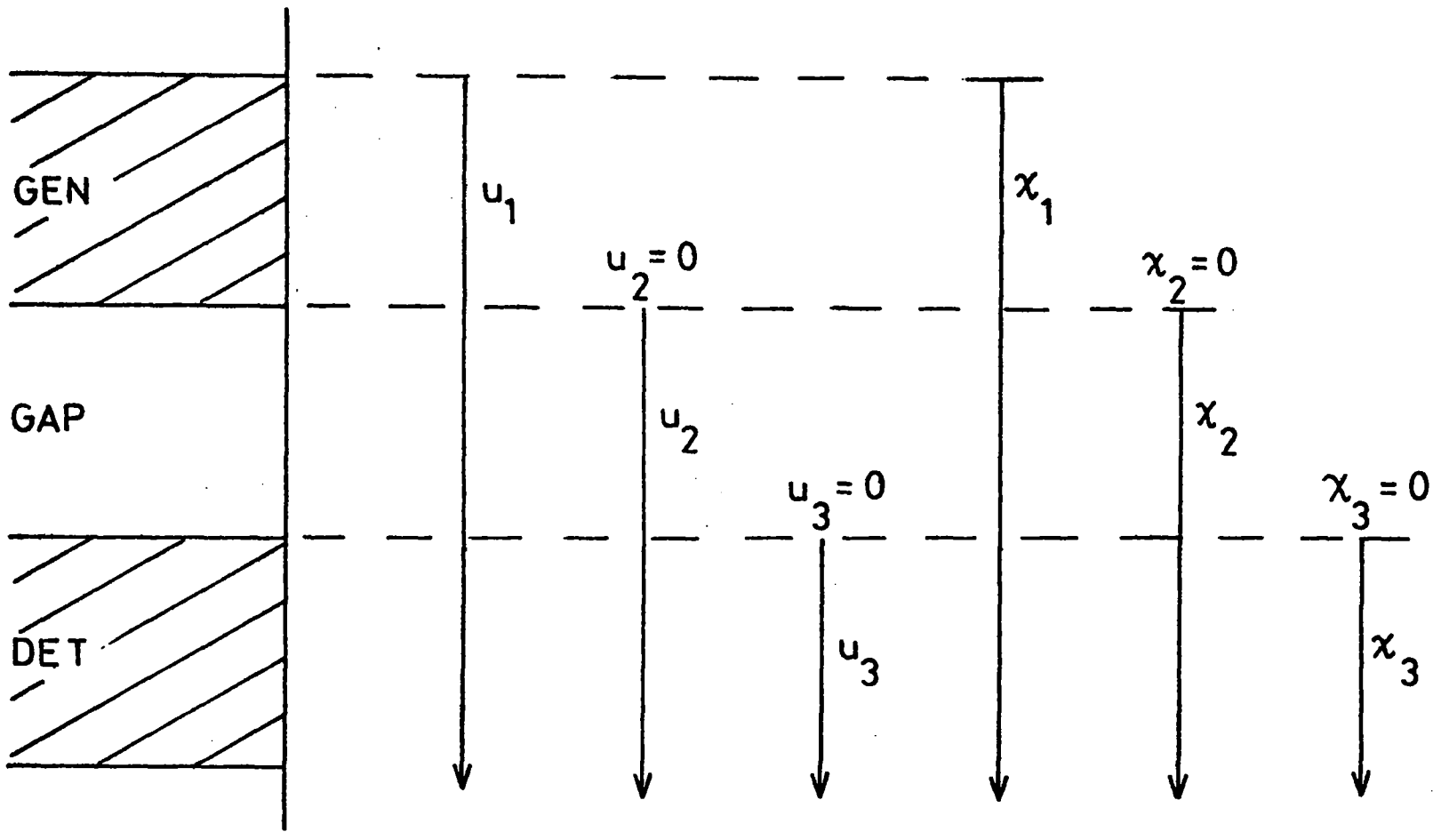

Figure 11.2. The functions u and χ at the TDE

whose solution can be expressed in terms of Airy functions (Appendix 2):

$$\bar{u}_n = \text{constant} \times \text{Ai}\,(s_n^{1/3}\rho)$$

the constant being fixed for each $\bar{u}_n$ by the boundary condition for the $\bar{u}_n$ at the wall of the tube. The normalised concentration gradient, in Laplace space, is therefore

$$\frac{\partial \bar{u}_n}{\partial \rho} = \text{constant} \times s_n^{1/3}\,\text{Ai}'\,(s_n^{1/3}\rho) \qquad \text{(II.14)}$$

This approach is now applied to the TDE assuming a uniform surface concentration, which is equivalent to Braun's assumption; the boundary conditions are

Generator $u_1 = 1$ (II.15)

Gap $$\left(\frac{\partial u_2}{\partial \rho} = -\frac{\partial u_1}{\partial \rho}\right)_{\rho = 0} \qquad \text{(II.16)}$$

Detector $u_3 = -u_1 - u_2 = -1 - u_2$ (II.17)

Since $u = \Sigma u_n$, the boundary condition II.16 means that $(\partial u/\partial \rho)_o = 0$, i.e. B is inactive at the wall of the tube in the region of the gap. Condition II.17 expresses the fact that $u = 0$ at the surface of the detector electrode, since B is being collected as a limiting current. The dimensions of the generator, gap and detector are l_1, l_2 and l_3 respectively, so that

$$l = l_1 + l_2 + l_3$$

and it is helpful to recast these lengths in dimensionless form:

$$\lambda_1 = l_1/l \quad \lambda_2 = l_2/l \quad \lambda_3 = l_3/l \qquad \text{(II.18)}$$

where $\lambda_1 + \lambda_2 + \lambda_3 = 1$.

The collection efficiency is defined as $-i_{det}/i_{gen}$; these fluxes can be found by multiplying the diffusion coefficient of B by the concentration gradient (integrated over the length of the relevant electrode), so that

$$N_o = \frac{\int_o^{\lambda_3} (\partial u_3/\partial \rho)_o d\chi_3}{\int_o^{\lambda_1} (\partial u_1/\partial \rho)_o d\chi_1} \qquad \text{(II.19)}$$

Therefore it is necessary to find, and integrate, these concentration gradients in the zones of the generator and detector.

a) Generator zone

The solution to equation II.11 in the generator zone using boundary condition II.15 is, in Laplace space,

$$\bar{u}_1 = \frac{Ai\ (s_1^{1/3} \rho\ )}{s_1 Ai\ (o)} \qquad (II.20)$$

Differentiation of this expression gives the concentration gradient at the surface of the electrode

$$\left(\frac{\partial \bar{u}_1}{\partial \rho}\right)_o = \frac{Ai'\ (o)}{s_1^{2/3}\ Ai(o)}$$

which can be inverted to give

$$\left(\frac{\partial u_1}{\partial \rho}\right)_o = \frac{Ai'\ (o)\, \chi_1^{-1/3}}{Ai\ (o)\ \Gamma(2/3)} = \frac{Ai'\ (o)\ (\lambda_1 + \chi_2)^{-1/3}}{Ai\ (o)\ \Gamma\ (2/3)} \qquad (II.21)$$

This gradient must be integrated to find the denominator in equation II.19:

$$\int_o^{\lambda_1} \left(\frac{\partial u_1}{\partial \rho}\right) d\chi_1 = \frac{Ai'\ (o)\ \lambda_1^{2/3}}{Ai\ (o)\ \Gamma\ (5/3)} \qquad (II.22)$$

Returning to equation II.20, this expression describes, in Laplace space, the distribution of intermediate B in the zone of the generator electrode. When $\rho = 0$ ($r = r_o$) then $\bar{u}_1 = 1/s$, so that at the wall of the tube $u_1 = 1$, which is the boundary condition used. The Airy function Ai (z) is shown below

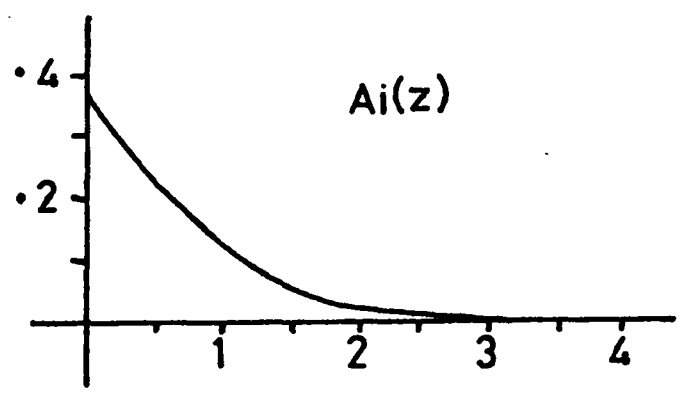

and in this case $z = s_1^{1/3} \rho$; ρ describes the distance from the wall of the tube so that as ρ increases the transformed concentration (and real concentration) falls. The form of the Airy function clearly indicates the existence of the diffusion layer (the region of solution in which

concentration gradients arise). The concentration gradient (and therefore flux) is described by equation II.21, and is seen to depend on $\chi^{-1/3}$, which demonstrates that the tubular electrode is not a uniformly accessible surface (section I.2.b).

b) Gap zone

In this zone the concentration profile is described by u_1, which is given above, and by u_2. This second function is found by solution of equation II.11, with boundary condition II.16, so that

$$\bar{u}_2 = \frac{-\mathcal{L}_2 (\lambda_1 + \chi_2)^{-1/3} \, Ai\,(s_2^{1/3} \rho)}{Ai\,(o)\,\Gamma\,(2/3)\, s_2^{1/3}} \qquad (II.23)$$

and at $\rho = 0$ (the electrode wall)

$$\bar{u}_{2,o} = - \frac{\mathcal{L}_2 (\lambda_1 + \chi_2)^{-1/3}}{\Gamma\,(2/3)\, s_2^{1/3}}$$

It is necessary to invert this expression since u_2 is required as a boundary condition in the detector zone; the inversion is achieved by using the convolution theorem (Appendix 1)

$$u_{2,o} = - \frac{\int_o^{\chi_2} t^{-2/3} (\lambda_1 + \chi_2 - t)^{-1/3} \, dt}{B\,(1/3,2/3)} \qquad (II.24)$$

$$= - \mathrm{I}_{\frac{\chi_2}{\lambda_1 + \chi_2}}\,(1/3,2/3) \qquad (II.25)$$

Integrals of the form appearing in equation II.24 can be written (66) as incomplete Beta functions (see Appendix 4), where

$$B_x\,(a,b) = \int_o^x t^{a-1} (1 - t)^{b-1} \, dt$$

$$B(a,b) = \Gamma\,(a)\ \Gamma(b)$$

and $$\frac{B_x(a,b)}{B\,(a,b)} = \mathrm{I}_x\,(a,b)$$

c) Detector zone

The third function u_3 can be found by combining equation II.25 and boundary condition II.17:

$$u_{3,o} = -\left[1 - I_{\frac{\chi_2}{\lambda_1 + \chi_2}}(1/3,2/3)\right]$$

$$= -I_{\frac{\lambda_1}{\lambda_1 + \chi_2}}(2/3,1/3)$$

$$= -I_{\frac{\lambda_1}{\lambda_1 + \lambda_2 + \chi_3}}(2/3,1/3) \qquad \text{(II.26a)}$$

To evaluate the collection efficiency (equation II.19) it is necessary to integrate the gradient of the concentration function u_3 in the zone of the detector electrode. The integration is best performed in Laplace space, since this merely involves division by the Laplace variable. Therefore

$$\bar{u}_3 = -\bar{I}_{Ai}(s_3^{1/3}\rho)/Ai(o) \qquad \text{(II.26b)}$$

$$(\partial \bar{u}_3/\partial \rho)_o = -s_3^{1/3} I Ai'(o)/Ai(o)$$

and $$\int_o^{\lambda_3}\left(\frac{\partial u_3}{\partial \rho}\right)_o = \mathcal{L}_3^{-1} - \frac{1}{s_3^{2/3}} \bar{I}_{\frac{\lambda_1}{\lambda_1 + \lambda_2 + \chi_3}}(2/3,1/3)\ \frac{Ai'(o)}{Ai(o)}$$

$$= -\frac{Ai'(0)}{Ai(o)\ \Gamma(2/3)}\int_o^{\lambda_3}\frac{1}{t^{1/3}}\ I_{\frac{\lambda_1}{1-t}}(2/3,1/3)\,dt \qquad \text{(II.27)}$$

Equations II.22 and II.27 express the integrated concentration gradients at the generator and detector electrodes, so that division of the latter by the former gives an expression for the collection efficiency:

$$N = \frac{2/3}{\lambda_1^{2/3}}\int_o^{\lambda_3}\frac{1}{t^{1/3}}\ I_{\frac{\lambda_1}{1-t}}(2/3,1/3)\,dt \qquad \text{(II.28)}$$

This integral is evaluated in Appendix 3, and equation II.28 becomes

$$N = \frac{\lambda_3^{2/3}}{\lambda_1^{2/3}} \mathrm{I}_{\frac{\lambda_1}{\lambda_1+\lambda_2}}(2/3,1/3) - \frac{1}{\lambda_1^{2/3}} \mathrm{I}_{\frac{\lambda_1\lambda_3}{(\lambda_1+\lambda_2)(\lambda_2+\lambda_3)}}(2/3,1/3) + \mathrm{I}_{\frac{\lambda_3}{\lambda_2+\lambda_3}}(2/3,1/3) \qquad \text{(II.29)}$$

It can be shown (see appendix 4) that the functions of the form I_x (a,b) can be related to functions of the form of F(x) (see equation I.26) which arose in the derivation of the RRDE collection efficiency:

$$\mathrm{I}_x(1/3,2/3) = F(x/1-x)$$

Therefore at this point the paths taken by the new approach and by the triple Laplace transform approach meet, and the collection efficiency is given by

$$N = \frac{\lambda_3^{2/3}}{\lambda_1^{2/3}} [1 - F(\lambda_2/\lambda_1)] + 1 - F(\lambda_2/\lambda_3) - \frac{1}{\lambda_1^{2/3}} [1 - F(\lambda_2/\lambda_1\lambda_3)] \qquad \text{(II.30)}$$

In this expression $\lambda_n = 1_n/1$; Braun's expression (equation II.1) uses ϑ ($= 1_2/1_1$) and λ ($= 1_3/1_1$) but it can be seen to be equivalent to equation II.30 (remembering that $1 + \vartheta + \lambda = 1/1_1$). This then is the final expression for the collection efficiency of a tubular double electrode, for the particular case of a reversible reaction at the generator electrode; as with the RRDE, the TDE collection efficiency is purely a function of the geometry of the electrode.

2. THE TUBULAR DOUBLE ELECTRODE - TITRATION CURVES

The diffusion layer titration technique has been described in section I.2.d for the case of the rotating ring disc electrode. This technique can also be used with the tubular double electrode, and the qualitative remarks made in section I.2.d. apply to both electrode systems. To describe a TDE titration curve it is necessary to describe the concentration profiles of both B (the electrogenerated titrant) and A (the

added substrate), and the transport equations for these species are

$$v_o[\,1 - (r/r_o)^2]\,\frac{\partial b}{\partial x} = D_B\left(\frac{\partial^2 b}{\partial r^2} + \frac{1}{r}\frac{\partial b}{\partial r}\right) - k_2 ba \qquad \text{(II.31)}$$

$$v_o[\,1 - (r/r_o)^2]\,\frac{\partial a}{\partial x} = D_A\left(\frac{\partial^2 a}{\partial r^2} + \frac{1}{r}\frac{\partial a}{\partial r}\right) - k_2 ba \qquad \text{(II.32)}$$

The difference between these equations and equation II.3 is the term $-k_2 ba$ describing the very fast irreversible reaction between A and B. If it is assumed that $D_B = D_A$ then subtraction of the two equations removes the non linear term, so that

$$v_o\,[\,1 - (r/r_o)^2\,]\,\frac{\partial u}{\partial x} = D\left(\frac{\partial^2 u}{\partial r^2} + \frac{1}{r}\frac{\partial u}{\partial r}\right) \qquad \text{(II.33)}$$

where

$$u = \frac{b - a + a_\infty}{b_o + a_\infty} \qquad \text{(II.34)}$$

Equation II.33 can be reduced to the form of equation II.11, by the substitutions and approximations described in section 1 of this chapter,

$$\rho\,\frac{\partial u_n}{\partial \chi_n} = \frac{\partial^2 u_n}{\partial \rho^2} \qquad \text{(II.35)}$$

and once again the function u is split into different contributions at different regions of the tube.

The form of u is such that

$$u \to 0 \quad \text{as} \quad \rho \to \infty$$

since in the bulk of solution $b = 0$ and $a = a_\infty$. At the generator electrode surface a uniform concentration boundary condition is assumed ($u_1 = 1$) and in the region of the gap $\partial u/\partial \rho = 0$, which are the same boundary conditions as encountered in the collection efficiency case (equations II.15 and II.16). The boundary condition at the detector electrode differs because it is necessary to describe the passage of the reaction boundary along the detector. The position of this boundary is described by a value of $\chi = \chi_J$. In the B-dominated region

$$\chi < \chi_J \quad \text{and} \quad u_o = a_\infty / (b_o + a_\infty) \qquad \text{(II.36)}$$

since in this region a = 0, and b = 0 at the electrode surface. In the A dominated region

$$\chi > \chi_J \quad \text{and} \quad \partial u/\partial \rho = 0 \qquad \text{(II.37)}$$

since b = 0 in this region and it is assumed that A is not electroactive.

The shape of the titration curve is described by values of i_{gen} and i_{det}; it is convenient to calculate a value of a normalised generator current, i_{gen}/M (where M is the limiting flux of A to the generator), and a corresponding value of N' ($= i'_{det}/ i'_{gen}$). This value of N' is (by analogy with equation II.19):

$$N' = \frac{\int_o^{\lambda_3} (\partial u_3/\partial \rho)_o d\chi_3}{\int_o^{\lambda_1} (\partial u_1/\partial \rho)_o d\chi_1} \qquad \text{(II.38)}$$

where the integration limits in the numerator are from the upstream edge of the detector electrode to the reaction boundary. The normalised generator current is given by

$$\frac{i_{gen}}{M} = \frac{b_o + a_\infty}{a_\infty} \qquad \text{(II.39)}$$

M has been defined in section I.2.d, and is equal to the diffusion limited current of A (if A were electractive). When $i_{gen} = M$ then $b_o = 0$, but only just since a slight increase in i_{gen} will enable B to exist in solution and $b_o > 0$.

The denominator in equation II.38 has already been determined (equation II.22): u is identical in this case and in the collection case, except in the region of the detector electrode. The boundary condition in this region for collection is given by equation II.17

$$u_3 = -(u_1 + u_2)$$

whereas for titration

$$u_3 = -(u_1 + u_2) + u_o$$

where u_o is given in equation II.36

$$u_o = \frac{a_\infty}{b_o + a_\infty} = \frac{M}{i_{gen}}$$

Therefore, from equation II.26b

$$\bar{u}_3 = -\bar{\bar{I}}_{\frac{\lambda_1}{\lambda_1+\lambda_2+\chi_3}}(2/3,1/3)\ \frac{Ai\ (s_3^{1/3}\rho)}{Ai(o)} + \frac{u_o}{s_3}\ \frac{Ai\ (s_3^{1/3}\rho)}{Ai\ (o)} \qquad (II.40)$$

$$\text{and } \left(\frac{\partial \bar{u}_3}{\partial \rho}\right)_o = -s_3^{1/3}\ \bar{\bar{I}}_{\frac{\lambda_1}{\lambda_1+\lambda_2+\chi_3}}(2/3,1/3)\ \frac{Ai'(o)}{Ai\ (o)} + \frac{u_o}{s_3^{2/3}}\ \frac{Ai'\ (o)}{Ai\ (o)} \qquad (II.41)$$

At the reaction boundary both boundary conditions II.36 and II.37 are satisfied, and $(\partial \bar{u}_3/\partial \rho)_o = 0$ when

$$\mathcal{L}^{-1}\frac{u_o}{s_3^{2/3}} = \mathcal{L}^{-1}\bar{\bar{I}}_{\frac{\lambda_1}{\lambda_1+\lambda_2+\chi_3}} s_3^{1/3} \qquad (II.42)$$

Therefore this equation fixes χ_J the position of the reaction boundary.

If χ_J is greater than χ_3, corresponding to the reaction boundary being past the downstream edge of the detector, then

$$\int_o^{\chi_3}\left(\frac{\partial u_3}{\partial \rho}\right)_o = \text{Braun terms} + \mathcal{L}^{-1}\frac{u_o}{s_3^{5/3}}\ \frac{Ai'\ (o)}{Ai\ (o)} \qquad (II.43)$$

where "Braun terms" refer to the right hand side of the equation II.27; the second term in equation II.43 has been integrated in Laplace space (division by s_3). Division of equation II.43 by equation II.22 gives N' (see equation II.38)

$$N' = N_o - \frac{Ai'\ (o)\ u_o\ \lambda_3^{2/3} / Ai\ (o)\ \Gamma\ (5/3)}{Ai'\ (o)\ \lambda_1^{2/3} / Ai\ (o)\ \Gamma\ (5/3)} \qquad (II.44a)$$

so that, since $u_o = M/i_{gen}$

$$i_{det} = N_o i_{gen} - \left(\frac{\lambda_3}{\lambda_1}\right)^{2/3} M \qquad (II.44b)$$

This equation describes the linear portion of the titration curve, encountered when the detector electrode lies entirely in the B-dominated region; the equation is of the same form as equation I.30 which describes

the RRDE curve.

When $\chi_J < \chi_3$ then the integral of equation II.41 may be written

$$\int_0^{\chi_J} \left(\frac{\partial \bar{u}_3}{\partial \rho}\right)_o d\chi = \int_{\chi_3=\lambda_J}^{-1} -\frac{Ai'(o)}{Ai(o)} \left[\frac{1}{s_3^{2/3}} \bar{I}_{\frac{\lambda_1}{\lambda_1+\lambda_2+\chi_3}}^{(2/3,1/3)} - \frac{u_o}{s_3^{5/3}}\right] \qquad (II.45)$$

where once again the integration has been performed in Laplace space. The first term in equation II.45 may be inverted using the convolution theorem

$$\int_3^{-1} \frac{1}{s_3^{2/3}} \bar{I}_{\frac{\lambda_1}{\lambda_1+\lambda_2+\chi_3}}^{(2/3,1/3)} = \frac{1}{\Gamma(2/3)} \int_0^{\lambda_J} t^{-1/3} I_{\frac{\lambda_1}{\lambda_1+\lambda_2+\lambda_J-t}}^{(2/3,1/3)} dt \qquad (II.46)$$

and this integral has the same form as that encountered for the collection efficiency (equation II.28) where $\lambda_J = \lambda_3$ and $\lambda_1 + \lambda_2 + \lambda_3 = 1$. The result for N_o from appendix 3 may be used (replacing λ_n by $\lambda_n/[\lambda_1 + \lambda_2 + \lambda_J]$) to write an expression for N', where N' is the quotient of the detector flux (equation II.45) and the generator flux (equation II.22)

$$N' = \frac{\lambda_J^{2/3}}{\lambda_1^{2/3}} I_{\frac{\lambda_1}{\lambda_1+\lambda_2}}^{(2/3,1/3)} - \frac{(\lambda_1+\lambda_2+\lambda_J)^{2/3}}{\lambda_1^{2/3}} \chi I_{\frac{\lambda_1\lambda_J}{(\lambda_1+\lambda_2)(\lambda_2+\lambda_J)}}^{(2/3,1/3)}$$

$$+ I_{\frac{\lambda_J}{\lambda_2+\lambda_J}}^{(2/3,1/3)} - \frac{u_o \lambda_J^{2/3}}{\lambda_1^{2/3}}$$

$$= \frac{\lambda_J^{2/3}}{\lambda_1^{2/3}} \left[G\left(\frac{\lambda_1}{\lambda_2}\right) - \frac{M}{i_{gen}}\right] + G\left(\frac{\lambda_J}{\lambda_2}\right) - \frac{(\lambda_1+\lambda_2+\lambda_J)^{2/3}}{\lambda_1^{2/3}} G\left(\frac{\lambda_1\lambda_J}{\lambda_2(\lambda_1+\lambda_2+\lambda_J)}\right) \qquad (II.47)$$

The expression for N' therefore requires the evaluation of u_o (= M/i_{gen}). Returning to equation II.42

$$\frac{M}{i_{gen}} \frac{\lambda_J^{-1/3}}{\Gamma(2/3)} = \int^{-1} s_3^{1/3} \bar{I}_{\frac{\lambda_1}{\lambda_1+\lambda_2+\chi_3}}^{(2/3,1/3)} \qquad (II.48)$$

but (from equations II.45 and II.22)

$$N' = \frac{\Gamma(5/3)}{\lambda_1^{2/3}} \left[\int_{\chi_J=\lambda_J}^{-1} \frac{1}{s_3^{2/3}} \bar{I}_{\frac{\lambda_1}{\lambda_1+\lambda_2+\chi_3}}^{(2/3,1/3)}\right] - \frac{M}{i_{gen}} \frac{\lambda_J^{2/3}}{\lambda_1^{2/3}} \qquad (II.49)$$

Therefore the inverse transform in equation II.48 may be expressed as

$$\mathcal{L}^{-1}\left\{s_3^{1/3}\,\bar{I}^{(2/3,1/3)}_{\frac{\lambda_1}{\lambda_1+\lambda_2+\chi_3}}\right\} = \frac{\partial}{\partial\lambda_J}\mathcal{L}^{-1}\left\{\frac{1}{s_3^{2/3}}\,\bar{I}^{(2/3,1/3)}_{\frac{\lambda_1}{\lambda_1+\lambda_2+\chi_3}}\right\}$$

$$= \frac{\partial}{\partial\lambda_J}\frac{\lambda_1^{2/3}}{\Gamma(5/3)}\left[N' - \frac{M}{i_{gen}}\,\frac{\lambda_J^{2/3}}{\lambda_1^{2/3}}\right]$$

and using the expression for N' from equation II.47

$$\mathcal{L}^{-1}\left\{s_3^{1/3}\,\bar{I}^{(2/3,1/3)}_{\frac{\lambda_1}{\lambda_1+\lambda_2+\chi_3}}\right\} = \frac{\lambda_1^{2/3}}{\Gamma(2/3)}\,\frac{3}{2}\,\frac{\partial}{\partial\lambda_J}\left[\frac{\lambda_J^{2/3}}{\lambda_1^{2/3}}G\left(\frac{\lambda_1}{\lambda_2}\right) + G\left(\frac{\lambda_J}{\lambda_2}\right) - \frac{(\lambda_1+\lambda_2+\lambda_J)^{2/3}}{\lambda_1^{2/3}}\,G\left(\frac{\lambda_1\lambda_J}{\lambda_2(\lambda_1+\lambda_2+\lambda_J)}\right)\right] \qquad \text{(II.50)}$$

This equation may be differentiated (appendix 7) to give

$$\frac{M}{i_{gen}} = G\left(\frac{\lambda_1}{\lambda_2}\right) - \frac{\lambda_J^{1/3}}{(\lambda_1+\lambda_2+\lambda_J)^{1/3}}\,G\left(\frac{\lambda_1\lambda_J}{\lambda_2(\lambda_1+\lambda_2+\lambda_J)}\right) \qquad \text{(II.51)}$$

which describes the reciprocal of the normalised generator current as a function of χ_J. This may be substituted into equation II.47 to produce an expression for N'

$$N' = G\left(\frac{\lambda_J}{\lambda_2}\right) - G\left(\frac{\lambda_1\lambda_J}{\lambda_2(\lambda_1+\lambda_2+\lambda_J)}\right)\left[\frac{(\lambda_1+\lambda_2+\lambda_J)^{2/3}}{\lambda_1^{2/3}} - \frac{\lambda_J}{\lambda_1^{2/3}(\lambda_1+\lambda_2+\lambda_J)^{1/3}}\right]$$

$$N' = G\left(\frac{\lambda_1}{\lambda_2}\right) - \frac{\lambda_1+\lambda_2}{\lambda_1^{2/3}(\lambda_1+\lambda_2+\lambda_J)^{1/3}}\,G\left(\frac{\lambda_1\lambda_J}{\lambda_2(\lambda_1+\lambda_2+\lambda_J)}\right) \qquad \text{(II.52)}$$

The non-linear region of the titrationcurve at a TDE is therefore described by equations II.51 and II.52. The detector current begins to rise when the reaction boundary reaches the inside edge of the detector ($\lambda_J = 0$):

$$M/i_{gen} = G(\lambda_1/\lambda_2) \qquad \text{(II.53)}$$

The linear region of the curve (described by equation II.44b) begins when the reaction boundary reaches the outside edge of the detector electrode ($\lambda_J = \lambda_3$, $\lambda_1 + \lambda_2 + \lambda_3 = 1$):

$$M/i_{gen} = G(\lambda_1/\lambda_2) - \lambda_3^{1/3} G(\lambda_1\lambda_3/\lambda_2) \qquad (II.54)$$

3. THE ROTATING RING DISC ELECTRODE - EXTENSION OF THE TITRATION CURVE THEORY

The titration curve theory for the RRDE (section I.2.d) and TDE (section II.2) has assumed that the diffusion coefficients of substrate (A) and titrant (B) are equal. This section extends the theory for cases where this assumption is not valid. The RRDE is considered here, since its theoretical treatment is simpler than that of the TDE; however it is necessary to assume that the RRDE is of thin gap - thin ring configuration.

The steady state transport equation for the titrant is (68)

$$D_B\frac{\partial^2 b}{\partial z^2} - v_r\frac{\partial b}{\partial r} - v_z\frac{\partial b}{\partial z} = 0 \qquad (II.57)$$

which omits the radial diffusion term since this is negligible compared to radial convection. The third term in equation II.57 describes normal convection and may be omitted for a thin gap - thin ring (tgtr) electrode, so that equation II.57 becomes

$$D_B\frac{\partial^2 b}{\partial z^2} - Czr\frac{\partial b}{\partial r} = 0 \qquad (II.58)$$

where the convective constant $C = 0.510\omega^{3/2}\nu^{-1/2}$

The equation may be normalised with

$$\chi = z\,(C/D_B)^{1/3} \qquad (II.59)$$

and the function b is again split into three parts (figure II.3)

$$b = b_1 + b_2 + b_3$$

The function b_1 may be obtained from the rotating disc electrode solution, and is zero outside the diffusion layer; both b_2 and b_3 tend to zero inside the reaction zone and the boundary conditions at the electrode surface are

	b_1	b_2	b_3
Disc	b_1^o, $\left(\frac{\partial b_1}{\partial \chi}\right)_o$	–	–
Gap	"	$\left(\frac{\partial b_2}{\partial \chi}\right)_o = -\left(\frac{\partial b_1}{\partial \chi}\right)_o$	–
Ring	"	"	$b_3^o = -b_1^o - b_2^o$ (II.60)

The boundary condition for b_2 in the zone of the gap states that $(\partial b/\partial \chi)_o = 0$, i.e. b is not electroactive at the gap surface. At the ring electrode surface b = 0 and the ring flux is given by $(\partial b_3/\partial \chi)_o$.

The above boundary conditions are for the case when the substrate concentration, a, is zero, and evaluation of the ring flux leads to the collection efficiency. Figure II.4 presents schematic concentration profiles in the disc zone for the titration of A by B; this diagram is drawn for the case where $D_A < D_B$. The disc surface concentration, b_1^o, during titration is lower than that in the absence of titration, b_I^o and may be expressed as (figure II.4)

$$b_1^o = b_I^o - b_{II}^o \qquad \text{(II.61)}$$

The surface concentration may also be related to the surface concentration gradient through the RDE result

$$b_I^o = -A_1 (\partial b_1/\partial \chi)_o \qquad \text{(II.62)}$$

This concentration gradient is constant at constant disc current, and it can be seen (figure II.4) that the gradient of b_{II} is zero.

The splitting of b_1 into two parts enables the boundary conditions II.60 to be rewritten for titration.

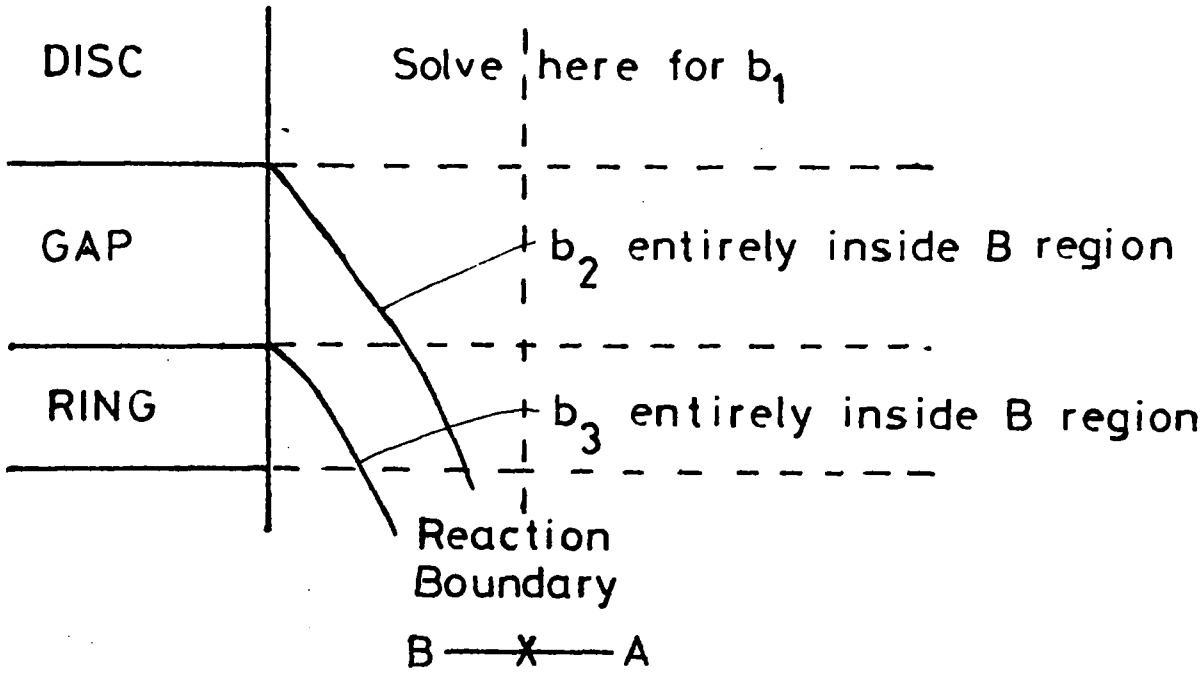

Figure II.3 The function b at the RRDE

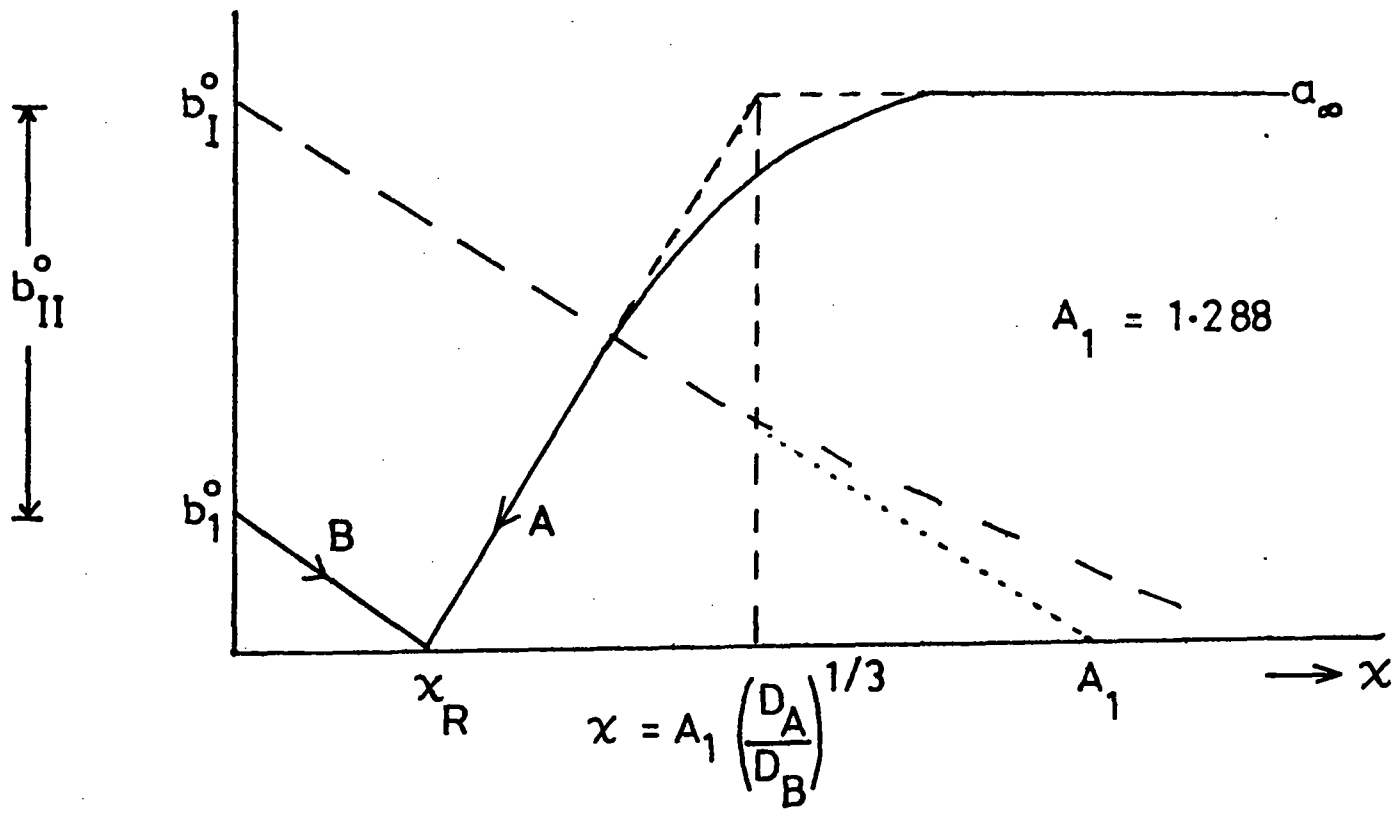

$$-D_B(\partial b/\partial \chi) = D_A(\partial a/\partial \chi)\ ; \quad b_I^\circ = -A_1(\partial b/\partial \chi)$$

Figure II.4 Disc zone concentration profiles

Disc $\quad b_I^o,\ (\partial b_I/\partial \chi)_o$

Gap $\quad (\partial b_2/\partial \chi)_o = - (\partial b_I/\partial \chi)_o$

Ring $\quad b_3^o = - b_I^o - b_2^o + b_{II}^o$

$$b_4^o = + b_{II}^o \qquad \text{(II.63)}$$

The ring flux is now given by

$$(\partial b_3/\partial \chi)_o + (\partial b_4/\partial \chi)_o; \qquad \text{(II.64)}$$

the first term is the same as that encountered in the collection efficiency case, while the second term gives a limiting ring current

$$i_R = Ni_D - i_{R,L} \qquad \text{(II.65)}$$

To obtain the second term in equation II.65 it is necessary to find b_{II}^o. This is evaluated below, but first some useful relations are developed. At the reaction boundary the flux of A is equal to the flux of B (figure II.4)

$$D_A \frac{\partial a}{\partial \chi} = \frac{D_A a_\infty}{A_1 \left(\frac{D_A}{D_B}\right)^{1/3} - \chi_R} = -\frac{D_B b_1^o}{\chi_R} = - D_B \left(\frac{\partial b}{\partial \chi}\right)_o \qquad \text{(II.66)}$$

The limiting flux of A to the disc electrode surface is usually termed M (section I.2.d). If M is normalised with respect to D_B then

$$M' = \left(\frac{D_A}{D_B}\right)^{2/3} \frac{a_\infty}{A_1} = \frac{M}{D_B}\ ; \qquad \text{(II.67)}$$

this is the flux when the reaction boundary is at the electrode surface ($\chi_R = 0$), and is of course equal to the flux of B, so that

$$f = - (\partial b/\partial \chi)_o/M' = 1 \qquad \text{(II.68)}$$

Generally (from equations II.66,67)

$$f = \frac{1}{1 - \frac{\chi_R}{A_1}\left(\frac{D_B}{D_A}\right)^{1/3}} \qquad \text{(II.69)}$$

and f increases to ∞ as χ_R approaches the outside edge of A's diffusion layer. Equation II.69 may be rearranged to

$$\frac{\chi_R}{A_1}\left(\frac{D_B}{D_A}\right)^{1/3} = 1 - \frac{1}{f} \qquad \text{(II.70)}$$

The function b_{II} at the electrode surface is given by (equation II.61)

$$b_{II}^{o} = b_{I}^{o} - b_{1}^{o} \qquad \text{(II.71)}$$

This can be expressed as (figure II.4)

$$b_{II}^{o} = -\left(\frac{\partial b}{\partial \chi}\right)_o [A_1 - \chi_R]$$

and using equation II.70

$$b_{II}^{o} = -\left(\frac{\partial b}{\partial \chi}\right)_o A_1 \left[1 - \left(\frac{D_A}{D_B}\right)^{1/3}\left\{1 - \frac{1}{f}\right\}\right]$$

If this expression for b_{II}^{o} is multiplied by f/f, then it can be further rearranged using equations II.67 and II.68 to give

$$b_{II}^{o} = \left(\frac{D_A}{D_B}\right)^{2/3} a_\infty \left[f\left\{1 - \left(\frac{D_A}{D_B}\right)^{1/3}\right\} + \left(\frac{D_A}{D_B}\right)^{1/3}\right] \qquad \text{(II.72)}$$

When $D_A = D_B$ then equation II.72 reduces to

$$b_{II}^{o} = a_\infty \qquad \text{(II.73)}$$

Returning to $D_A \neq D_B$ and equation II.72, the function f may be written

$$f = 1 + F' \qquad \text{(II.74)}$$

and the diffusion coefficient ratio may be written

$$(D_A/D_B)^{1/3} = 1 - D' \qquad \text{(II.75)}$$

Substituting these expressions into equation II.72 gives

$$b_{II}^{o} = \left(\frac{D_A}{D_B}\right)^{2/3} a_\infty \left[(1 + F')\, D' + 1 - D'\right]$$

$$= (1 + F'D')\left(\frac{D_A}{D_B}\right)^{2/3} a_\infty \qquad \text{(II.76)}$$

For a tgtr electrode then the linear portion of the titration curve will be encountered at a value of f which is not much greater than 1; f is the normalised disc current and f = 1 when the B-dominated zone is just beginning. Because of the tgtr configuration a slight increase in disc current will

result in this B-dominated zone extending past the outside edge of the ring, so that F' (equation II.74) will be small. Furthermore if D_A and D_B are similar then D' (equation II.75) and the product $F'D'$ will also be small,

$$F'D' = (f - 1)\,[1 - (D_A/D_B)^{1/3}].$$

Therefore equation II.76 may be simplified to

$$b_{II}^{o} \simeq (D_A/D_B)^{2/3}\, a_\infty \qquad \text{(II.77)}$$

Equations II.73 and II.77 therefore present two expressions for b_{II}^{o} which may be used with equation II.64 to determine the ring flux. The result for $D_A = D_B$ ($b_{II}^{o} = a_\infty$) is already known (equations I.29, I.30)

$$i_R = Ni_D - M\beta^{2/3} \qquad \text{(II.78)}$$

$$M = 0.62nFA\omega^{1/2}\nu^{-1/6} D^{2/3} a_\infty$$

When $D_A < D_B$ ($b_{II}^{o} = (D_A/D_B)^{2/3} a_\infty$) then the form of M to be used in equation II.78 will be modified by the diffusion coefficient ratio:

$$M = 0.62nFA\,\omega^{1/2}\nu^{-1/6} D^{2/3} a_\infty \left(\frac{D_A}{D_B}\right)^{2/3} \qquad \text{(II.79)}$$

The diffusion coeficient D in equation II.79 is in fact D_B, since the transport equation and fluxes have been normalised with respect to D_B (equation II.59, II.67). Therefore equation II.79 simplifies to

$$M = \text{constant} \times D_A^{2/3}\, a_\infty \qquad \text{(II.80)}$$

and the ring electrode sees a limiting current due to a_∞ and D_A. If $D_A < D_B$ (the usual case) the displacement of the linear portion of the titration curve is less than if $D_A = D_B$.

III EXPERIMENTAL

This third chapter describes some of the experimental aspects of the work presented in this thesis. The rotating electrode assembly and tubular electrode assembly are described in sections 1 and 2 respectively. The supporting electronics are outlined in section 3, while section 4 presents details of the chemicals and solutions used.

1. THE ROTATING ELECTRODE ASSEMBLY

The rotating ring disc electrode is illustrated in figure I.9 (page 23); the electrodes used in this work consisted of platinum disc and ring electrodes, with a Teflon gap and surrounding mantle. The electrode was initially mechanically polished using 6μm and 3μm diamond; this was followed by hand polishing with 1μm alumina, a slurry of alumina in double distilled water being applied with cotton wool. A highly polished surface was obtained and maintained by hand polishing with 0.3μm alumina. This polishing is necessary since surface irregularities will induce turbulence at low Reynolds numbers, and will also protrude into the diffusion layer. The electrode was stored at 25^{o}C (in the thermostat tank) to prevent the 'creeping' of Teflon which accompanies temperature changes.

The electrode was inserted into bearings which were mounted in a brass block, and the brass block was supported on two steel rods, which allowed the electrode to be raised or lowered. An aluminium rotor clamped to the top of the electrode shaft, and a similar rotor clamped to the motor shaft enabled rotation of the electrode, using a rubber drive belt for transmission. The motor used was a printed armature DC motor (Printed Motors Limited, GPM 12M 4B), and its rotation speed was controlled by a servo-controller (constructed by this laboratory's electronics workshop). Since the motor used does not have a tachometer output, feedback to the servo-controller was

provided optically. A disc of 1/32" copper clad board, etched to give a spoke pattern, was clamped to the motor shaft above the drive pulley. The alternating copper and clear board sectors modulate the transmission of infra-red radiation which is emitted and detected by a slotted opto-switch (Radio Spares 306 - 061) situated above and below the copper disc. The pulse waveform produced is shaped and its frequency converted to a voltage; this voltage is compared with a reference voltage to control the rotation speed, and is also used to drive a LED display which indicates the rotation speed of the electrode. Rotation speeds of 1 - 50 Hz are obtainable with this equipment.

The electrode and electrochemical cell are shown in figure III.1. Electrical contact to the ring and disc electrodes was made with silver-carbon brushes, brush noise being reduced by regular cleaning. The cell was made of glass, with an outer jacket through which water from a thermostatted tank was passed to maintain the cell solution at a constant temperature ($25 \pm 0.1^{o}C$). The control of temperature is necessary to ensure reproducibility of viscosity, diffusion coefficients and rate constants. The cell was fitted with a Teflon lid to exclude oxygen, a central hole allowing the electrode to enter the cell. Other holes in this lid accommodate the counter electrode, the reference electrode, the nitrogen supply and enable the addition of further solution by pipette. Oxygen-free nitrogen can be bubbled through or above the solution to remove and exclude oxygen. The counter electrode consisted of a large piece of platinum gauze (1 cm^2), and the reference electrode was a saturated calomel electrode (Radiometer).

2. THE TUBULAR ELECTRODE ASSEMBLY

The tubular double electrode is illustrated in figure I.14 (page 28). The generator and detector electrodes consisted of platinum discs, whose thickness were measured using a micrometer. The two discs were then cemented together using Araldite to form a generator-gap-detector sandwich;

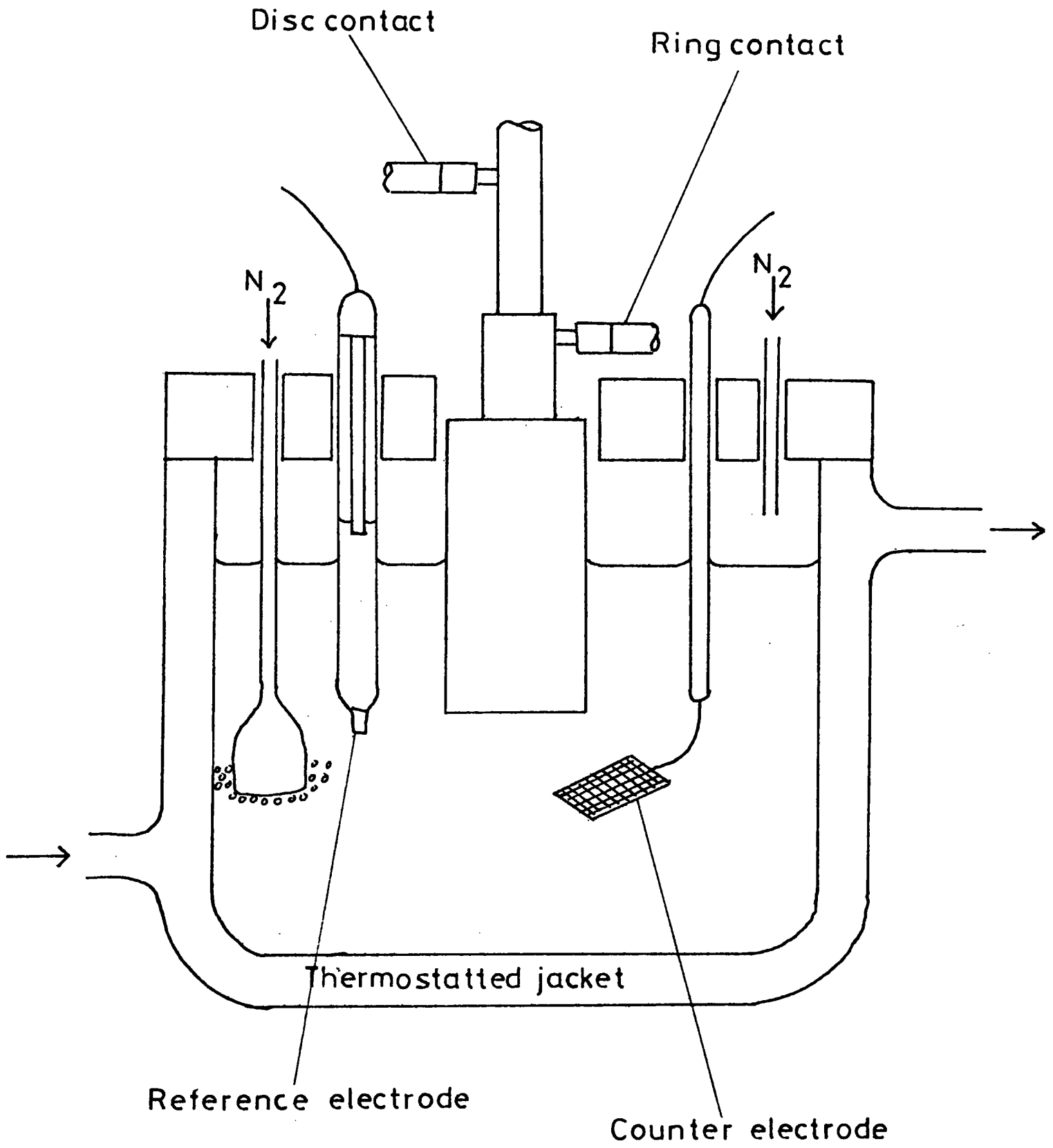

Figure III.1 The cell used with the RRDE

the thickness of this assembly was measured to obtain the gap thickness. An axial hole was then drilled through the electrode sandwich so that the latter would tightly fit a zinc wire of uniform diameter (1.06mm). Electrical contacts were silver-soldered to the electrodes, and the zinc wire was made taut. Araldite was then poured around the electrodes and zinc wire to produce a cylindrical casting. After curing of the casting Araldite the zinc wire was removed by etching with concentrated hydrochloric acid, the acid being introduced into the tubular recess through a fine capillary. This capillary was made by drawing out a dropping pipette. The electrode casting was held vertically and the upper end of the pipette was also clamped so that the capillary assumed a bow shape; this resulted in the capillary tip following the receding zinc wire and providing a continuous flow of fresh acid to the zinc surface. The zinc wire ($\sim$10cm) was thus removed in 8 hours to produce a tubular double electrode. The ends of the araldite casting were turned to conform to S13 ball joints, and 1 mm sockets were soldered to the electrical contacts and cemented to the casting. The electrodes were polished with alumina, down to 0.3μ m, using a silver steel wire and alumina slurry.

A forced flow of solution was provided by two pumping systems. When thermostatting of the solution was not important a peristaltic pump was used (Pharmacia Fine Chemicals, P3, 3 channel pump); this pump can produce flow rates of 0.6 - 400 ml hr^{-1} (1.6×10^{-4} - 0.1 ml s^{-1}). When thermostatting was desirable a motor driven syringe was used, which could produce flow rates of 5×10^{-3} - 0.1 ml s^{-1}. This latter pump consists of a 50 ml syringe (Hamilton 1050LL) which is surrounded by a thermostatting jacket; it was designed by Chadwick (80) and constructed in this laboratory's workshop. A DC servo-motor, operating at 2 - 100Hz , is coupled to the syringe through a gearbox and worm; servo-control of the motor again uses an optical feedback system. Neither of these pumps produced a pulse free flow, and the effects of this pulsation are evident in the results presented

in chapter V.

The syringe was coupled to 1/8" Teflon tubing (Altex) using a luer adapter, and this tubing coupled to an S13 glass socket using a tubing-to-glass connector (Altex). The tubing-to-glass connector was also used with the peristaltic pump to connect the pump and associated tubing (Pharmacia Fine Chemicals) with an S13 glass socket. The counter electrode was situated downstream of the TDE, while the reference electrode was used, in a sintered compartment, upstream of the TDE in order to eliminate Ohmic drop between the reference and working electrodes (figure III.2). The solutions used in the TDE experiments were not deoxygenated, since at the potentials used oxygen does not interfere.

3. SUPPORTING ELECTRONICS

The control and measurement of electrode currents and potentials was achieved using operational amplifiers. FET input operational amplifiers were used (LH0042CD, Radio Spares 305-945), and important characteristics of this particular amplifier are

Open loop gain (A_o)	100 dB
Input bias current	10 pA
Maximum output voltage	15 V
Maximum output current	2 mA

An operational amplifier has two inputs and an output (with respect to ground) as depicted in figure III.3; a is termed the non-inverting input, b the inverting input. The output voltage is proportional to the voltage difference between the inputs.

$$v_o = A_o (v_+ - v_-) \qquad \text{(III.1)}$$

and for the operational amplifier above A_o = 100dB (= 10^5). Because of this high gain only a narrow range of input voltages can be used with an open loop amplifier, and negative feedback is almost invariably used in practical circuits. Figure III.4 is a general example of the use of

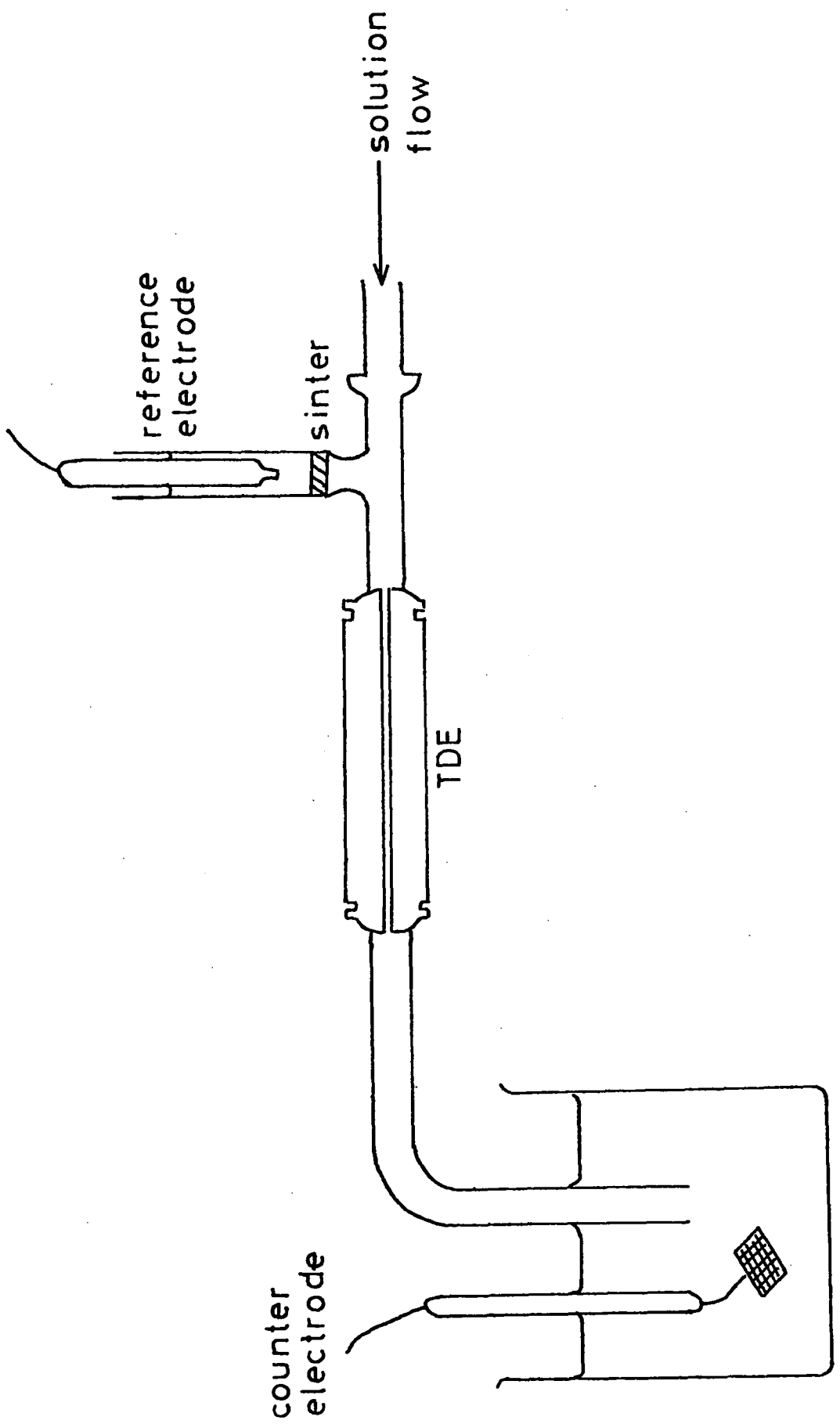

Figure III.2 Positions of electrodes in TDE experiments

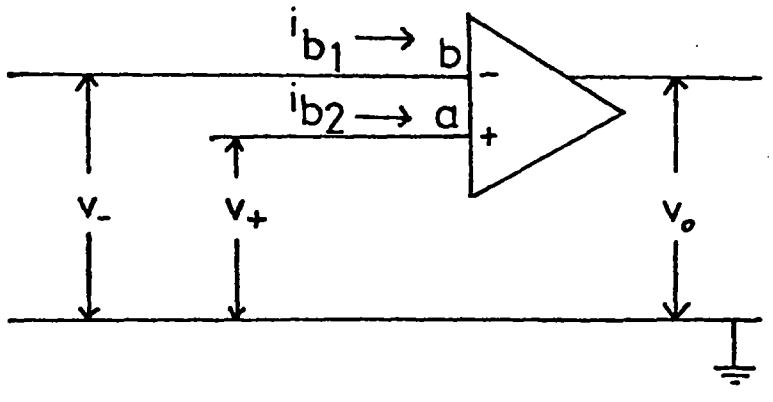

$$i_b = (i_{b_1} + i_{b_2})/2$$

Figure III.3 Schematic operational amplifier

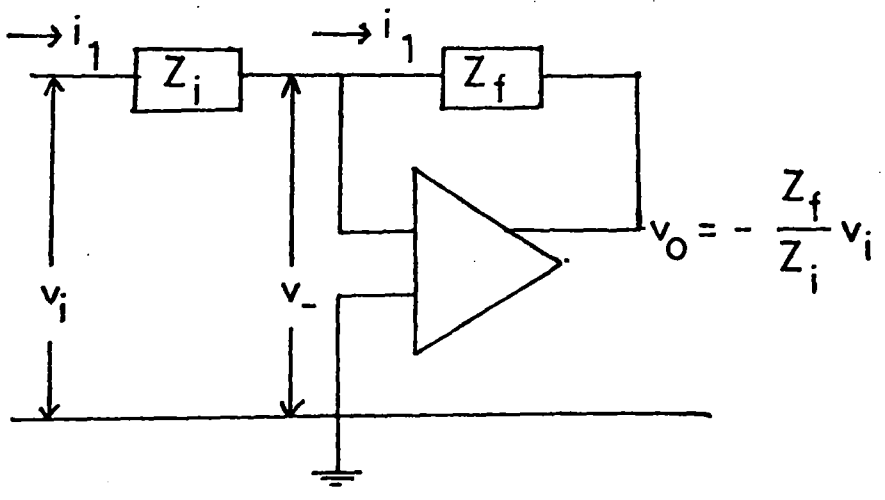

$v_- \sim 0$; $i_1 = v_i / Z_i = -v_o / Z_f$

Figure III.4 Use of negative feedback

negative feedback; the ratio of the feedback impedance (Z_f) to that of the input impedance (Z_i) determines the closed loop gain $A_{o,f}$ if $Z_f/Z_i \ll A_o$. In this circuit equation III.1 is still applicable, but the closed loop control of v_o means that $v_+ \sim v_-$ (e.g. if v_o = 1V then $v_+ - v_-$ = 10 μV). Therefore in the analysis of closed loop circuits it can be assumed that the operational amplifier inputs are at the same potential; if the non-inverting input is held at ground potential, then the inverting input is referred to as a virtual ground.

The second characteristic given above is the input bias current, i_b. This is the mean of the currents which flow into the operational amplifier inputs. For an ideal operational amplifier $i_{b1} = i_{b2} = i_b = 0$. The response of feedback circuits may be simply analysed using Ohm's and Kirchoff's Laws if ideality is assumed ($v_+ = v_-$; $i_b = 0$). Using the first assumption and Ohm's Law it is possible to determine the current flowing through the input impedance, Z_i. The second assumption and Kirchoff's Law means that this current must flow through the feedback impedance, so that the re-use of Ohm's Law will give the output voltage (figure III.4). The operational amplifiers used in this work have i_b = 10pA, so that feedback circuits will behave as predicted if currents in excess of 1nA are used.

The high input impedance of the amplifier used (10^{12} Ω) allows feedback and input impedances of up to 10^{10} Ω to be used without affecting the ideal response of a circuit. The amplifiers are powered by a dual ± 15V supply, ground potential being the midpoint of this range. This supply restricts output voltages to ± 15V, but these voltages and the maximum output current of 2mA are adequate for the applications in this thesis.

Some feedback circuits used in this work are illustrated in figure III.5; operational amplifiers are so named because of the mathematical operations which they may thus perform. The integrator may be used, with a constant input potential, to provide an output voltage which varies linearly with time (a ramp) since the capacitor is charged with a constant current. These

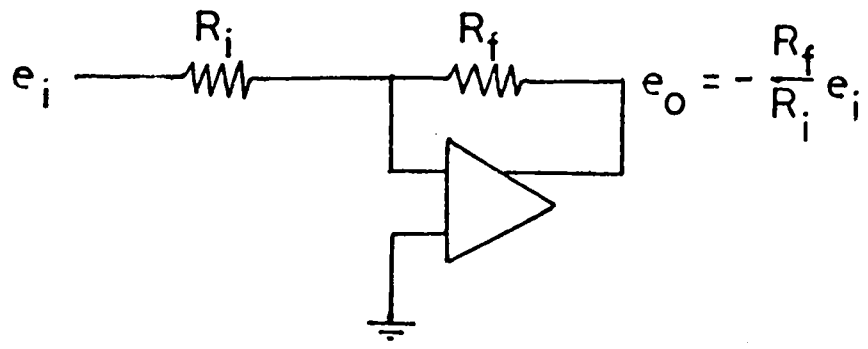

INVERTING AMPLIFIER

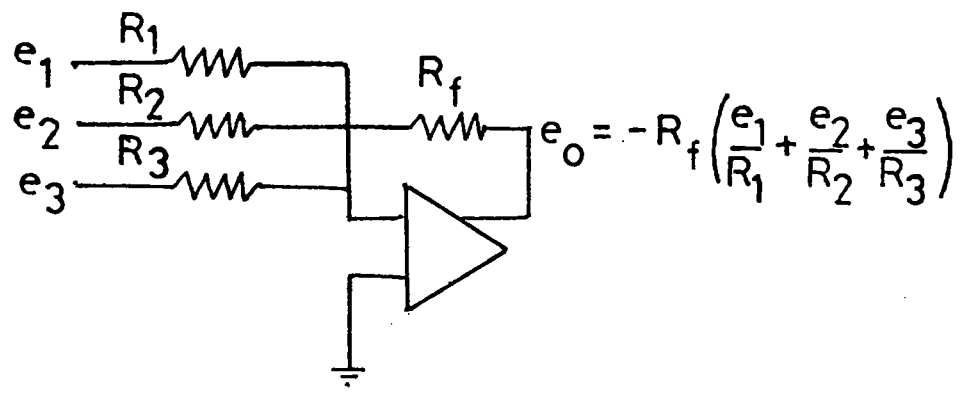

SUMMING AMPLIFIER

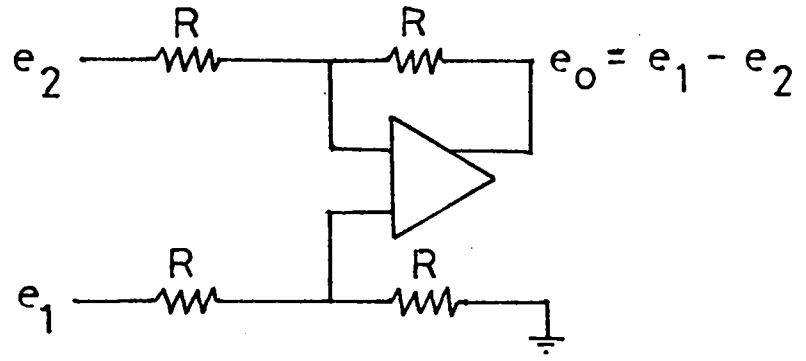

SUBTRACTOR

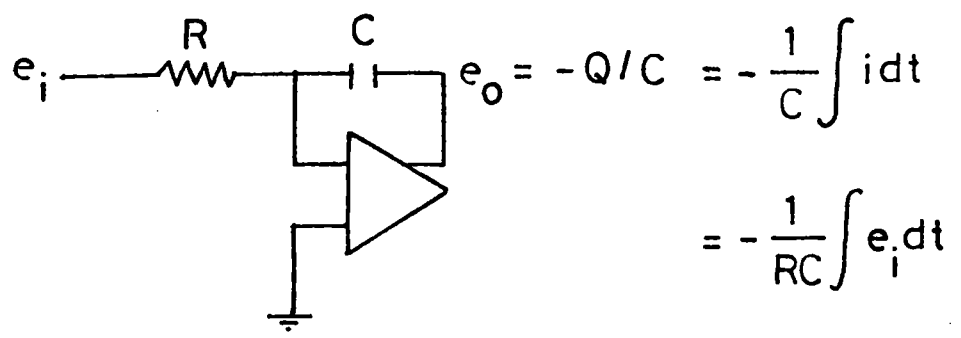

INTEGRATOR

Figure III.5 Feedback circuits

circuits may be used to control and measure electrode currents and potentials, but must first be interfaced with the electrodes (figure III.6). The voltage follower may be used to measure an electrode potential without drawing any current (only the input bias current will flow). The galvanostat enables control of the current flowing between two electrodes - the working and counter electrodes; electrode B will also be held at ground potential. The potentiostat is used to control an electrode potential, and the electrode current may be determined by measuring the potential difference across resistor R. However this latter potential will be floating (i.e. not related to ground potential). If a non-floating potential is required then the current-to-voltage converter can be used, with the potentiostat, to measure the electrode current and control the electrode potential. It is preferable to maintain the working electrode potential at ground and alter the reference electrode potential, rather than vice versa, since this produces less noisy signals.

The feedback and interfacing circuits are combined to produce experimental control circuits. The potentiostat is used when recording rotating disc electrode or tube electrode polarograms and the integrator provides a linearly varying voltage for the non-inverting input. Titration curves at the ring disc electrode and tubular double electrode require the disc (generator) current to be varied while the ring (detector) electrode is held at a constant potential and its current is measured. The circuit in figure III.7 performs this function, and the potential sources V_1 and V_2 are derived from batteries. The recording of ring polarograms requires the disc current to be held constant while the ring potential is varied. This has been achieved using the galvanostat and bridge potentiostat illustrated in figure III.8; omission of the 1nF capacitor usually results in circuit instability.

Six amplifiers were mounted in a box so that connections could be easily made to them using banana plugs and sockets; all the other components required for the above circuits were also contained in the box, and the amplifiers were zeroed regularly. Polarograms and titration curves were

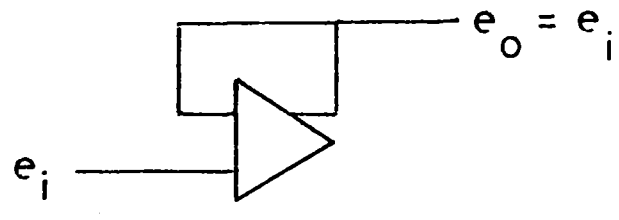

FOLLOWER

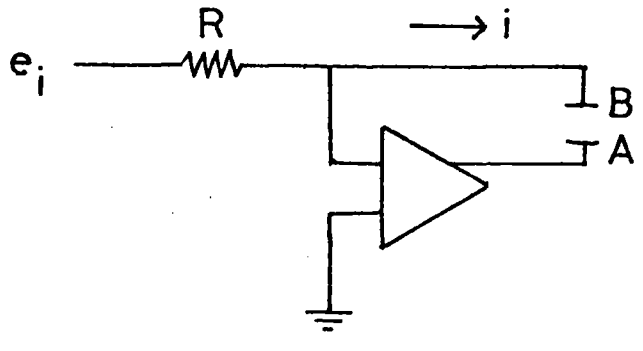

$i = e_i / R$

NB electrode B is at ground potential

GALVANOSTAT

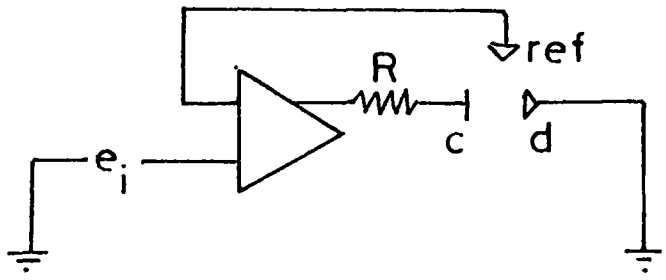

$E_d = -e_i$ (w.r.t. ref)

POTENTIOSTAT

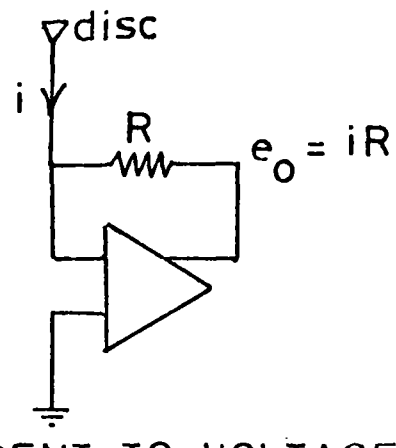

CURRENT-TO-VOLTAGE CONVERTER

Figure III.6 Interfacing circuits

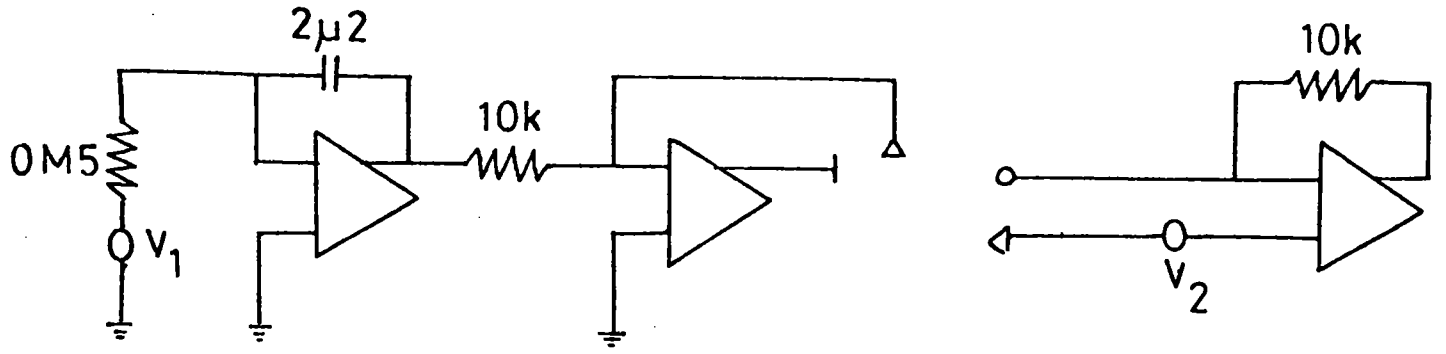

Figure III.7 Circuit for titration curves

▷— disc/generator
o— ring/detector
⊢ counter
◁— reference

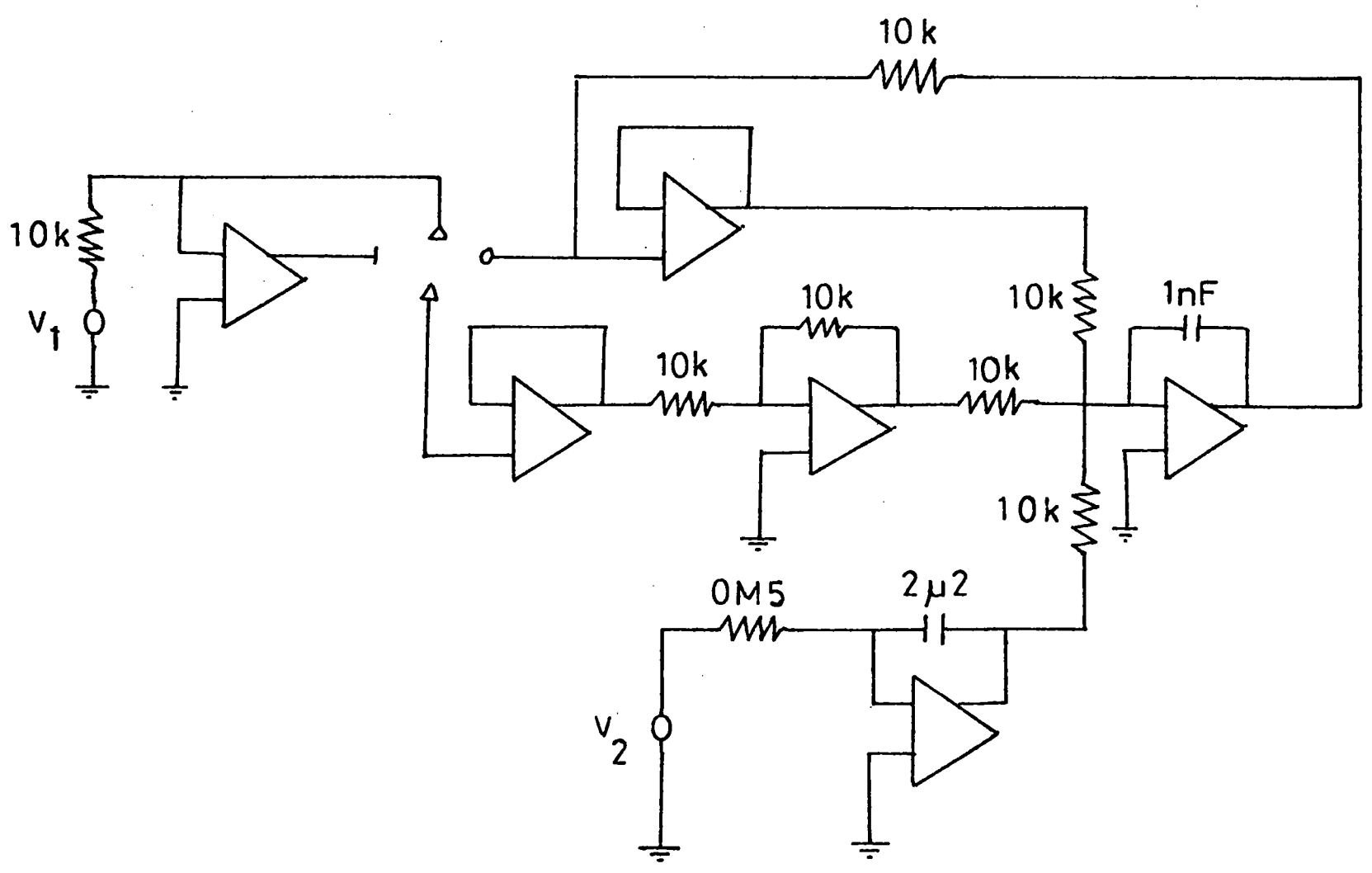

Figure III.8 Circuit for ring polarograms

plotted on a Hewlett-Packard 7035B X-Y recorder, and a Fluke 8000A digital multimeter was used to monitor currents and voltages. A Servoscribe RE 541.20 t-Y recorder was used to monitor automated titrations (chapter V). All connections from the electrodes to the operational amplifier manifold, and to the X-Y recorder were made using screened leads to reduce noise.

4. CHEMICALS

All glassware was cleaned by soaking in "Decon 90" solution. This glassware was thoroughly rinsed, and solutions were prepared, using water which had been deionized and distilled twice; this water is referred to as doubly distilled water (DDW).

Inorganic chemicals used were all of AnalaR grade: disodium tetraborate decahydrate, sodium dihydrogen orthophosphate, anhydrous disodium hydrogen orthophosphate, arsenic trioxide and potassium bromide. This last chemical contains 0.001% nitrogen compounds and since 0.5M KBr solutions are used this impurity must be removed. Two clean-up methods were used, both of which involved treatment of the stock solution of bromide and borate (pH 9.2). The first method involves addition of bromine to the stock solution, and removal of excess bromine by heating; heating for ~6 hours is necessary, and this method was used to treat large volumes (1 l) of stock solution. A second method of pretreatment may be used exclusively with the RRDE. Stock solution is added to the electrochemical cell, and hypobromite is generated at the disc electrode until the impurity concentration is reduced to a negligible level. The second technique may be completed in ~15 minutes.

AnalaR glycine was obtained from Hopkin and Williams. Other amino acids were DL - Lysine Monohydrochloride (BDH 37130), DL - methionine (BDH 37132), DL-tryptophan (BDH 37154), L - tyrosine (BDH 37156) and L - cystine (BDH 37057).

The peptide bacitracin (50,000 units g^{-1}) was obtained from ICN Pharmaceuticals Inc., Plainview, New York. The peptides tri-tyrosine, pentaglycine, tetraalanine and glycyl-leucyl-tyrosine were obtained from Sigma.

All proteins used were obtained from Sigma:

Serum Albumin - bovine (A - 6003); prepared from fraction V albumin.

Serum Albumin - human (A-9511); crystallised and lyophilised.

Haemoglobin - human type IV (H - 7379); 2 x crystallised.

Phosvitin - from egg vitellin (P - 1253).

Thyroglobulin - bovine type I (T-1001).

Cytochrome c-horse heart type III (C - 2506).

α - Amylase - bacterial type II-A (A-6380); from bacillus Subtilis,1270 units mg^{-1}.

CHAPTER IV. ROTATING RING DISC ELECTRODE TITRATIONS

The diffusion layer titration technique has been qualitatively described in section I.2.d. Chapter II presents a derivation of the theoretical TDE titration curve, for the case where $D_{titrant} = D_{substrate}$, and also presents an extension of the RRDE theory, for the case where the diffusion coefficients differ. This fourth chapter presents the results of diffusion layer titrations performed with the RRDE, electrogenerated hypobromite having been used to titrate amino acids and peptides (section 2) and also proteins (sections 3 and 4). The RRDE was used for these experiments in preference to the TDE, firstly because the control of rotation speed is better than that of flow rate, and secondly because maintenance of the electrode surface is easier. The first section of this chapter is an introduction to the practical use of the RRDE, and includes those experiments which were necessary to confirm the proper functioning of the particular electrodes used; this section also includes details of the choice of the background electrolyte which was used in subsequent experiments.

1. INTRODUCTION

In the attempt to develop an electroanalytical technique for the determination of proteins, it was decided to firstly investigate the diffusion layer titration of amino acids. These compounds are the building blocks from which proteins are constructed; it was felt that a study of them would be helpful before progressing to the more complex protein molecules, and that this study might provide a technique for the determination of amino acids themselves. An analytical method for all amino acids must involve that part of the molecule which is common to all amino acids, i.e. the - COOH

group or the $-NH_2$ group. Therefore the approach of Christian (29 - 32) and Claeys and Velghe (22 - 24) was followed: reaction of $-NH_2$ with hypobromite to give, initially, $-NBr_2$; any simultaneous bromination of side chains (26, 33 - 36) will enhance the sensitivity of the method in particular cases.

The choice of pH and background electrolyte for these experiments was based on the experience of previous workers who had investigated the bromination of ammonia and amino compounds. Kolthoff, Stricks and Morren (21), whose paper is the first reference to hypobromite amperometric titrations, used sodium bicarbonate buffer at pH 8.6 and sodium hypobromite solution to determine ammonia; later workers have used borate buffers at pH 8.5 - 8.9. Arcand and Swift (69) recommend pH 8.5; this was because their determination requires the complete bromination of ammonia:

$$2NH_3\ (aq.) + 3OBr^- \longrightarrow N_2 + 3Br^- + 3H_2O$$

At pH < 8.5 the formation of nitrogen oxides results in more hypobromite being used, while at pH > 8.5 there is loss of ammonia from solution. In this laboratory Cook (39) investigated the bromination of ammonia in borate buffers of pH 8.5 - 9.5, and performed diffusion layer titrations with the RRDE exclusively at pH 9.0 - 9.2. Since amino acids are not volatile, and the pK_a of the amino group is generally in the range 8.9 - 9.6, it was decided to use 0.025M borate buffer at pH 9.2

Those workers who generated hypobromite coulometrically, instead of using standard hypobromite solution, used a solution of 0.5M or 1M bromide, which serves as the background electrolyte and is oxidised as follows

$$Br^- + H_2O \longrightarrow OBr^- + 2H^+ + 2e^-$$

Figure IV.1 shows a voltammogram recorded at the platinum disc of a RRDE using a solution of 0.025M borate (pH 9.2) and 0.4M potassium sulphate (background electrolyte). The cathodic current observed at $E_D < -700mV$ is due to solvent decomposition (evolution of hydrogen) and that at -100mV

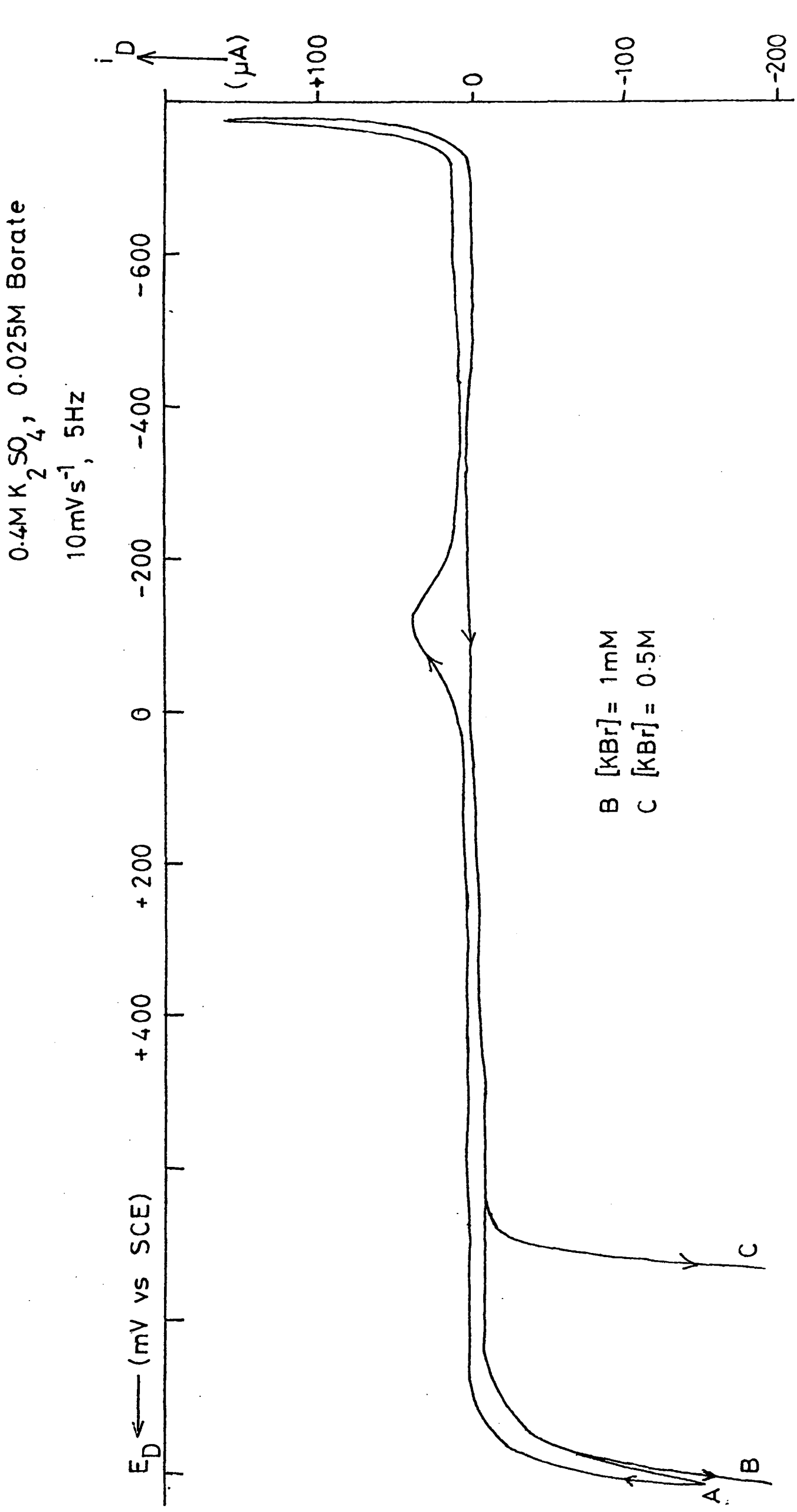

Figure IV.1 Disc polarograms at pH 9.2

is due to reduction of surface oxides (these having been formed at E_D > + 100mV). The anodic current labelled A (at E_D = +1000mV) is again solvent decomposition

$$2H_2O \longrightarrow O_2 + 4H^+ + 4e^-$$

Potassium bromide was then added to the solution so that [KBr] = 1mM, and another voltammogram recorded (figure IV.1). The only point of difference is labelled B; this extra anodic current is due to the oxidationof bromide to form hypobromite. It can be seen that the generation of hypobromite is not 100% current efficient, since it occurs at the same potential as oxygen evolution. However by increasing the bromide concentration to 0.5M (for voltammogram see figure IV.1, labelled C) the contribution of solvent decomposition to the total current is rendered negligible. An alternative method of achieving 100% efficiency of bromide oxidation, at low bromide concentration, is to shift the anodic solvent decomposition to more positive potentials. This can be achieved by lowering the pH of the solution, and was investigated at pH 8.0 (the acidic limit of borate buffers) but figure IV.2 shows that an even greater pH change is necessary to remove the interference due to oxygen evolution. It was therefore decided that the background electrolyte should be 0.025M borate (pH 9.2) plus 0.5M potassium bromide; reduction of the bromide concentration is not possible since it would reduce the efficiency of generation of hypobromite.

In order to observe experimentally the theoretical collection efficiency of a RRDE both the disc generation and ring detection of the intermediate must be 100% efficient, i.e. the intermediate must be detected as a limiting current. Hypobromite was generated at the disc electrode using a current of 200 μ A and a rotation speed of 5 Hz; the electrochemical behaviour of this hypobromite at the ring electrode was investigated by varying the potential of the ring and measuring the observed current. The lower polargram (A) in figure IV.3 shows the observed ring current when the

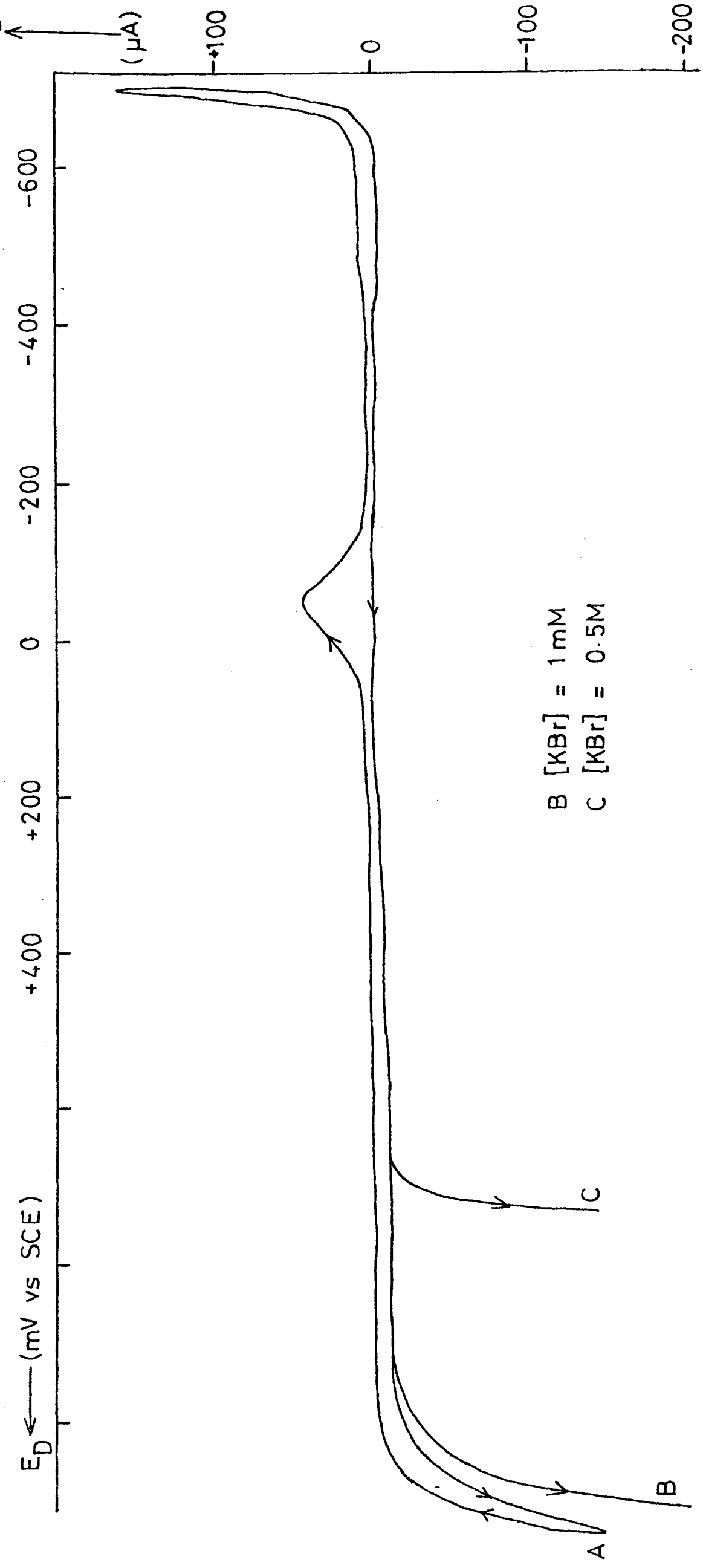

Figure IV.2 Disc polarograms at pH 8.0

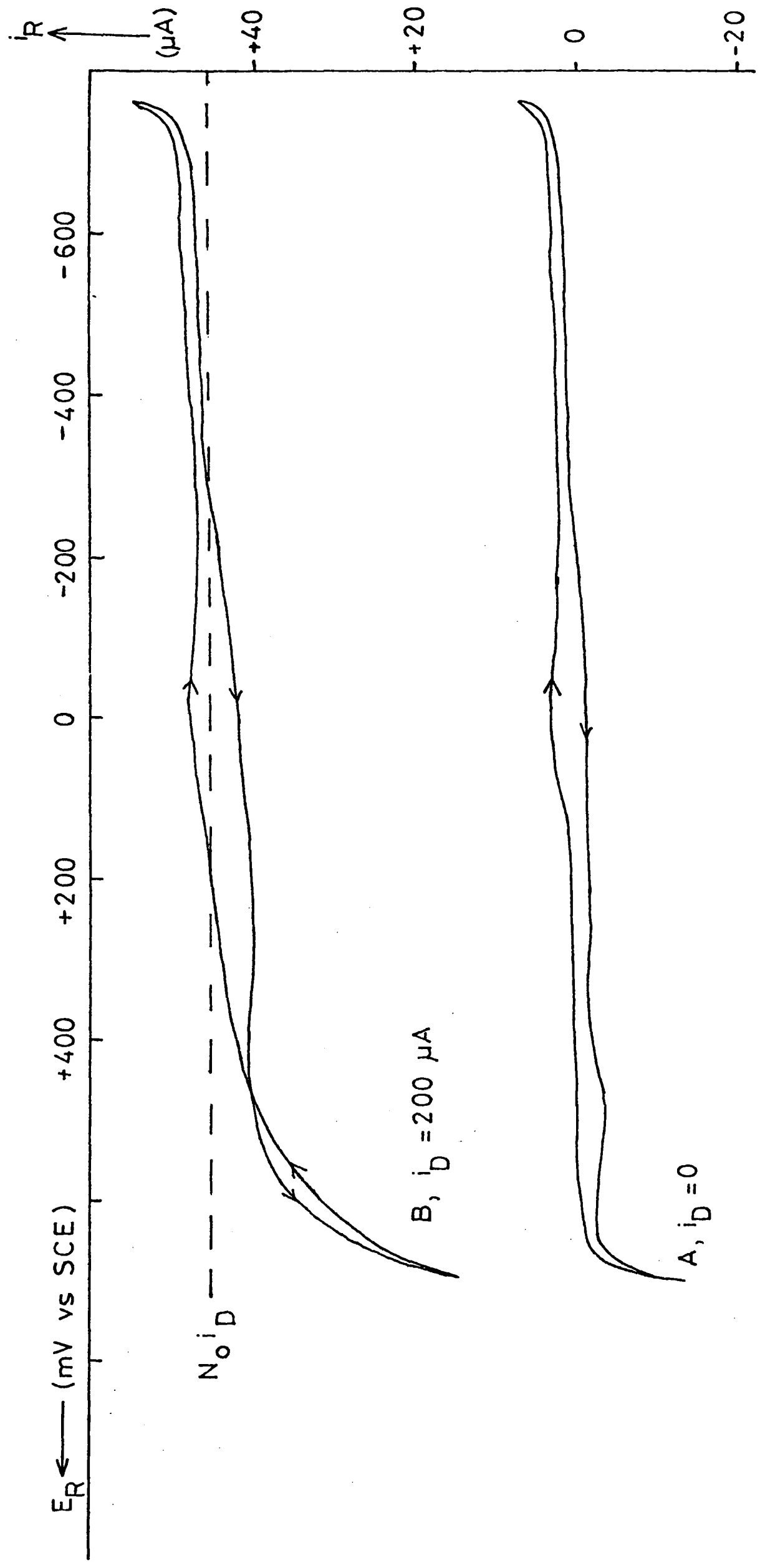

Figure IV.3 Ring polarograms with disc generation of hypobromite

disc is inactive, while the upper polargram (B) shows the collection of hypobromite (with i_D = 200 μA). The hysteresis evident in both polarograms is due to oxidation and subsequent reduction of the platinum electrode surface, an unavoidable problem with this metal. The theory of the RRDE predicts that when the generated species is collected as a limiting current at the ring then that ring current is given by

$$i_R = -N_o\, i_D \;;$$

this value of N_o is drawn on the diagram. To enable clarification of interpretation, polarogram A in figure IV.3 has been subtracted from B and the result is presented in figure IV.4; this shows that the predicted collection efficiency is observed if $E_R < +400mV$. At higher ring potentials the reduction of hypobromite is no longer diffusion controlled, and it can be seen that hysteresis due to surface oxides is still evident in the subtracted polarogram. These polarograms were recorded in a deoxygenated solution; the reduction of any oxygen present in solution is evidenced by the appearance of a wave at $E_R < -100mV$.

The radii of the RRDE used in this experiment are:

$$r_1 = 3.659 \pm 0.006 \text{ mm}$$

$$r_2 = 3.803 \pm 0.007 \text{ mm}$$

$$r_3 = 4.134 \pm 0.004 \text{ mm}$$

and theoretically $N_0 = 0.225 \pm 0.006$.

The collection efficiency was checked by the more usual method, in which the ring electrode is held at a constant potential and the ring current measured while the disc current is varied. The results, at different ring potentials, E_R, are presented in figure IV.5, and are in good agreement with the theoretical value; the collection efficiency was also found to be independent of rotation speed. However the collection efficiency measured at E_R =+450mV was observed to decrease slowly with time, falling from 0.227 to 0.204 in 60 minutes. This decrease in collection is caused by oxidation of the platinum ring electrode (figure IV.3 shows much hysteresis in this potential range); the ring electrode can be rejuvenated by holding it at

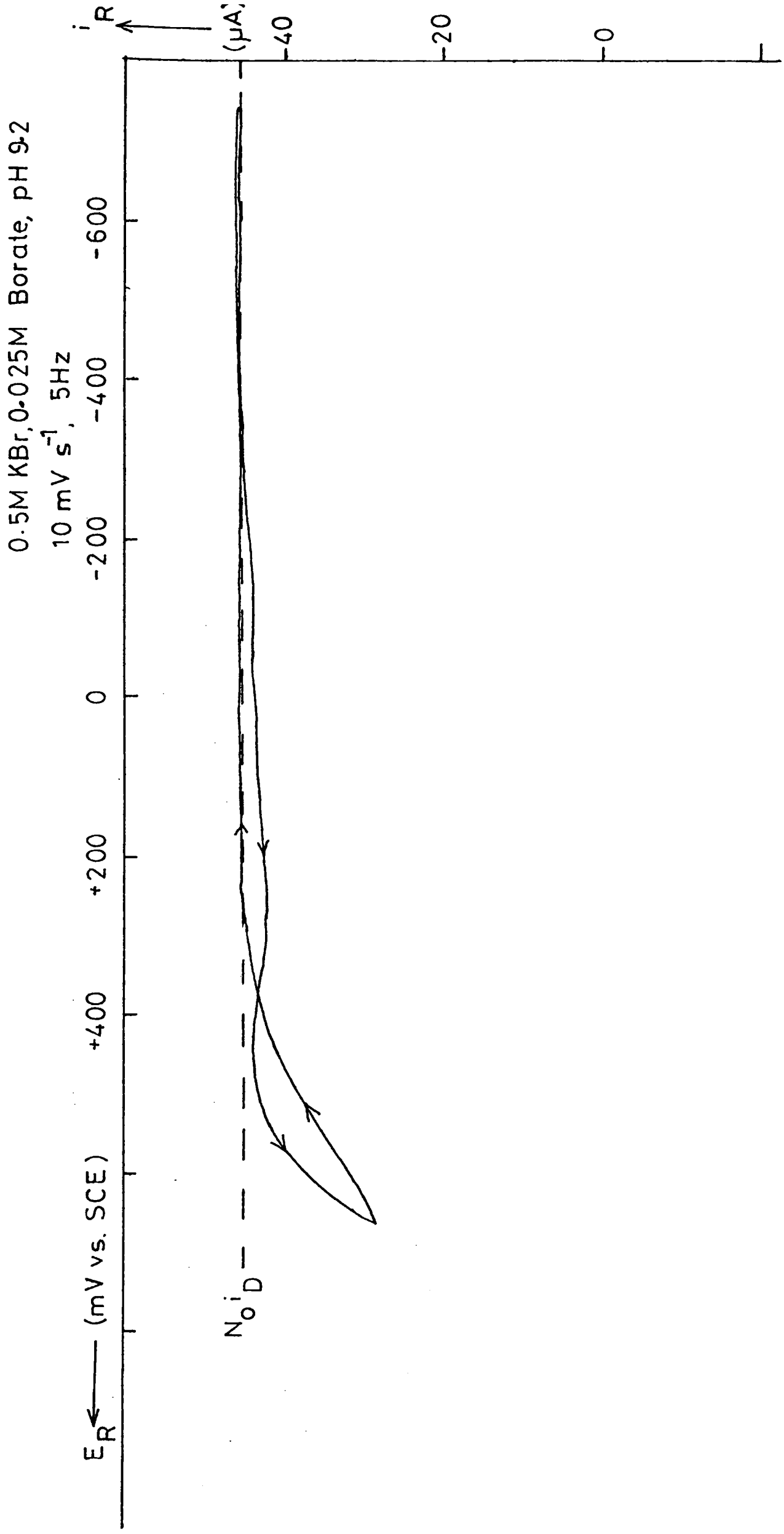

Figure IV.4 Difference between polarograms A and B in figure IV.3

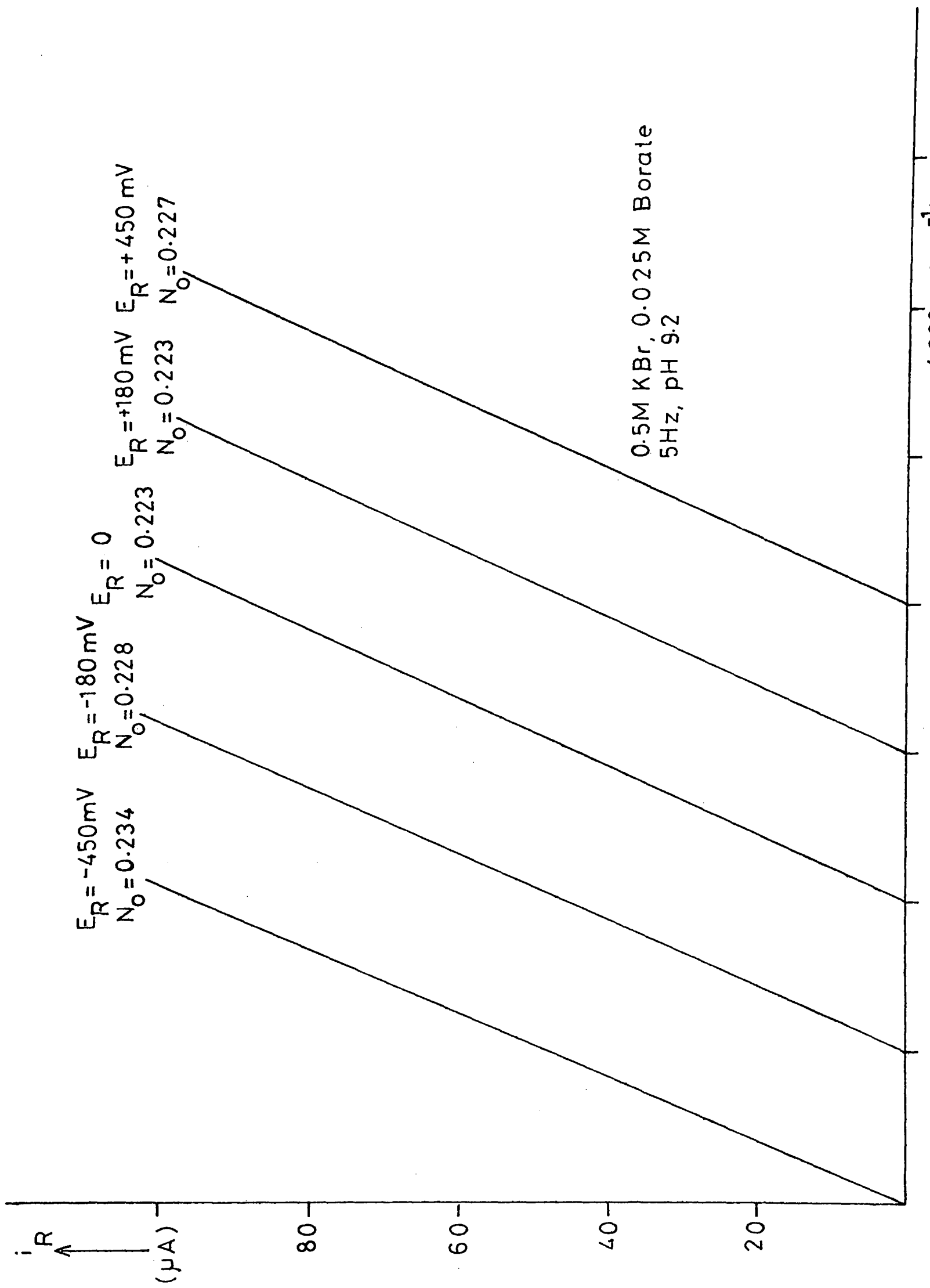

Figure IV.5 Collection efficiencies at the RRDE

- 450mV for 60 seconds (at this potential surface oxides are reduced), but this treatment is not always successful, and longer periods of cathodisation are sometimes required.

The experiments described in this section have suggested a background electrolyte solution of 0.5M KBr, 0.025M $Na_2B_4O_7$ at pH 9.2. The high bromide concentration is necessary to ensure efficient generation of hypobromite at the pH used. The pH of 9.2 has been chosen to ensure that amine groups will react with hypobromite; at a lower pH protonation of the amine groups will prevent their reaction with hypobromite, while a higher pH will decrease the efficiency of hypobromite generation.

2. THE TITRATION OF AMINO ACIDS AND PEPTIDES

This section is divided into two parts. The first part presents experiments which were performed to investigate the effect of ring electrode potential on the recorded titration curve. The second part of this section presents titration curves for several amino acids and peptides at an optimised ring electrode potential, i.e. optimised for greatest sensitivity as an analytical technique.

a. Effect of Ring Electrode Potential

The experiments described in the previous section suggested a background electrolyte solution suitable for hypobromite generation and that this hypobromite could be detected as a limiting current in the ring potential range $+ 450 > E_R > - 600$mV. However the titration curve theory, as outlined in section I.2.d, requires that the products of the titration reaction are inactive at the ring electrode.

The overall reaction of hypobromite with ammonia is

$$3OBr^- + 2NH_3 \longrightarrow N_2 + 3H_2O + 3Br^-$$

and this reaction proceeds through the intermediates NH_2Br, $NHBr_2$ and NBr_3. Johanneson (70) prepared monobromoamine and dibromoamine and found them to be electroactive, $NHBr_2$ being more easily reduced than NH_2Br. These intermediates, and their electroactivity, were also observed by Cook (39) in his RRDE studies of the bromination of ammonia at pH 9.2. Claeys and Velghe (24) reported the amperometric titration of aliphatic amines with hypobromite

$$RNH_2 + 2OBr^- \longrightarrow RNBr_2 + 2OH^-$$

and found these bromoamines also to be electroactive.

It was therefore expected that the reaction of hypobromite with amino acids would produce electroactive bromoamino acids. The consequences of this were that before attempting to titrate amino acids with hypobromite it was necessary to investigate the electrochemical activity of the reaction products, and to determine an electrode potential at which hypobromite, but not bromoamino acid, could be detected. The easiest way to perform this is by generating hypobromite at the disc electrode, in a solution containing amino acid, and to record ring polarograms. This is shown in figure IV.6; polarogram A was recorded (before the addition of amino acid) at a disc current of 200 μ A and demonstrates the collection of hypobromite. The ring electrode was held at a potential of + 450mV (point P) and glycine (the simplest amino acid) was added to the solution, so that the resultant glycine concentration was $\sim 10^{-4}$M. The ring current immediately decreased, showing that the added glycine is reacting with the electrogenerated hypobromite, reducing the amount of the latter which reaches the ring. On decreasing the potential of the ring electrode the ring current is seen to increase (polarogram B); this is due to reduction of the brominated glycine compound, and at - 700mV the observed ring current is equal to that observed in the absence of glycine. Results presented in part (b) of this section show that glycine reacts with two molecules of hypobromite:

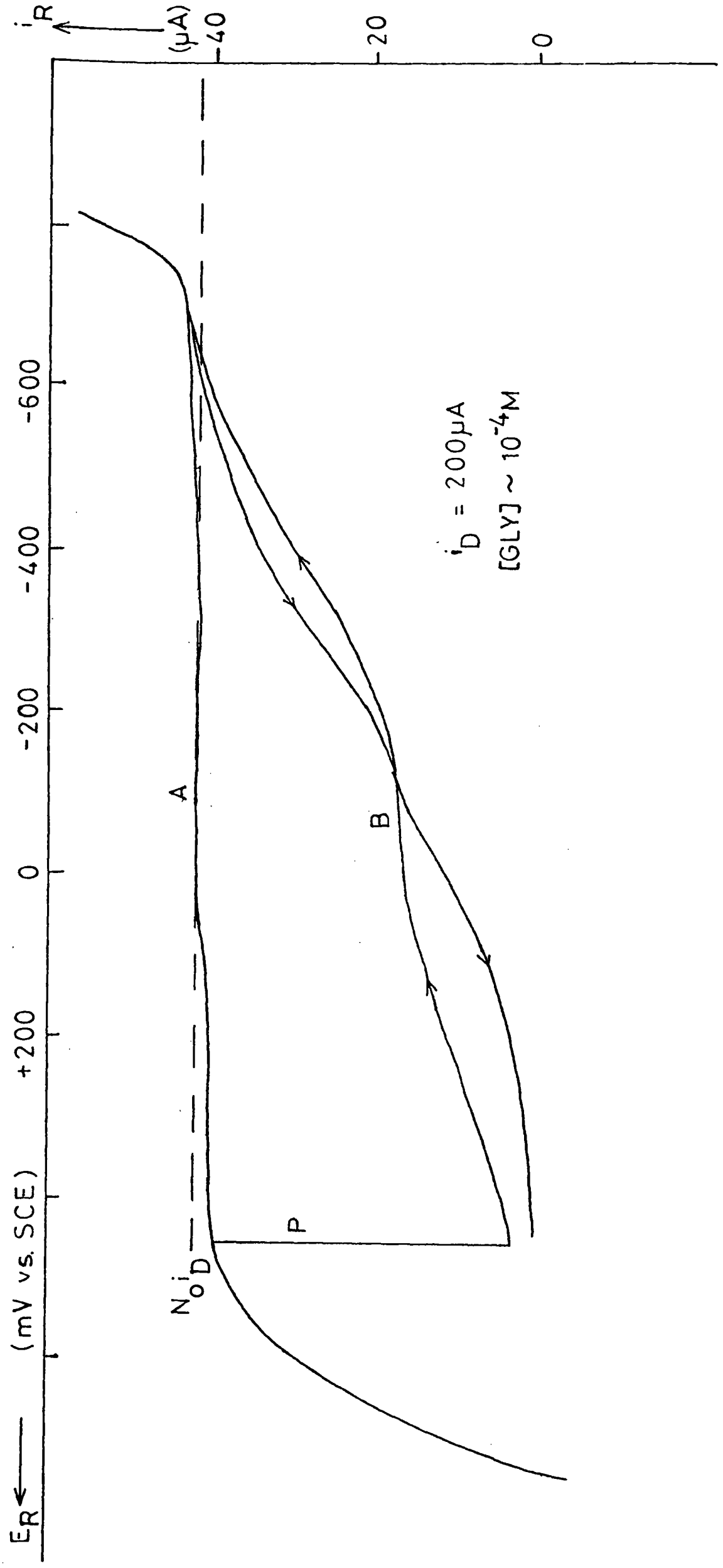

Figure IV.6 Ring polarograms of hypobromite and glycine

$$HOOC — CH_2 — NH_2 + 2OBr^- \rightarrow HOOC — CH_2 — NBr_2 + 2OH^-$$

and the double wave observed in figure IV.6 suggests that the reduction of N,N - dibromoglycine proceeds in two steps:

$$- NBr_2 + H^+ + 2e^- \rightarrow - NHBr + Br^-$$

$$- NHBr + H^+ + 2e^- \rightarrow - NH_2 + Br^-$$

Dibromoglycine, by analogy with dibromoamine ($NHBr_2$), is expected to be more easily reduced than monobromoglycine so that the wave observed at $+ 450 > E_R > - 100mV$ corresponds to the first step in the above reduction, while the wave at $- 100 > E_R > - 700mV$ corresponds to the second step (the reduction of monobromoglycine, as soon as it is formed from dibromoglycine). The double wave is easily observed when recorded in the cathodic (negative - going) direction, but is less distinct when recorded in the anodic (positive-going) direction. The hysteresis is due to formation, and subsequent reduction, of platinum oxides on the surface of the electrodes, and because of this, and the poor reproducibility, the waves were not further analysed.

The information obtained from figure IV.6 is important in deciding at which potential to hold (potentiostat) the ring electrode in titration curve experiments. A potential of + 450mV was chosen; this is not the ideal potential for hypobromite detection, since collection efficiencies recorded at this ring potential have been observed to decrease slowly due to oxidation of the electrode surface, but a lower potential will result in bromoamino acid interference. This interference is illustrated in figure IV.7 which presents titration curves recorded at different ring potentials. Curve A was recorded at $E_R = + 450mV$ and has the normal features of a titration curve. The titration curve parameters for the particular RRDE used are given in Appendix 5 and the line labelled N' is the theoretical ring current: disc current ratio corresponding to the reaction boundary being situated at the outside edge of the ring electrode ($\beta_J = 1$). This line intersects the titration curve at the commencement of the linear region (equation I.30)

$$i_R = N_o i_D - M\beta^{2/3}$$

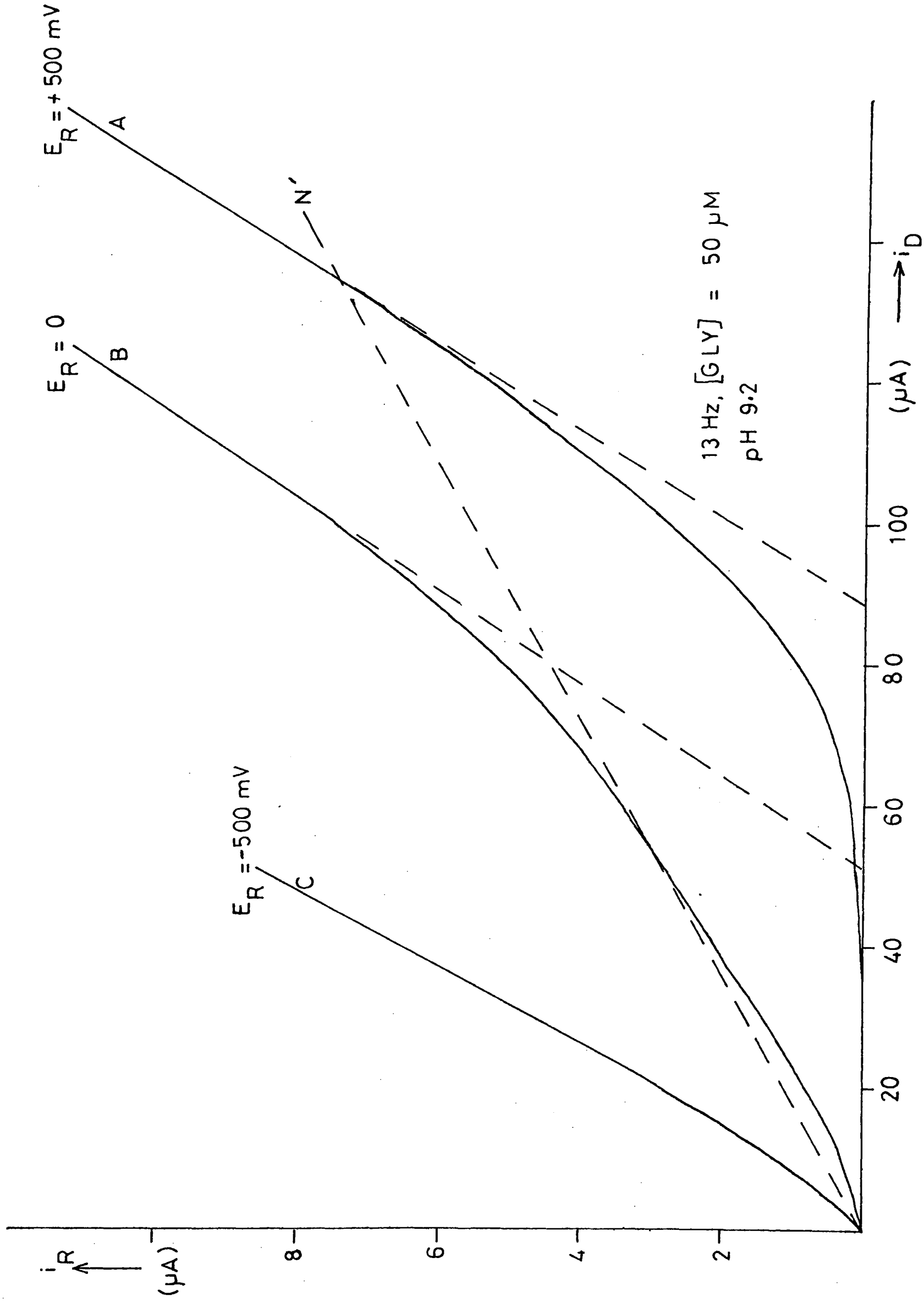

Figure IV.7 Effect of ring potential on glycine titration curve

and extrapolation of the linear region to $i_R = 0$ gives a disc current ($i_D \sim 90$ μA) which is proportional to the glycine concentration. Curve B was recorded at a potential of 0 V (vs SCE), at which potential dibromoglycine is reduced to monobromoglycine. This activity of the reaction products noticeably alters the shape of the titration curve, which shows two linear regions. In the first linear region (at 10 μA $< i_D <$ 60 μA) the ring current is due entirely to reduction of the dibromoglycine, since curve A shows zero ring current in this range. As the disc current is further increased hypobromite reaches the ring electrode, the slope of the titration curve increases and the second linear region commences at $\sim$ 110 μA. Extrapolation of the second linear region to $i_R = 0$ gives a disc current intercept of $\sim$50 μA which is approximately half of that observed at $E_R = +$ 450mV. Thus the activity of the reaction product has also altered the displacement of the titration curve; this is because half of the hypobromite which has reacted with the glycine (and would normally be irretrievably consumed) is recovered in the reduction of dibromoglycine to monobromoglycine. Curve C illustrates the titration recorded at a ring potential of - 500mV; at this potential dibromoglycine is almost completely reduced to glycine and very little titration is observed since most of the reacted hypobromite is recovered at the ring electrode.

The optimum ring potential for titration of amino acids is therefore + 450mV since this gives greatest sensitivity. Returning to curve A of figure IV.7 the disc current at the point of intersection of the N' line corresponds to a theoretical value of the normalised disc current i_D/M. The value of i_D/M for $\beta_J = 0$ (Appendix 5) enables indentification of the point on curve A at which the reaction boundary is situated on the inside edge of the ring:

β_J / β	1	0
i_D/M	2.755	1.665

This point is at i_D = 80 μA, and a finite ring current exists here; this is because hypobromite is penetrating past the reaction boundary due to the relative slowness of the reaction. The effect of pH on the rate of reaction is indicated by figure IV.8 which compares titration curves at pH 9.2 and pH 8 and clearly shows that the reaction is slower at lower pH. Increase of the pH above 9.2 to obtain a faster titration reaction is not practical because of the difficulties of generating and detecting hypobromite with 100% efficiency.

b) Titration Curves Recorded at E_R = +450mV

After optimisation of the experimental conditions several amino acids and simple peptides were titrated with hypobromite. The amino acids studied were glycine, lysine, cysteine, methionine, tryptophan and tyrosine; As (III) was also titrated, as a standard, since it is known to react with one molecule of hypobromite:

$$As(III) + OBr^- + 2H^+ \longrightarrow As(V) + Br^- + H_2O$$

The titrations were investigated by placing 100 ml of the background electrolyte solution (0.5M KBr + 0.025M Borate, pH 9.2) in the electrochemical cell. The concentration of brominatable impurities present in this solution was reduced in situ, by generating hypobromite at the disc electrode until a collection efficiency showing little or no titration could be recorded. The amino acids were then titrated by pipetting solution, usually in 1 ml aliquots, into the cell and titration curves at 5Hz rotation speed were recorded using the XY recorder. Each amino acid was titrated at several different concentrations so that the concentration response could be examined; the recorded titration curves are presented in figures IV.9 - 15. The curves for all compounds show the effect of kinetics since the reaction of hypobromite with the amino group is not infinitely fast.

The concentration dependence of these titration curves has been investigated by constructing a line of gradient N' = 0.0558 to intersect the curves. This line, as explained above, intersects the titration curve at the

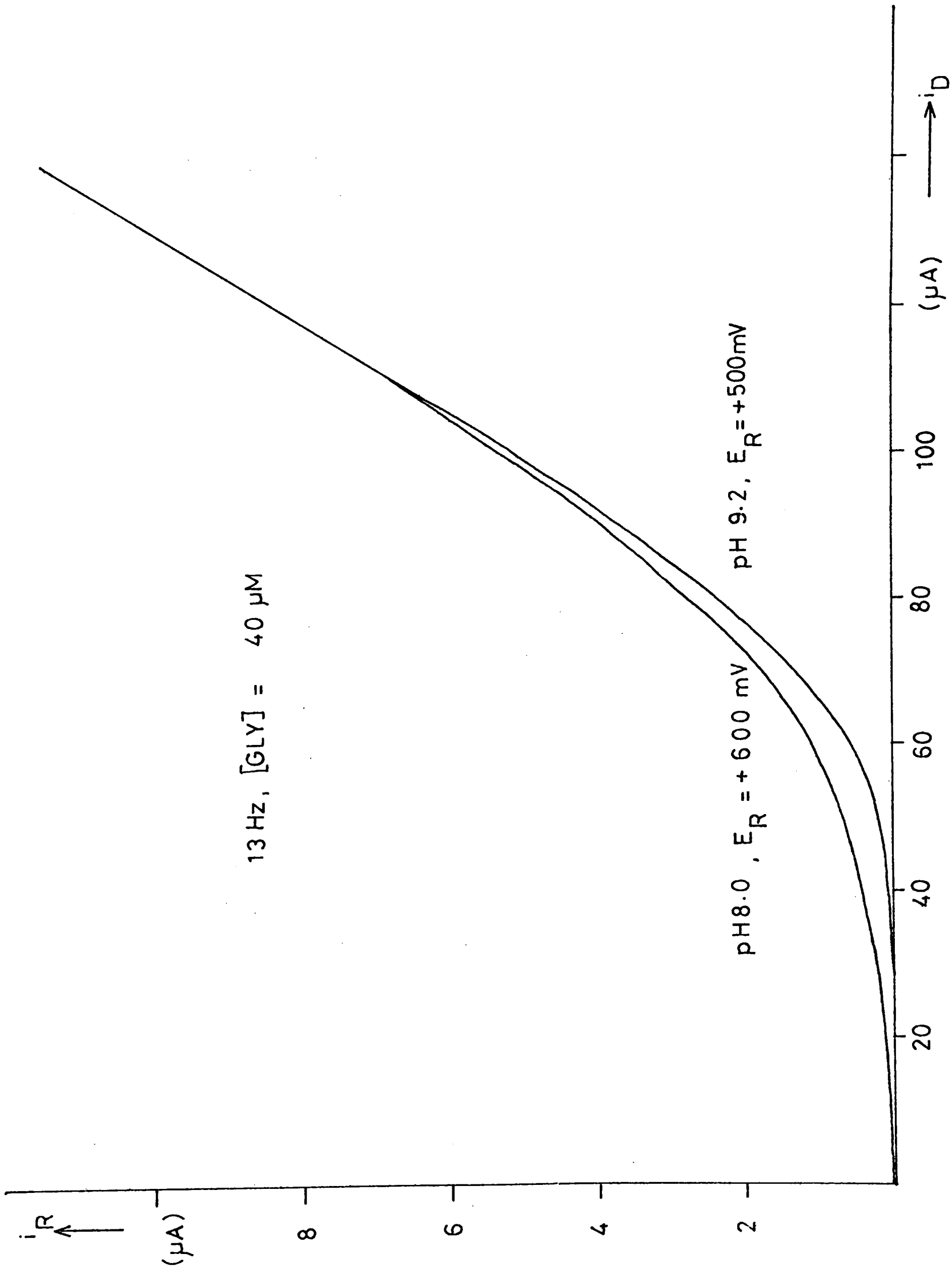

Figure IV. 8 Effect of pH on titration of glycine

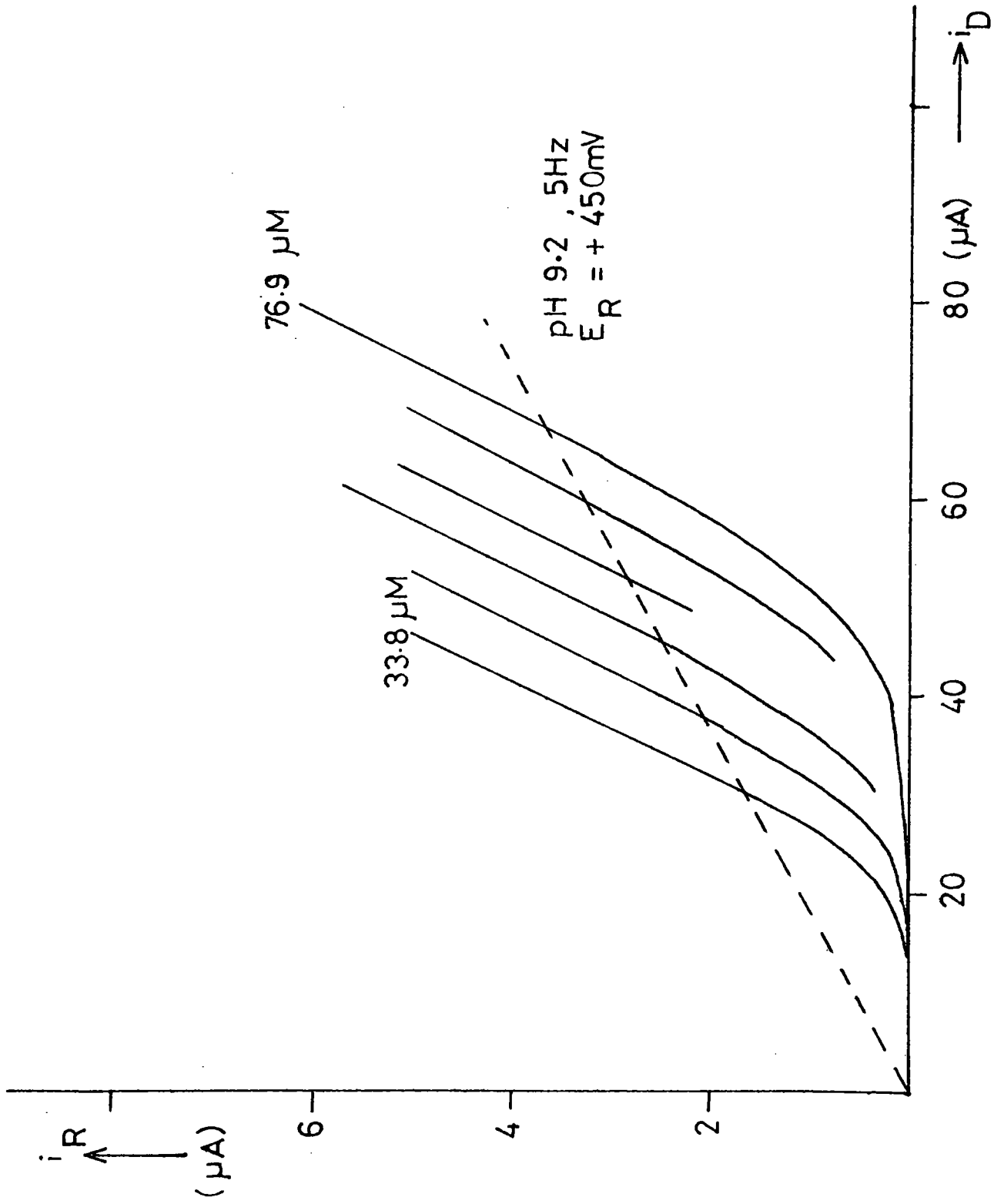

Figure IV. 9 Titration of arsenic (III)

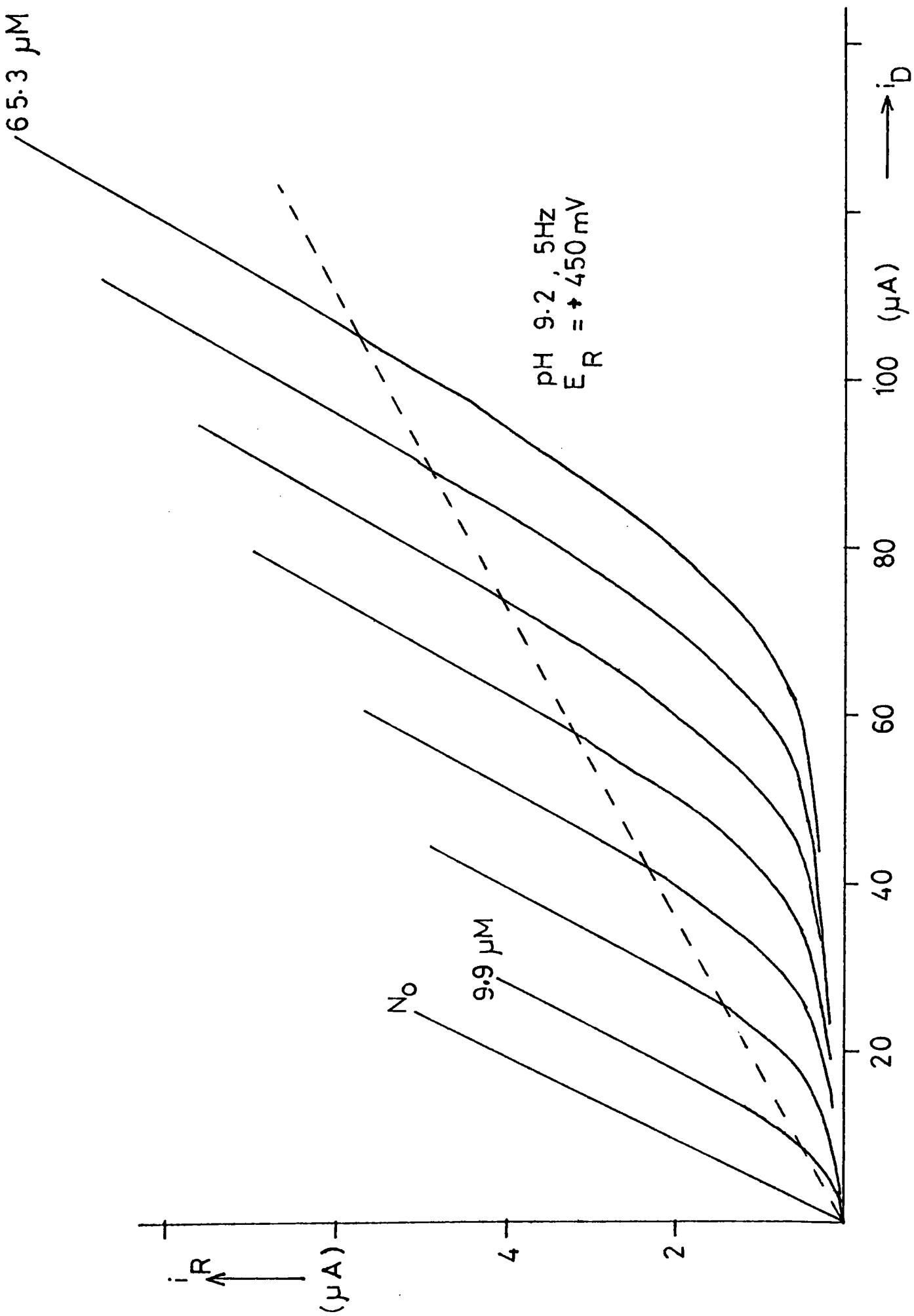

Figure IV. 10 Titration of glycine

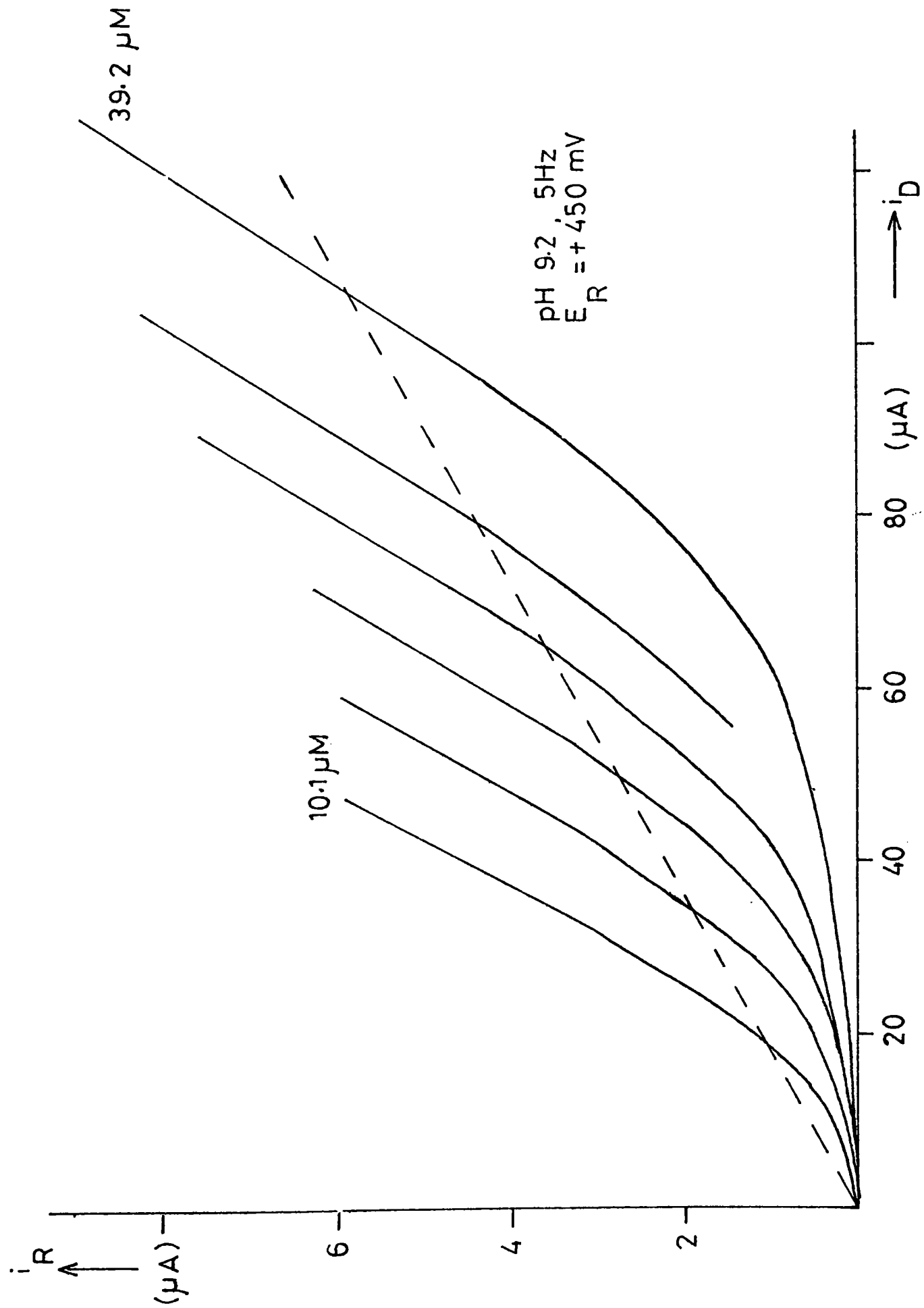

Figure IV. 11 Titration of lysine

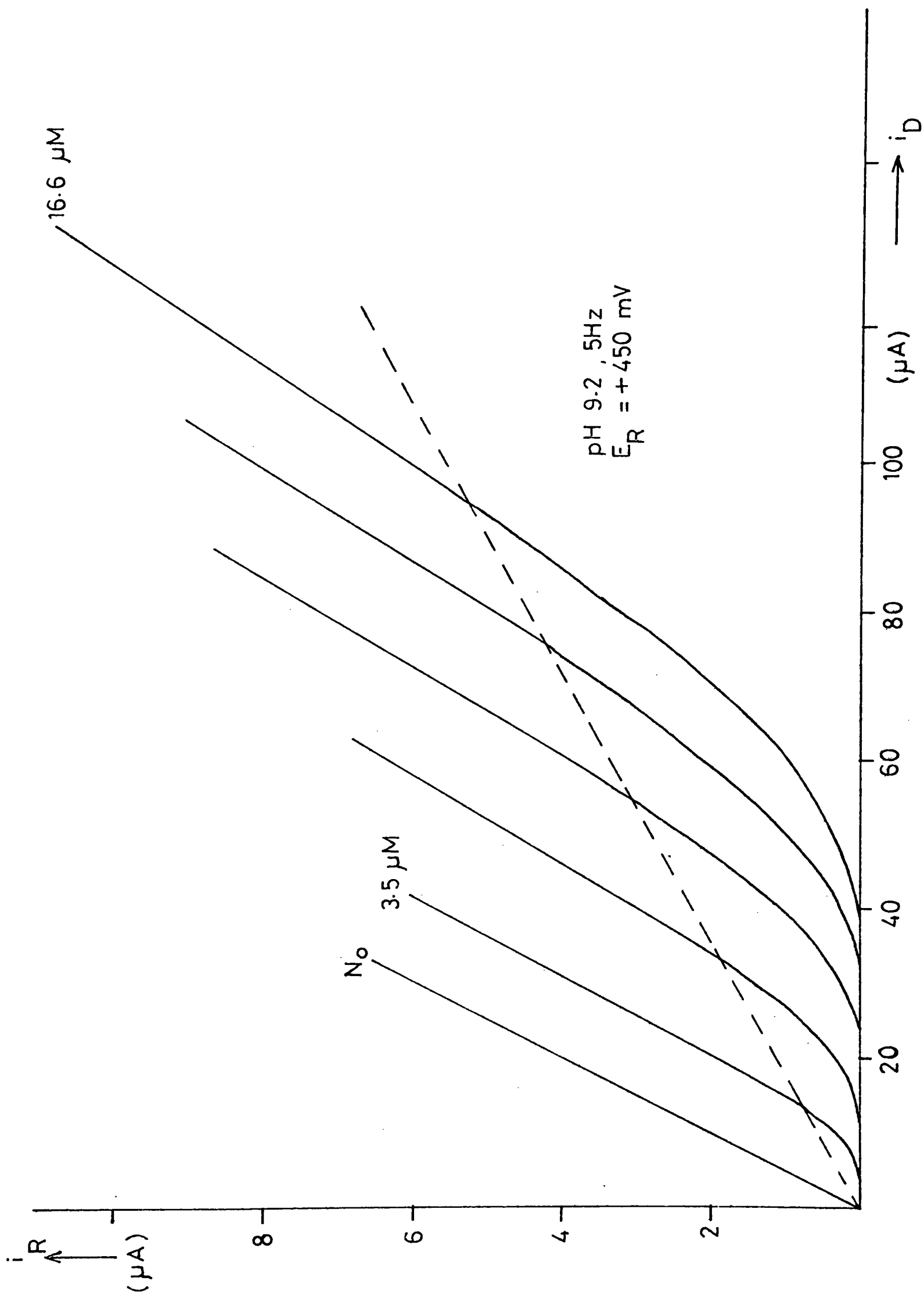

Figure IV.12 Titration of cystine

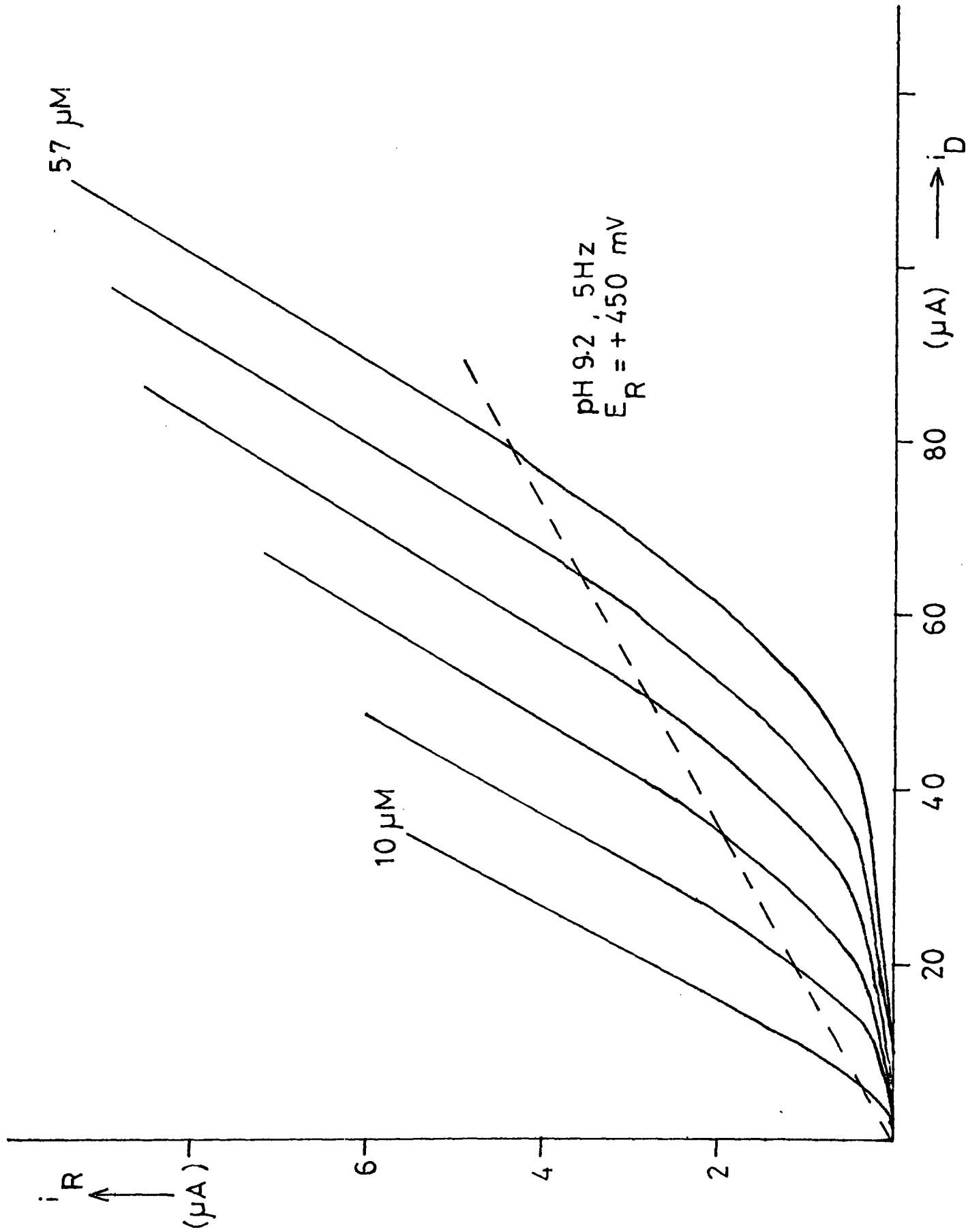

Figure IV.13 Titration of methionine

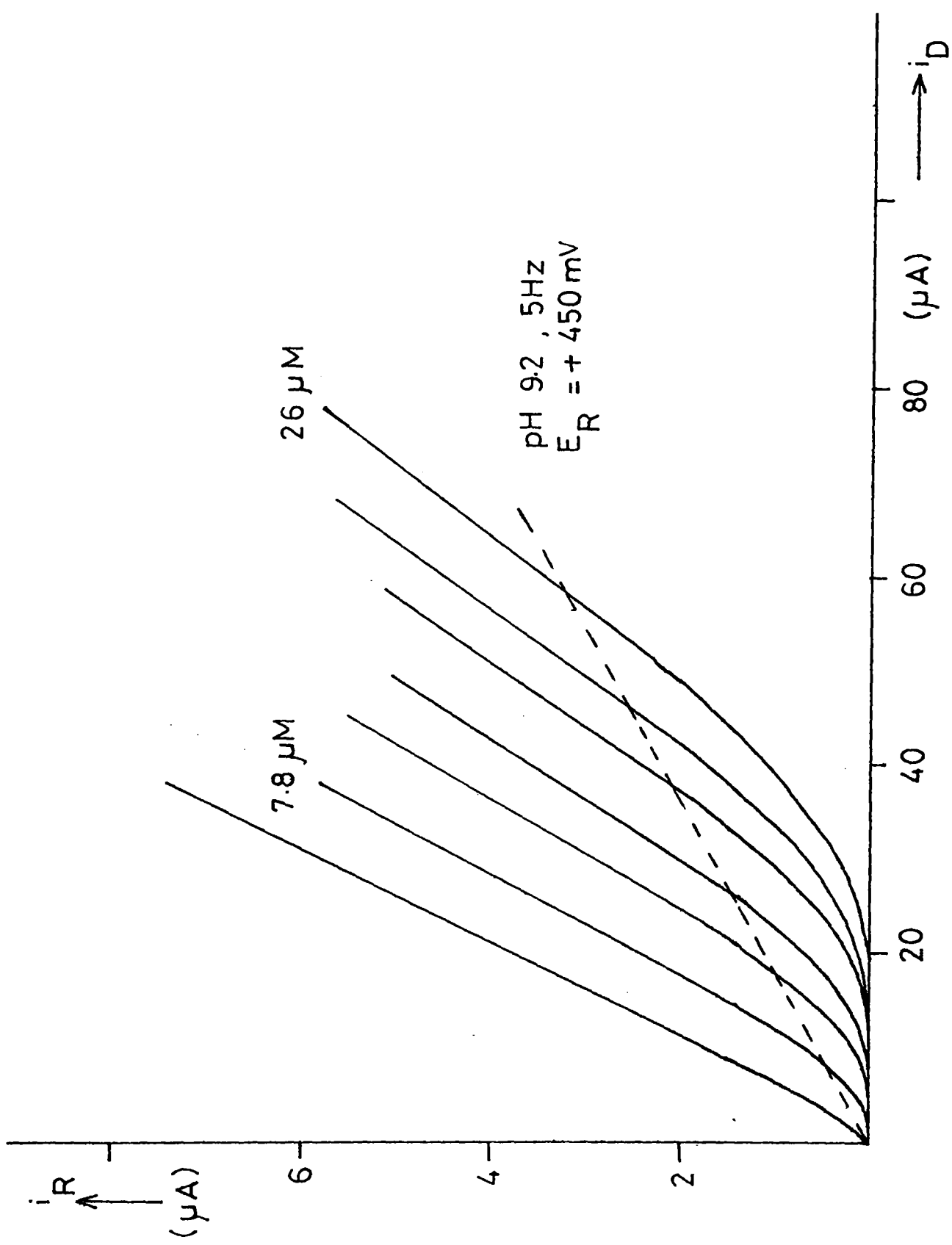

Figure IV.14 Titration of tryptophan

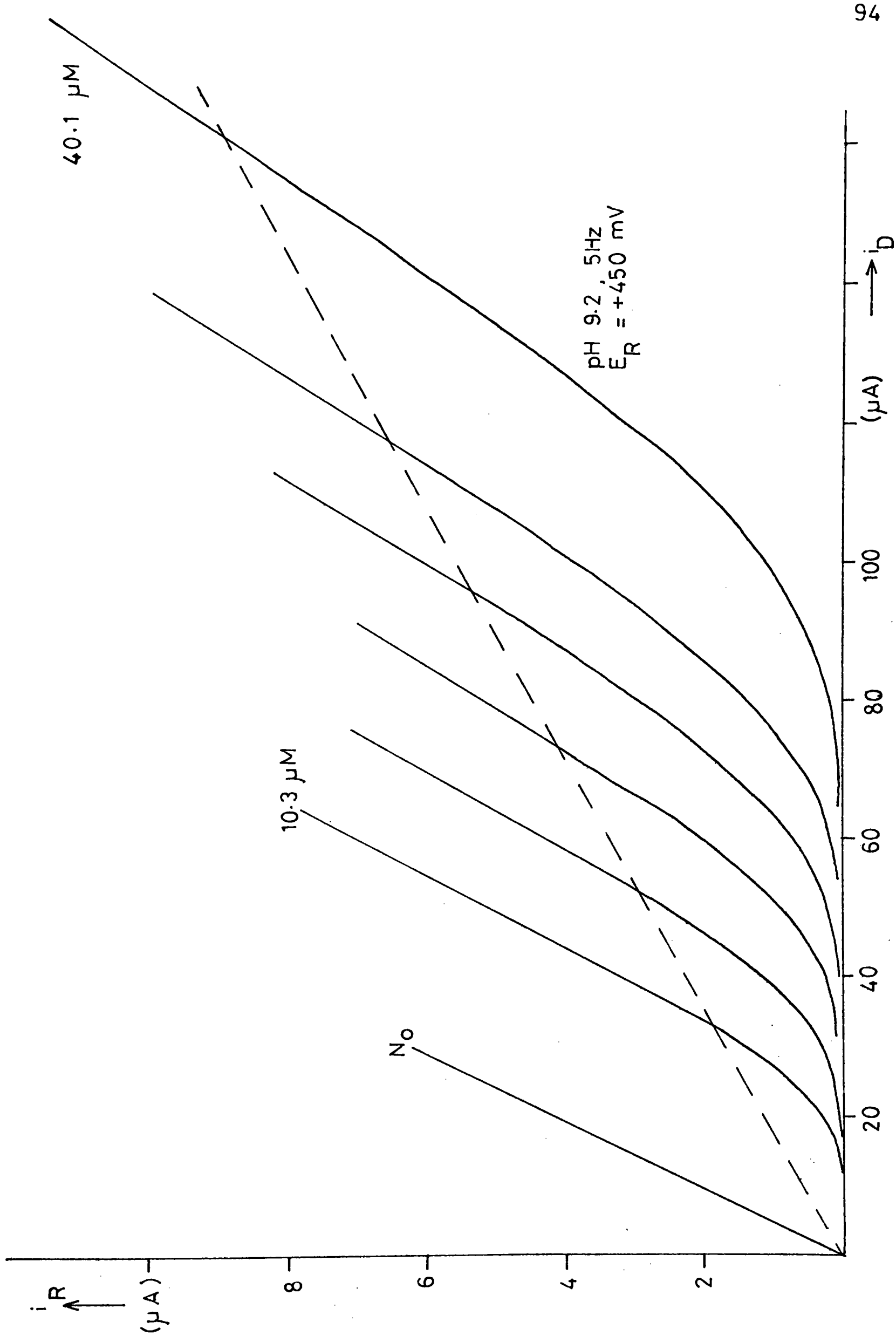

Figure IV. 15 Titration of tyrosine

commencement of the linear region

$$i_R = N_o i_D - \beta^{2/3} M$$

The value of the disc current, i_D' , at the point of intersection should be proportional to M and to a_∞ , the bulk concentration of amino acid. Therefore the titration curves were analysed by measuring values of i_D' and plotting this against the concentration of amino acid. This method of analysis is better than extrapolation of the linear portion to $i_R = 0$, since it is sometimes difficult to be certain where the titration curve becomes linear and the extrapolation may be inaccurate.

The plots of i_D' vs a_∞ show non-zero intercepts due to excess OBr^- or impurities in the background electrolyte which were not completely removed in the prebromination clean up technique. The plots collected in figures IV.16 and IV.17 have been adjusted to pass through the origin; this has been done so that the gradients may be compared. Figure IV.16 presents the results for glycine, lysine and cystine; all show good straight lines, the standard deviation being 1 - 2%. The values of the gradients vary and As (III) is included as a standard. The gradient for glycine is twice that for As(III) which demonstrates that the amine group, as expected, reacts with two molecules of hypobromite. Lysine, which contains two amine groups, has a greater gradient and for cystine, which consists of two amine groups and a disulphide bridge, the even greater gradient suggests that the sulphur linkage is also reacting with hypobromite. The results plotted for glycine and lysine are the product of two seperate experiments, which demonstrates the reproducibility of the technique. Figure IV.17 presents the results for the sulphur-containing methionine and for the aromatic amino acids tryptophan and tyrosine. Once again the gradients reflect that the amino acid side chains are reacting with differing numbers of hypobromite molecules. Some difficulty was encountered in reproducing the methionine titration, as is shown by the pairing of plotted values. The relative magnitudes of the

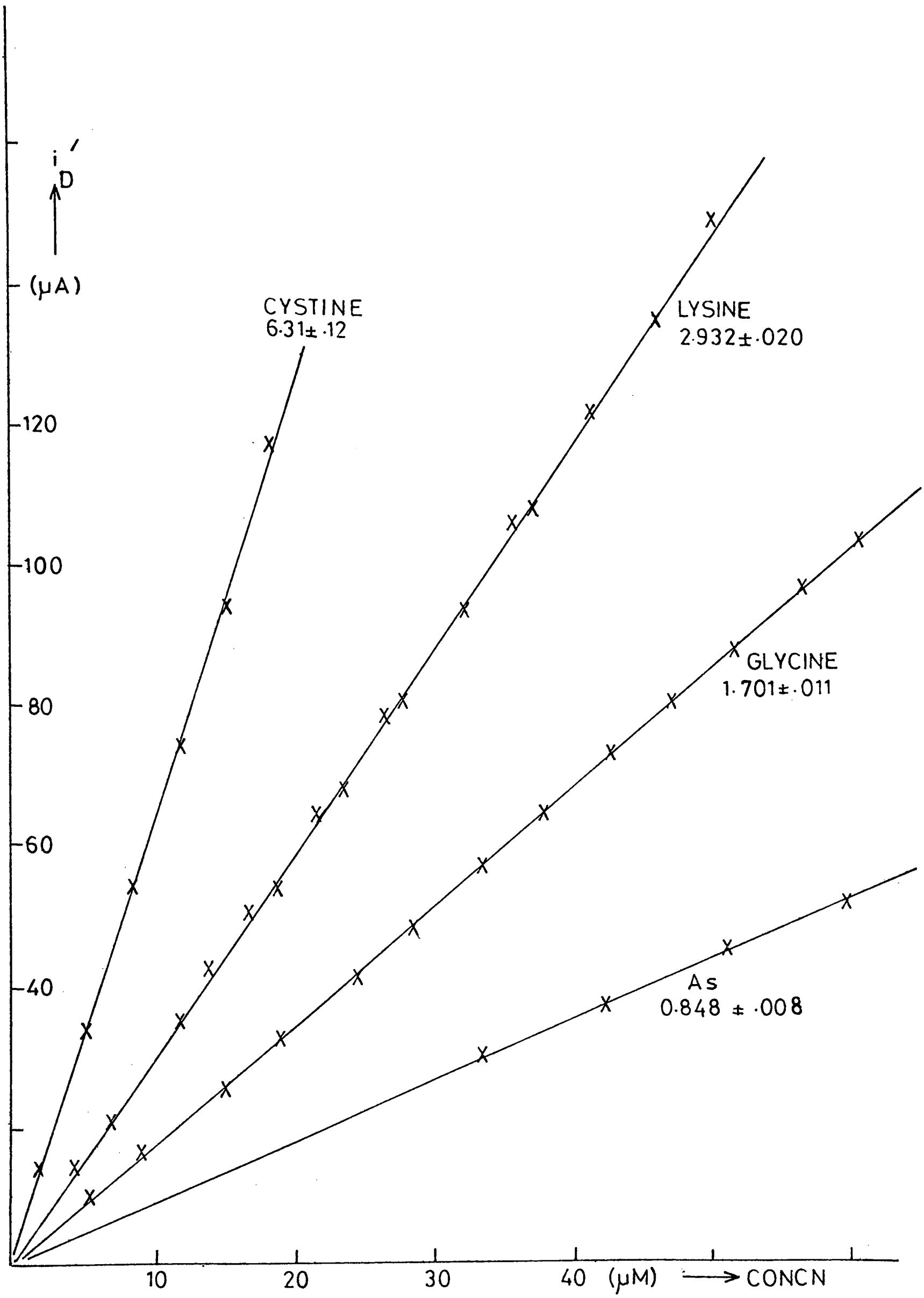

Figure IV.16 Titration response of amino acids at pH 9·2

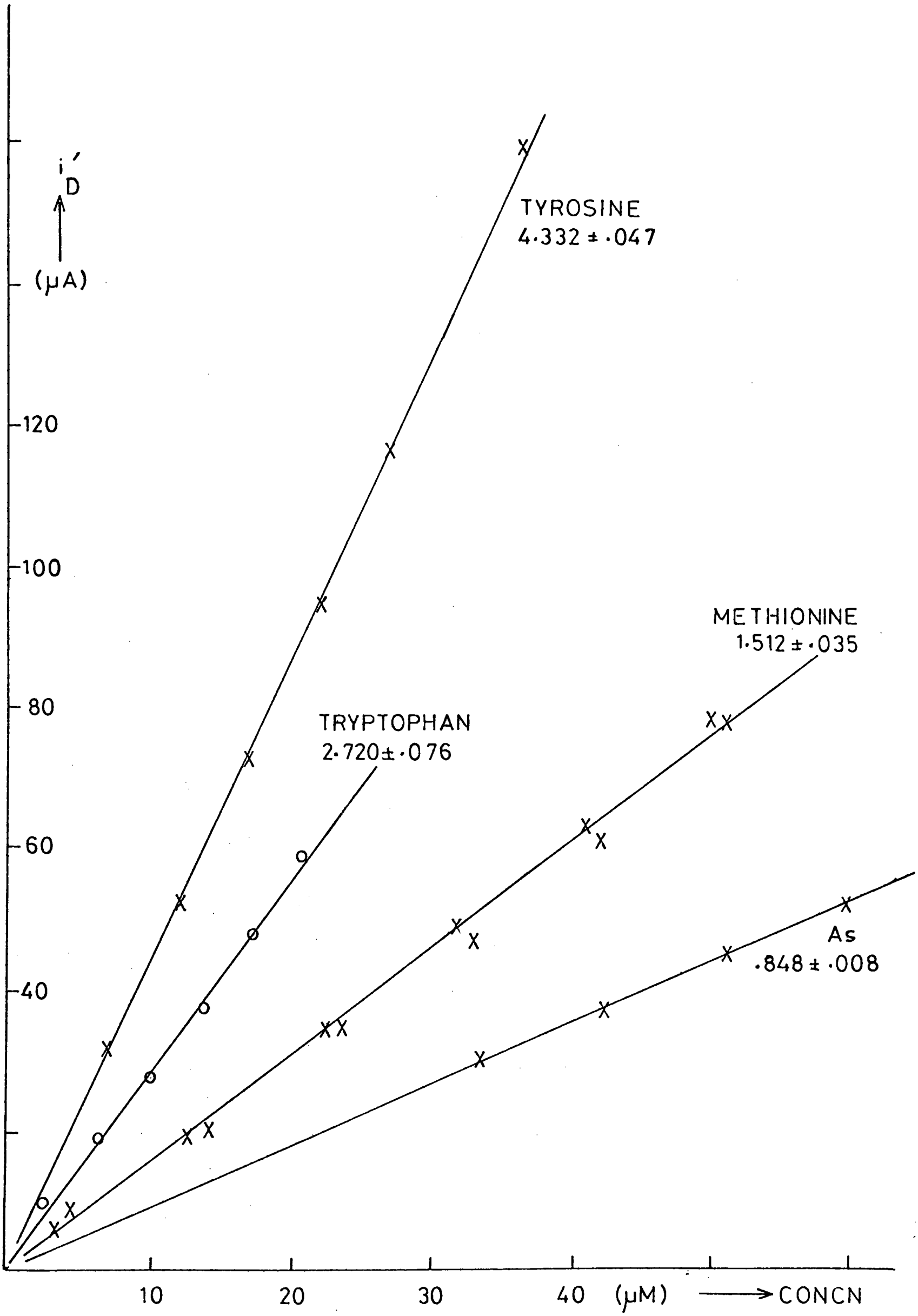

Figure IV.17 Titration response of amino acids at pH 9·2

gradients are further analysed below.

In addition to the above amino acids some simple synthetic peptides were investigated. These peptides were penta-glycine, tetra-alanine, glycyl-leucyl-tyrosine and tri-tyrosine; alanine has a methyl side chain and leucine has an iso-butyl side chain. The titration curves for these peptides are presented in figures IV.18 - 21. The response with respect to concentration has been analysed in the same manner as the amino acid titrations and plots of i_D' vs a_∞ are presented in figure IV.22. The gradients for penta-glycine and tetra-alanine are the same, with a standard deviation of $\sim$2%; these peptides both have only a terminal amine group capable of reacting with hypobromite, the peptide bonds being resistant to bromination. The two other peptides studied, glycyl-leucyl-tyrosine and tri-tyrosine,possess phenolic side chains, the bromination of which accounts for their greater gradients.

The value of N' used to measure i_D' intersects the titration curve at a theoretical normalised disc current of $i_D/M = 2.755$; therefore the gradient of an i_D' vs a_∞ plot should be

$$\text{grad} = 2.755M/a_\infty$$

$$= 2.755 \times 0.62\ FAn_B D^{2/3}\ \omega^{1/2}\ \nu^{-1/6} \qquad \text{(IV.1)}$$

M is the limiting current which would be observed if the substrate were electroactive at the disc electrode. The term n_B is equal to $2n_{Br}$, where n_{Br} is the number of molecules of titrant (hypobromite) which react with one molecule of substrate; the factor of 2 is necessary since two electrons are exchanged in the production of one molecule of hypobromite. The above equation also contains the term $D^{2/3}$, but the simple theory of diffusion layer titrations, outlined in section I.2.d, assumes that D (substrate) = D (titrant). The diffusion coefficient of hypobromite has been measured, at pH 9.1, using the rotating disc electrode (39):

$$D_{OBr^-} = 1.06 \pm 0.06 \times 10^{-9}\ m^2\ s^{-1}$$

Since arsenic (III) is known to react with one molecule of hypobromite the

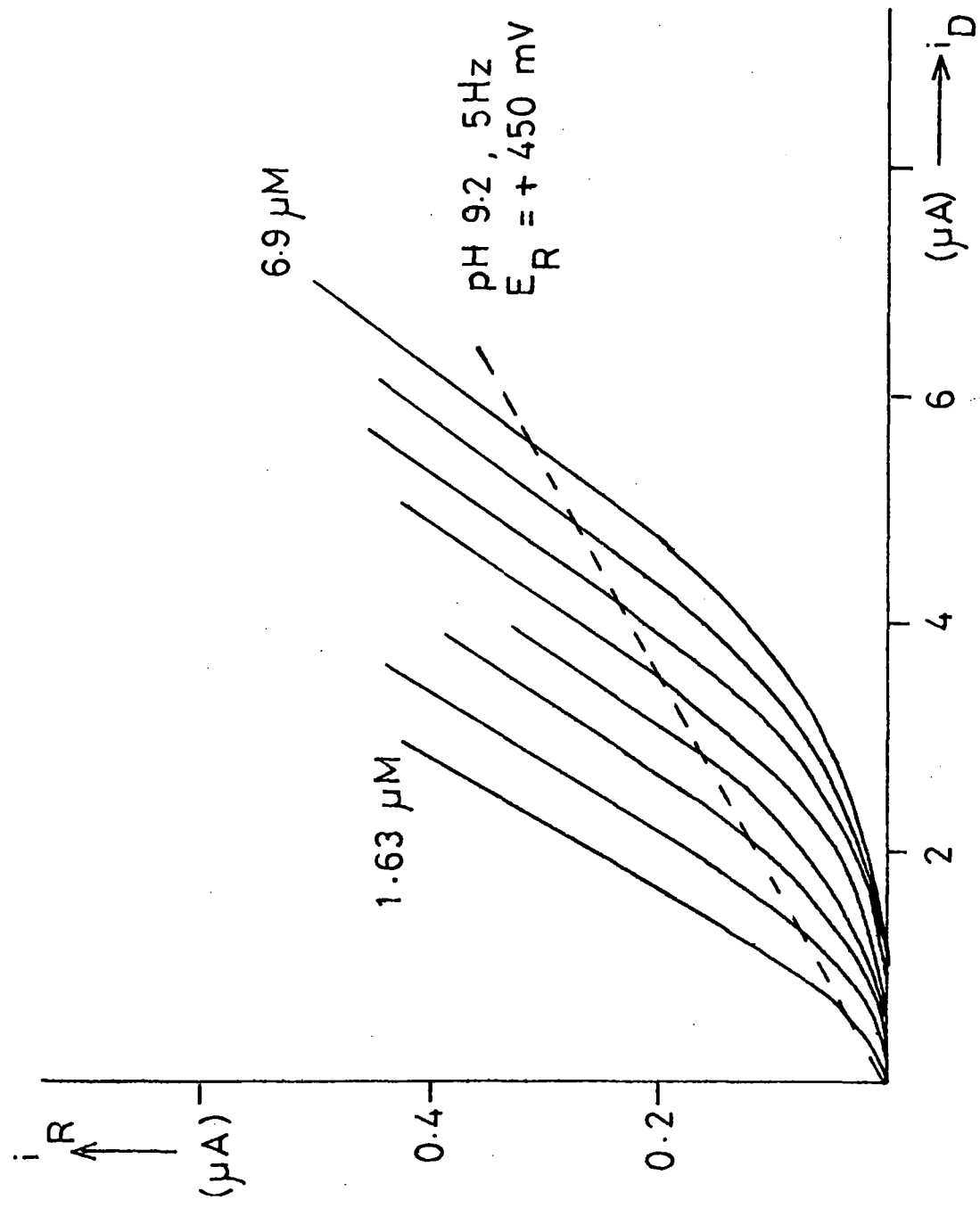

Figure IV. 18 Titration of penta-glycine

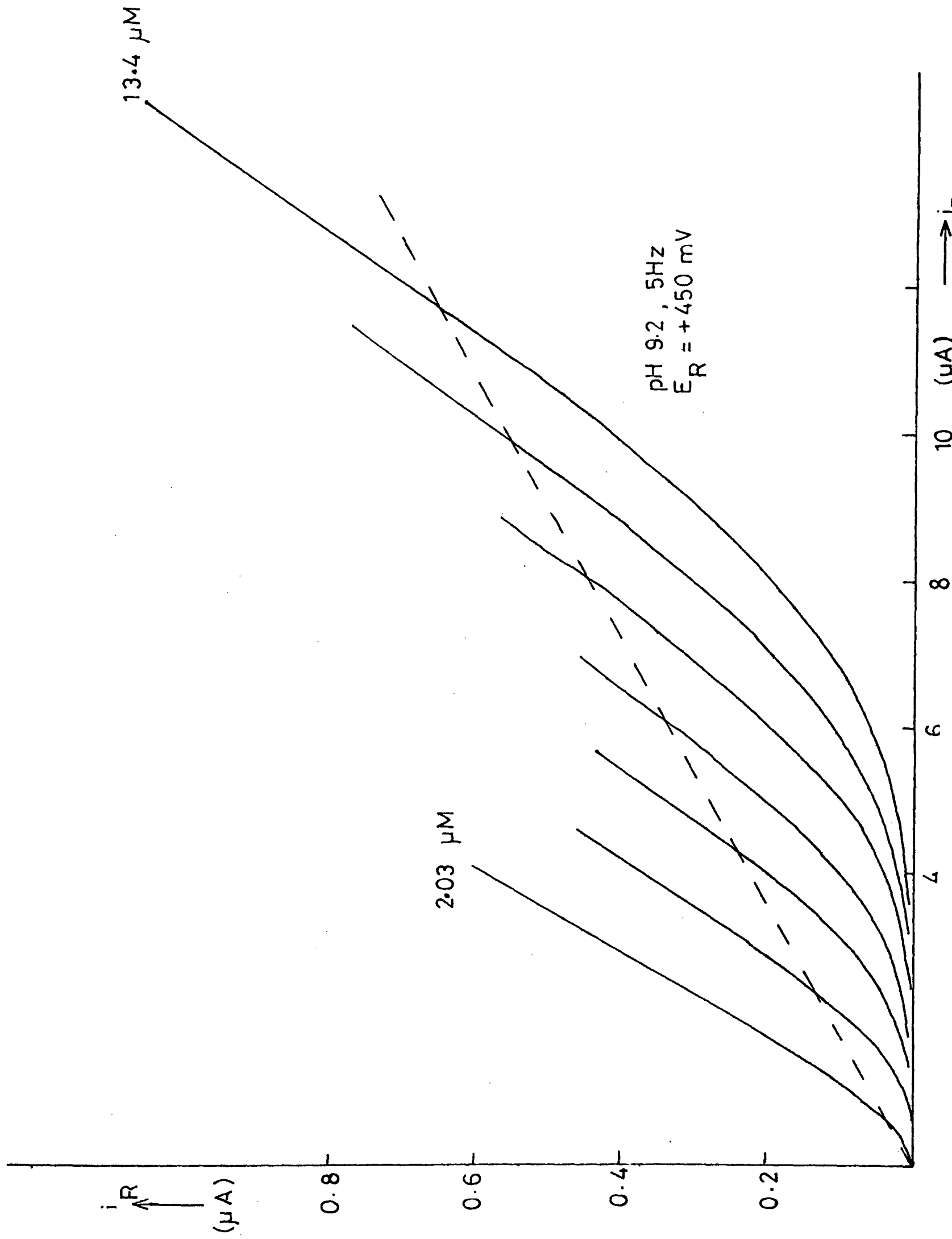

Figure IV. 19 Titration of tetra-alanine

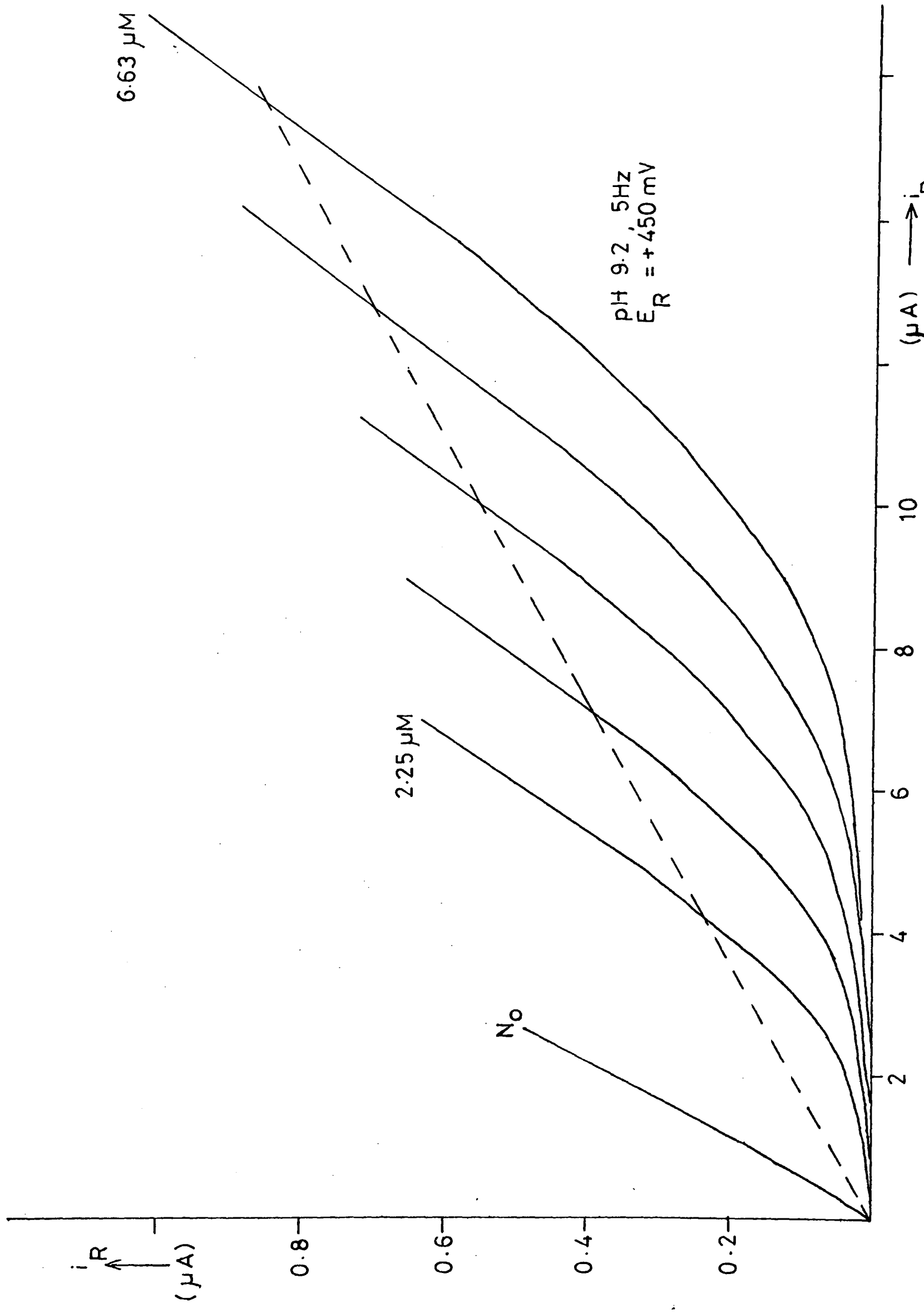

Figure IV. 20 Titration of glycyl-leucyl-tyrosine

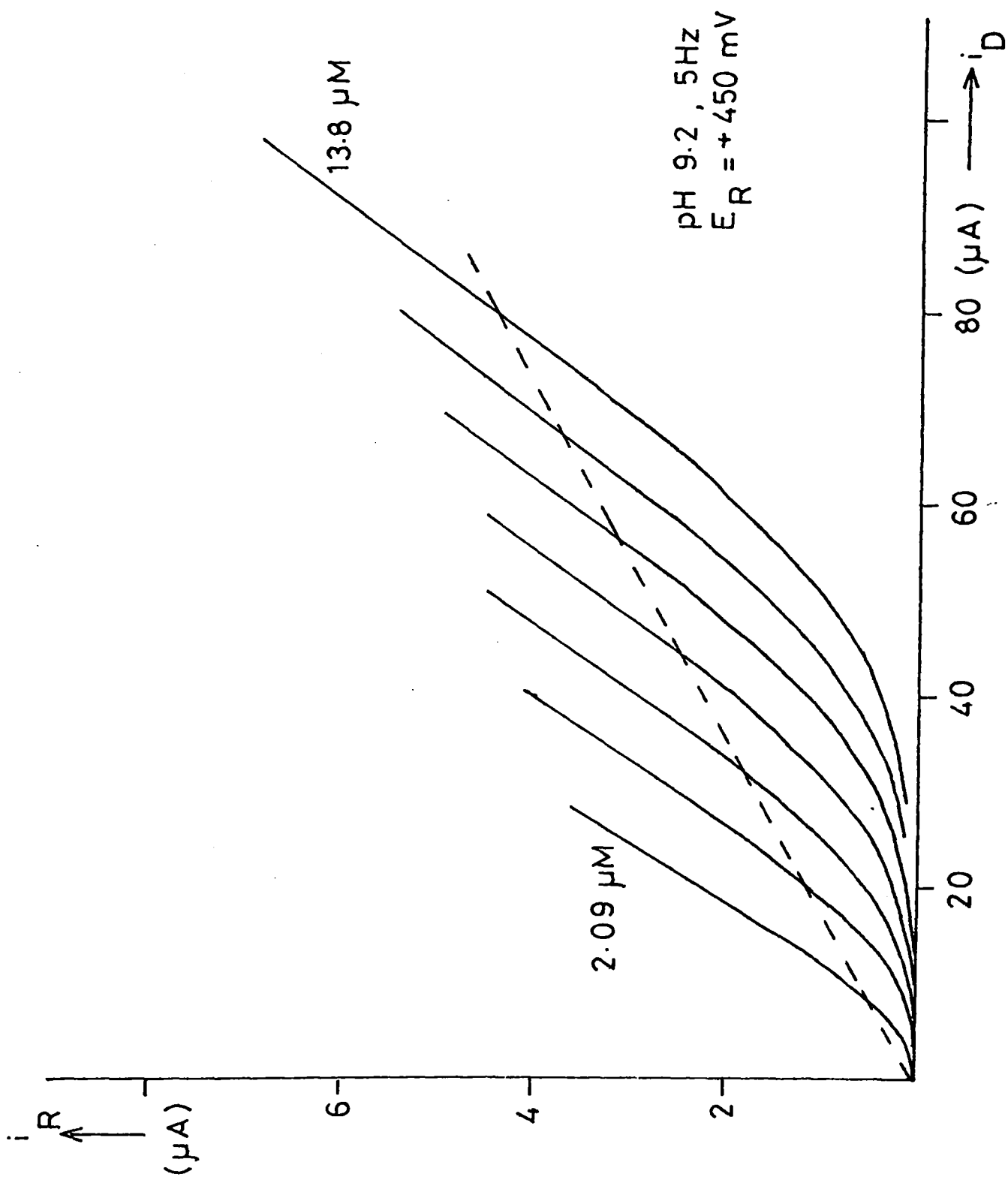

Figure IV. 21 Titration of tri-tyrosine

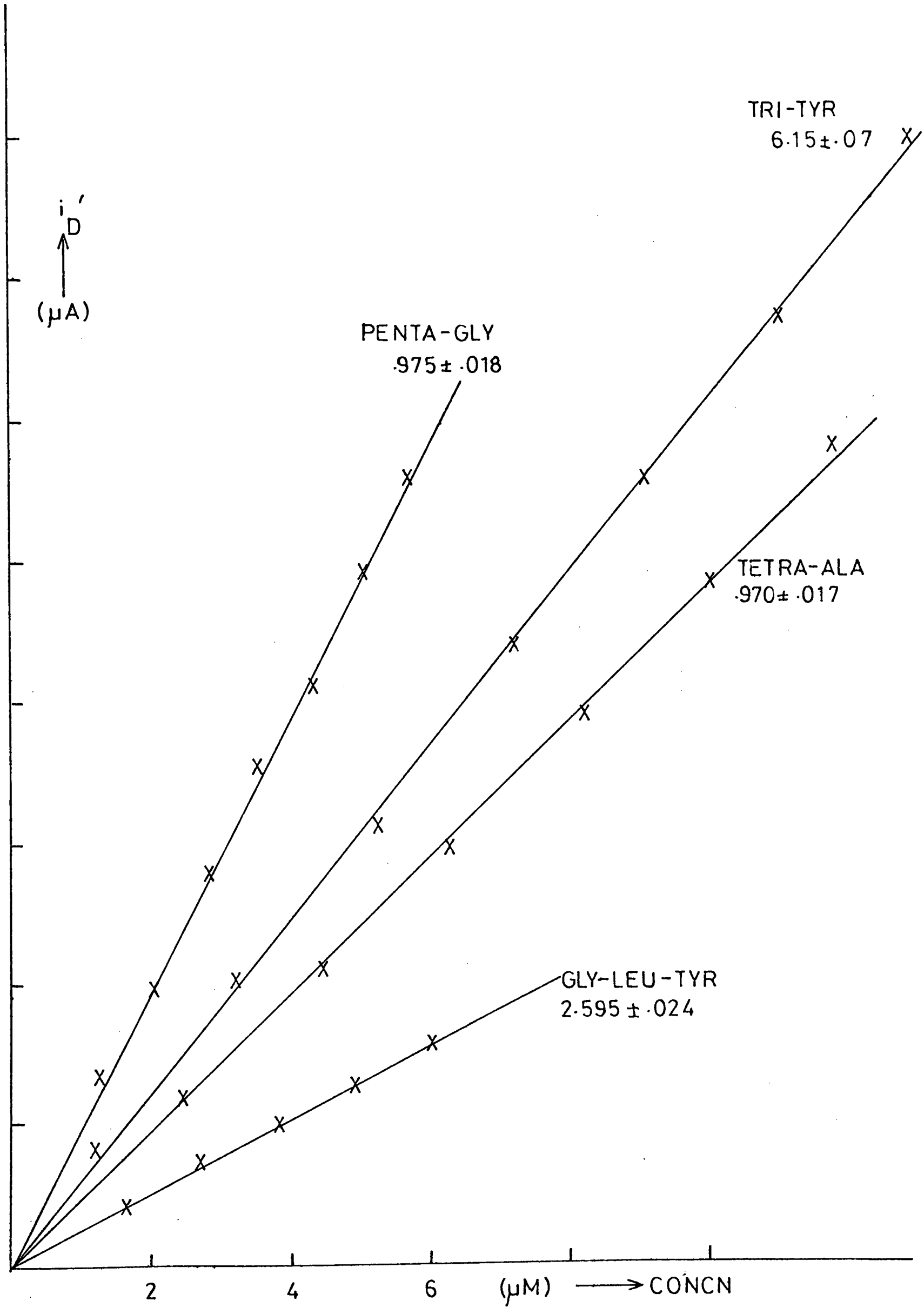

Figure IV. 22 Titration response of peptides at pH 9·2

diffusion coefficient for this system may be evaluated from the gradient of the arsenic titration plot; using $\nu = 9.45 \times 10^{-7}\ m^2\ s^{-1}$ (39) and $\omega = 10\pi\ rad\ s^{-1}$

$$D = 1.12 \pm .02 \times 10^{-9}\ m^2\ s^{-1}$$

The close agreement of this value with that above confirms that the assumption of equal diffusion coefficients is justified for the titration of arsenic (III) with hypobromite.

The amino acids and peptides studied vary in size so that their diffusion coefficients will vary. Therefore the assumption that D (substrate) = D (titrant) is not valid for all of these compounds. The RRDE titration curve theory has been extended to apply to this situation (section II.3) and this new theory predicts that the gradients of the i_D' vs a_∞ plots should be

$$\text{grad} = 2.755.\ 0.62FA\ n_B\ \omega^{1/2}\ \nu^{-1/6} D_A^{2/3} \qquad \text{(IV.2)}$$

The gradients have been collected in table IV.1 (first column), and have been normalised with respect to the arsenic gradient to produce a bromine number, N_{Br} (second column).

i) The Bromine Number, N_{Br}

The experimentally determined bromine number is given by (equation IV.2)

$$N_{Br} = n_{Br} \left(\frac{D_{AA}}{D_{As}}\right)^{2/3} \qquad \text{(IV.3)}$$

This quantity reflects the number of molecules of hypobromite which react with one molecule of substrate,. For glycine $N_{Br} = 2.01 \pm .02$, which implies that the diffusion coefficient ratio in equation IV.3 is unity for this compound. The diffusion coefficient of glycine has been reported (81).

$$D = 1.055 \pm .001 \times 10^{-9}\ m^2\ s^{-1}$$

This was determined at 25°C by a refractometric method, at a concentration of 0.6 wt. %; the viscosity of the solution was not reported, but the diffusion coefficient is in good agreement with those of hypobromite and arsenic reported above.

TABLE IV.1 Bromination of Amino Acids and Peptides

	Gradient ($\mu A/\mu M$)	Bromine Number (N_{Br})
Arsenic	0.848 ± .008	1
Glycine	1.701 ± .011	2.01 ± .02
Lysine	2.932 ± .020	3.46 ± .04
Cystine	6.31 ± .12	7.44 ± .16
Methionine	1.512 ± .035	1.78 ± .05
Tryptophan	2.720 ± .076	3.21 ± .09
Tyrosine	4.332 ± .047	5.11 ± .07
Penta-gly	0.975 ± .018	1.15 ± .02
Tetra-ala	0.970 ± .017	1.14 ± .02
Gly-leu-tyr	2.595 ± .024	3.06 ± .04
Tri-tyr	6.15 ± .07	7.26 ± .10

The other values of N_{Br} in table IV.1 are non-integral due to the effect of diffusion coefficients. This effect may be clearly seen by comparing the bromine numbers of glycine and pentaglycine; both of these molecules possess a single amino group capable of reacting with hypobromite, but the peptide exhibits a lower bromine number (1.15 $\pm$ .02) due to its lower diffusion coefficient. The bromine number may be corrected, if the amino acid diffusion coefficients are known, to give n_{Br}:

$$n_{Br} = N_{Br} \left(\frac{D_{As}}{D_{AA}} \right)^{2/3} \qquad \text{(IV.4)}$$

ii) The Corrected Bromine Number, n_{Br}

If the extended RRDE titration theory presented in section II.3 is accurate, then the corrected bromine number will be equal to the number of hypobromite molecules reacting with one molecule of substrate. The diffusion coefficients of 23 amino acids and peptides have been published by Longsworth (81), including

	10^9 D/m^2 s^{-1}
Glycine	1.0554
Diglycine	0.7909
Triglycine	0.6652
Alanine	0.9097
Leucine	0.7255
Phenylalanine	0.7074
Tryptophan	0.6592
Leu-gly-gly	0.5507

Only two of these compounds coincide with those titrated; it was therefore decided to calculate diffusion coefficients for the substances of interest.

The estimation of diffusion coefficients has been described by Edward (82) and by Bidstrup (83); the former method was followed (Appednix 6) and the calculated values are presented in table IV.2. These are diffusion coefficients at infinite dilution in water, at 25^{o}C; the viscosity used was that of water (8.904 x 10^{-4} kg m^{-1} s^{-1}). In the background electrolyte

Table IV.2 Estimated Diffusion Coefficients and Corrected Bromine Numbers of Amino Acids and Peptides.

	D^{o}_{25} ($\times 10^{9}/m^{2}\ s^{-1}$)	n_{Br}
Glycine	.984	2
Lysine	.769	4.08 ± .05
Methionine	.785	2.07 ± .05
Cystine	.655	9.76 ± .21
Tyrosine	.715	6.32 ± .08
Tryptophan	.713	3.98 ± .11
Penta-gly	.631	1.55 ± .03
Tetra-ala	.609	1.57 + .03
Gly-leu-tyr	.562	4.45 ± .06
Tri-tyr	.484	11.65 ± .16

solution ($\eta = 9.84 \times 10^{-4}$ kg m^{-1} s^{-1}) the estimated diffusion coefficient of glycine is 0.89×10^{-9} m^2 s^{-1} which is lower than that of hypobromite and arsenic above. However the integral number, N_{Br}, obtained for glycine implies that no correction is necessary for this compound and that $D_{GLY} = D_{As}$. It was therefore decided to correct the amino acid bromine numbers using the relationship

$$n_{Br} = N_{Br} \left(\frac{D_{GLY}}{D_{AA}} \right)^{2/3} \qquad \text{(IV.5)}$$

Since the ratio of two estimated diffusion coefficients is used some of the errors and assumptions inherent in their estimation will cancel. The corrected bromine numbers n_{Br}, are presented in table IV.2, and for the amino acids (with the exception of tyrosine) these are close to integral values. The peptide corrected bromine numbers are however non-integral and this is discussed below (iv).

iii) The Stoichiometric Bromine Number, n_{Br} (s).

The number of molecules of hypobromite which react with one molecule of substrate may be predicted by considering the structure and reactivity of the amino acid side chains; this predicted value will be termed the stoichoimetric bromine number, n_{Br} (s), and Table IV.3 presents this analysis.

Some further comment is necessary for the stoichiometric bromine numbers of tryptophan, tyrosine, glycyl-leucyl-tyrosine and trityrosine. Tryptophan possesses an indole side chain. Generally the direct electrophilic substitution of indoles yields 3 - derivatives; if this postion is blocked (as it is in tryptophan) then the substituent enters position 2. This reaction, together with the reaction of three molecules of hypobromite at the 1 position (secondary amine) and α - amino group, suggests a stoichiometric bromine number of 4 for this amino acid.

TABLE IV.3 STOICHIOMETRIC BROMINE NUMBERS OF AMINO ACIDS AND PEPTIDES

	SIDE CHAIN	REACTION PRODUCT	n_{Br} (s)	EVIDENCE
LYSINE	$-(CH_2)_4NH_2$	$-(CH_2)_4NBr_2$	2+2 = 4	Reaction of glycine
METHIONINE	$-(CH_2)_2-S-CH_3$	$-(CH_2)_2-SO-CH_3$	2+1 = 3	MET + BrCl + H_2O ⟶ $HO_2C(NH_2)CHCH_2CH_2SOCH_3$ + HBr + HCl
CYSTINE	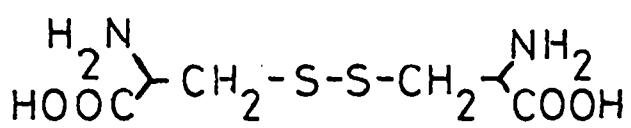	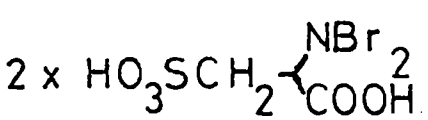	4+5 = 9	CYS_2 + 5BrCl + $6H_2O$ ⟶ $2HO_2C(NH_2)CHCH_2SO_3H$ + 5HBr + 5HCl
TYROSINE	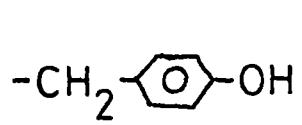	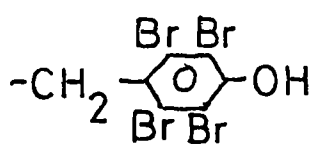	2+4 = 6	See text
TRYPTOPHAN	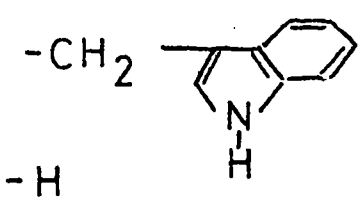	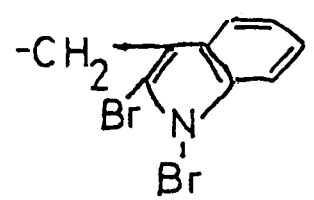	2+2 = 4	See text
PENTA-GLY	5 x -H		2	Peptide bonds inactive
TETRA-ALA	4 x $-CH_3$		2	Peptide bonds inactive
GLY-LEU-TYR	$-H + -C_4H_9$ + -TYR	See tyrosine	2+4 = 6	
TRI-TYROSINE	3 x -TYR	See tyrosine	2+12 = 14	

The tyrosine side chain is phenolic, and the hydroxyl group will direct substitution to the ortho-positions, the para-position being blocked. The amino acid group which is situated para to the hydroxyl will itself direct substitution to the meta-positions (with respect to the hydroxyl group). Thus electrophilic attack is directed to all four unsubstituted ring positions, but the stepwise substitution of bromine will deactivate this ring. The corrected bromine numbers of the four peptides, two of which contain phenolic side chains, were found to be helpful in determining the extent of ring substitution. The corrected bromine numbers for these peptides are themselves in the approximate ratio 1:1:3:7, and if it is assumed that the amine group in each peptide is fully brominated then these figures show that four molecules of hypobromite react with each phenolic side chain. Therefore the stoichiometric bromine number of tyrosine is 6.

iv) Comparison of n_{Br} and $n_{Br}(s)$.

The corrected and stoichiometric bromine numbers are compared in table IV.4. For the amino acids, with the exception of methionine (see below), there is good agreement between the two numbers. The peptides however all exhibit corrected bromine numbers which are considerably lower than their stoichiometric numbers. The peptide diffusion coeficients were estimated assuming the molecules to be spherical although they certainly are not. If this non-sphericity is taken into account then the estimated diffusion coefficients will be smaller, thus raising the value of the correcting ratio and corrected bromine number.

The amino acids studied were selected for their side chains rather than for their diffusion coefficients. The limited amount of data obtained from these compounds however confirms the validity of the extended RRDE titration theory, considering the limited accuracy of the estimated diffusion coefficients.

The results for methionine show poor agreemnt. This amino acid reacts with one molecule of BrCl, and has been reported (71) to react at pH 7

Table IV.4 Corrected and Stoichiometric Bromine Numbers

	n_{Br}	$n_{Br}(s)$	Agreement
Glycine	2	2	
Lysine	4.08 ± .05	4	Good (+ 2%)
Methionine	2.07 ± .05	3	Poor (- 30%)
Cystine	9.76 ± .21	9	Good (+ 8%)
Tyrosine	6.32 ± .08	6	Good (+ 5%)
Tryptophan	3.98 ± .11	4	Good (- 0.5%)
Penta-gly	1.55 ± .03	2	(- 23%)
Tetra-ala	1.57 ± .03	2	(- 22%)
Gly-leu-tyr	4.45 ± .06	6	(- 26%)
Tri-tyr	11.65 ± .16	14	(- 17%)

with one molecule of N - bromosuccinimide. This latter brominating reagent is hydrolysed in an aqueous medium to form succinimide and hypobromous acid. In both cases the reaction product is a sulphoxide (table IV.3), and at pH 7 the amine groups are not brominated. The bromination of methionine at pH 9.2 was further investigated by recording ring polarograms of hypobromite generated in a solution containing methionine. This technique was used in investigating the titration of glycine, and polarograms similar to figure IV.6 would be expected if the methionine side chain were unreactive (as sugguested by the corrected bromine number). Figure IV.23 presents the recorded polarograms; curves A and B were recorded before the addition of methione, the former at $i_D = 0$ and the latter at $i_D = 120\,\mu A$ (generating hypobromite). 10 ml of 10^{-3} M methionine solution were then added to the 100 ml of solution in the cell. Curve C was recorded at $i_D = 0$ and the wave at $E_R < -100$ mV is due to oxygen present in the methionine stock solution. The disc current was then restored to 120 μA and curve D was recorded; the virtual absence of any ring current at $E_R = +450$mV confirms the titration of methionine. At $E_R = -600$ mV the ring current is greater than the background level, but the recovery of hypobromite is not complete (cf figure IV.6). This result conflicts with the titration curve analysis: the ring polarogram results suggest that there is a side chain reaction in addition to the electrochemically reversible bromination of the amine group, while the corrected bromine number suggests that the side chain is unreactive. The reproducibility of polarogram D was poor, as was the titration of methionine, and repetition of these experiments is necessary to resolve this case.

The experiments described above were successful in the development of an electroanalytical technique for the determination of amino acids. The detection limit of the technique was pursued by titrating glycine at concentration increments of 10^{-7}M; the titration curves are presented in figure IV.24 where the effect of kinetics is again evident. These curves

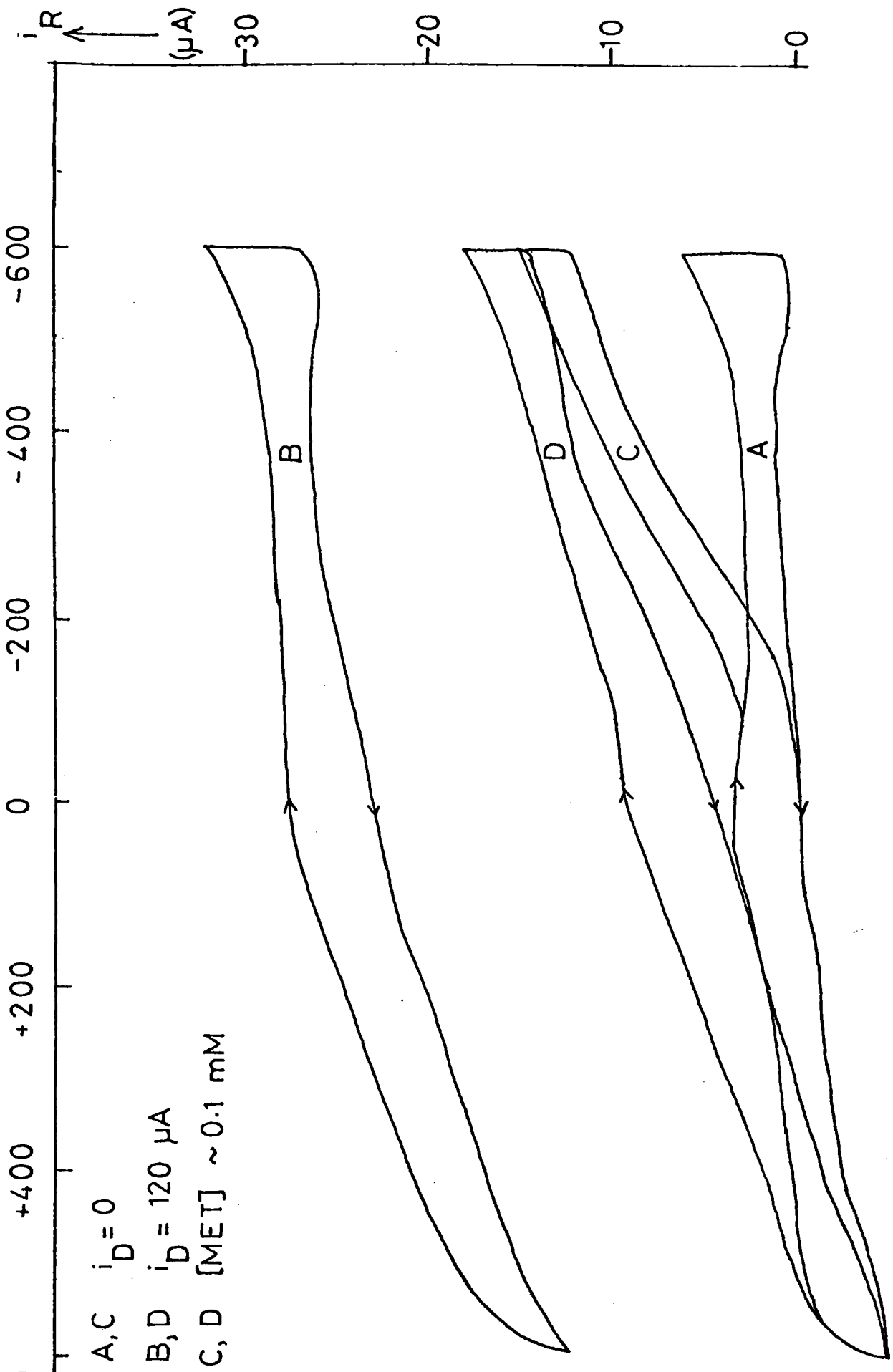

Figure IV. 23 Ring polarograms of hypobromite and methionine

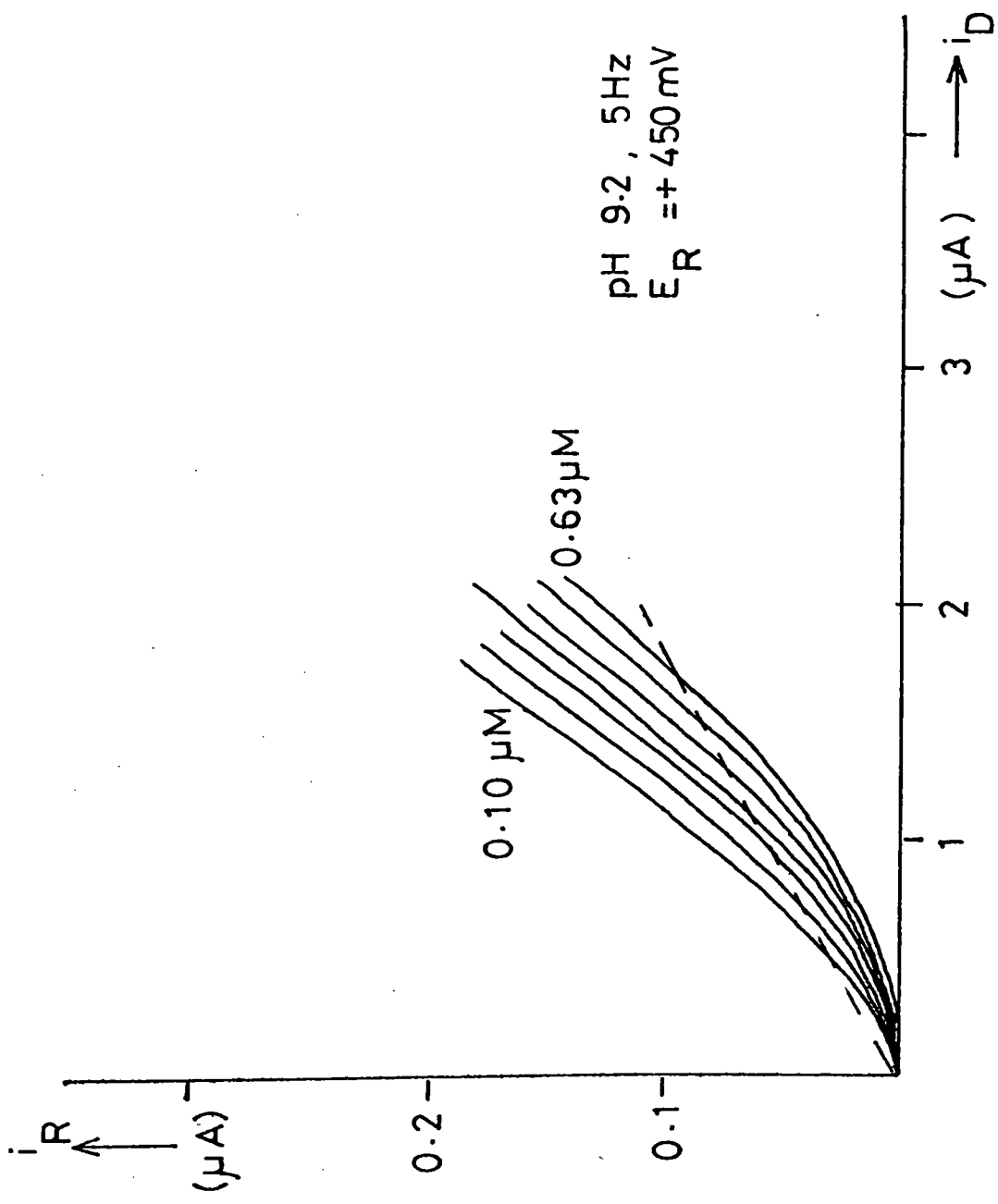

Figure IV. 24 Titration of glycine

have been analysed by the usual method, and the i_D' vs. a_∞ plot is shown in figure IV.25. The non-zero intercept is due to impurities in the background electrolyte which were not completely removed. Further reduction of this impurity level was not attempted because of evidence of impurities in the double distilled water (DDW) used to prepare the glycine stock solution - on adding 1 ml of DDW to the cell the displacement of the titration curve was observed to increase by the thickness of a line. The gradient of figure IV.25 is greater than that in figure IV.16 ($1.701 \pm .011$), which was recorded at a higher concentration range; the increase in gradient is presumably due to the impurities in the DDW. This plot implies a detection limit of 10^{-8}M, which may be lowered if the background electrolyte is further purified. The detection limit for other amino acids will be similar, and will be enhanced by side chain bromination.

3. THE TITRATION OF PROTEINS

The successful development of the determination of amino acids led to the titration of proteins under the same conditions. The proteins selected were the haem proteins, cytochrome c and haemoglobin; human and bovine serum albumins; the globulin, thyroglobulin; the phosphoprotein, phosvitin; and the enzyme α- amylase. These proteins were titrated over a range of concentrations- the titration curves are presented in figures IV.26 - 32 and all show kinetic effects. The curves have been analysed in the usual manner, and plots of i_D' vs. a_∞ are presented in figure IV.33. These plots show some curvature, which is most apparent for haemoglobin and human serum albumin. This is probably due to the large number of hypobromite molecules (see below) reacting with each molecule of protein at differing reaction rates - the simple titration curve theory was derived for the reaction $A + B \rightarrow C + D$. However the straight lines obtained indicate the feasibility of the titration as an analytical technique, and the

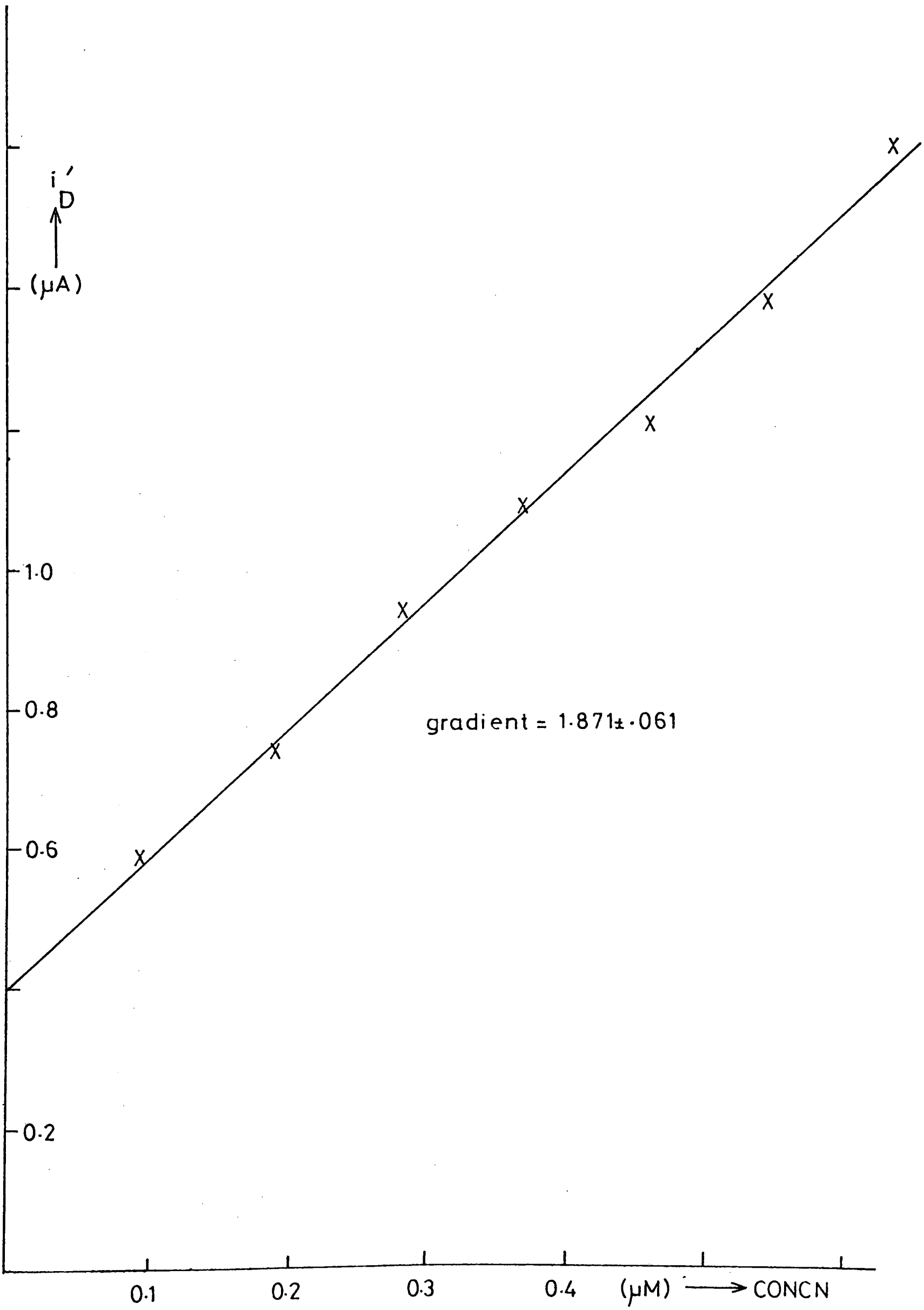

Figure IV. 25 Titration response of glycine at pH 9·2

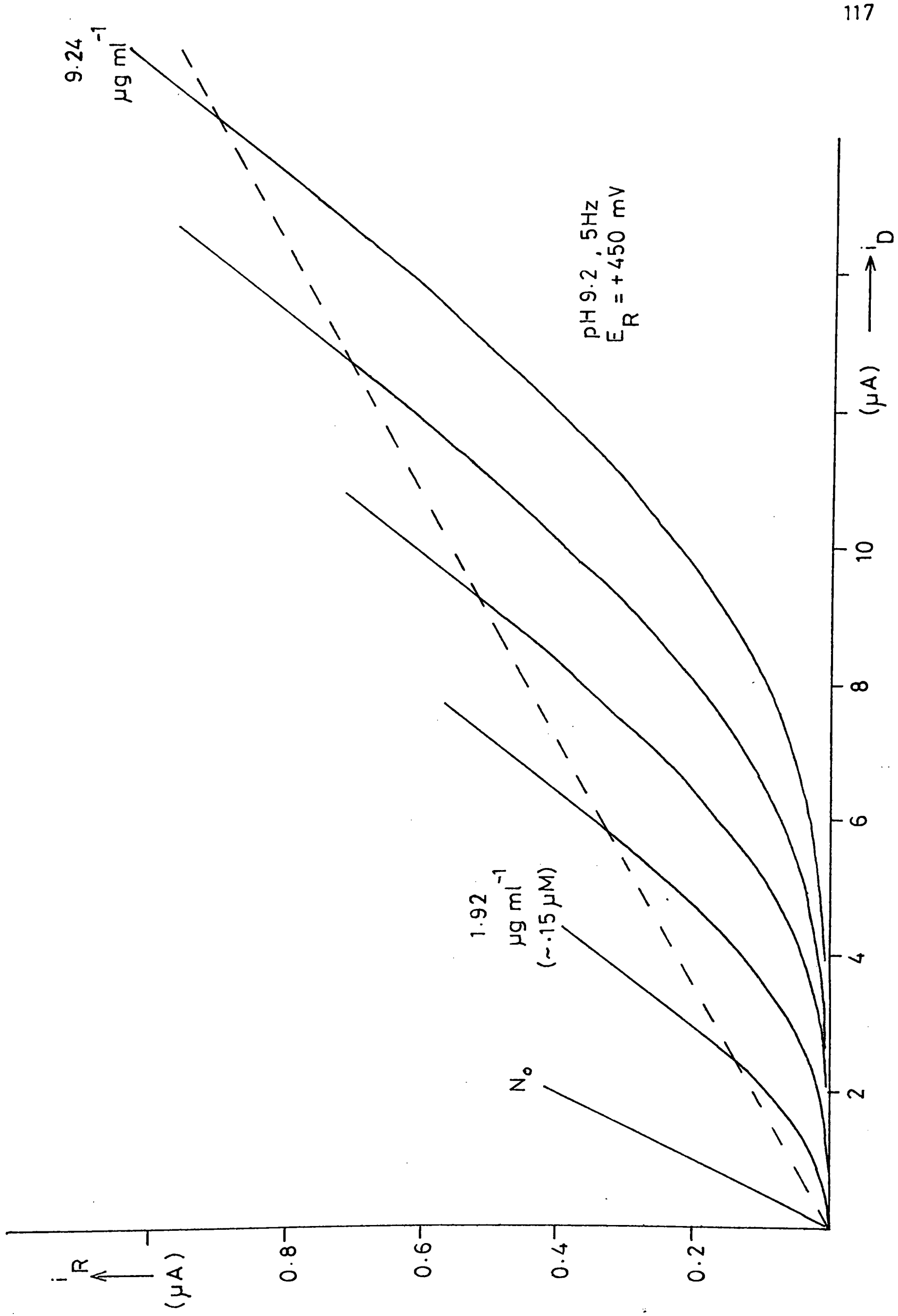

Figure IV. 26 Titration of cytochrome c

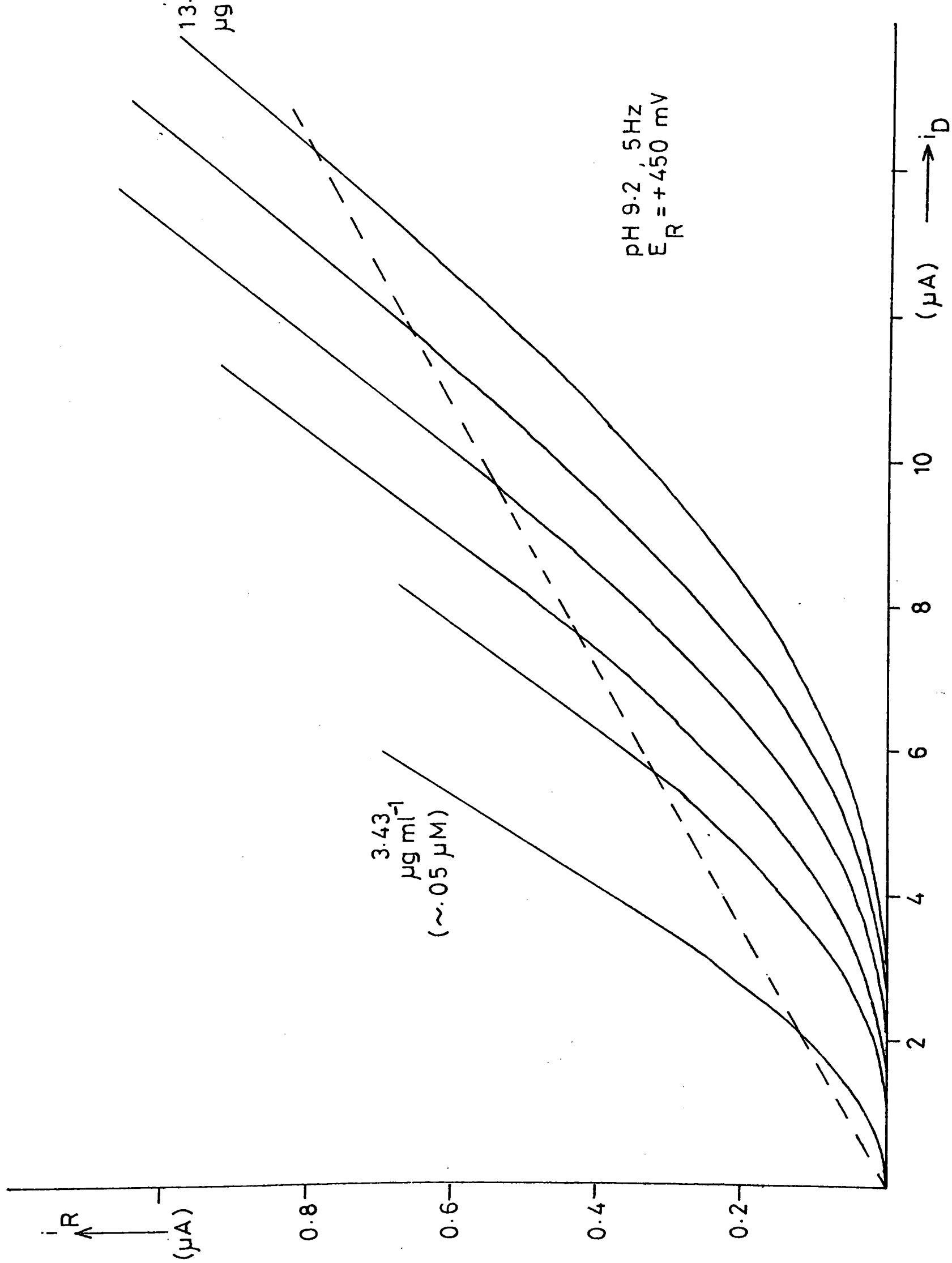

Figure IV. 27 Titration of haemoglobin

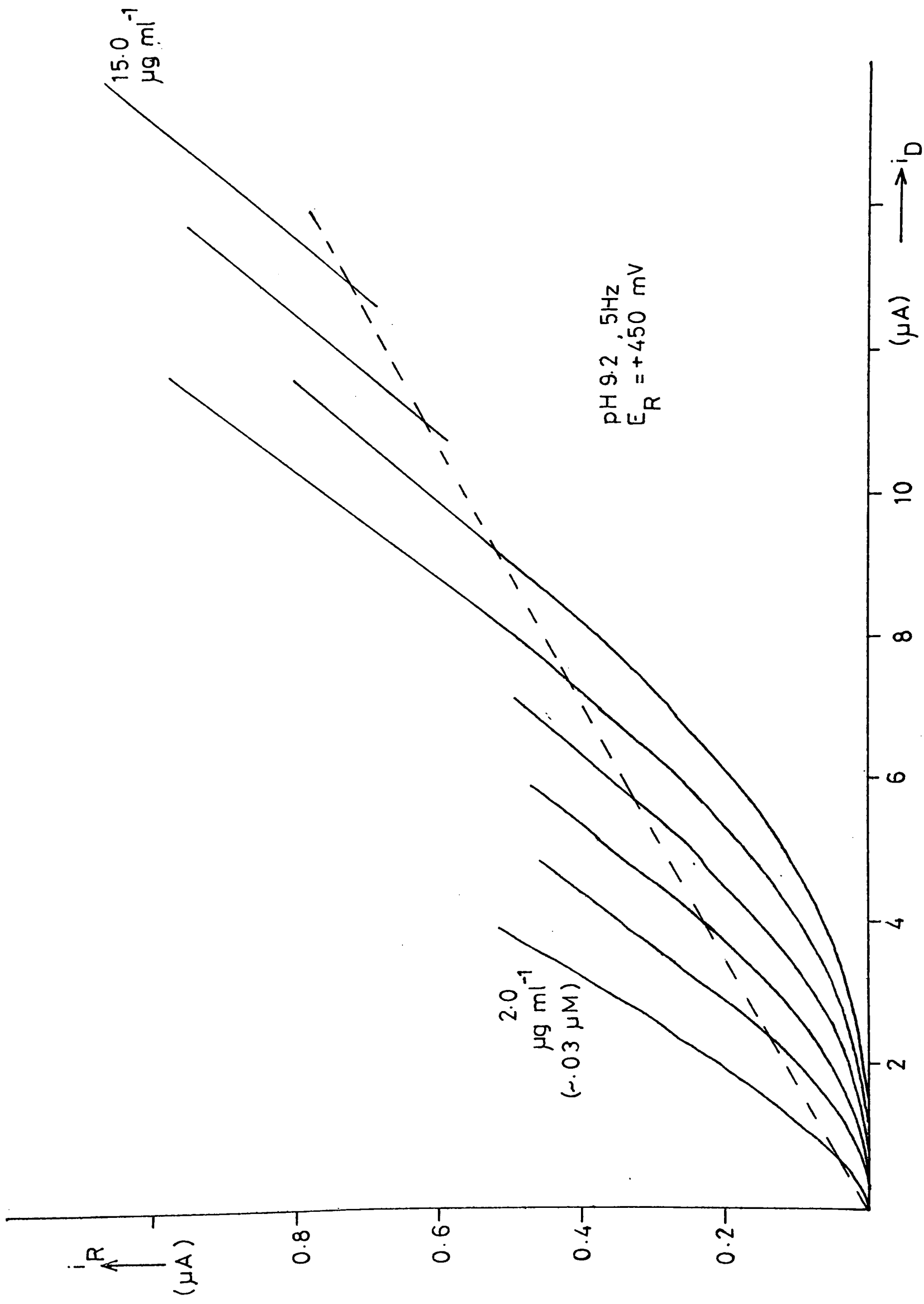

Figure IV. 28 Titration of HSA

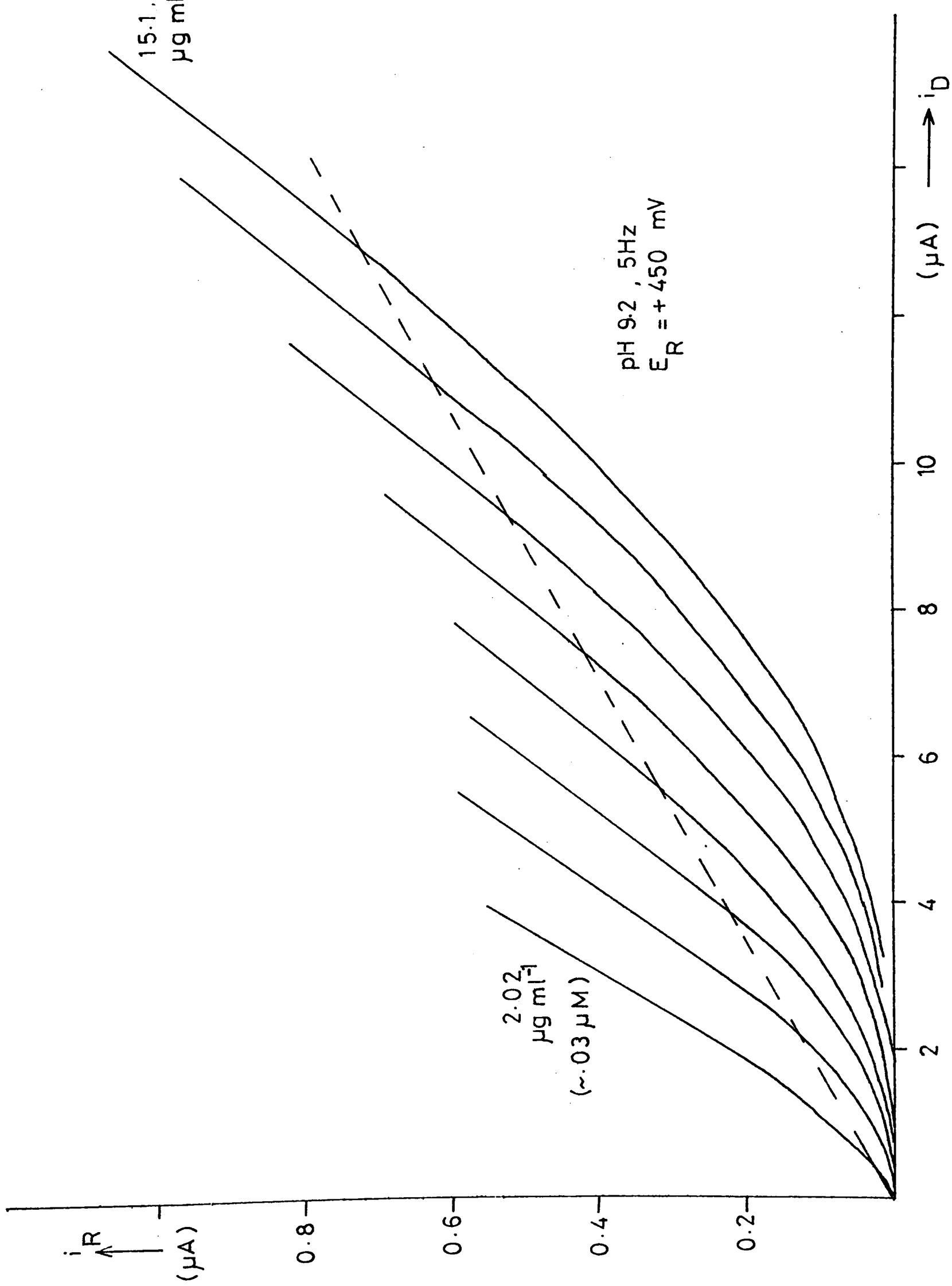

Figure IV. 29 Titration of BSA

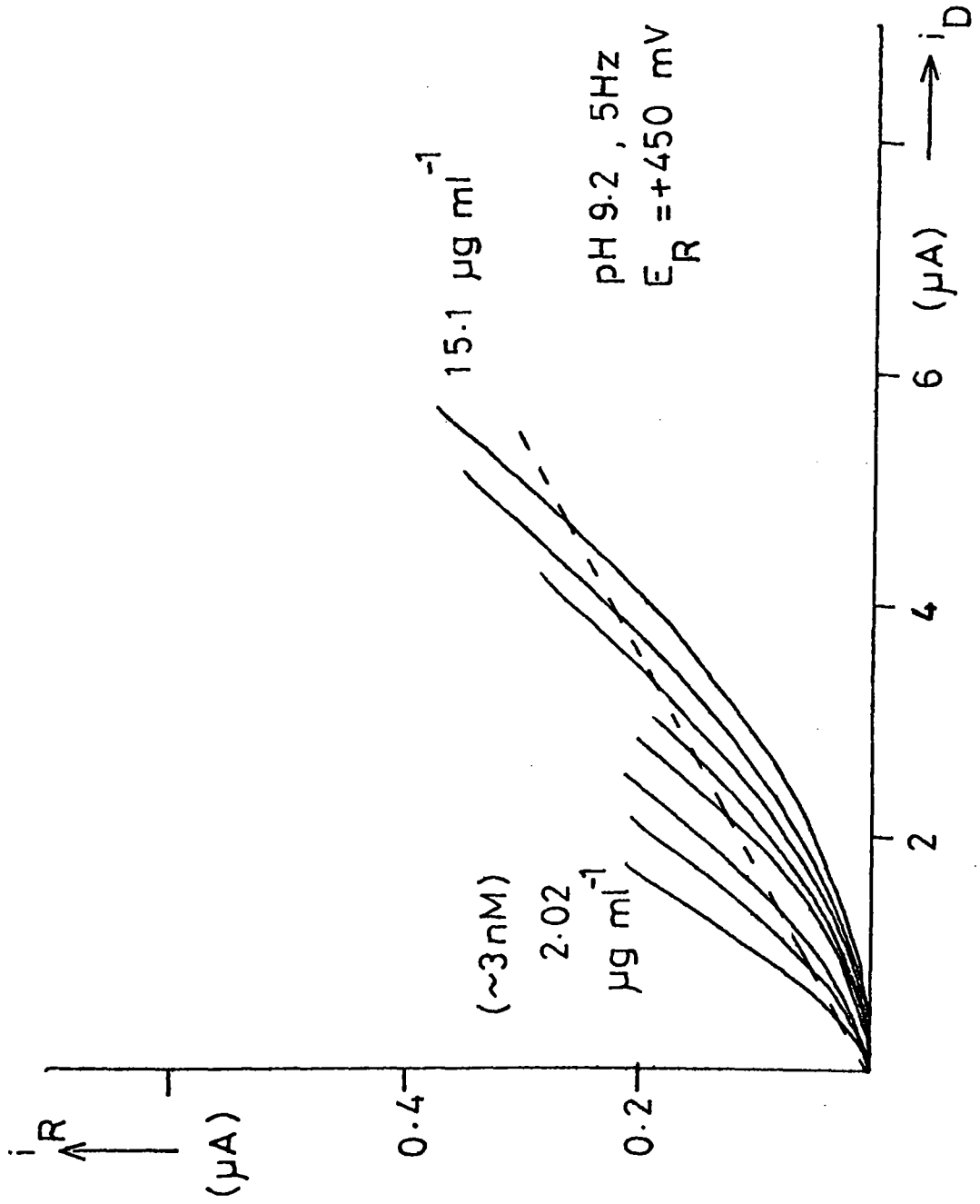

Figure IV. 30 Titration of thyroglobulin

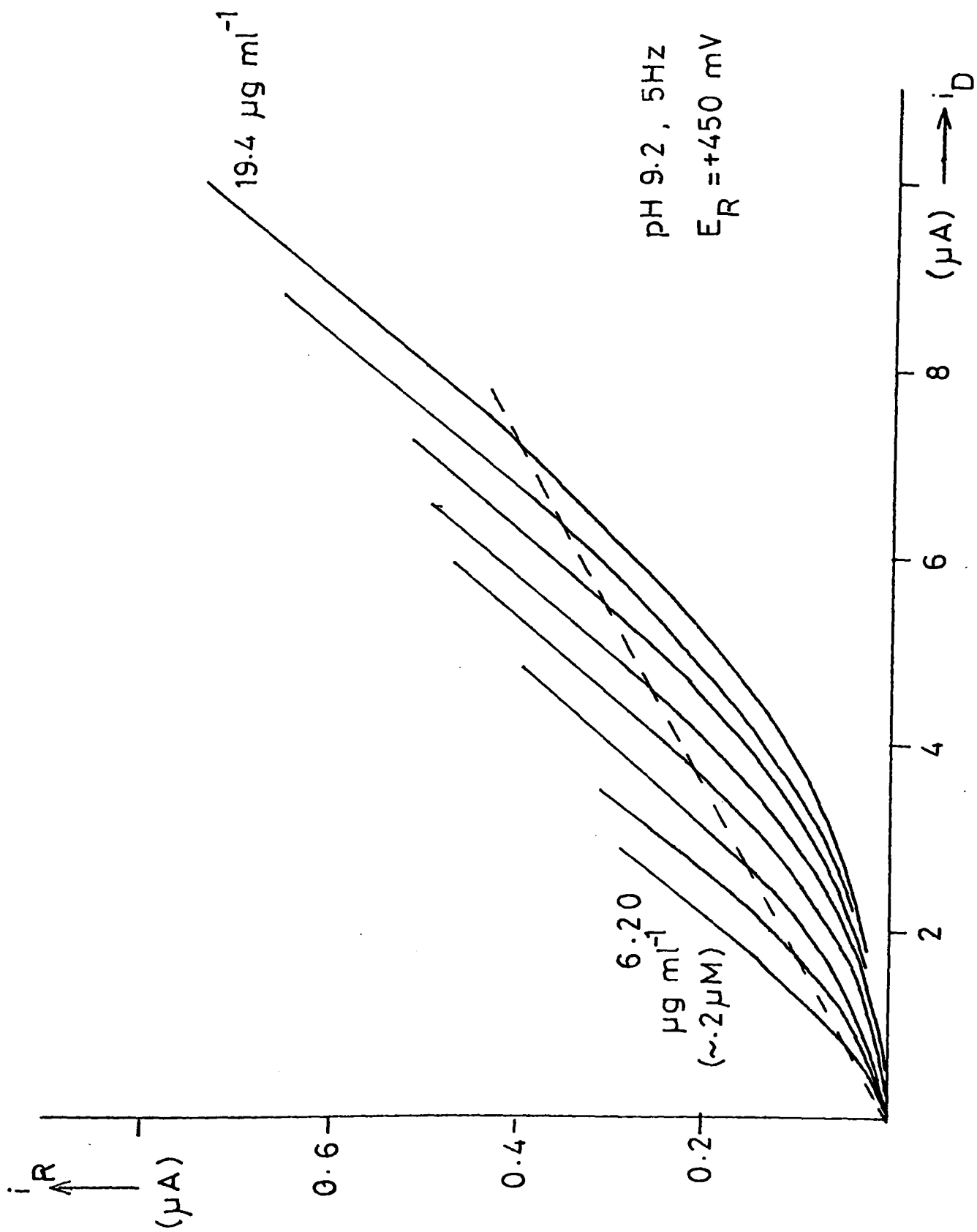

Figure IV. 31 Titration of phosvitin

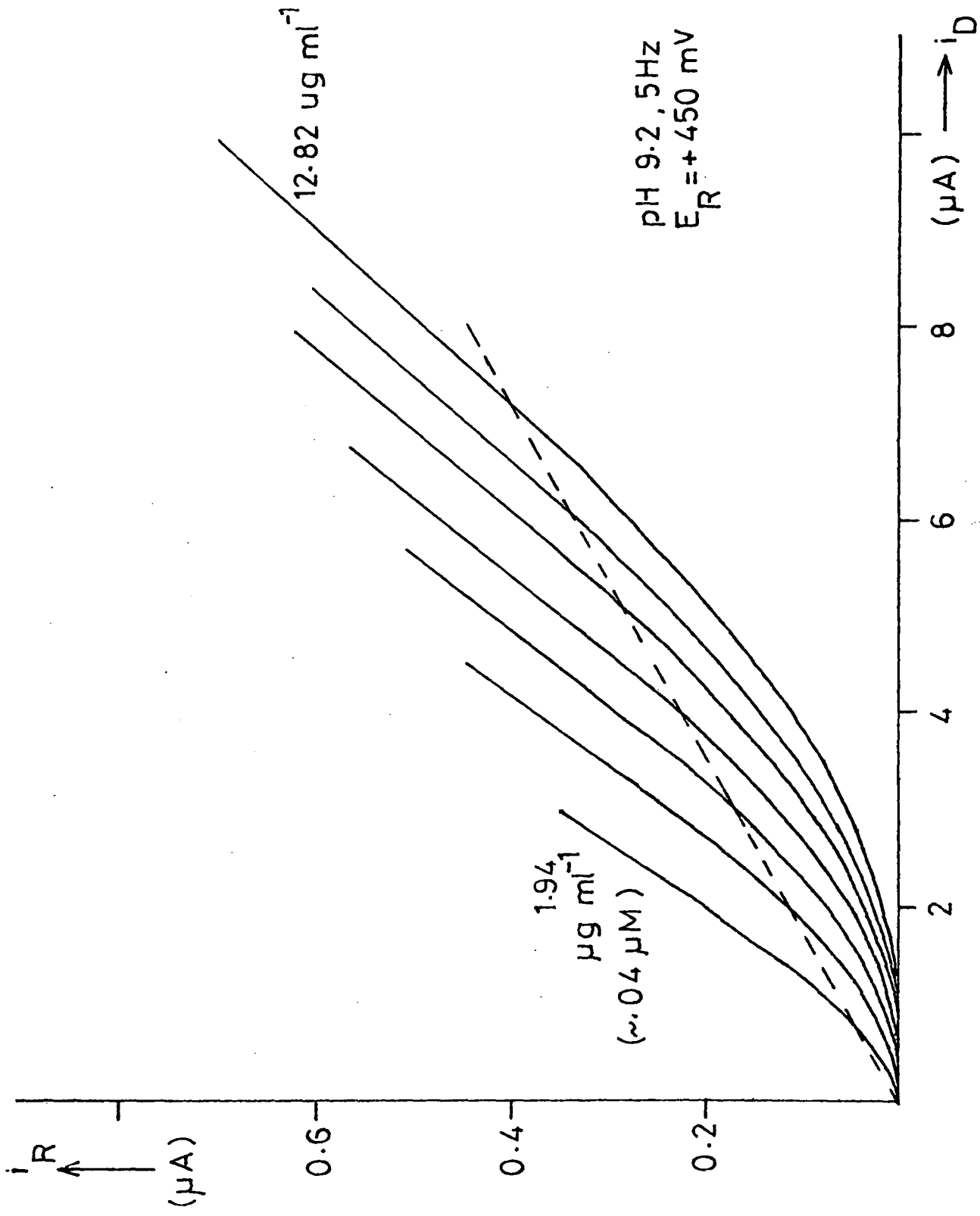

Figure IV.32 Titration of α-amylase

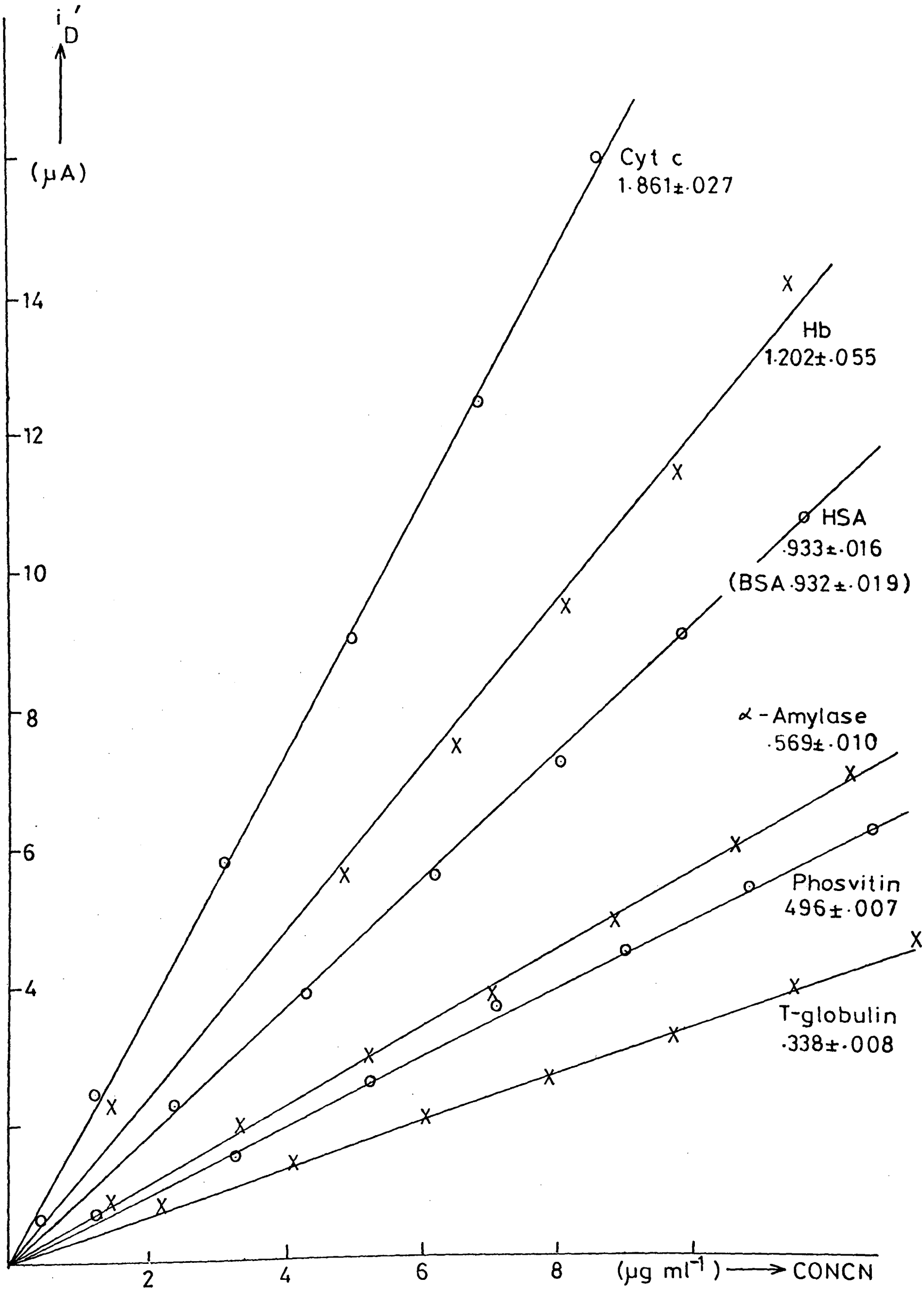

Figure IV.33 Titration response of proteins at pH 9·2

reproducibility of this method is demonstrated by the gradients for human serum albumin and bovine serum albumin being equal.

i) The Bromine Number, N_{Br}

In figure IV.33 the protein concentration is plotted as $\mu g\ ml^{-1}$, and the gradients are seen to vary between different proteins. In this form the gradients reflect the molecular weights and diffusion coefficients of the proteins in addition to the stoichiometry of their titration. The gradients are collected in table IV.5, column 1 and have been converted to μA/μM in column 2. This enables division by the arsenic gradient (table IV.1) to give the bromine number which is presented in column 3. This experimental bromine number already demonstrates that many molecules of hypobromite are reacting with each protein molecule.

ii) The Corrected Bromine Number, n_{Br}

The diffusion coefficients of many proteins have been determined, and values were found for all the proteins studied in this work. Some of these values were determined at 20°C, and they have been converted to 25°C using the Stokes - Einstein equation and the viscosity of water; the diffusion coefficients are listed in table IV.6. Those of bovine serum albumin and human serum albumin differ by 3%, and the quoted values are for preparations of MW 67,000 and 68,500 respectively. These variations with protein preparation appear to be common, so that the diffusion coefficient of human serum albumin has been used to correct both albumin bromine numbers. The corrected bromine number has been determined using the estimated diffusion coefficient of glycine.

$$n_{Br} = N_{Br} \left(\frac{D_{GLY}}{D_{PROT}} \right)^{2/3}$$

and is presented in table IV.6

Table IV 5 Bromination of Proteins

	Gradient		
	$\mu A/\mu g\ ml^{-1}$	$\mu A/\mu M$	Bromine number
Cytochrome c (MW 12,384)	1.861 ± .027	23.04 ± 0.33	27.2 ± 0.5
Haemoglobin (MW 64,500)	1.202 ± .055	77.5 ± 3.5	91.4 ± 4.3
HSA (MW 69,000)	.933 ± .016	64.4 ± 1.1	76.0 ± 1.5
BSA (MW 69,000)	.932 ± .020	64.3 ± 1.3	75.8 ± 1.7
Thyroglobulin (MW 660,000)	.3376 ± .0081	233 ± 5.3	263 ± 7
Phosvitin (MW 34,000)	.4959 ± .0066	16.86 ± 0.22	19 ± 0.3
α - Amylase (MW 48,7000)	.569 ± .010	27.71 ± 0.48	32.7 ± 0.6

Table IV.6 Diffusion Coefficients and Corrected Bromine Numbers of Proteins

	D^{o}_{25}		n_{Br}
	($x10^{11}/m^2s^{-1}$)		
Cytochrome c	14.9	(73)	95.7 ± 1.8
Haemoglobin	7.9	(74)	491 ± 23
HSA	7.00	(73)	443 ± 9
BSA	6.8	(73)	442 ± 10
Thyroglobulin	2.93	(75)	2740 ± 70
Phosvitin	5.28	(73)	140 ± 2
α - Amylase	9.15	(73)	159 ± 3

iii) The Stoichiometric Bromine Number, $n_{Br}(s)$

The published amino acid compositions of α- amylase (76), haemoglobin (77), cytochrome c (78), human serum albumin (79) and bovine serum albumin (79) are summarised in table IV.7 (the other amino acids do not possess brominatable side chains). Amino acid stoichiometric bromine numbers are given in the last column of table IV.7, and are lower than those in table IV.4 since the amine groups are participating in peptide bonds; the stoichiometric bromine number for the haem group assumes total bromination. This data enables the calculation of protein stoichiometric bromine numbers which are compared with the corrected numbers in table IV.8

iv) Comparison of n_{Br} and n_{Br} (s)

For the haem proteins and albumins there is good agreement between the two bromine numbers. The calculation of stoichiometric bromine numbers has assumed that the protein is totally accessible, but the observation that this number is, for α-amylase, in this case higher than the corrected bromine number suggests that this assumption is incorrect. The ratio of n_{Br} to n_{Br} (s) cannot be correlated with molecular weight, but might be related to protein tertiary structure.

These bromine numbers indicate the large number of hypobromite molecules reacting with each protein molecule. It is upon this that the sensitivity of the technique depends - the reaction of 100 molecules of hypobromite with a protein is equivalent to the exchange of 200 electrons. This chemical amplification gives the amperometric titration of proteins much greater sensitivity than a DC voltammetric techniqe. The titration of low concentrations of cytochrome c is illustrated in figure IV.34, the concentration increments being 0.1 μg ml^{-1}. The plot of i_D' vs a_∞ is presented in figure IV.35, where the non-zero intercept is again due to residual impurities in the background electrolyte. The gradient of this line

Table IV.7 Amino Acid Compositions (moles/mole) of Proteins

Amino Acid	α- Amylase (Bacillus Subtilus)	Haemoglobin (Human)	Cytochrome c (Horse Heart)	HSA	BSA	Amino Acid Stoichiometric Bromine Number
Lysine	25	44	17	58	59	2
Cystine	-	3	1	17	17	5
Tyrosine	24	12	4	18	19	4
Tryptophan	15	6	1	1	2	2
Methionine	5	6	2	6	4	1 (71)
Cysteine	-	-	-	1	1	3 (71)
Histidine	12	38	3	16	17	3
Phenylalanine	18	30	3	30	27	3
Haem	-	4	1	-	-	24

Table IV.8 Corrected and Stoichiometric Bromine Numbers of Proteins

	n_{Br}	$n_{Br}(s)$	Agreement
Cytochrome c	95.7 ± 1.8	103	- 7%
Haemoglobin	491 ± 23	477	+ 3%
HSA	443 ± 9	424	+ 4%
BSA	442 ± 10	424	+ 4%
Thyroglobulin	2740 ± 70	-	
Phosvitin	140 ± 2	-	
α - Amylase	159 ± 3	273	- 42%

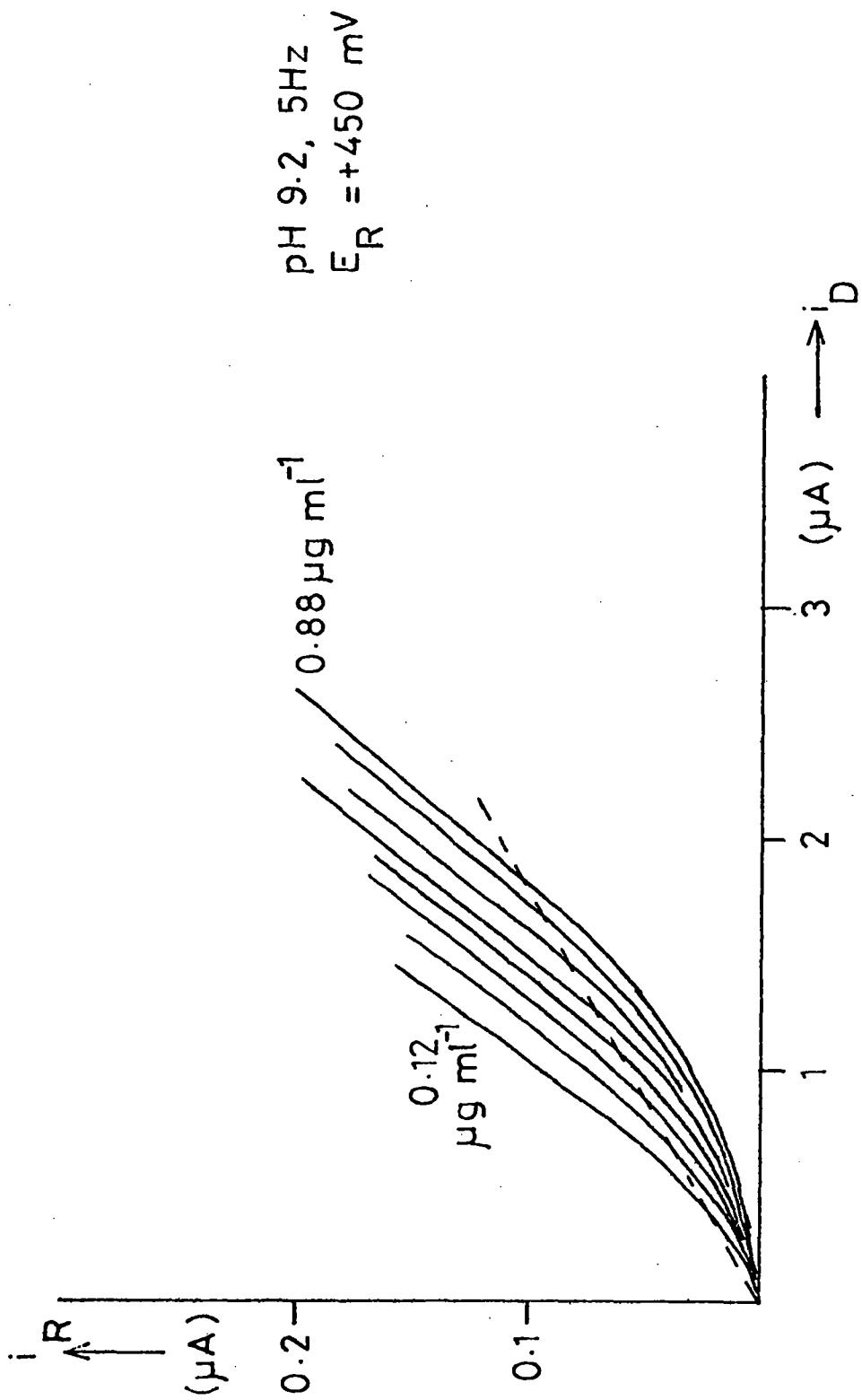

Figure IV. 34 Titration of cytochrome c

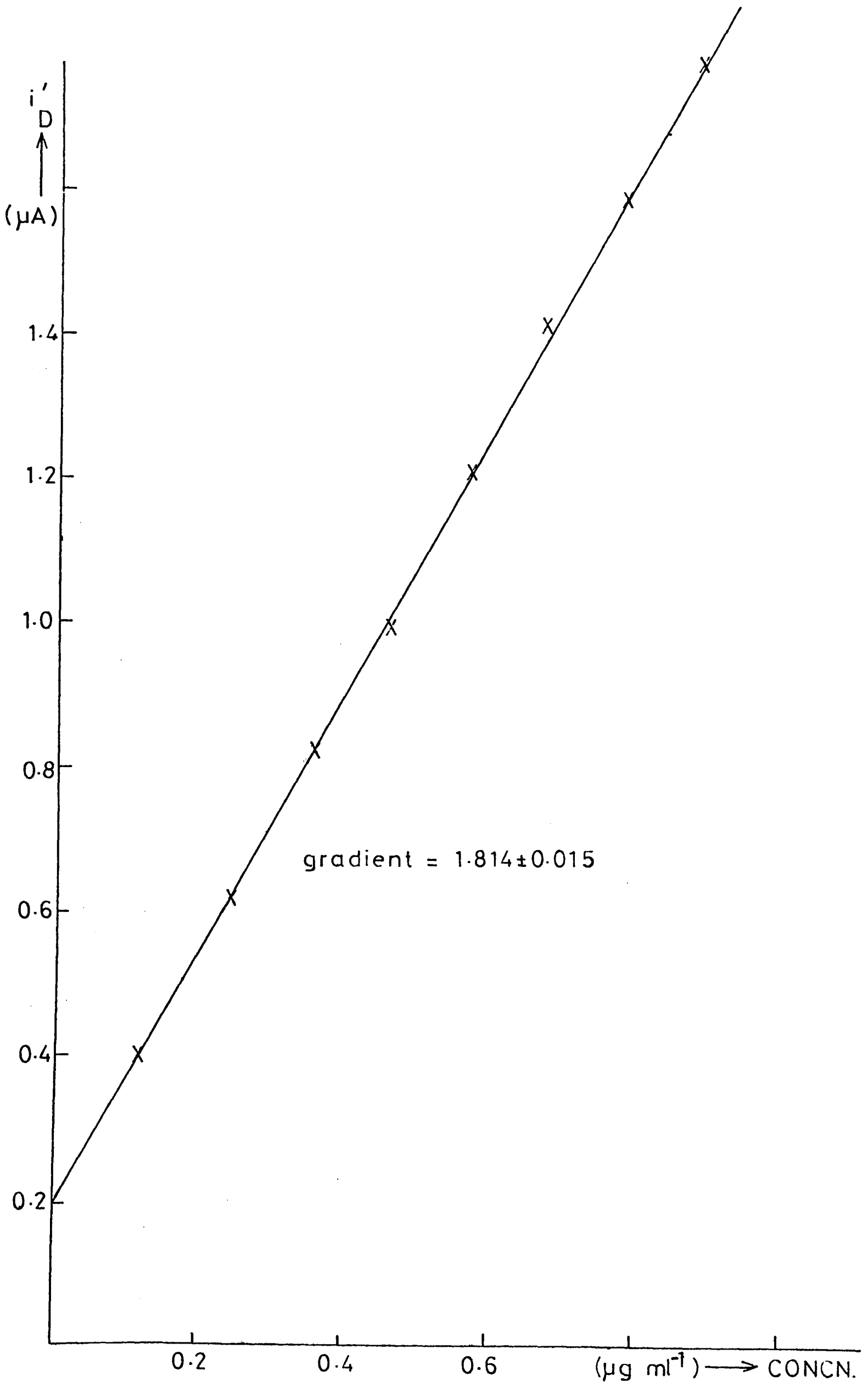

Figure IV.35 Titration response of cytochrome c at pH 9.2

(1.814 $\pm$ .015) agrees well with that in figure IV.33 (1.861 $\pm$ .027) and suggests a detection limit for this protein of 10 ng ml^{-1} which may be lowered if the background electrolyte is further purified. This detection limit is equivalent to $\sim 10^{-9}$M, the chemical amplification being $\sim$150 ($\sim$25 due to N_{Br}, a factor of 2 because of the two electrons transferred in making one molecule of hypobromite, and a further factor of 3 since i_D' corresponds to a normalised disc current of $i_D/M \sim 3$).

4. THE IDENTIFICATION OF PROTEINS

The development of a general (i.e. non-specific) electroanalytical technique for the determination of proteins has been described in the preceding sections of this chapter. In order to determine absolute concentrations it is necessary to know which protein is present, since the response varies for different proteins. This is not a great disadvantage in chromatography since a detector is primarily required to indicate changes in concentration. However it would be a bonus if some indication of the identity of a protein could be obtained during its titration. In the first part (a) of this section additional measurements at pH9.2 are described; the second part (b) of this section presents the results of titrations performed at pH5.

a) Titrations at pH9.2

The bromination of the amine group has been shown to be electrochemically reversible (section IV.2.a, figure IV.6), i.e. the bromoamine group can be reduced back to the amine group. Figure IV.7 demonstrated that the displacement of an amine/hypobromite titration curve can be altered by varying the ring electrode potential. The implications of this are that the bromination of amine-containing side chains can be "switched off" by using a reducing ring electrode potential, and the titration curve displacement of a protein will differ at E_R = + 450mV and - 500mV. The relative displacements will reflect the ratio of all brominatable side chains (+ 450 mV) to non-amine side chains (-500 mV). This ratio might be useful in identifying proteins, and the data in table IV.7 enables the estimation of two stoichiometric bromine numbers; the first, n_{Br} (s, total), is for the reaction of all brominatable side chains; the second, n_{Br} (s, partial), omits the reaction of amine containing side-chains. The amino acid partial stoichiometric bromine numbers are the same as the total numbers in

table IV.7 except for lysine (= 0), tryptophan (= 1) and histidine (= 2). Thus the partial and total protein stoichiometric bromine numbers are

	n_{Br}(s, partial)	n_{Br}(s, total)	ratio
HSA	289	424	1.47
α - Amylase	194	273	1.41
Haemoglobin	337	477	1.42
Cytochrome c	63	103	1.63

The ratios show that for cytochrome c 40% of the titration is due to amine containing groups, while for the other proteins only 30% of the total displacement may be ascribed to amines.

The feasibility of this method of identification was first tested using the peptide bacitracin. The composition of this natural product is illustrated in figure IV.36; the terminal amine group and ornithyl will be reversibly brominated while the cysteinyl,phenylalanyl and histidinyl residues will be irreversibly brominated. The recorded titration curves are shown in figure IV.37 and do display different displacements.

The method was then applied to proteins, but without success. This failiure was investigated by generating hypobromite at the disc electrode and recording ring polarograms in a solution containing protein. The results are presented in figure IV.38 (human serum albumin) and figure IV.39 (haemoglobin), and may be interpreted in the same manner as figure IV.6 and IV.23. The reduction in ring current from B to D is constant throughout the range investigated, there being no indication of electrochemical reversing of bromination. The analysis above predicted that human serum albumin and haemoglobin should exhibit ~30% reversibility. The failure to observe this must be due to the inability of the bromoamine groups to exchange electrons with the ring electrode. During homogeneous reaction in solution most amine groups will encounter and react with hypobromite molecules; but when the "bromo-protein" arrives at the ring electrode surface only those bromoamine groups which are near to the electrode can be reduced.

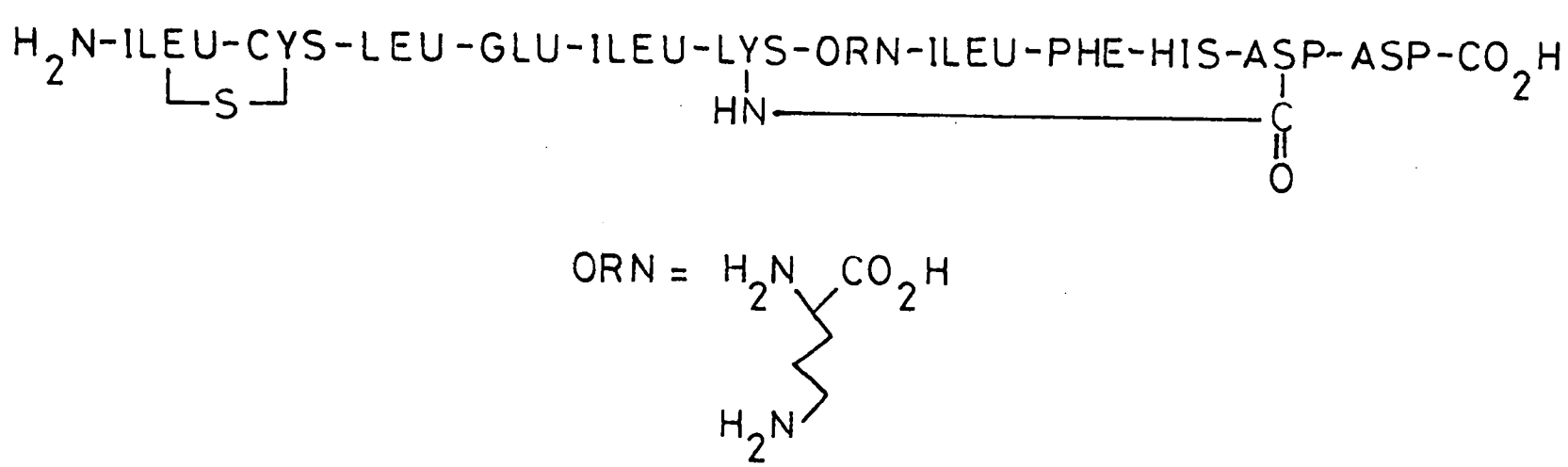

Figure IV.36 Bacitracin

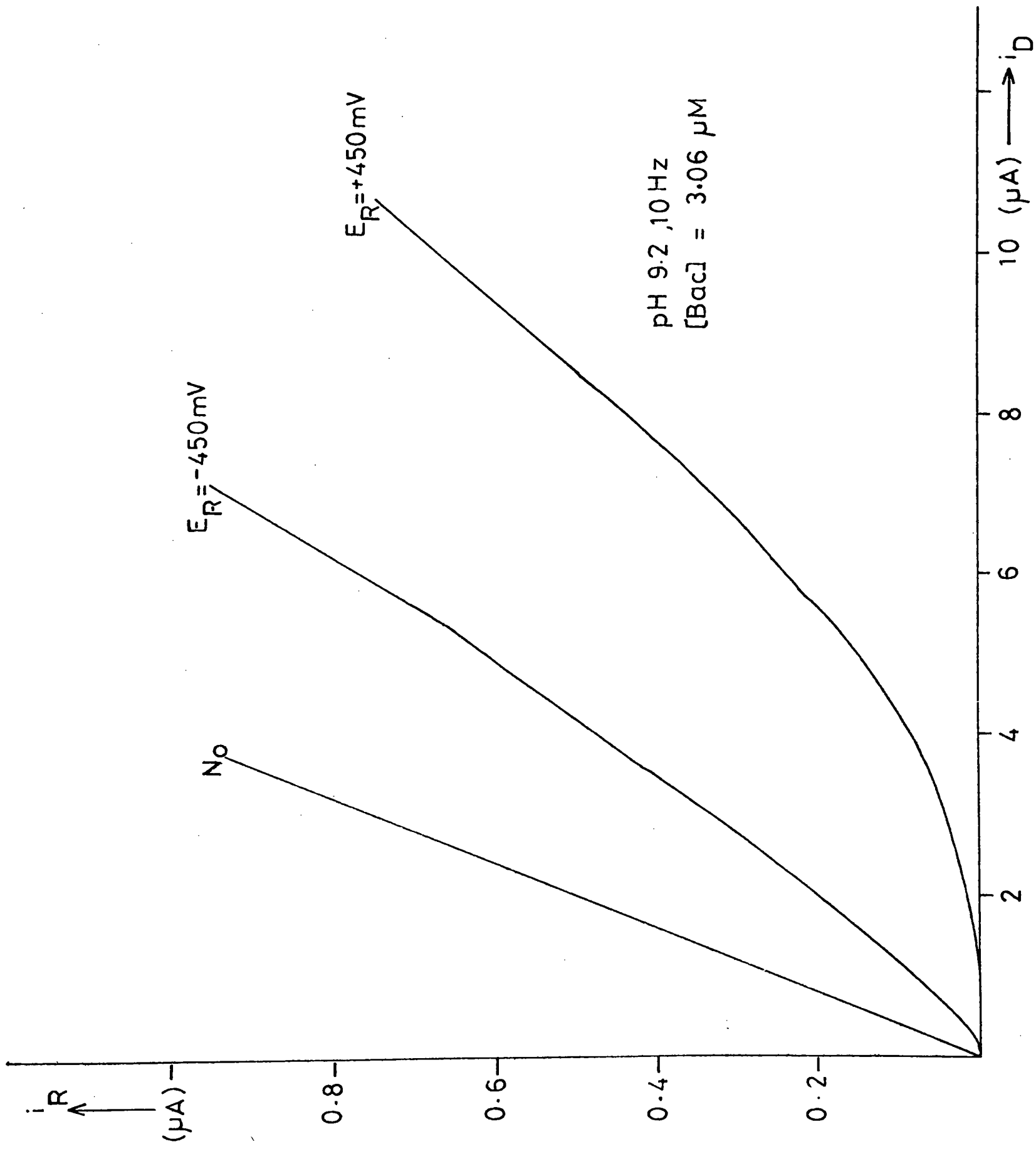

Figure IV.37. Effect of ring potential on bacitracin titration curves.

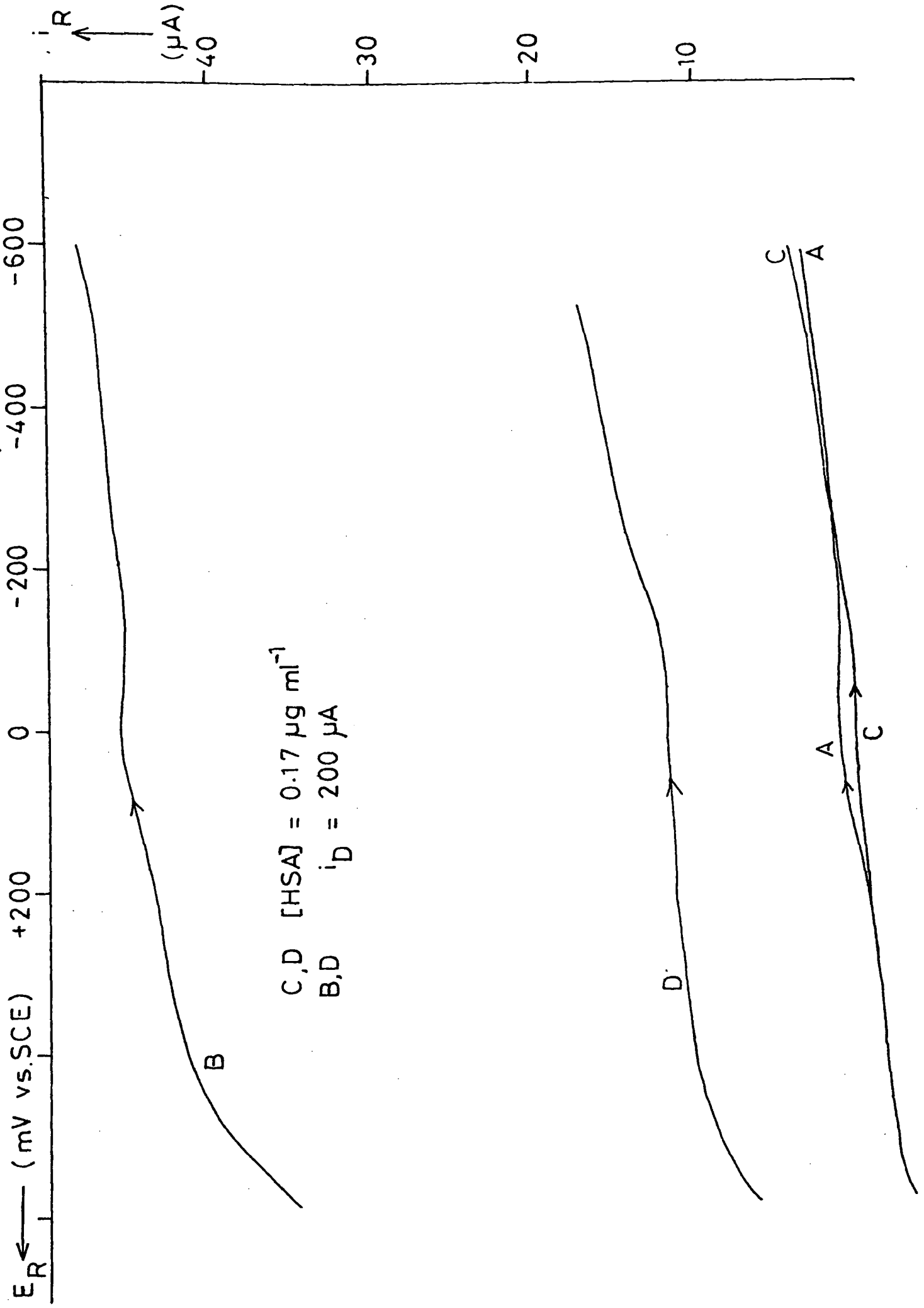

Figure IV. 38 Ring polarograms of hypobromite and HSA

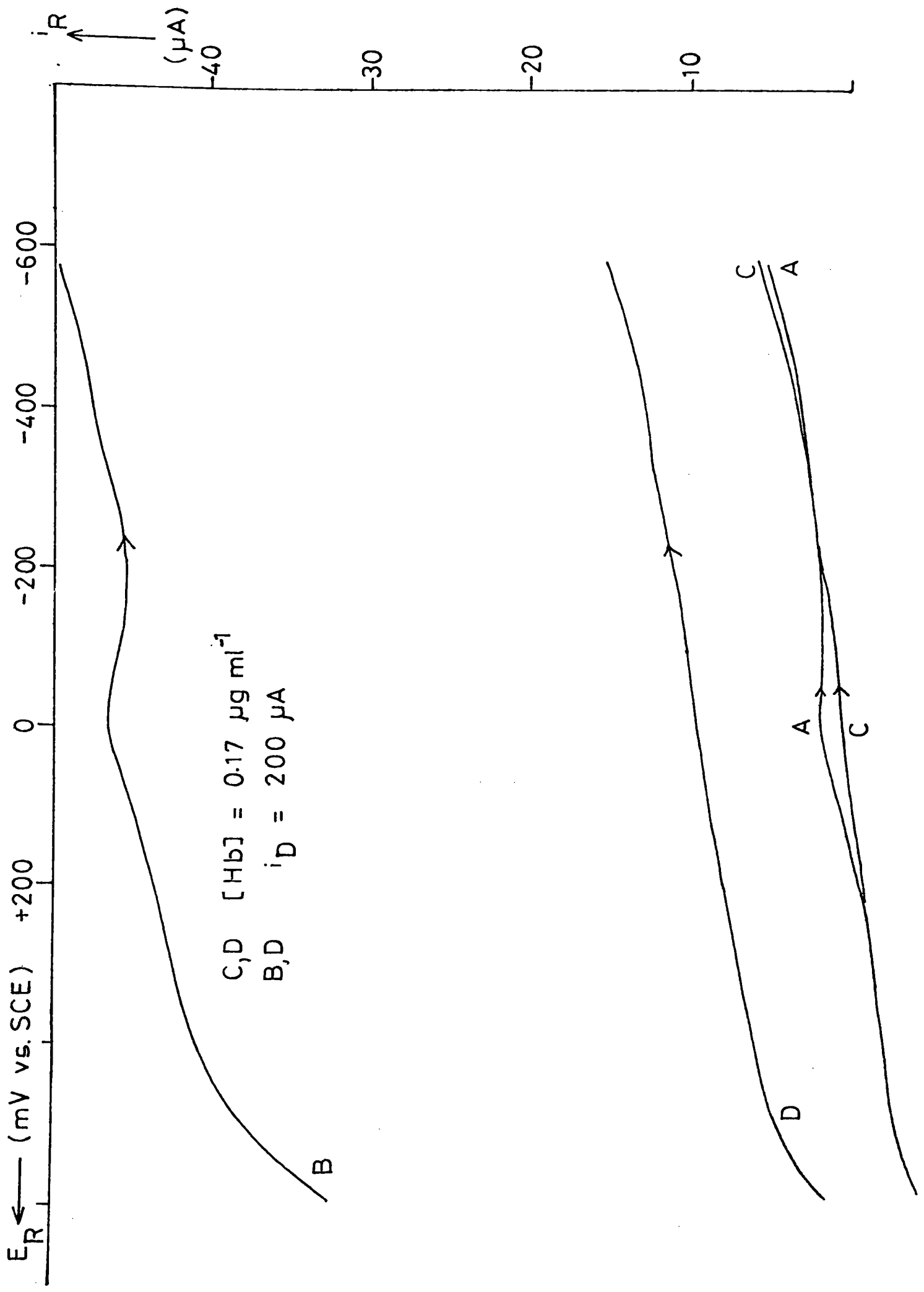

Figure IV.39. Ring polarograms of hypobromite and haemoglobin

All of the titration curves presented in this chapter have exhibited kinetic effects - increased ring currents, in the non-linear region of the titration curve, due to penetration of hypobromite past the reaction boundary. The extent of penetration, and the size of the kinetic ring currents, depends upon the rate of reaction. The RRDE theory of second order reactions predicts that (equation I.33)

$$i_{R,\varkappa} = 0.21\pi\, r_1^2\, nFD\omega^{3/2}\, \nu^{-1/2}\, k_2^{-1}$$

where k_2 is the rate constant and $i_{R,\varkappa}$ is the ring current observed at the point on the titration curve corresponding to the reaction boundary being situated on the inside edge of the ring electrode ($\beta_J = 0$). This ring current is independent of concentration (section I.2.d) and, through the size of the rate constant, may indicate what titration reaction is occuring. The applicability of this to protein bromination was investigated by measuring $i_{R,\varkappa}$ values for haemoglobin and human serum albumin. These are plotted against concentration in figure IV.40 and it can be seen that equation I.33 is not obeyed. This failure may again be attributed to the fact that the RRDE theory was derived for the simple reaction A + B $\rightarrow$ C + D whereas this work has shown that many molecules of titrant react with one molecule of protein.

b) Titration at pH5

Since additional measurements at pH9.2 were not helpful it was decided to repeat the titration of proteins at a different pH. The pH chosen was 5 since amine groups will be protonated and unreactive in this acidic medium (at pH5 the oxidised bromide product is bromine rather than hypobromite). The ratio of bromine numbers determined at the two pH values may then help to identify the protein concerned. This method of identification therefore returns to the total and partial bromine numbers of section IV.4.a., the amine group bromination being "switched off" by protonation instead of a ring electrode potential change. However the

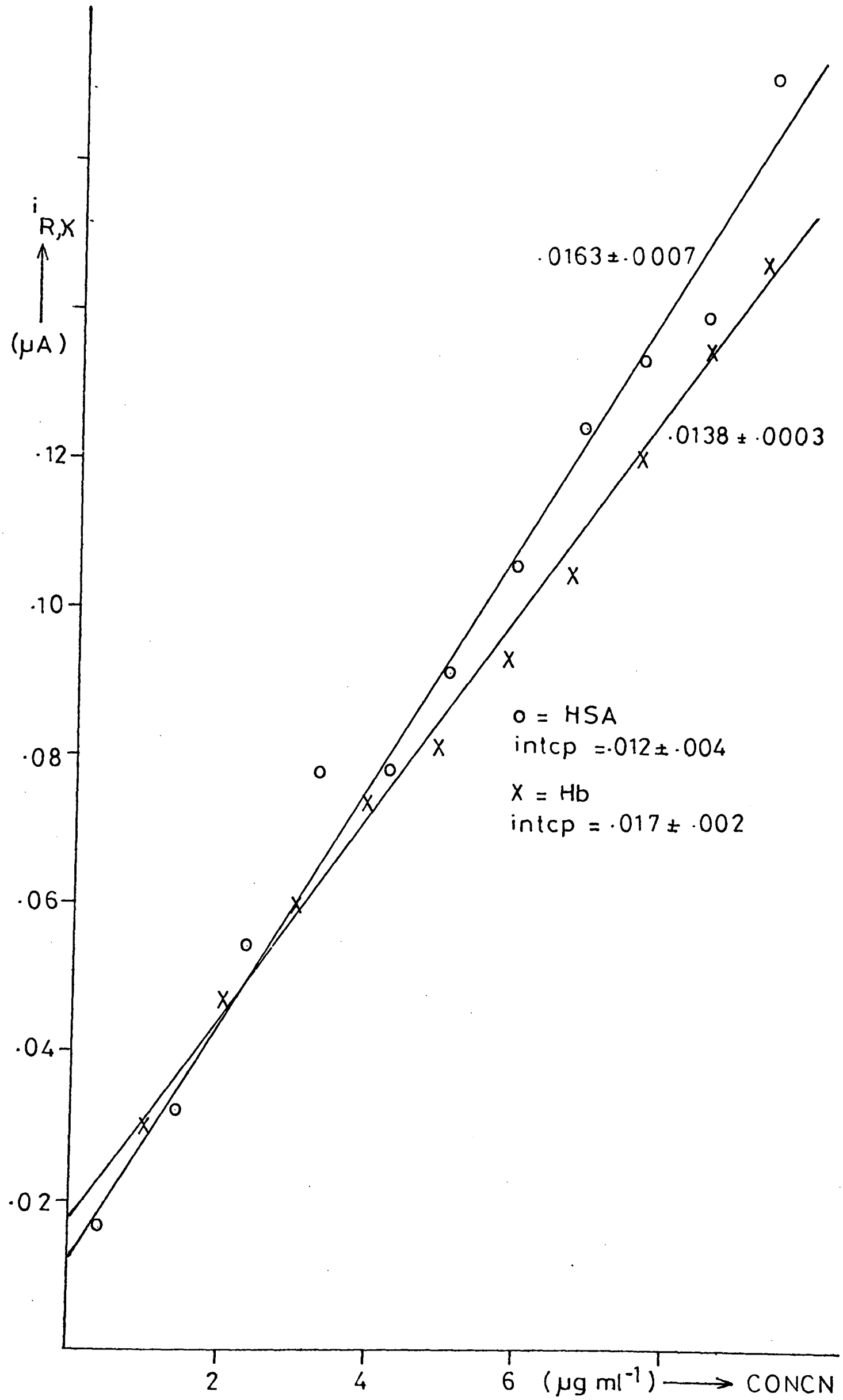

Figure IV.40 Kinetic ring currents of HSA and Hb

reaction of other groups may be affected by the pH change.

The titration of proteins at pH5 was investigated using a phosphate buffer (10 ml 0.2M Na_2HPO_4 + 470 ml 0.2M NaH_2PO_4, diluted to 1 litre) containing potassium bromide at a concentration of 0.5M. The pH of this solution was measured and found to be 4.9. The proteins were titrated at the RRDE using a ring potential of +100 mV (vs. SCE), and the titration curves are presented in figures IV.41 - 47.

The curves were analysed by the usual method, and the plots of i_D' vs. concentration, which have again been adjusted to pass through the origin, are presented in figures IV.48 and IV.49. As at pH 9.2 the gradients vary from protein to protein, and BSA and HSA show similar responses. The gradients are collected in table IV.9, where they may be compared with those obtained at pH 9.2. Once again arsenic (III) was titrated as a reference - the gradient differs at the two pH values used since electrodes of different geometry were used (Appendix 5; in both cases a line of gradient $N' = 0.0558$ was used to analyse the curves). It can be seen that the extent of titration at pH 5 is much less than at pH 9.2; the last column of table IV.9 presents the ratio of the titration responses, allowance having been made for the difference between electrodes. The total/partial stoichiometric bromine number ratios calculated in section IV.4a are smaller than these pH ratios which indicates that other groups, in addition to amines, are inactivated by the pH change. The calculation and correlation of corrected and stoichiometric bromine numbers has not been attempted at pH 5.

The pH ratios presented in the last column of table IV.9 do enable some degree of protein identification, although they would not permit differentiation of haemoglobin and thyroglobulin or human and bovine serum albumin. A proposed application of these ratios in the identification of proteins is further described in chapter VI.

Table IV.9 Titration of Proteins at pH 5

	Gradient		pH 9.2/pH 5
	pH 9.2	pH 5	
Arsenic	0.848 ± 0.008	0.9140 ± 0.0034	1
Cytochrome c	1.861 ± 0.027	0.3394 ± 0.0133	5.91 ± .25
Haemoglobin	1.202 ± 0.055	0.3527 ± 0.0092	3.67 ± .20
HSA	0.933 ± 0.016	0.1144 ± 0.0027	8.80 ± .26
BSA	0.932 ± 0.020	0.1091 ± 0.0036	9.20 ± .36
Thyroglobulin	0.338 ± 0.008	0.0980 ± 0.0028	3.71 ± .14
Phosvitin	0.496 ± 0.007	0.0345 ± 0.0011	15.50 ± .54
α -Amylase	0.569 ± 0.010	0.1887 ± 0.0101	3.25 ± .18

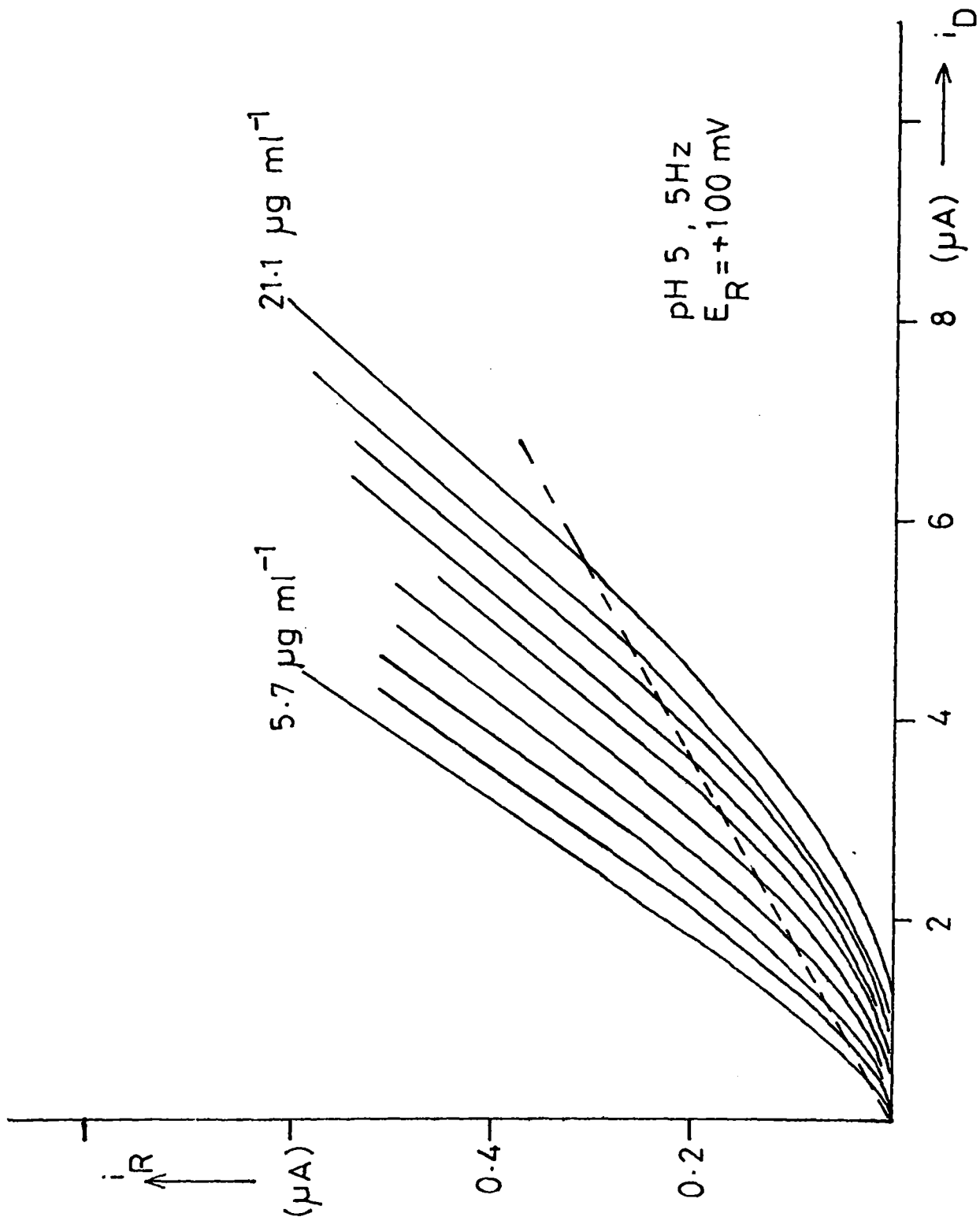

Figure IV.41 Titration of haemoglobin

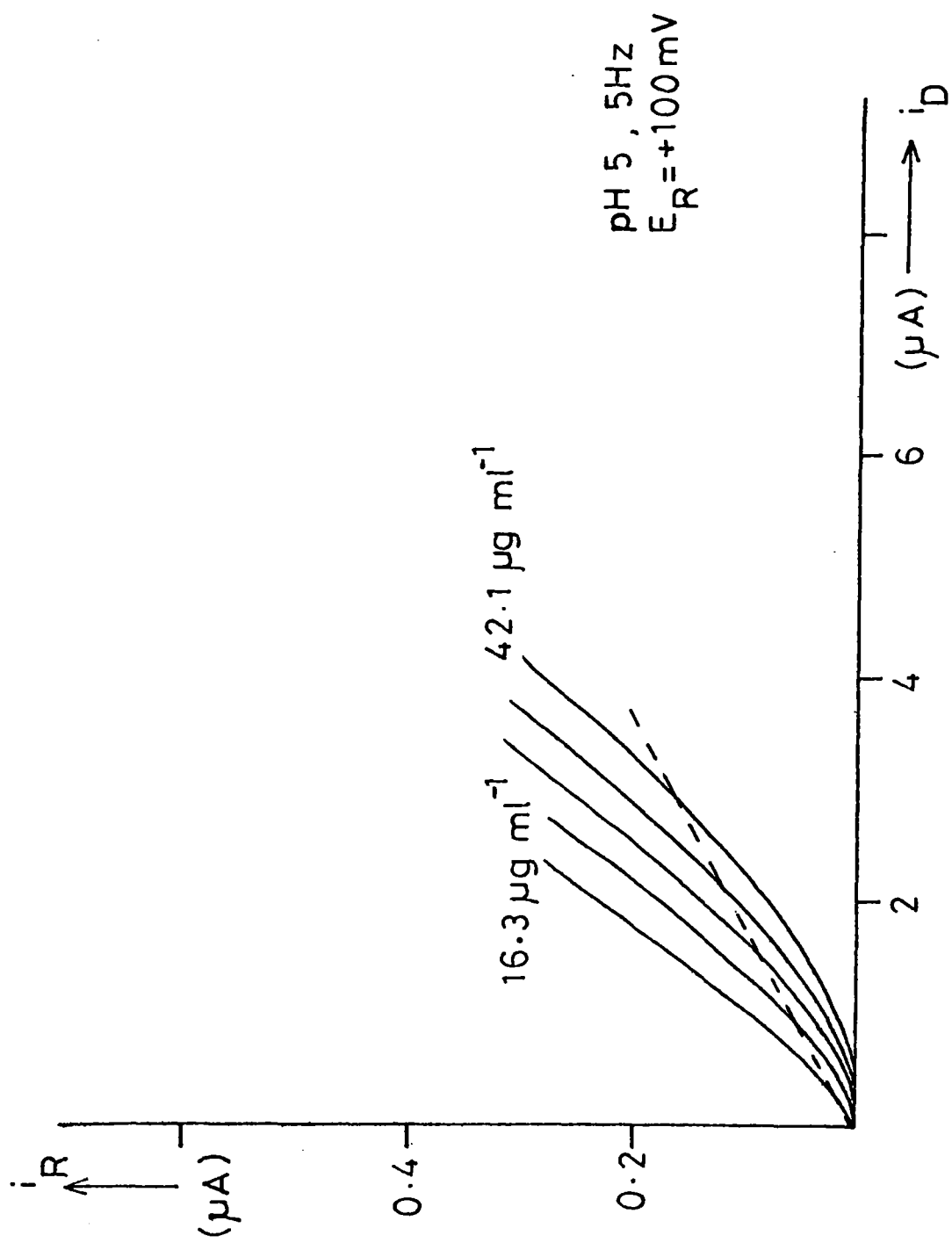

Figure IV.42 Titration of human serum albumen

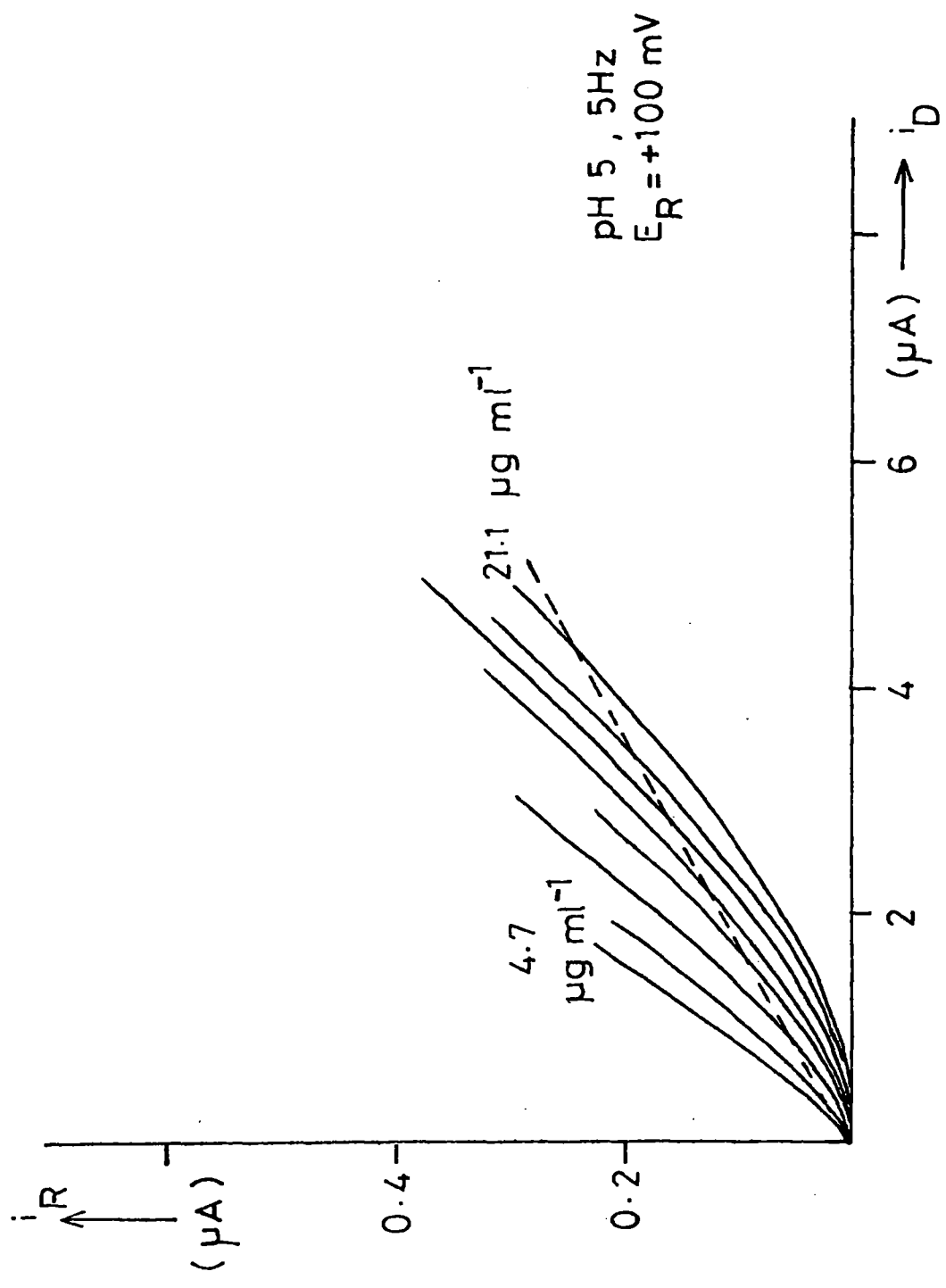

Figure IV.43 Titration of cytochrome c

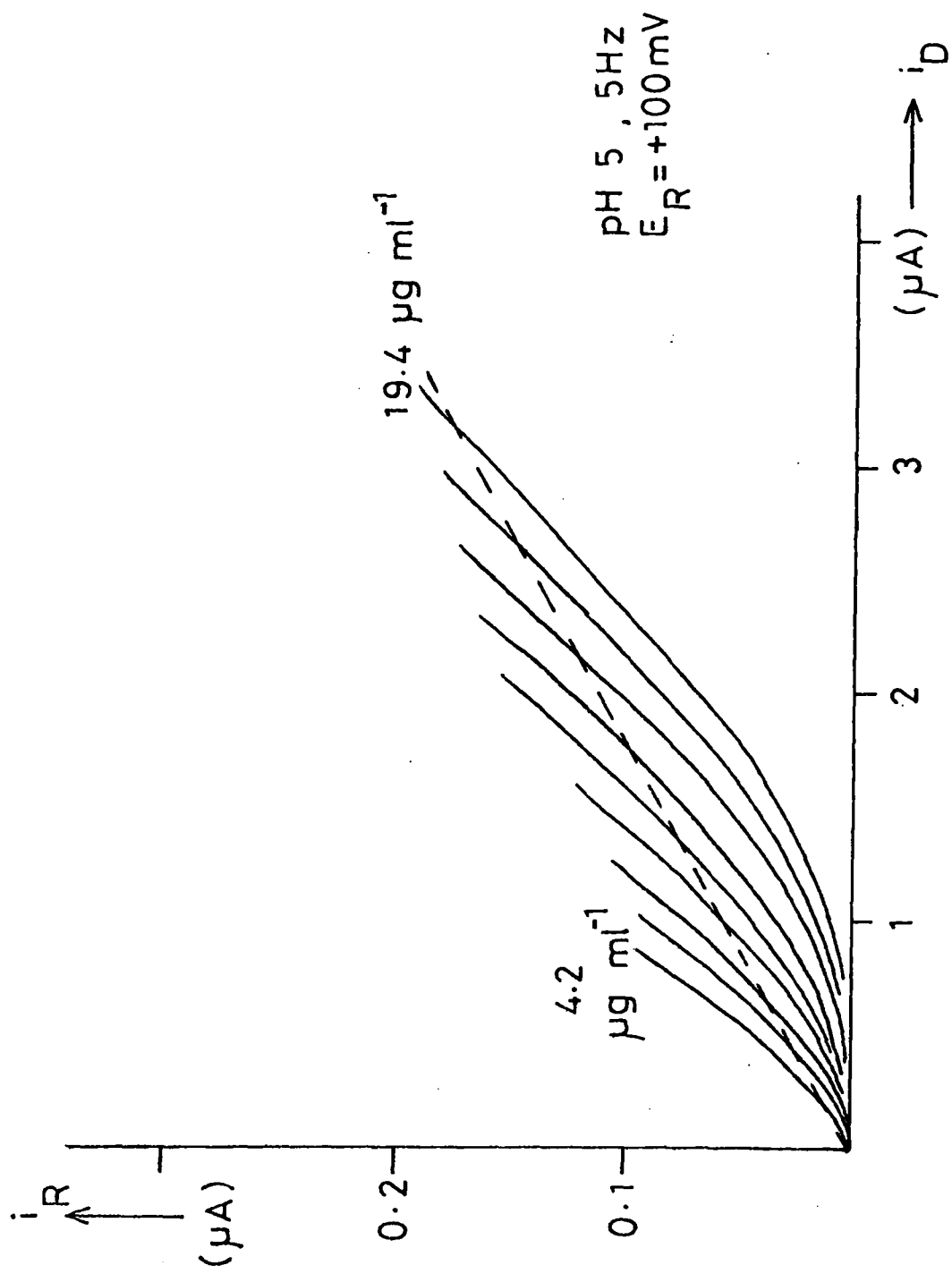

Figure IV.44 Titration of α-amylase

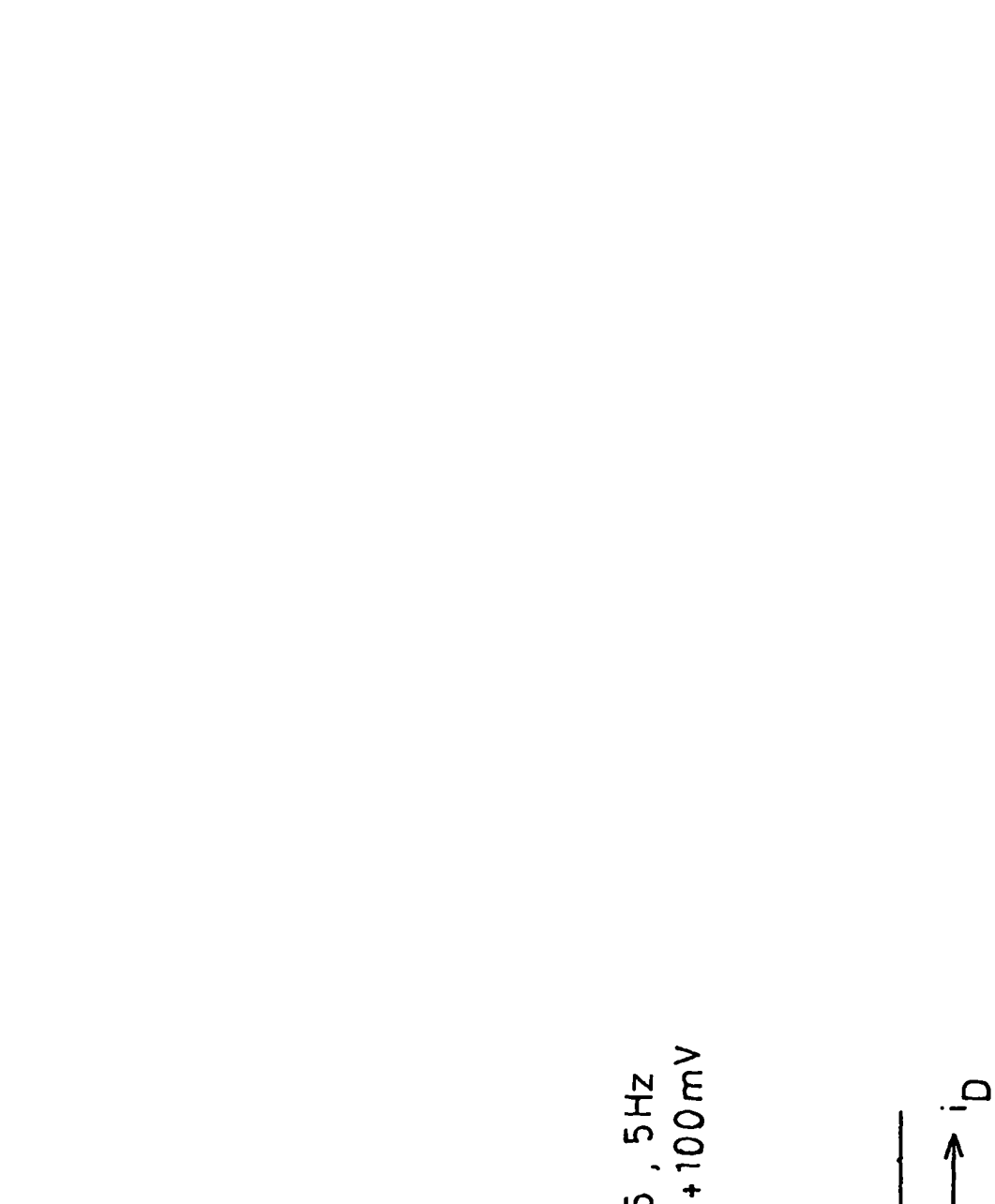

Figure IV.45 Titration of phosvitin

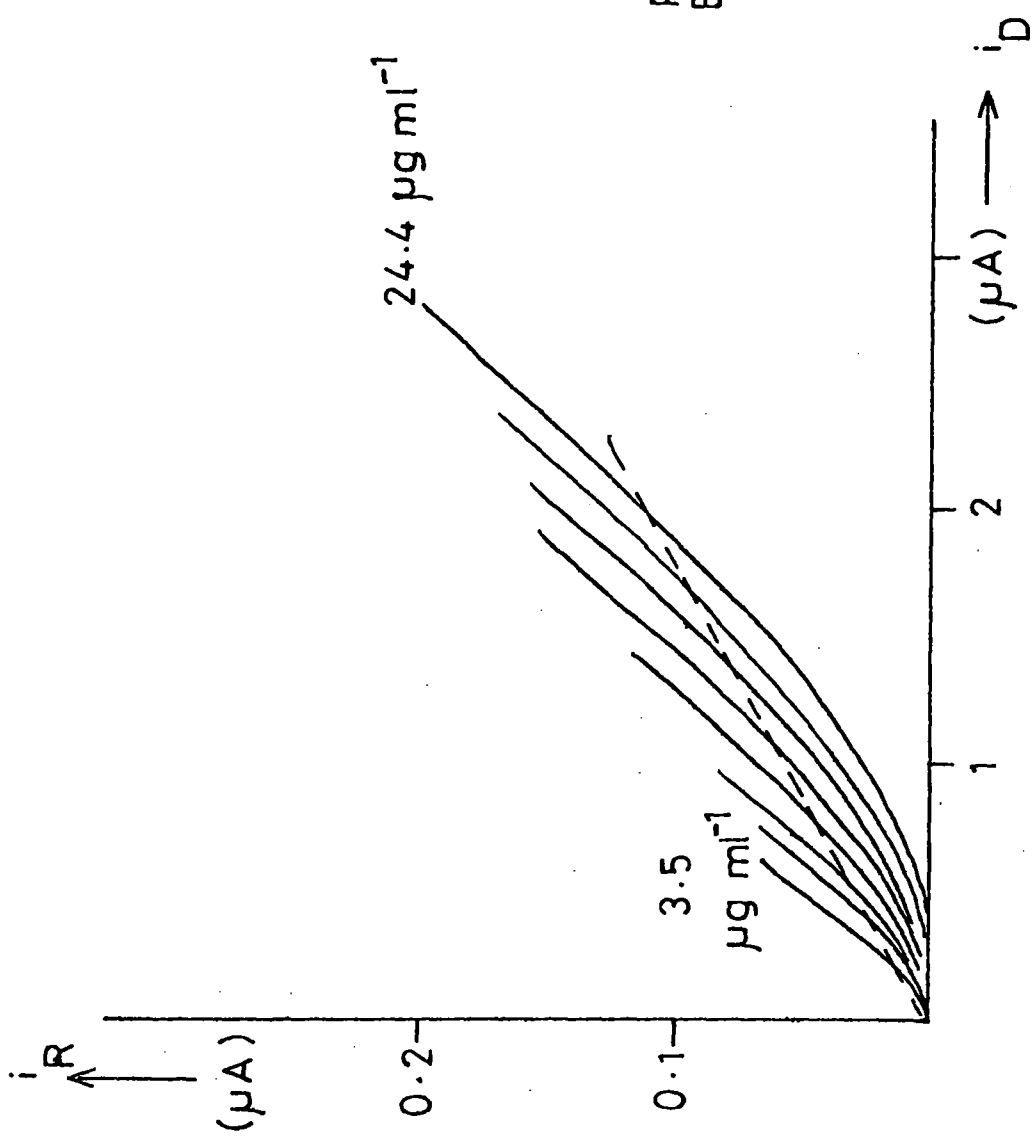

Figure IV.46 Titration of thyroglobulin

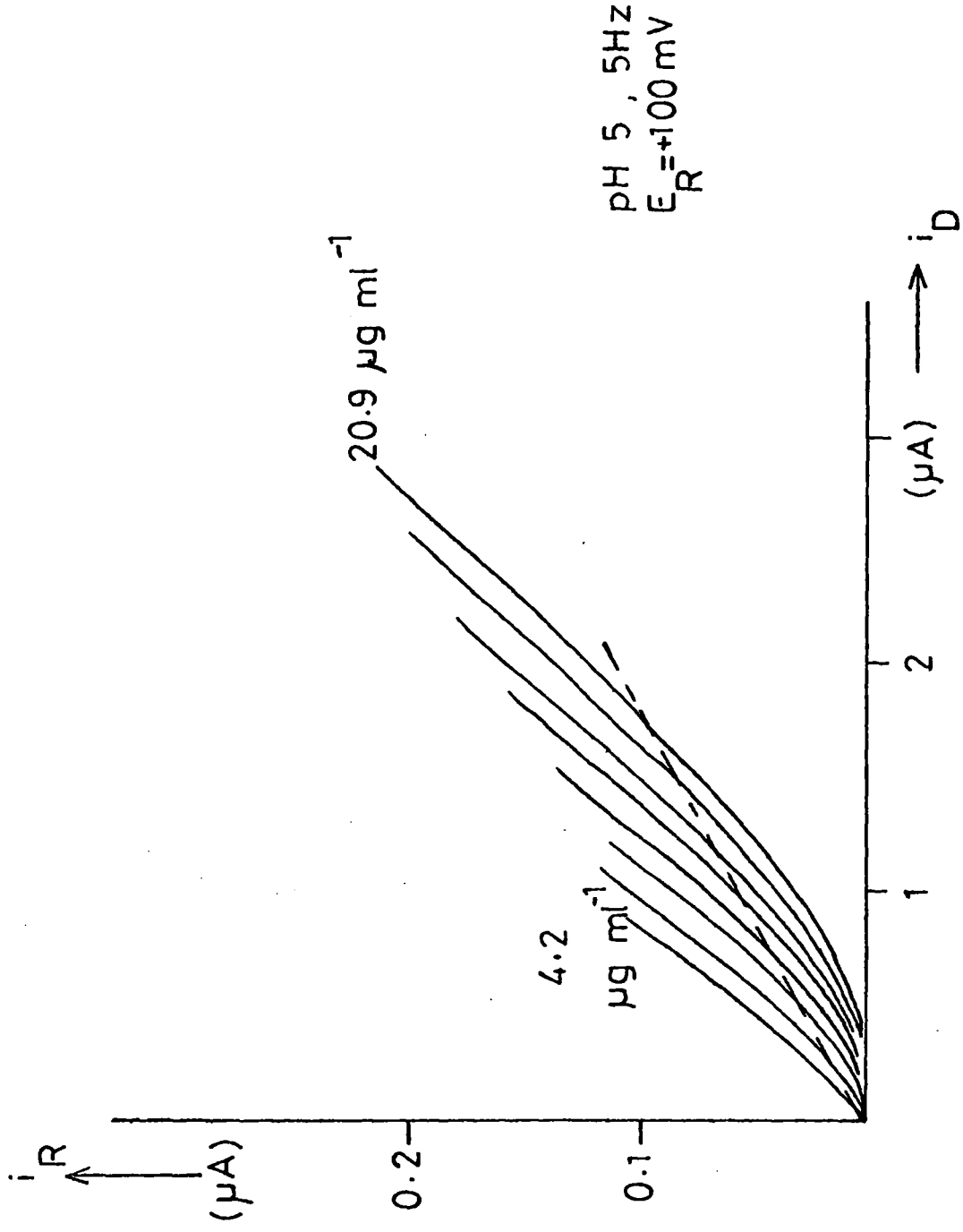

Figure IV.47 Titration of bovine serum albumen

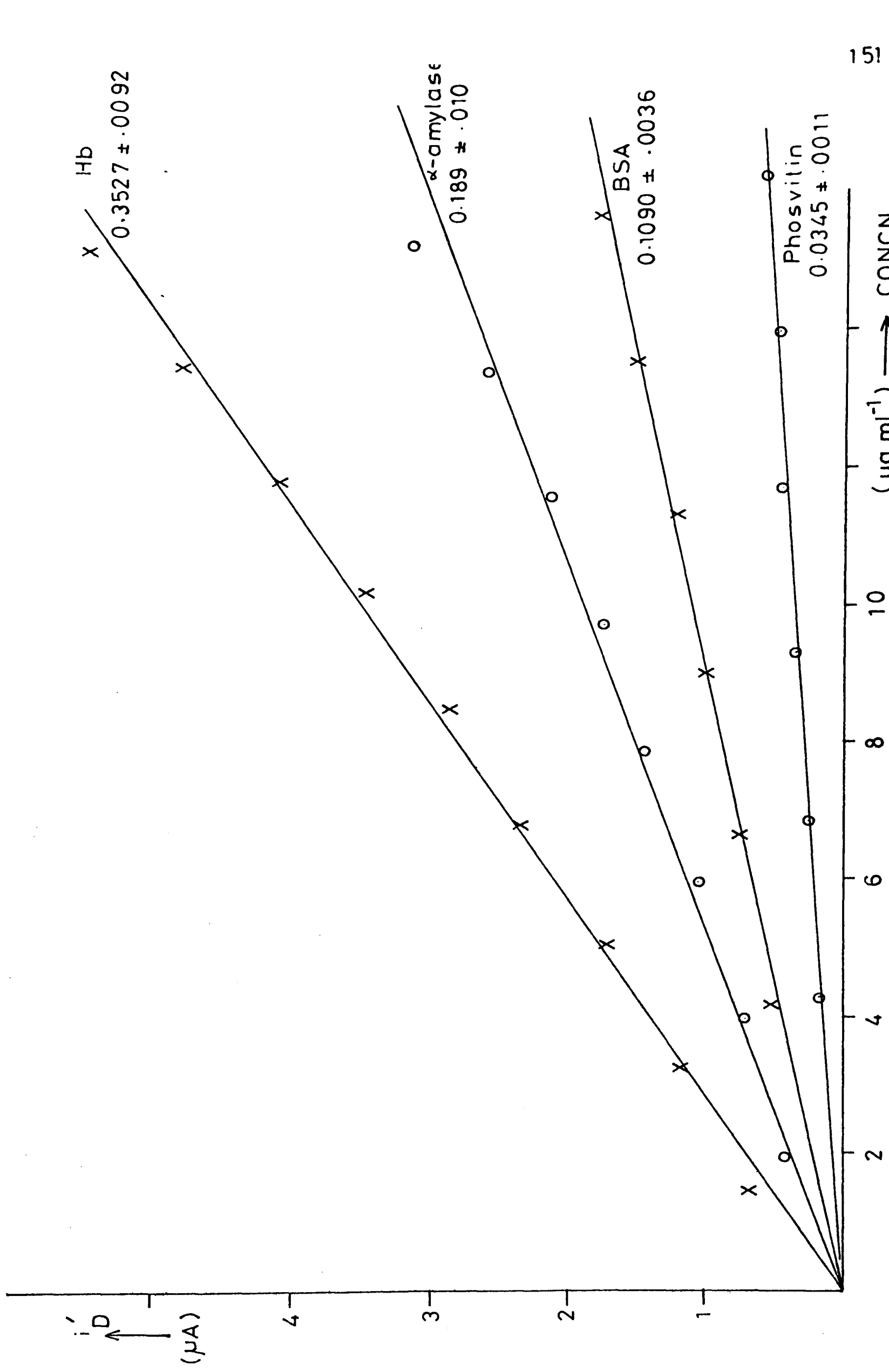

Figure IV.48 Titration response of proteins at pH 5

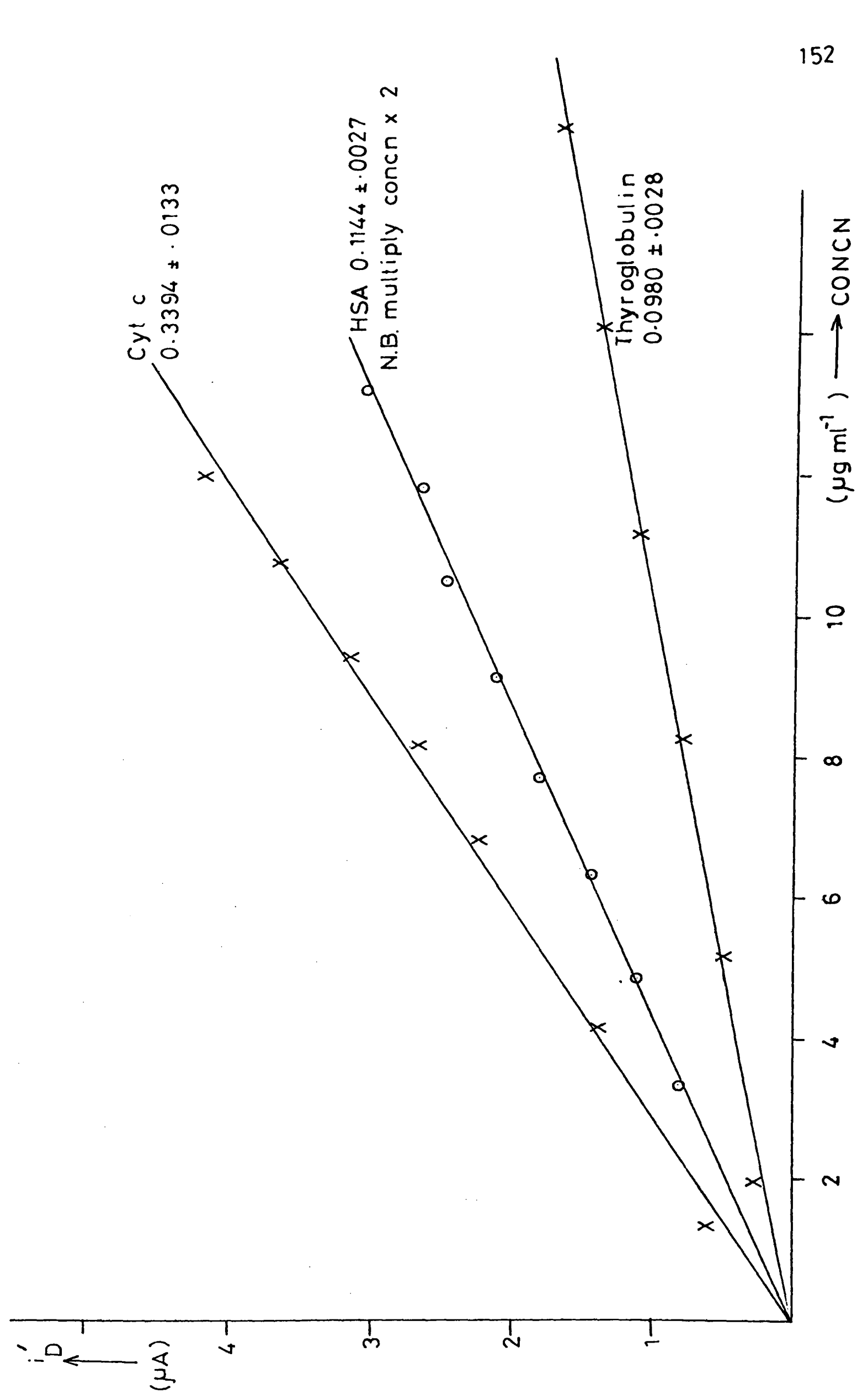

Figure IV.49 Titration response of proteins at pH 5

CHAPTER V. THE DEVELOPMENT OF A CONTINUOUS FLOW - THROUGH DETECTOR

The rotating ring disc electrode (RRDE) experiments described in chapter IV have shown that amino acids and proteins may be titrated with hypobromite. However the RRDE is only suitable for batch analysis, and the titration technique must be transferred to the tubular double electrode (TDE) before flow through analysis may be performed. Section 1 of this chapter therefore presents experiments which were carried out to check the performance of the TDE, and sections 2 and 3 describe the development of a method of continuous analysis.

1. THE TUBULAR DOUBLE ELECTRODE

The tubular double electrode is illustrated in figure I.14, and its method of construction has been described in section III.2.

The dimensions of the electrodes are

generator = 0.072" = 1.83 mm

gap = 0.006" = 0.15 mm

detector = 0.020" = 0.51 mm

The TDE was first tested by recording polarograms at each electrode. The theory of the tubular electrode predicts that

$$i_L = 5.31 \times 10^5 \, n \, D^{2/3} \, X^{2/3} \, V_f^{1/3} \, c_\infty \qquad (I.20)$$

and polarograms were recorded at varying flow rates using a solution of 10^{-2}M KBr in 0.5M H_2SO_4. The syringe drive was used so that this solution could be thermostatted (at 25^oC), and some of the results are presented in figure V.1. The fluctuations in current in the potential range 1000-1400 mV are due to fluctuations in the flow rate delivered by the syringe drive. Values of the limiting current were measured at +1200 mV and log-log plots against V_f are shown for the generator and detector electrodes in figures V.2 and V.3. Least mean squares analysis of the results gives the gradients as

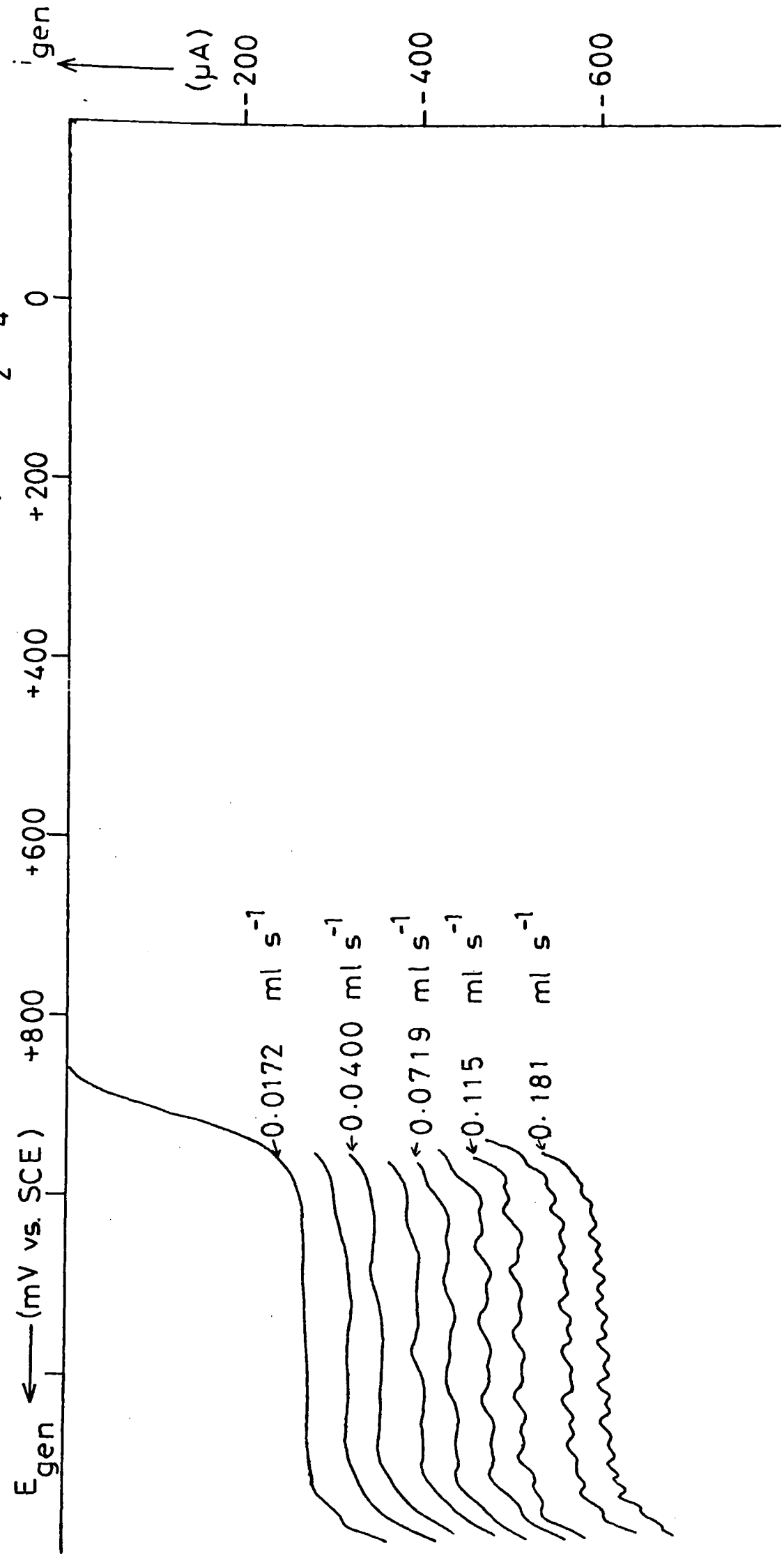

Figure V.1 Polarograms at a tubular electrode

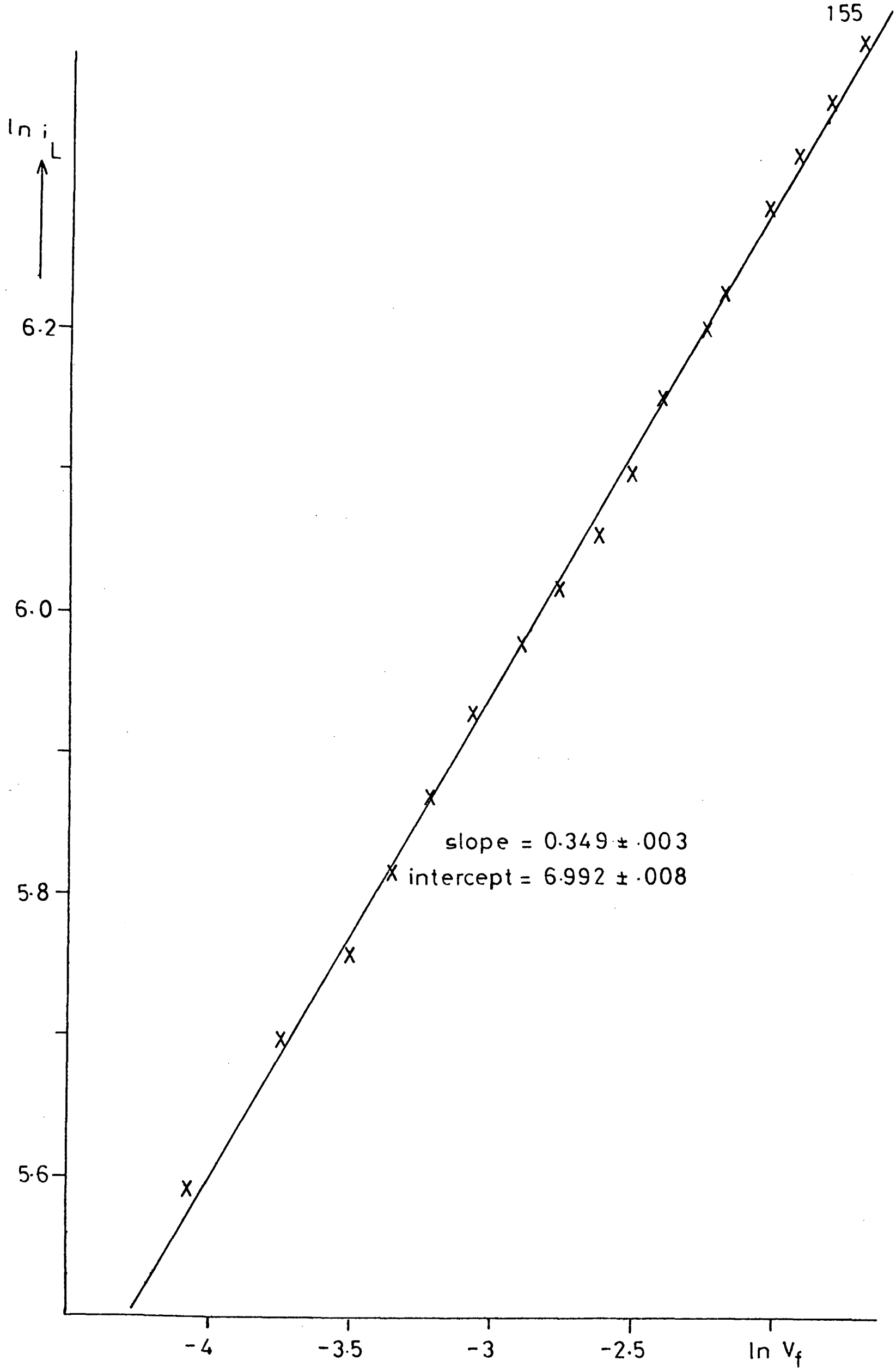

Figure V.2 Flow-rate dependence of current at generator electrode

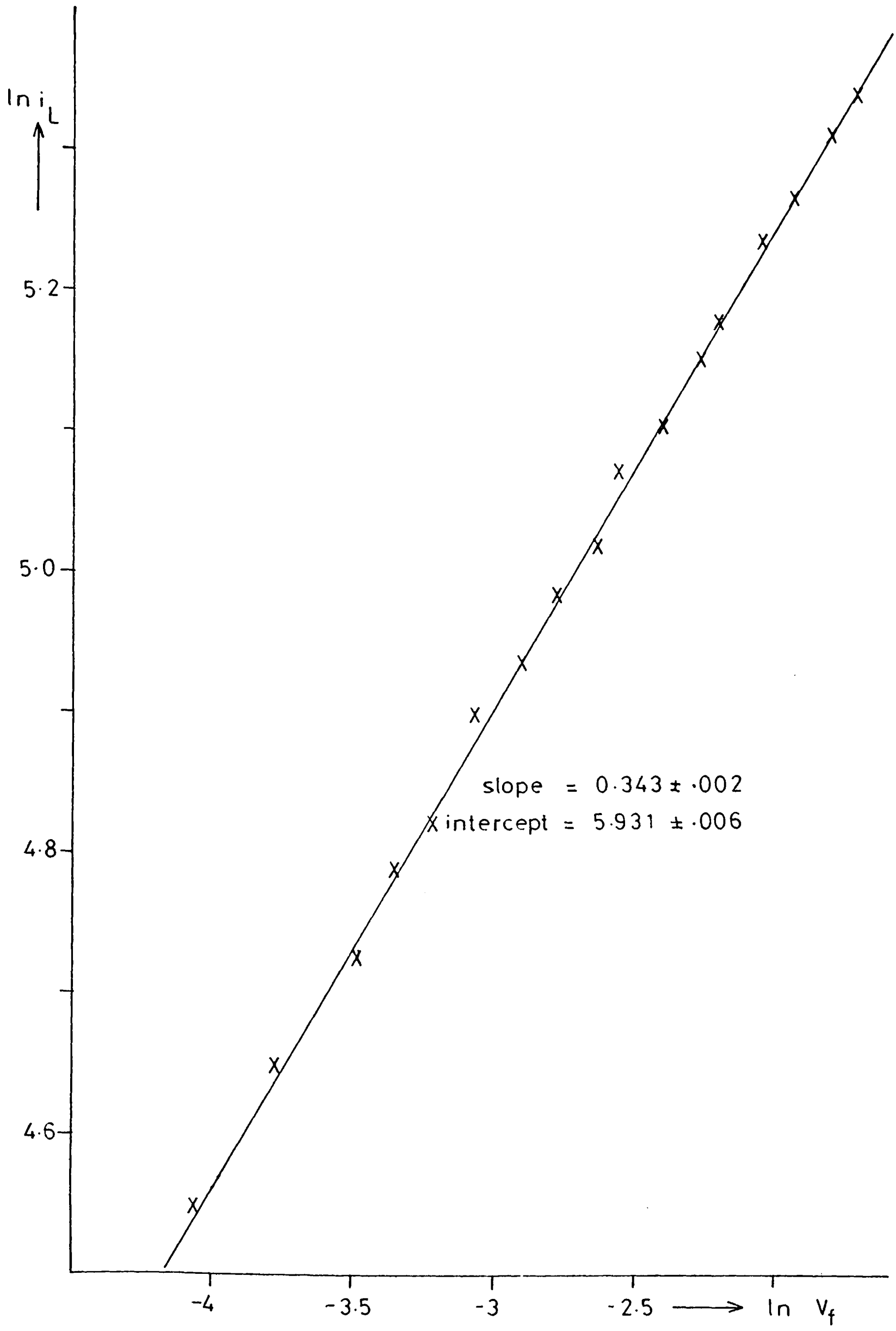

Figure V. 3 Flow-rate dependence of current at detector electrode

generator 0.349 ± 0.003

detector 0.343 ± 0.002

which are higher than the theoretical 0.333 indicating some turbulence; this is further discussed below.

The intercepts of the graphs enable evaluation of the diffusion coefficient of bromide; this gives

generator $D = 1.61 \pm .02 \times 10^{-9}\ m^2 s^{-1}$

detector $D = 1.12 \pm .01 \times 10^{-9}\ m^2 s^{-1}$

The generator electrode result agrees well with that determined using the rotating disc electrode (86) ($1.58 \pm .06 \times 10^{-9}\ m^2 s^{-1}$). However the detector electrode result is low which implies that the electrode length is shorter than measured, i.e. some of the electrode surface is blocked. This is due to Araldite creeping between the zinc wire and the electrode surface when the casting Araldite is poured around the electrode assembly.

These results were obtained after lapping of the tube using alumina. Araldite is softer than platinum and further lapping was not desirable as it could result in the production of a step at the edges of the electrodes. Some turbulence was in fact observed and was presumably due to preliminary polishing. The inlet length used was 60 d, where d is the tube diameter, following the recommendation of Cook (39). This length ensures the development of laminar flow for $Re < 1200$ since

$$h \sim 0.05\ dRe \qquad (I.17)$$

and at $Re > 2000$ turbulence is unavoidable. The Reynolds number for a tube is

$$Re = \frac{2V_f}{\pi R \nu} \qquad (I.22)$$

and the maximum flow rate obtainable from the pumping systems used in this work is $0.1\ ml\ s^{-1}$. This corresponds to

$$Re = 127$$

so that the inlet length need only be 6 d; equations I.17 and I.22 may be combined to give (using $\nu = 10^{-7}\ m^2 s^{-1}$)

$$h \sim 6V_f \quad cm \qquad (V.I)$$

where V_f is expressed in ml s^{-1}.

The peristaltic pump was also used to record polarograms, and these polarograms again showed fluctuations in the limiting current region. The limiting current varied by 6% peak-to-peak, indicating (through the $V_f^{1/3}$ dependence) that the flow rate from the pump varies by $\sim$ 20%. This modulation of the flow rate is similar to that observed with the syringe drive, and is rather large so that a pulse damping system was improvised. This system consisted of a half-filled 10 ml weighting bottle and a 1 m coil of tubing, situated between the pump and electrode (figure V.4), which is analogous to an RC low-pass filter. The performance of this pulse damper may be seen in the polarograms presented in figure V.5. The frequency of the oscillations is dependent upon the rate of rotation of the pump roller cage, and increases with flow rate; the cut-off frequency of the hydrodynamic filter is $\sim$ 0.2 Hz.

The testing of the TDE was continued by measuring its collection efficiency. Using the measured electrode dimensions the theoretical value (equation II.30) is

$$N_o = 0.219 \pm .006$$

The experimental value was found to be 0.193 - 0.195, and this low value is again due to blockage of the detector electrode surface. The bromide diffusion coefficient obtained from the detector suggests that its effective length is 0.014" (a 30% decrease due to the 30% discrepancy in D) and if this dimension is used in equation II.30 then

$$N_o = 0.182 \pm .006$$

This second theoretical value is lower than the experimental value; it has assumed that the gap is as measured and that the detector electrode is uniformly obscured at the downstream edge.

The titration of As (III) in an acidic medium was also performed with the TDE. The theoretical parameters describing this titration curve are

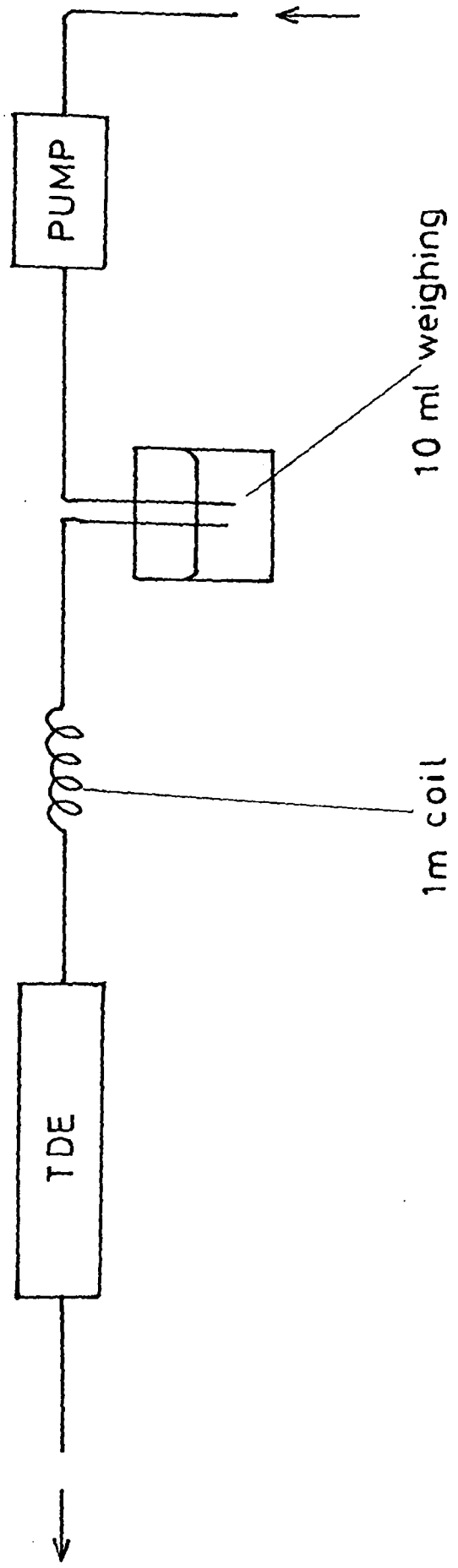

Figure V.4 Pulse damping system

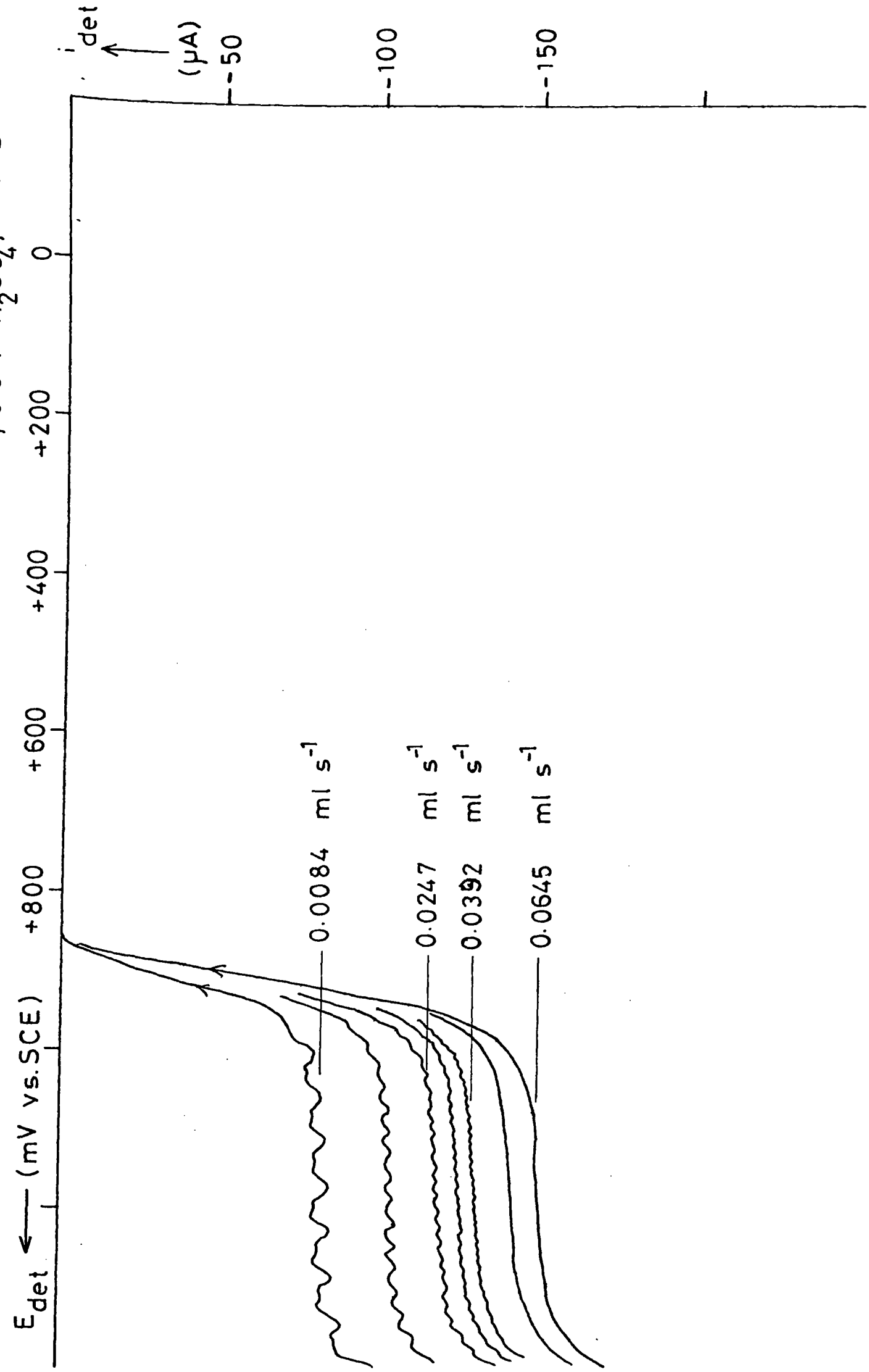

Figure V.5 Effect of pulse damper on polarograms

l_1 = 0.072"
l_2 = 0.006"
l_3 = 0.020"

λ_J/λ_3	i_{gen}/M	N'
1.0	2.575	0.0542
0.9	2.484	0.0483
0.8	2.392	0.0423
0.7	2.298	0.0364
0.6	2.202	0.0304
0.5	2.105	0.0243
0.4	2.004	0.0184
0.3	1.899	0.0126
0.2	1.790	0.0072
0.1	1.674	0.0026

Some of the recorded titration curves are illustrated in figure V.6. A complete analysis of the curves using the above parameters was not attempted because of the imperfections of the TDE. The curves were analysed by superimposition of a line of gradient N' = 0.0542; this corresponds to λ_J/λ_3 = 1 but it can be seen from figure V.6 that the point of intersection is after the start of the linear region of the titration curve (this is to be expected if the detector electrode is shorter than assumed). Measured values of i_D' (at the intersection point) are plotted against concentration in figure V.7 and this graph shows that the titration curve displacement is proportional to concentration. The gradients of these plots have been plotted against $V_f^{1/3}$ in figure V.8 which again shows a straight line passing close to the origin. Thus while this particular TDE does not behave exactly as predicted by theory it does show the expected titration response with respect to concentration and flow rate, and may be used to perform titrations on flowing solutions.

2. THE AUTOMATION OF TITRATION CURVE RECORDING

The TDE may be used to perform titrations on flowing solutions but the technique, as used in this thesis so far, is unsuitable for continuous analysis. This technique involves increasing the disc current linearly with

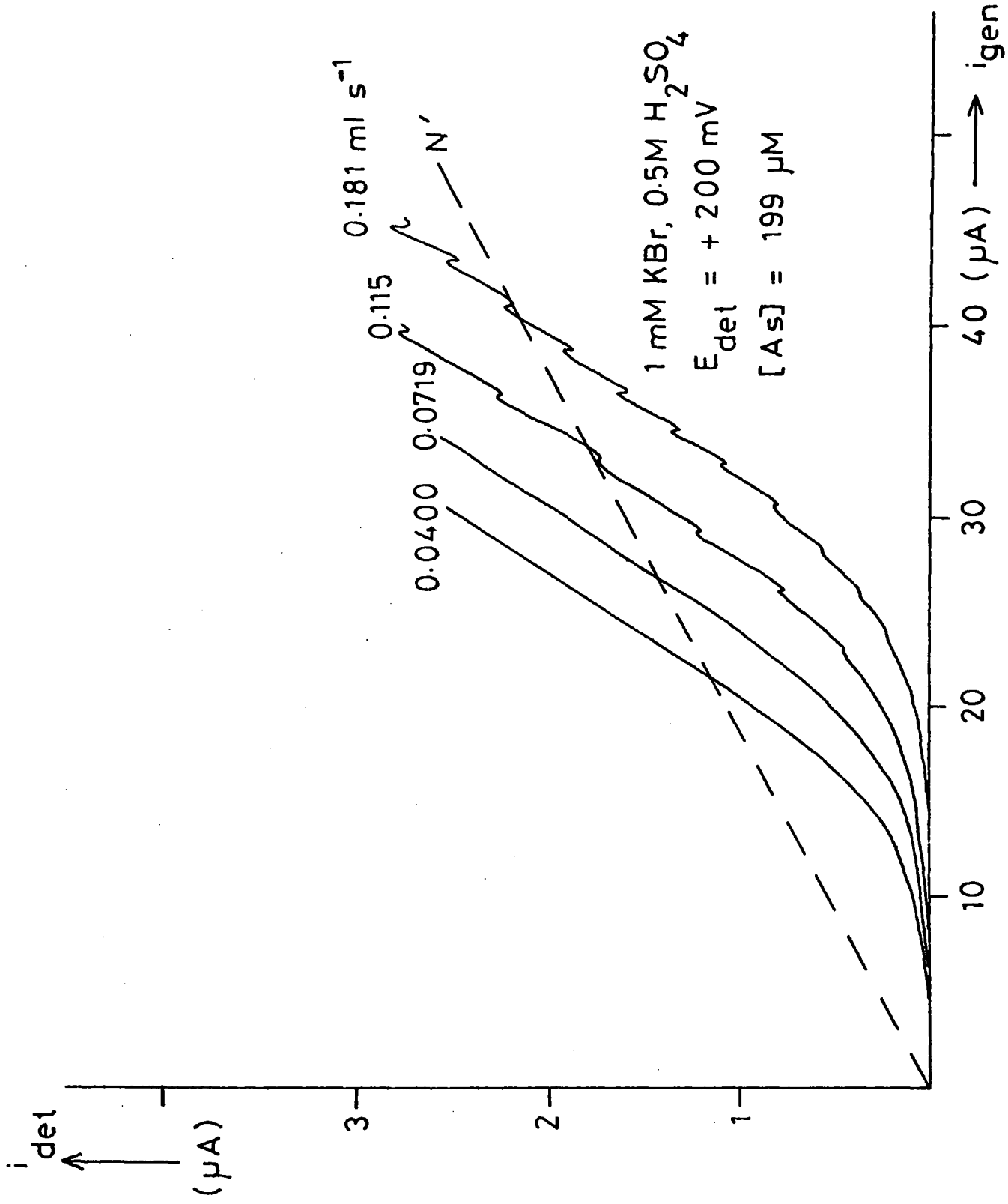

Figure V.6 Titration curves at the TDE

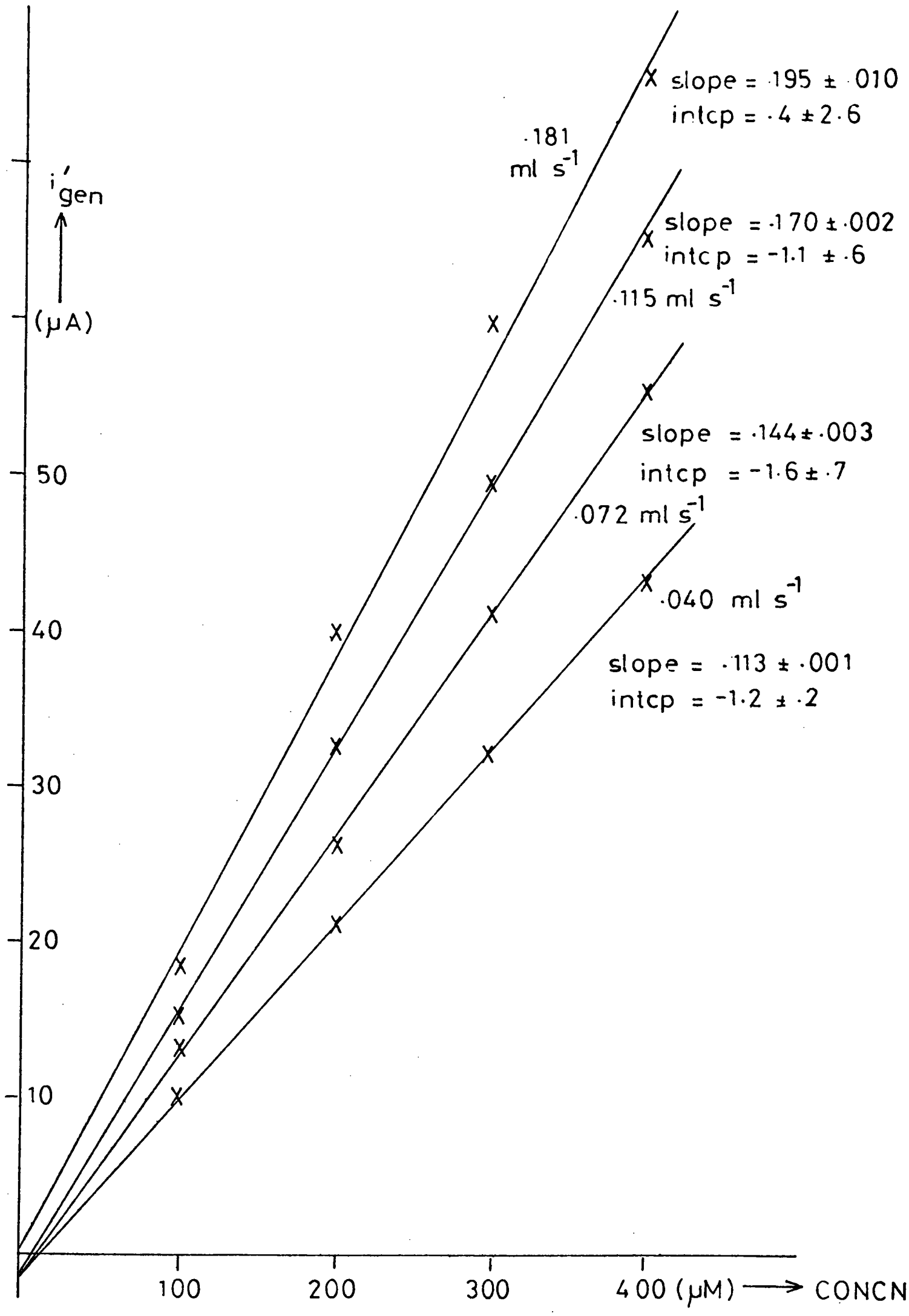

Figure V. 7 Concentration dependence of TDE titration curve displacement

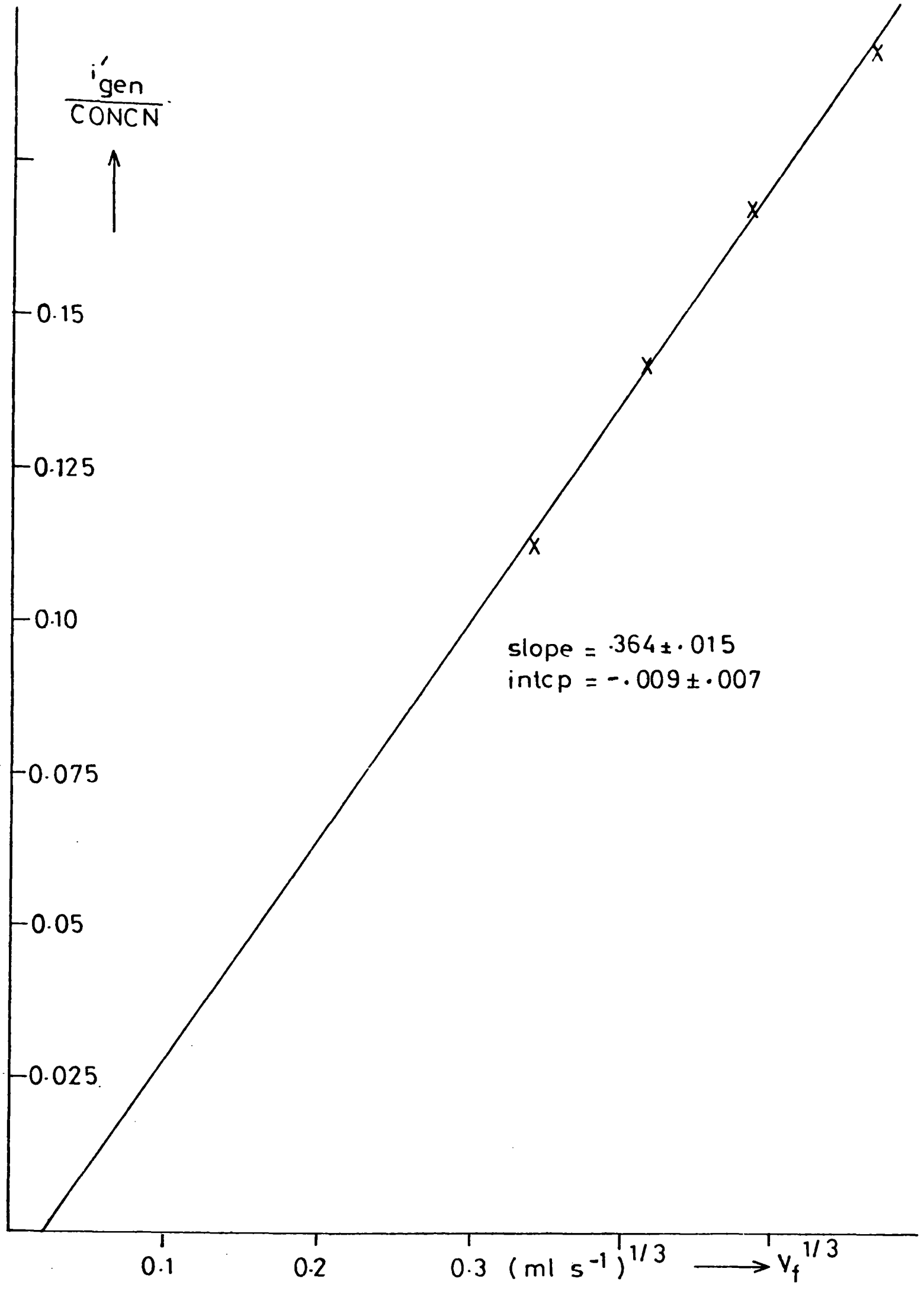

Figure V. 8 Flow-rate dependence of TDE titration curve displacement

time and measuring the ring current; the titration curves are plotted on a X - Y chart recorder, and the time required to record a single curve is approximately 60 seconds. The ring current-disc current plots must then be manually analysed to obtain the bulk concentration of substrate. This methodology is summarised in figure V.9.

The concentration dependence of titration curves presented above has been analysed by constructing a line of gradient N' which intersects the titration curve at the commencement of the linear region (figure I.12). The value of the disc current, i_D' , at the point of intersection is then proportional to a_∞ . The line N' represents a ring current/disc current ratio of less than N_o. If, during the performance of titrations, electronic control circuitry is used to maintain $i_R/i_D = N'$ then this constraint can only be satisfied at the point where the line N' intersects the titration curve. Therefore the value of i_D observed under this constraint is proportional to a_∞ ; this novel method is summarised in figure V.10. The ring (detector) electrode controls the rate at which the titrant B is generated, as opposed to the previously used method in which generation of B is controlled manually. If the concentration of A changes then the disc current must change to satisfy the condition $i_R/i_D = N'$. The value of N' should be such that it intersects the titration curve in or near to the linear region; in manual analyses above N' intersected at the commencement of the linear region since at this point the angle of intersection and accuracy is greatest.

The electronic control circuitry necessary to maintain $i_R/i_D = N'$ has been developed and is shown in figure V.11. Disc (generator) and ring (detector) currents are measured by determining the potential drop across known resistors, R_D and R_R. If $R_D/R_R = N'$ then the desired control condition corresponds to $i_R R_R = i_D R_D$. Amplifier 1 potentiostats the ring electrode with respect to a reference electrode, and is a current-to-voltage convertor. The voltages $E_R - i_R R_R$ and E_R (via a follower) are fed to a subtractor (amplifier 3) along with $i_D R_D$ (see below). The output of this subtractor

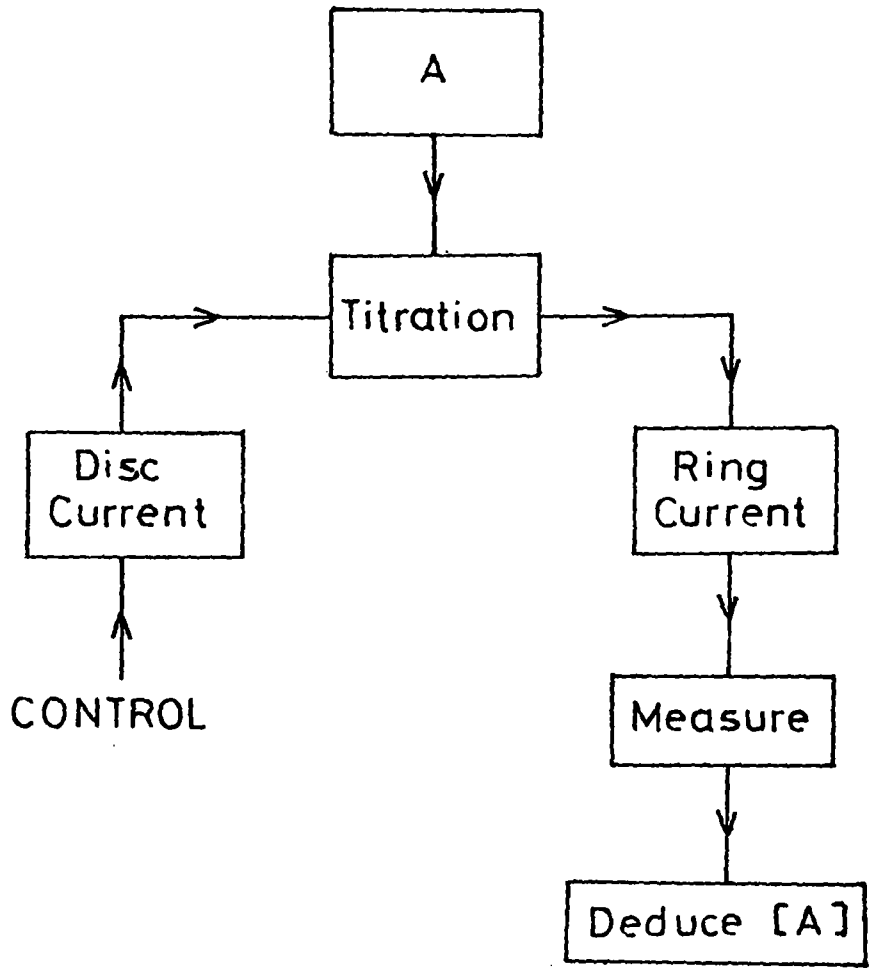

Figure V.9 Manual recording of titration curves

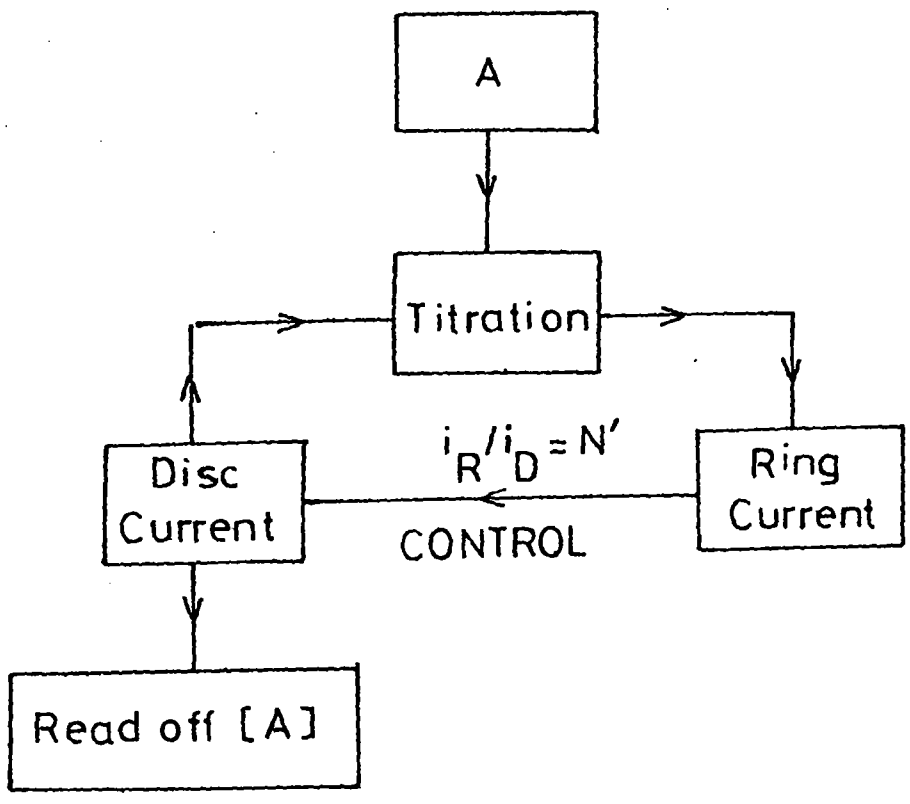

Figure V.10 Automated recording of titration curves

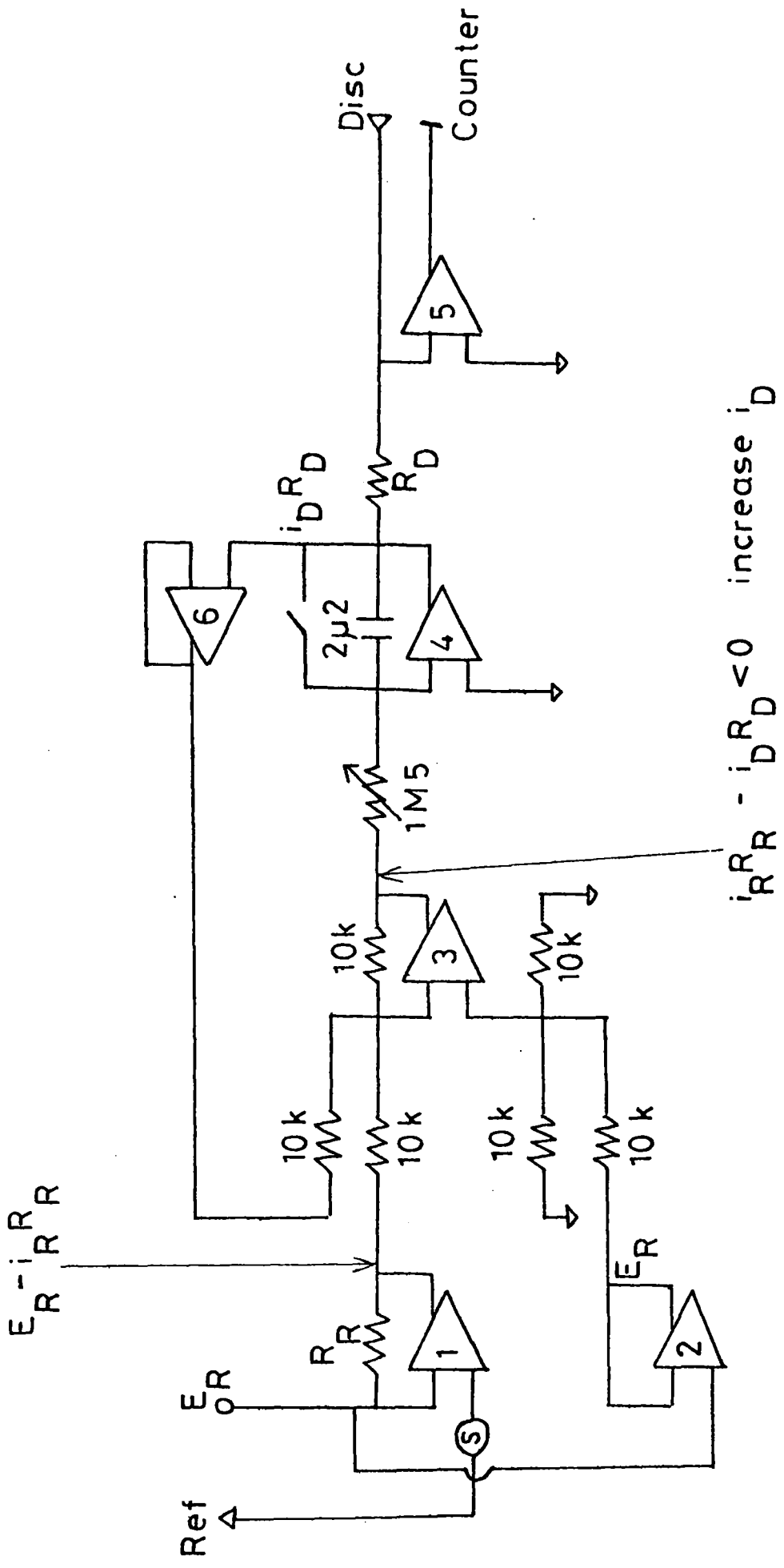

$i_D R_D - i_R R_R < 0$ increase i_D

> 0 decrease i_D

$= 0$ hold i_D

Figure V.11 Autotitrator circuit

is $i_R R_R - i_D R_D$ and a finite output potential represents an error signal. Amplifier 5 is a galvanostat which controls the disc current, the controlling potential being the output of amplifier 4 (an integrator). The input to this integrator is the error signal from the subtractor - thus if $i_R R_R - i_D R_D = 0$ the output potential remains constant, i.e. the disc current is unchanged because the condition $i_R/i_D = N'$ is satisfied. A finite error signal will cause the integrator output potential, and hence disc current, to change in the appropriate direction. A second purpose of the integrator is to provide an electronic delay; this is necessary since there is a transport delay in the electrode system between the disc and the ring - it takes a finite time for an increase in disc current to affect the ring current ($\sim$0.1s for the RRDE, $\sim$1s for the TDE).

The circuit has been used to brominate arsenic (III) at the RRDE using $N' = 0.06$. 100 ml of background electrolyte solution (0.5 M H_2SO_4, 1mM KBr) were added to the electrochemical cell. The electrode was inserted, rotated at 20 Hz, and the control circuitry connected, potentiostatting the ring electrode at +200 mV (vs SCE). A disc current of 3.2 μA was observed, indicating the prescence of impurities in the background electrolyte solution. Then 1 ml of 10^{-3} M arsenic (III) solution was added to the cell, and the system responded by generating bromine (the background electrolyte is acidic) at a disc current of 19.2 μA. Further aliquots of arsenic were added and the response was monitored using a t-Y recorder (figure V.12). This shows that the disc current does increase with concentration and a plot of i_D vs. a_∞ is presented in figure V.13. The graph shows good linearity, and the positive intercept agrees with that observed before the addition of arsenic. The gradient may be compared with that for arsenic in figure IV.16 (0.848 ± 0.008) which was obtained at 5 Hz. The ratio of $1.94 \pm .02$ may be corrected for rotation speed ($i \alpha \omega^{1/2}$), N' and slight differences between electrodes (appendix 5) to give 0.96 ± 0.01. The deviation from unity is due to the differing diffusion coefficients of arsenic in acidic solution and at pH 9.2. The autotitrator circuit therefore performs as expected and

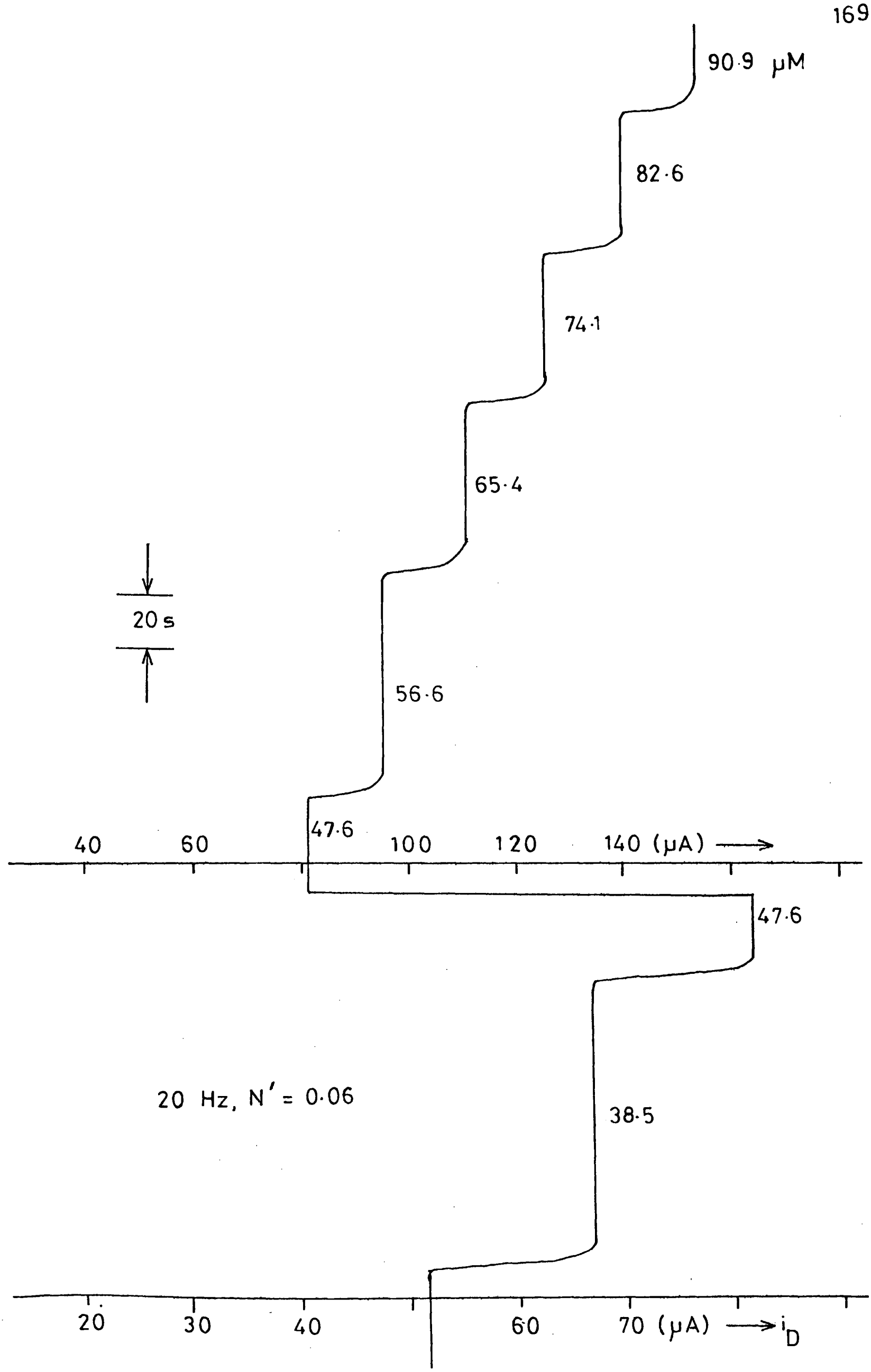

Figure V.12 RRDE autotitration of arsenic

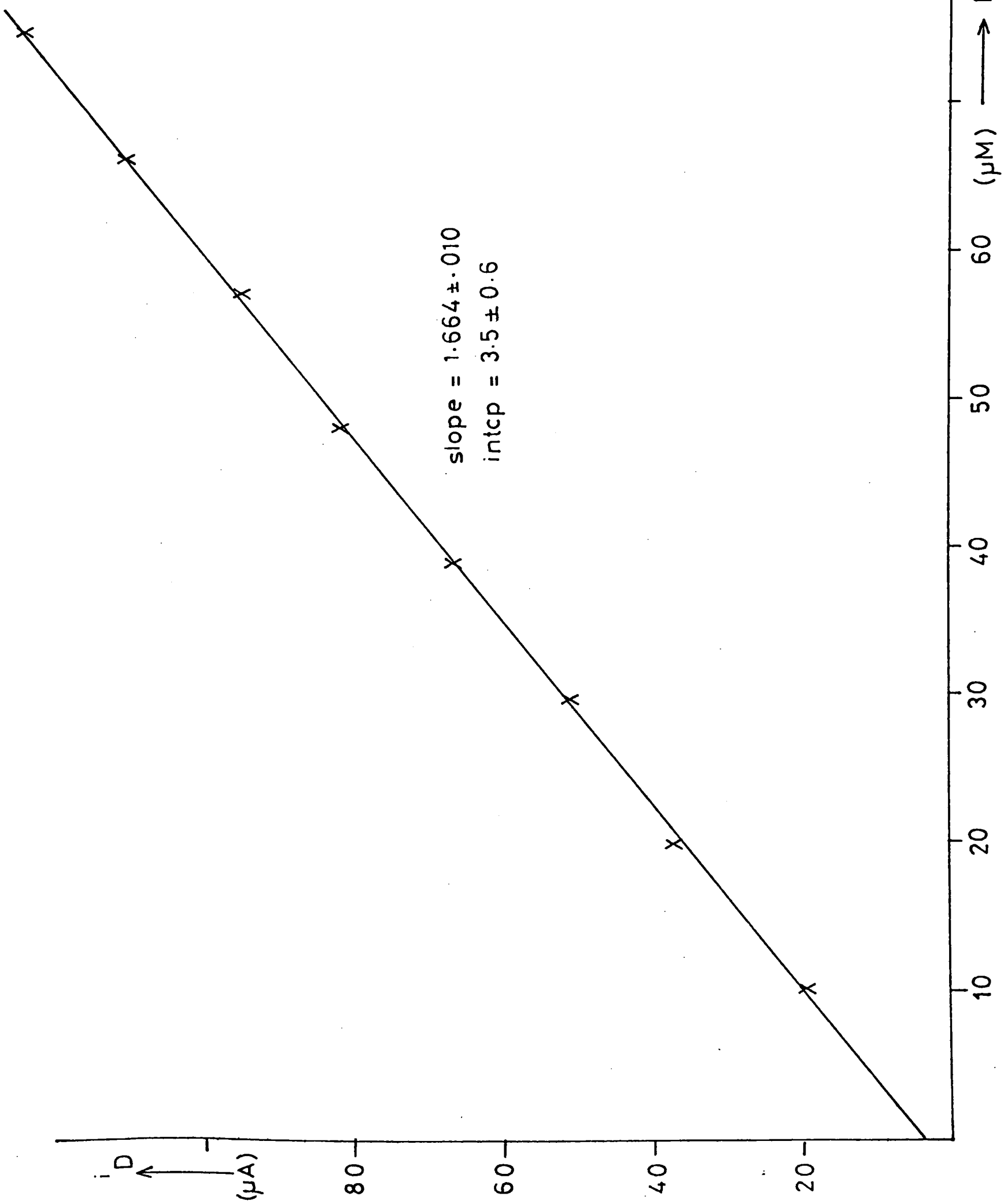

Figure V.13 RRDE autotitration of arsenic

delivers a single current proportional to substrate concentration.

The autotitrator was next applied to the TDE, using the bromination of arsenic (III) in a background electrolyte solution of 0.5M KBr + 0.025 M borate. The three channel peristaltic pump was used to perform this experiment. One channel delivered the background electrolyte solution using 2 mm pump tubing and a pulse damping system. The other channels, using 1 mm tubing, delivered two arsenic solutions of differing concentration one of which was mixed with the background electrolyte using a three-way tubing connector. The arsenic concentration was changed using a two channel four way valve. The dead volume between this valve and the TDE was minimised by using short lengths of tubing and by omitting the reference electrode compartment (and consequently the reference electrode). The generator electrode was therefore used to provide a reference potential of $\sim$ + 650 mV vs. SCE. This is the potential at the foot of the bromide wave, and will change as the generator current changes. However the change in potential is small (except at low i_{gen}), and the detector was potentiostatted at E_{det} = - 400 mV (vs. E_{gen}). The automated titration was monitored using a t-Y recorder, and part of the trace is shown in figure V.14. The large response time is mainly due to the dead volume between the mixing point and TDE (the volume of the tubing to glass connector is $\sim$0.5 ml); the electronic response time is $\sim$5s. A plot of i_D vs. a_∞ (figure V.15) once again shows a linear response. The gradient of this graph (0.288 µA/µM at 0.0625 ml s^{-1}) is less than that obtained with the RRDE (1.644 µA/µM at 20 Hz) since in the TDE forced convection is a less efficient transport process (compared to diffusion) than in the rotating ring disc electrode.

3. A DETECTOR FOR LIQUID CHROMATOGRAPHY

The combination of the TDE and the autotitration technique should enable the continuous titration of proteins as they are eluted from a chromatographic column. This experiment has not been performed since in the final months of

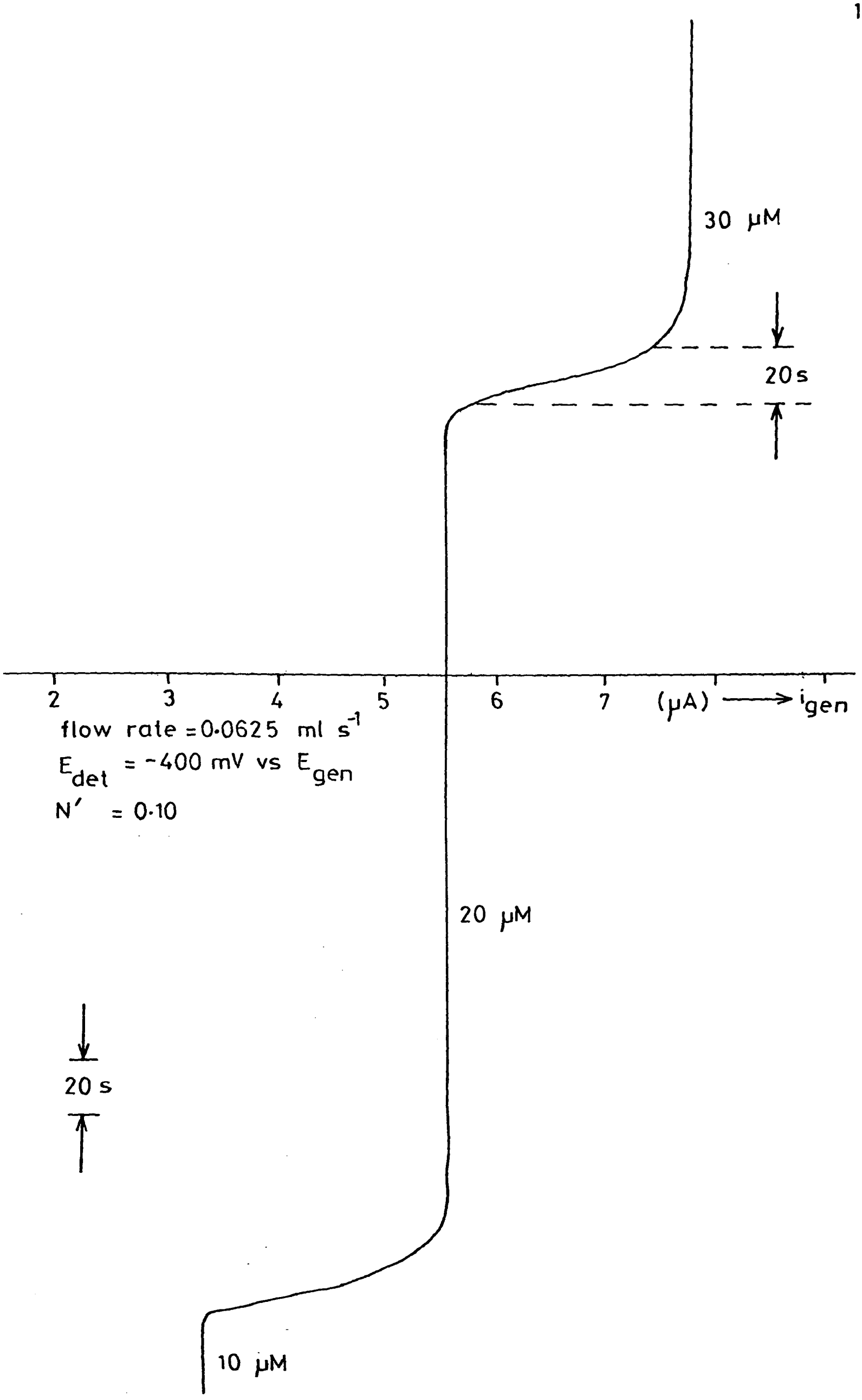

Figure V. 14 TDE autotitration of arsenic

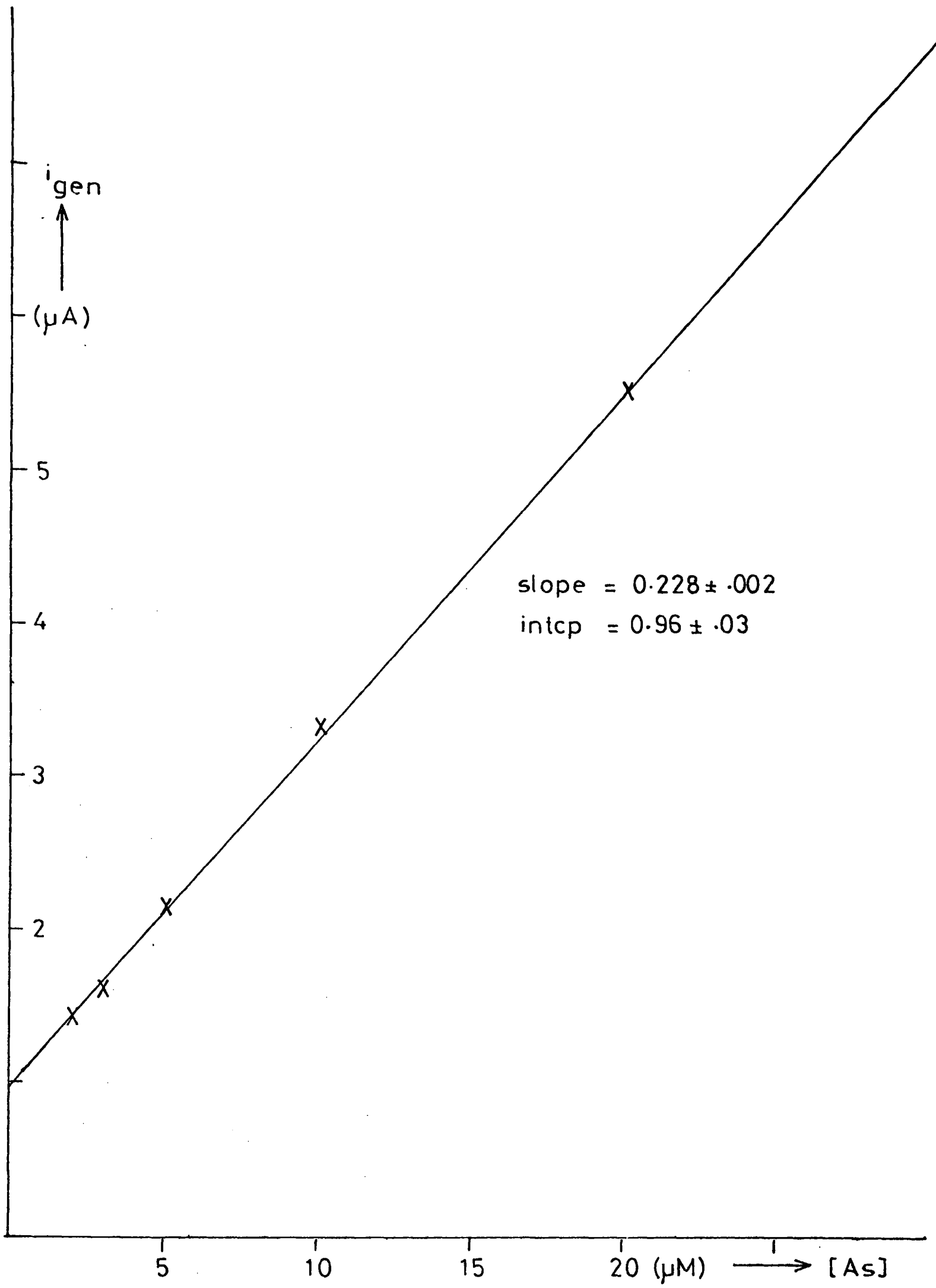

Figure V.15 TDE autotitration of arsenic

this work priority was given to the development of a method for the identification of proteins. However this section describes the configuration and operation of a tubular double electrode diffusion layer titration detector.

The tubular double electrode used in this work had a volume of ~100 µl. The diameter of the tube may be reduced to 0.5 mm and its total length may be reduced to ~4 cm (an inlet length of 0.6 cm is sufficient for flow rates of 0.1 ml s^{-1}) to produce a detector of ~10 µl volume. A new electrode has been designed to these dimensions and the ends of the Araldite casting will be tapped to accommodate standard chromatographic two way tubing connectors; this will remove the dead volume associated with the tubing to glass connector. The electrode will also incorporate the counter and reference electrodes (figure V.16). In the TDE autotitration experiment (figure V.14) the generator electrode was used to provide a quasi-reference potential. This enabled the titration of µM solutions but might be unsatisfactory at lower concentrations. If this is so then the platinum wire reference electrode may be galvanostatted at the foot of the bromide oxidation wave to provide a stable reference potential. This new electrode will also be short enough to enable a reamer to be used to clear any Araldite from the electrode surfaces. This will then enable a full investigation of the theoretical description of the TDE titration curve.

Proteins are separated on columns at various pH values. The pH of the eluant must be adjusted to 9.2, and bromide added, before passing through the detector (figure V.17). The background electrolyte stream must therefore contain borate and sufficient hydroxide to neutralise the separation buffer. The impurity level in both streams must also be decreased below the detection limit of the technique. This may be achieved by preelectrolysis (if a small amount of bromide is added to the eluant stock solution). This preelectrolytic clean up technique is similar to the in situ technique used with the RRDE (chapter IV) and large volumes of solution may be treated. The technique involves electrogeneration of hypobromite; the concentration of hypobromite

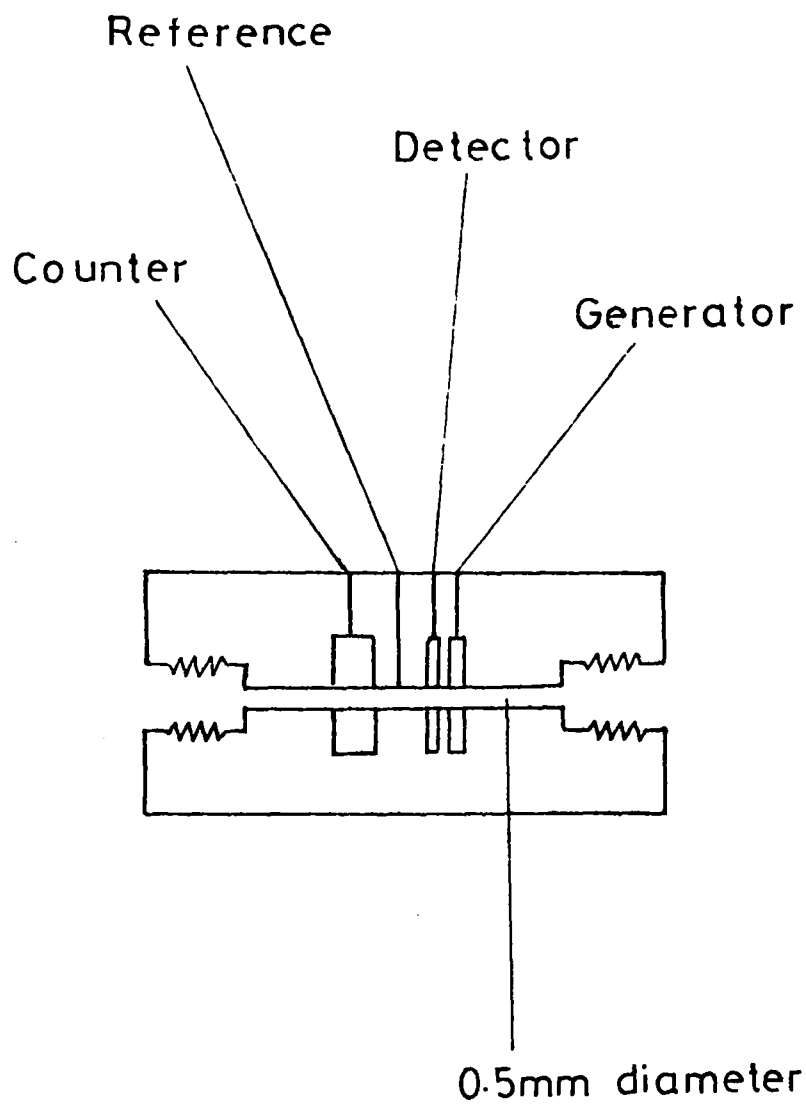

Figure V.16 New design for TDE

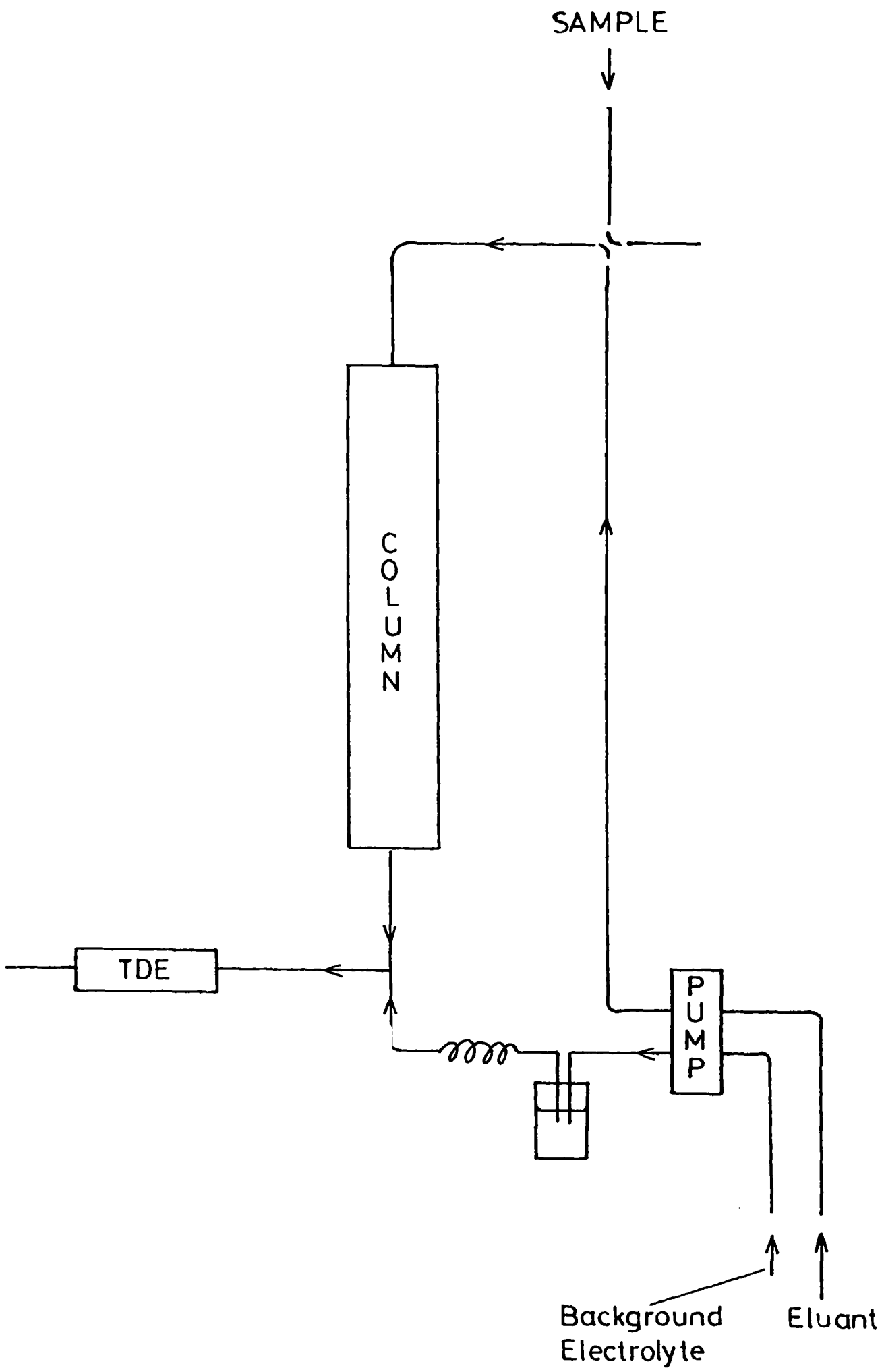

Figure V.17 Configuration of TDE titration detector

surviving in solution may be monitored electrometrically and this concentration will rise after the bromination of all impurities. This rise may then be used to switch off the hypobromite generation. The use of hypobromite as a titrant however will not permit the presence of some substances commonly used in eluants, e.g. ammonia, glycine, tris and barbiturate buffers, ascorbic acid, urea.

Some properties of the TDE titration detector have been given in table I.1. The detection limit of the RRDE titration of proteins is $\sim 10^{-8}$ g ml^{-1} (section IV.3) and should be similar for the TDE. This sensitivity is comparable to the refractometric detector and is close to that of uv absorption. The linear dynamic range has not yet been determined. The autotitration technique enables concentration information to be obtained from one current measurement and a patent application has been submitted to cover this technique.

CHAPTER VI. FURTHER DEVELOPMENT OF THE DETECTOR

This final chapter reviews the work described in this thesis presenting suggestions for further work.

Amino acids were the first compounds to be studied in this work. The actual compounds studied were selected on the basis of their expected side-chain reactivity since the titration of proteins relies entirely upon side-chain reactions. The amino acid results indicated the effect of diffusion coefficients on the measured titration response and prompted the extension of the RRDE titration curve theory. This theory may be further tested by titrating the series of amino acids (glycine, alanine, valine, leucine, serine, threonine, aspartic acid, glutamic acid) which have unreactive side chains. These compounds all have a stoichiometric bromine number of 2 and their diffusion coefficients have been reported by Longsworth (81). However the RRDE titration technique itself may be used to determine diffusion coefficients without knowledge of the bromine number. The autotitration method gives a current which is proportional to concentration. If a prolonged titration is performed then the substrate is consumed and the disc current will fall. The decay is first order and the time constant may be related to the diffusion coefficient. This is a refinement of the technique published by Hitchman and Albery (87) in which the disc current was maintained at a constant value and the increase in ring current was monitored.

The technique developed for the titration of amino acids was then used successfully with proteins. However it was subsequently discovered that the electrochemical reduction of bromoamine groups in proteins does not occur. Therefore protein titrations need not be performed using E_R = + 450 mV at which potential electrode surface oxidation may produce drifting currents. Less positive ring potentials may be used but at $E_R < \sim +$ 100 mV any oxygen present in solution will interfere.

The above failure to observe bromoamine reduction was made while

attempting to develop a method for the identification of proteins, which consequently also failed. The titration of proteins was repeated at pH 5; the ratio of titration responses (table IV.9) shows promise as the basis of an identification method when combined with uv absorption measurements. The signal, S_{td}, obtained from a titration chromatographic detector may be expressed as

$$S_{td} = k_{td} N_{Br} [\text{Protein}] \qquad \text{(VI.1)}$$

i.e. it is proportional to the protein bromine number which may be related to the amino acid composition of the protein and individual amino acid bromine numbers. The signal, S_{uv}, obtained from a uv chromatographic detector may be expressed as

$$S_{uv} = k_{uv} \varepsilon [\text{Protein}] \qquad \text{(VI.2)}$$

where ε is the extinction coefficient. The extinction coefficient of a protein may also be correlated with the amino acid composition and individual amino acid extinction coefficients. At 280 nm (the most commonly used wavelength for uv detectors) the amino acids which absorb uv radiation are tyrosine (ε 1340), tryptophan (ε 5550) and cystine (ε 150). The protein extinction coefficient may be written as

$$\varepsilon = N_{Ar} \bar{\varepsilon} \qquad \text{(VI.3)}$$

where N_{Ar} is an aromatic number (related to the number of aromatic side chains) and $\bar{\varepsilon}$ is an arbitrary "average" aromatic extinction coefficient. Thus the uv signal (equation VI.2) may be written as

$$S_{uv} = k'_{uv} N_{Ar} [\text{Protein}] \qquad \text{(VI.4)}$$

which is of the same form as equation VI.1. Since the amino acids which absorb radiation at 280 nm have also been shown to react with hypobromite (section IV.2) the aromatic and bromine numbers provide complementary information.

Division of equation VI.4 by equation VI.1 gives

$$S_{uv}/S_{td} = k_1 N_{Ar}/N_{Br} \qquad \text{(VI.5)}$$

where $k_1 = k'_{uv}/k_{td}$. Table VI.1 presents the extinction coefficients (89) of some of the proteins studied in this work (values for haemoglobin and phosvitin could not be found, and an approximate value is given for haemoglobin). This table also presents the aromatic number, N_{Ar}, which has been calculated using $\bar{\varepsilon} = 2000$. The aromatic number has been divided by the bromine number at pH 9.2, and this is plotted in figure VI.1 against the titration response pH ratio (= N_{Br} [pH 9.2]/N_{Br}[pH 5]). This plot now allows the differentiation of haemoglobin and thyroglobulin which was not possible using only the titration response pH ratio. This method of identifying proteins is the subject of a second patent application. The identification of proteins as they are eluted from a column may be achieved by first passing the eluant through a uv detector and then splitting the stream to pass through two titration detectors (at pH 5 and pH 9.2). The three signals obtained may then be combined to give the two independent ratios plotted in figure VI.1.

This work has been confined to proteins and amino acids but the technique of gel filtration chromatography is also used to separate nucleic acids. O'Reilley (88) has reported the coulometric determination of nucleotides (cytosine, thymine and uracil compounds) by bromination at pH 4.6 and 5.75. These compounds contain aromatic rings and amine groups, and may therefore be detected by the tubular double electrode diffusion layer titration detector; a RRDE study of their bromination would also be useful.

The titration detector is complementary to the voltammetric detectors which are being increasingly used in HPLC detection. These latter detectors have been used in catecholamine detection and these compounds may also be amenable to bromination. They consist of a catechol ring and amine-containing side chain and their biosynthetic precursor is the amino acid tyrosine which has been successfully titrated in this work. The voltammetric detectors include the wall jet electrode, and a logical extension of this would be to construct a wall jet double electrode to perform diffusion layer titrations. One advantage of such an electrode over the TDE with the high flow rates used in

Table VI.1 Identification of Proteins

	ε	N_{Ar}	N_{Br}[pH 9.2]	N_{Ar}/N_{Br} [pH 9.2]	N_{Br} [pH 9.2]/N_{Br}[pH 5]
HSA	40,000	20	76.0 ± 1.5	.263 ± .005	8.80 ± .26
BSA	43,600	22	75.8 ± 1.7	.290 ± .007	9.20 ± .36
Cytochrome c	2,900	1.5	27.2 ± 0.5	.055 ± .001	5.91 ± .25
Thyroglobulin	693,000	347	263 ± 7	1.319 ± .035	3.71 ± .14
α-Amylase	125,000	62.5	33.6 ± 0.7	1.860 ± .039	3.25 ± .18
Haemoglobin	64,500	32	91.4 ± 4.3	.350 ± .016	3.67 ± .20

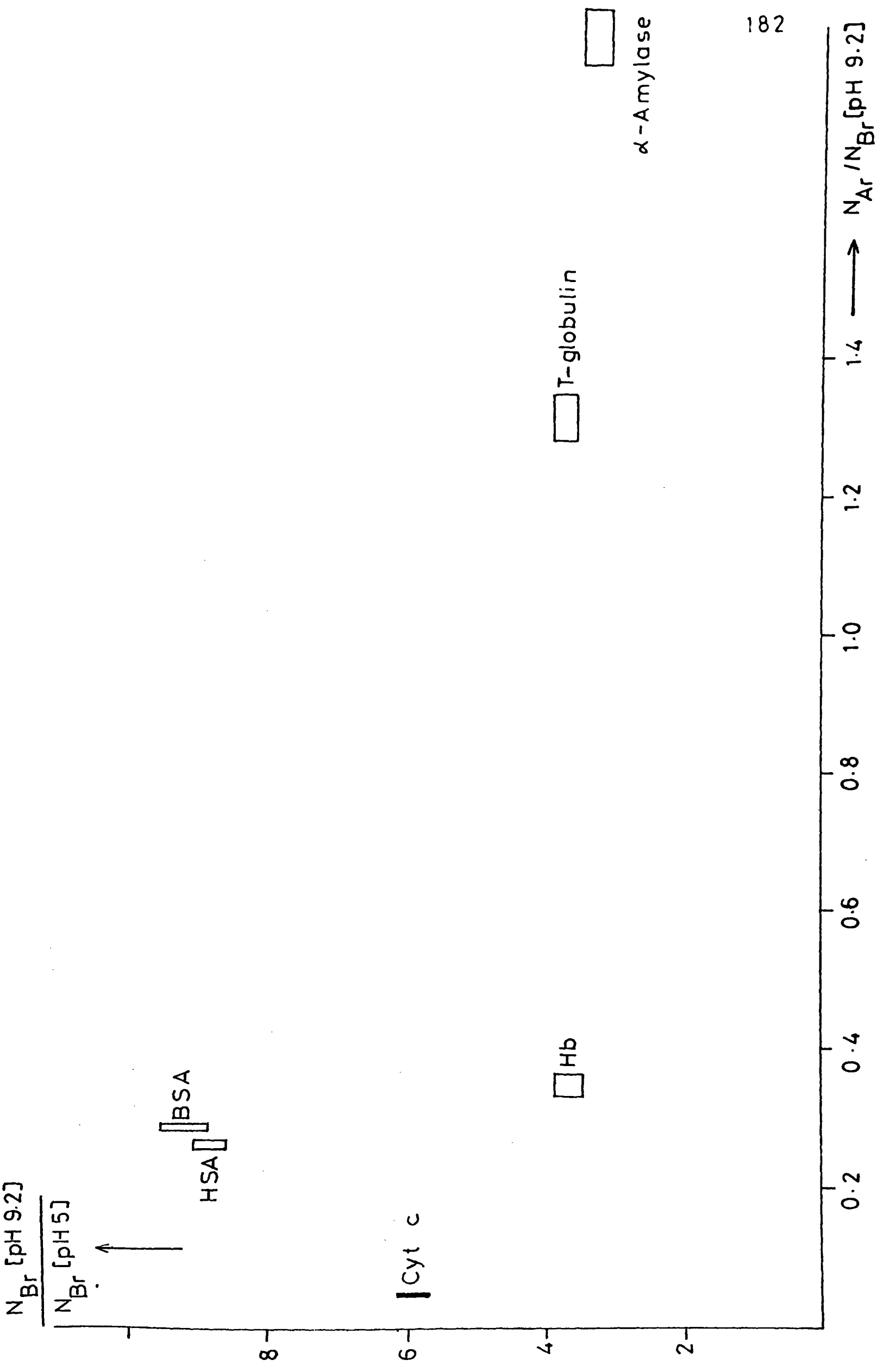

Figure VI.1 Identification of proteins

HPLC would be the increased efficiency of forced convection ($i \alpha V_f^{3/4}$ for the WJED, $\alpha V_f^{1/3}$ for the TDE) which would produce higher fluxes and currents.

The use of the titration technique is not confined to chromatography, and it may be applied to any compound which reacts reasonably quickly with bromine or hypobromite, e.g. phenols and cresols which are pollutants and occur in a variety of industrial wastes. The techniques developed in this thesis may therefore be applied to the continuous flow-through determination of a variety of compounds using coulometric titrant generation and amperometric end point detection.

APPENDIX 1. THE LAPLACE TRANSFORMATION

The Laplace transform, $\bar{f}(s)$, of a function, $F(t)$ is defined as

$$\bar{f}(s) = \mathcal{L} F(t) = \int_0^\infty e^{-st} F(t)\, dt \qquad \text{(A1.1)}$$

where s is the Laplace variable. The inverse operator $\mathcal{L}^{-1}$ is defined by

$$F(t) = \mathcal{L}^{-1} \bar{f}(s). \qquad \text{(A1.2)}$$

The Laplace transform of dy/dx is given by

$$\mathcal{L}(dy/dx) = s\bar{y}(s) - y(o) \qquad \text{(A1.3)}$$

where $y(o)$ is the value of $y(x)$ at $x = 0$.

The Laplace transform technique is useful in the solution of differential equations since the transformation firstly incorporates boundary conditions (equation A1.3) and secondly reduces an ordinary differential equation to an algebraic equation or reduces a partial differential equation to an ordinary differential equation. The result is obtained in terms of the transformed variable, and so must be inverted to obtain the solution of an equation. In practice the inversion is usually achieved by consulting tables of Laplace transforms, and some standard inversions used in this work are given below.

$\bar{f}(s)$	$F(t)$
$1/s^n$	$t^{n-1}/(n-1)!$ $(n = 1,2,3 \ldots)$
$1/s^k$	$t^{k-1}/\Gamma(k)$

If the desired inversion is not tabulated then the convolution theorem may be used. This states that if $\mathcal{L}^{-1} \bar{f}(s) = F(t)$ and $\mathcal{L}^{-1} \bar{g}(s) = G(t)$ then

$$\mathcal{L}^{-1} \bar{f}(s)\, \bar{g}(s) = \int_0^t F(u)\, G(t-u)\, du. \qquad \text{(A1.4)}$$

APPENDIX 2. AIRY FUNCTIONS

Airy functions arise in the solution of the differential equation

$$w'' - zw = 0 \qquad \text{(A2.1)}$$

and pairs of linearly independent solutions are

Ai (z)	Bi (z)
Ai (z)	Ai ($ze^{2\pi i/3}$)
Ai (z)	Ai ($ze^{-2\pi i/3}$)

Equation II.13

$$\rho\, s_n \bar{u}_n = \frac{\partial^2 \bar{u}_n}{\partial \rho^2}$$

can be reduced to the form of equation A2.1 if $z = s_n^{1/3}\rho$

The Airy function Ai (z) is illustrated in chapter II (below equation II.22) and some values are tabulated below:

z	Ai (z)
0	0.35502
0.5	0.23169
1.0	0.13529
1.5	0.06977
2.1	0.03089
3.3	0.00376
4.6	0.00024

APPENDIX 3. EVALUATION OF INTEGRAL IN EQUATION II.28

Division of the detector current (equation II.27) by the generator current (equation II.22) gives an expression for the collection efficiency of a TDE (equation II.28):

$$N = \frac{1}{\lambda_1^{2/3}} \int_0^{\lambda_3} \frac{2/3}{t^{1/3}} \; I_{\frac{\lambda_1}{1-t}}(2/3,1/3)\, dt$$

This can be integrated by parts

$$N = \left[\frac{1}{\lambda_1^{2/3}} \; t^{2/3} \; I_{\frac{\lambda_1}{1-t}}(2/3,1/3) \right]_0^{\lambda_3}$$

$$- \frac{1}{\lambda_1^{2/3}\, B(1/3,2/3)} \int_0^{\lambda_3} t^{2/3} \; \frac{\lambda_1}{(1-t)^2} \; \frac{\lambda_1^{-1/3}}{(1-t)^{-1/3}} \; \frac{(1-\lambda_1-t)^{-2/3}}{(1-t)^{-2/3}} dt$$

$$= \frac{\lambda_3^{2/3}}{\lambda_1^{2/3}} \; I_{\frac{\lambda_1}{1-\lambda_3}}(2/3,1/3) - \frac{1}{B(1/3,2/3)} \int_0^{\lambda_3} \frac{t^{2/3}}{(\lambda_2 + \lambda_3 - t)^{2/3}} \; \frac{dt}{(1-t)} \qquad (A3.1)$$

remembering that $1 = \lambda_1 + \lambda_2 + \lambda_3$. The integral in the second term in equation (A3.1) can be evaluated by using the substitution $\zeta = 1/t$, so that $dt = -d\zeta/\zeta^2$

$$\int = \int_{1/\lambda_3}^{\infty} \frac{\zeta^{-2/3} d\zeta . \zeta^{-2}}{[(\lambda_2 + \lambda_3)\,\zeta - 1]^{2/3} \zeta^{-2/3} (\zeta - 1)\zeta^{-1}}$$

$$= \int_{1/\lambda_3}^{\infty} \frac{d\zeta}{[(\lambda_2 + \lambda_3)\zeta - 1]^{2/3} (\zeta - 1)\zeta}$$

$$= \int_{1/\lambda_3}^{\infty} \frac{d\zeta}{[(\lambda_2 + \lambda_3)\zeta - 1]^{2/3}} \left[\frac{1}{(\zeta - 1)} - \frac{1}{\zeta} \right] \qquad (A3.2)$$

Equation A3.2 therefore requires the evaluation of two integrals. The first integral, which includes the $1/(\zeta - 1)$ term, is evaluated using the substitution $t = 1/(\zeta - 1)$. The integration limits become 0 and $\lambda_3/\lambda_1 + \lambda_2$ (since $\lambda_1 + \lambda_2 + \lambda_3 = 1$) and the integral is

$$\int_0^{\frac{\lambda_3}{\lambda_1+\lambda_2}} \frac{dt}{t^{1/3}[(\lambda_2+\lambda_3)-\lambda_1 t]^{2/3}}$$

A further substitution, $\vartheta = \lambda_1 t/(\lambda_2 + \lambda_3)$, reduces this to

$$\frac{1}{\lambda_1^{2/3}} \int_0^{\frac{\lambda_1\lambda_3}{(\lambda_1+\lambda_2)(\lambda_2+\lambda_3)}} \frac{d\vartheta}{\vartheta^{1/3}(\lambda-\vartheta)^{2/3}} \qquad \text{(A3.2)}$$

which can be recognised as an incomplete Beta function (see Appendix 4). The second integral in equation A3.2, containing the $1/\zeta$ term is evaluated similarly using the substitution $\vartheta = 1/\zeta\ (\lambda_2 + \lambda_3)$ to give

$$\int_0^{\frac{\lambda_3}{\lambda_2+\lambda_3}} \frac{d\vartheta}{\vartheta^{1/3}(1-\vartheta)^{2/3}}$$

which is again an incomplete Beta function. Equation A3.2 is therefore

$$B\ (1/3,2/3)\left[\frac{1}{\lambda_1^{2/3}} I_{\frac{\lambda_1\lambda_3}{(\lambda_1+\lambda_2)(\lambda_2+\lambda_3)}}(2/3,1/3) - I_{\frac{\lambda_3}{\lambda_2+\lambda_3}}(2/3,1/3)\right]$$

so that equation A3.1 becomes

$$N = \frac{\lambda_3^{2/3}}{\lambda_1^{2/3}} I_{\frac{\lambda_1}{\lambda_1+\lambda_2}}(2/3,1/3) - \frac{1}{\lambda_1^{2/3}} I_{\frac{\lambda_1\lambda_3}{(\lambda_1+\lambda_2)(\lambda_2+\lambda_3)}}(2/3,1/3)$$

$$+ I_{\frac{\lambda_3}{\lambda_2+\lambda_3}}(2/3,1/3)$$

APPENDIX 4. RELATIONSHIP BETWEEN FUNCTIONS IN EQUATIONS I.26 AND II.29

In the expression for the collection efficiency of a RRDE the function F(x) (see equation I.26) is given by the integral

$$F(x) = \frac{1}{B(1/3,2/3)} \int_o^x \frac{dt}{t^{2/3}(1+t)} \qquad (A4.1)$$

where $B(a,b) = \Gamma(a)\Gamma(b)/\Gamma(a+b)$ and $\Gamma(z)$ is the Gamma function

$$\Gamma(z) = \int_o^\infty t^{z-1}e^{-t}dt$$

In the derivation of the TDE collection efficiency equation II.29 contains functions of the type $I_x(2/3,1/3)$, where

$$I_x(a,b) = B_x(a,b)/B(a,b) \qquad (A4.2)$$

and $B_x(a,b)$ is an incomplete Beta function

$$B_x(a,b) = \int_o^x t^{a-1}(1-t)^{b-1}dt. \qquad (A4.3)$$

The symmetry of $I_x(a,b)$ is such that

$$I_x(a,b) = 1 - I_{1-x}(b,a) \qquad (A4.4)$$

The purpose of this appendix is to show that

$$I_x(1/3,2/3) = F\ (x/1-x) \qquad (A4.5)$$

Equations A4.2 and A4.3 give

$$I_x(1/3,2/3) = \frac{1}{B(1/3,2/3)} \int_o^x t^{-2/3}(1-t)^{-1/3}dt \qquad (A4.6)$$

Now let $t = \zeta/(1+\zeta)$, so that $dt = d\zeta/(1+\zeta)^2$, $\zeta = t/(1-t)$ and $1 - t = 1/(1+\zeta)$. Substituting these values into equation A4.5 gives

$$I_x(1/3,2/3) = \frac{1}{B(1/3,2/3)} \int_o^{\frac{x}{1-x}} \frac{\zeta^{-2/3}d\zeta}{1+\zeta}$$

$$= F(x/1-x) \quad \text{(Q.E.D.)}$$

The expression for N_o (the TDE collection efficiency) in terms of $I_x(a,b)$ is

$$N = \frac{\lambda_3^{2/3}}{\lambda_1^{2/3}} I_{\frac{\lambda_1}{\lambda_1+\lambda_2}}(2/3,1/3) - \frac{1}{\lambda_1^{2/3}} I_{\frac{\lambda_1\lambda_3}{(\lambda_1+\lambda_2)(\lambda_2+\lambda_3)}}(2/3,1/3)$$

$$+ I_{\frac{\lambda_3}{\lambda_2+\lambda_3}}(2/3,1/3) \qquad (II.29)$$

Therefore using the relationship above (A4.4 and A4.5)

$$I_{\frac{\lambda_1}{\lambda_1+\lambda_2}}(2/3,1/3) = 1 - F(\lambda_2/\lambda_1)$$

$$I_{\frac{\lambda_1\lambda_3}{(\lambda_1+\lambda_2)(\lambda_2+\lambda_3)}}(2/3,1/3) = 1 - F(\lambda_2/\lambda_1\lambda_3)$$

$$I_{\frac{\lambda_3}{\lambda_2+\lambda_3}}(2/3,1/3) = 1 - F(\lambda_2/\lambda_3)$$

These expressions are substituted into equation II.29 to give equation II.30.

APPENDIX 5. RRDE COLLECTION EFFICIENCY AND TITRATION CURVE PARAMETERS.

The expresion for the RRDE collection efficiency has been given by equations I.25 and I.26. The ideal titration curve (infinitely fast reaction, equal diffusion coefficients) has been described by Albery, Bruckenstein and Johnson (58). The linear region of the titration curve is described by

$$i_R = N_o i_D - M\beta^{2/3} \qquad (A5.1)$$

while the non-linear region may be described by a normalised disc current (i_D/M) and by a ring current: disc current ratio ($N' = i_R/i_D$):

$$\frac{M}{i_D} = 1 - F(\alpha) - \frac{\beta_J^{1/3}}{(1+\alpha+\beta_J)^{2/3}} \left[1 - F\left\{ \frac{(1+\alpha+\beta_J)\alpha}{\beta_J} \right\} \right] \qquad (A5.2)$$

$$N' = 1 - F(\alpha/\beta_J) - \frac{1+\alpha}{(1+\alpha+\beta_J)^{1/3}} \left[1 - F\left\{ \frac{(1+\alpha+\beta_J)\alpha}{\beta_J} \right\} \right] \qquad (A5.3)$$

The parameter β_J

$$\beta_J = (r_J/r_1)^3 - (r_2/r_1)^3 \qquad (A5.4)$$

describes the radial position, r_J, of the reaction boundary on the surface of the ring electrode. When $r_J = r_2$ (the inside edge of the ring) then $\beta_J = 0$, and when $r_J = r_3$ (the outside edge of the ring) then $\beta_J = \beta$. In practice equations A5.2 and A5.3 are evaluated for $\beta_J/\beta =$ 0,0.1,0.2, ...1.0.

For the RRDE used to perform titrations at pH9.2

$r_1 = 3.659 \pm .006$ mm

$r_2 = 3.803 \pm .007$ mm

$r_3 = 4.134 \pm .004$ mm

$\beta^{2/3} = 0.467 \pm .011$

$N_o = 0.225 \pm .006$

β_J/β	N'	i_D/M
1.0	.0558	2.755
0.9	.0496	2.656
0.8	.0434	2.555
0.7	.0371	2.453
0.6	.0309	2.350
0.5	.0246	2.245
0.4	.0184	2.137
0.3	.0125	2.026
0.2	.00707	1.911
0.1	.00251	1.792
0	0.	1.665

For the RRDE used to perform titrations at pH5

$r_1 = 3.501 \pm .009$ mm

$r_2 = 3.767 \pm .002$ mm

$r_3 = 4.009 \pm .003$ mm

$\beta^{2/3} = 0.403 \pm .008$

$N_o = 0.179 \pm .003$

1.0	.0314	2.734
0.9	.0275	2.660
0.8	.0235	2.586
0.7	.0197	2.511
0.6	.0160	2.435
0.5	.0124	2.359
0.4	.00897	2.281
0.3	.00586	2.203
0.2	.00316	2.124
0.1	.00106	2.043
0	0	1.961

The RRDE used with the autotitrator circuit was the same as that used at pH9.2. However the Teflon mantle had crept, due to temperature changes, which meant that the electrode had to be faced off on the lathe. This lead to slight changes in the configuration of the electrode.

$r_1 = 3.669 \pm .007$

$r_2 = 3.800 \pm .005$

$r_3 = 4.164 \pm .005$

$\beta^{2/3} = .497 \pm .010$

$N_o = .239 \pm .005$

The line N′ intersects the linear portion of the titration curve (equation A5.1) at

$$N' \, i_D = N_o i_D - M\beta^{2/3}$$

so that

$$i_D/M = \frac{\beta^{2/3}}{N_o - N'}$$

is the normalised disc current at the point of intersection. For the RRDE autotitration experiment N' = 0.06 so that

$$i_D/M = 2.776$$

The autotitration response (μA/μM) must therefore be multiplied by 0.992 (2.755/2.776) before comparing it with the result from figure IV.16.

APPENDIX 6. THE ESTIMATION OF AMINO ACID DIFFUSION COEFFICIENTS

Several workers have estimated diffusion coefficients, or correlated experimental values, through the Stokes - Einstein equation.

$$D^{o} = kT/6\pi\eta r \qquad (A6.1)$$

where D^{o} is the diffusion coefficient at infinite dilution. Wilke and Chang (84) showed that the group $T/D\eta$ is essentially independent of temperature and could be represented as a function of molar volume (V) for the diffusion of various solutes in a given solvent:

$$D\eta/T = 7.4 \times 10^{-8}. (XM)^{1/2} V^{-0.6}. \qquad (A6.2)$$

M is the molecular weight of the solvent and X (= 2.6) for water corrects this molecular weight for association of the solvent. The constant and exponent of V in equation A6.2 were obtained from a log-log plot of $D\eta/T$ vs. V. The molar volume (V cm^3/g– atom) is the value at the normal boiling point estimated by the atomic contributions of Le Bas (Le Bas found molar volumes at the boiling point to be approximately additive and produced a set of increments). The correlation of Wilke and Chang was developed for compounds which were mainly non-polar. Bidstrup and Geankoplis studied carboxylic acids in aqueous solutions and found a better correlation using a constant of 6.6×10^{-8} (cf equation A6.2).

Edward (82) has also published details of the calculation of diffusion coefficients, and his correlation includes some of Longsworth's amino acid data. This method has been used in this work to estimate amino acid and peptide diffusion coefficients. Edward considered data in the literature and produced a correction factor permitting the Stokes - Einstein equation to be applied to small solute molecules:

$$D^{o} = kT/n\pi\eta r_{w}. \qquad (A6.3)$$

r_w is the van der Waals radius of the diffusing molecule and may be calculated from atomic increments (see below). When $r_w < 5$ Å then the factor n in equation A6.3 must be reduced below the Stokes value of 6; the

TABLE A6.1

	ν_w ($\mathring{A}^3$)	r_w ($\mathring{A}$)	n	D ($\times 10^{-9}$ m^2 s^{-1})
Glycine	105.6	2.93	5.1	.984
Lysine	185.5	3.54	5.4	.769
Methionine	174.5	3.47	5.4	.785
Cystine	269.6	4.01	5.6	.655
Tyrosine	218.7	3.74	5.5	.715
Tryptophan	220.6	3.75	5.5	.713
Penta-gly	300.8	4.16	5.6	.631
Tetra-ala	320	4.24	5.7	.609
Gly-leu-tyr	384.3	4.51	5.8	.562
Tri-tyr	542.5	5.06	6.0	.484

empirical dependence of n on r_w is tabulated by Edward. Equation A6.3 assumes the molecule to be spherical, and this assumption is maintained in this work; however the effects of non-sphericity may be added to equation A6.3 if desired (see below).

The van der Waal's volume, v_w, of a molecule is calculated from atomic increments ($\mathring{A}^3$); these increments have been obtained from crystallographic data at ordinary temperatures, and are tabulated by Edward (82). The van der Waals radius is obtained from $r_w = (3v_w/4\pi)^{1/3}$ assuming sphericity. The experiments described in Chapter IV were performed at pH 9.2, so that the carboxylic acid group of the amino acids would be ionized. It is assumed, following the recommendation of Edward, that the carboxylate group is solvated, by two water molecules, and a hydrated volume of 71 $\mathring{A}^3$ is therefore used; the hydroxyl group of tyrosine is also assumed to be solvated by one water molecule, with a consequent increase of 18.6 $\mathring{A}^3$ in the van der Waals volume of the diffusing molecule. The calculated values of v_w, r_w and n are presented in table A6.1, and have been substituted in equation A6.3 using $\eta = 8.904 \times 10^{-4}$ kg m^{-1} s^{-1} (the viscosity of water at 25°C). Therefore

$$D^o = 1.471 \times 10^{-8}/nr_w$$

and these calculated diffusion coefficients are presented in table A6.1.

An ellipsoidal molecule will diffuse more slowly than a spherical molecule of equal volume; the former has a greater surface area and experiences a greater frictional drag. Equation A6.1 applies to a spherical particle since $f_o = 6\pi\eta r$, the frictional coefficient of a sphere, is used. Perrin (85) derived equations giving the frictional coefficients (f) of prolate and oblate ellipsoids, and $f > f_o$ for particles of equal volume. The frictional coefficients of ellipsoids having three unequal axes have also been calculated. Equation A6.3 may therefore be modified to

$$D^o = kT/n\pi\eta r_w(f/f_o)$$

The frictional ratio f/f_o is close to unity for all molecules having $r_w < 3.5$ $\mathring{A}$.

APPENDIX 7. DIFFERENTIATION OF EQUATION II.50

Equations II.50 and II.48 present an expression for the normalised generator current

$$\frac{M}{i_{gen}}\frac{1}{\lambda_J^{1/3}\Gamma(2/3)} = \frac{\lambda_1^{2/3}}{\Gamma(2/3)}\frac{3}{2}\frac{\partial}{\partial\lambda_J}\left[\frac{\lambda_J^{2/3}}{\lambda_1^{2/3}}G\left(\frac{\lambda_1}{\lambda_2}\right)+G\left(\frac{\lambda_J}{\lambda_2}\right)\right.$$

$$\left.-\frac{(\lambda_1+\lambda_2+\lambda_J)^{2/3}}{\lambda_1^{2/3}}G\left(\frac{\lambda_1\lambda_J}{\lambda_2(\lambda_1+\lambda_2+\lambda_J)}\right)\right] \qquad \text{(A7.1)}$$

The function G(x) is

$$G(x) = 1 - F(1/x)$$

and F(x) is given in appendix 4, so that

$$\frac{dG}{dx} = \frac{1}{x^2}\frac{dF}{dx} = \frac{3^{1/2}}{x^2 2\pi(1+1/x)(1/x)^{2/3}} = \frac{3^{1/2}}{2\pi x^{1/3}(1+x)}$$

Thus

$$\frac{\partial}{\partial\lambda_J}G\left(\frac{\lambda_J}{\lambda_2}\right) = \frac{3^{1/2}}{2\pi}\frac{\lambda_2^{1/3}\lambda_2}{\lambda_J^{1/3}(\lambda_2+\lambda_J)\lambda_2}$$

$$-\frac{\partial}{\partial\lambda_J}\frac{(\lambda_1+\lambda_2+\lambda_J)^{2/3}}{\lambda_1^{2/3}}G\left(\frac{\lambda_1\lambda_J}{\lambda_2(\lambda_1+\lambda_2+\lambda_J)}\right) =$$

$$-\frac{2/3}{\lambda_1^{2/3}(\lambda_1+\lambda_2+\lambda_J)^{1/3}}G\left(\frac{\lambda_1\lambda_J}{\lambda_2(\lambda_1+\lambda_2+\lambda_J)}\right) - \frac{3^{1/2}}{2\pi}\frac{(\lambda_1+\lambda_2+\lambda_J)^{2/3}}{\lambda_1^{2/3}} \times$$

$$\frac{\lambda_2^{1/3}(\lambda_1+\lambda_2+\lambda_J)^{1/3}}{\lambda_1^{1/3}\lambda_J^{1/3}}\frac{\lambda_2(\lambda_1+\lambda_2+\lambda_J)}{(\lambda_1+\lambda_2)(\lambda_2+\lambda_J)}\times\left[\frac{\lambda_1}{\lambda_2(\lambda_1+\lambda_2+\lambda_J)}-\frac{\lambda_1\lambda_J}{\lambda_2(\lambda_1+\lambda_2+\lambda_J)^2}\right]$$

$$= -\frac{2/3}{\lambda_1^{2/3}(\lambda_1+\lambda_2+\lambda_J)^{1/3}}G\left(\frac{\lambda_1\lambda_J}{\lambda_2(\lambda_1+\lambda_2+\lambda_J)}\right) - \frac{3^{1/2}}{2\pi}\cdot\frac{\lambda_2^{1/3}}{\lambda_J^{1/3}(\lambda_2+\lambda_J)}$$

Substituting these relations into equation A7.1 gives equation II.51.

REFERENCES

1) W.J. Albery "Electrode Kinetics" Oxford (1975)

2) G.C. Barker, A.W. Gardner; A.E.R.E. Harwell CR/2297 (1958)

3) G.C. Barker, A.W. Gardner; Z.Anal. Chem. 173, 79 (1960)

4) H.E. Keller, R.A. Osteryoung; Anal. Chem. 43, 342 (1971)

5) R.F. Lane, A.T. Hubbard, Anal. Chem. 48, 1287 (1976)

6) B. Fleet, C.J. Little; J. Chromatog. Sci. 12, 747 (1974)

7) P.T. Kissinger et.al., J. Chem. Ed. 54, 50 (1977)

8) P.T. Kissinger; Anal. Chem. 49, 447A (1977)

9) R. Brdicka; Coll. Czech. Chem. Comm. 8, 366 (1936)

10) R. Brdicka; Coll. Czech. Chem. Comm. 5, 112 (1933)

11) B. Drake; Acta.Chem. Scand. 4, 554 (1950)

12) O.H. Muller; Methods Biochem. Anal. (Interscience, New York) 11, 329(1963)

13) E. Palacek, Z Pechan; Anal. Biochem. 42, 59 (1971

14) T.Y. Toribara, L. Koval; Talanta 17, 1003 (1970)

15) B.S. Harrap, L.C. Gruen; Anal. Biochem. 42, 398 (1971)

16) W. Selig; Mikrochim. Acta 453 (1973)

17) J. Papp, J. Havas; Proc. 3rd Anal. Chem. Conf. 2, 41 (1970)

18) R. Benesch, R.E. Benesch; "Methods of Biochemical Analysis" (Interscience, New York) 10, 43 (1962)

19) P. Artman, A. Skrabal; Z. anal. Chem. 46, 5 (1907)

20) E. Rupp, E. Rossler; Arch. der Pharm. 243, 104 (1905)

21) I.M. Kolthoff, W. Stricks, L. Morren; Analyst 78, 405 (1953)

22) N. Velghe, A. Claeys; Bull. Soc. Chem. Belg. 77, 327 (1968)

23) N. Velghe, A. Claeys; Analyst 98, 372 (1973)

24) A. Claeys, N. Velghe; Proc. 3rd Anal. Chem. Conf. 2, 101-5 (1970)

25) P.K. Norkus, G.S. Shimkyavichyute; Zh. Anal. Khim 26, 2002 (1971) translation in Russ. J Anal. Chem. 26, 1788 (1971)

26) M.K. Abramov; Farmatsiya (Moscow) 24, 80 (1975)

27) L. Szebelledy, Z. Somogyi; Z. anal. Chem. 112, 385 (1938)

28) A.F. Krivis, G.R. Supp, E.S. Gazda; Anal. Chem. 35, 2216 (1963)

29) G.D. Christian, E.C. Knoblock, W.C. Purdy; Anal. Chem. 35, 2217 (1963)

30) G.D. Christian, E.C. Knoblock, W.C. Purdy; Clin. Chem. 11, 413 (1965)

31) G.D. Christian, E.C. Knoblock, W.C. Purdy; Clin. Chem. 11, 700 (1965)

32) G.D. Christian; Anal. Biochem. 14, 183 (1966)

33) Z.E. Kalinowska, J. Kochalska; Acta Polon. Pharm. 21, 239 (1964)
Electroanal. Abstr. 4, 407

34) V.P. Komov, M.A. Strelkova, N.A. Kogan; Lab. Delo. 9, 547 (1972)
Chem. Abstr. 78, 25973t

35) A.P. Kreshkov, L.B. Oganesyan; Zh. Anal. Khim. 26, 614 (1971)
translation in Russ. J. Anal. Chem. 26, 534 (1971)

36) P.E. Belliveau, R.W. Frei; Chromatographia 4, 189 (1971)

37) I. Covelli; J. Nucl. Biol. Med. 13, 43 (1969) Chem. Abstr. 73, 601d

38) J.L. Hamlin, E.R. Arquila; J. Biol. Chem. 249, 21 (1974)
Chem. Abstr. 80: 78586 s

39) R.M. Cook; D.Phil Thesis, Oxford (1973)

40) F. Rauwel, D. Thévenot; Bioelectrochem. Bioenerget. 3, 284 (1976)

41) J. Broome; Nature 214, 849 (1967)

42) R.K. Simon, G.D. Christian, W.C. Purdy; Clin. Chem. 14, 463 (1968)

43) Nernst; Z.Physik. Chem. 47, 52 (1904)

44) T. Von Karman; Angew. Math. Mech. 1, 233 (1921)

45) W.G. Cochran; Proc. Camb. Phil. Soc. Math. Phys. Sci. 30, 365 (1934)

46) V.G. Levich; Acta. "Physicochemical Hydrodynamics" Prentice Hall, (1962)

47) A.C. Riddiford; Adv. Electrochem. Electrochem. Eng. 4, 47 (1966)

48) V.G. Levich;"Physicochemical Hydrodynamics" Prentice Hall, New Jersey (1962)

49) "Conference on Physicochemical Hydrodynamics, Oxford, 1977" (Ed. D.B. Spalding) Vol I, p 413. Academic (1977)

50) W.J. Blaedel, C.L. Olson, L.R. Sharma; Anal.Chem. 35, 2100 (1963)

51) M.B. Glauert; J. Fluid.Mech. 1, 625 (1956)

52) J. Yamada, H. Matsuda; J. Electroanal. Chem. 44, 189 (1973)

53) H. Siegerman, G. O'Dom; Amer. Lab. June 1972.

54) Y.B. Ivanov, V.G. Levich; Dokl. Akad. Nauk. SSSR 126, 1029 (1959)

55) W.J. Albery; Trans Farad. Soc. 62, 1915 (1966)

56) W.J. Albery, S. Bruckenstein, Trans. Farad. Soc. 62, 1920 (1966)

57) M.L. Hitchman; D.Phil Thesis. Oxford (1968)

58) W.J. Albery, S. Bruckenstein, C.D. Johnson; Trans. Farad. Soc. 62, 1938 (1966)

59) W.J. Albery, S. Bruckenstein; Trans. Farad. Soc. 62, 2584 (1966)

60) W.J. Albery, M.L. Hitchman, J. Ulstrup; Trans. Farad. Soc. 65, 1101 (196

61) W.J. Albery, M.L. Hitchman. "Ring Disc Electrodes"Oxford (1971)

62) H. Gerischer, I. Mattes, R. Braun; J. Electroanal. Chem. 10, 553 (1965)

63) R. Braun; J. Electroanal. Chem. 19, 23 (1968)

64) G.W. Schieffer, W.J. Blaedel; Anal. Chem. 49, 49 (1977)

65) L.R. Snyder, J.J. Kirkland; "Introduction to Modern Liquid Chromatography" Wiley-Interscience (1974)

66) M. Abramovitz, I. Stegun; "Handbook of Mathematical Functions" Dover (1965)

67) W.J. Albery, B.A. Coles, A.M. Couper; J. Electroanal.Chem. 65, 901 (1975)

68) W.J. Albery; Trans Farad. Soc. 63, 1771 (1967)

69) G.M. Arcand, E.H. Swift; Anal. Chem. 28, 440 (1956)

70) J.K. Johannesson; J. Chem. Soc. 2298 (1959)

71) P.O. Schneider, R.J. Thibert, R.J. Walton, Mikrochim. Acta 925 (1972)

72) L.G. Longsworth; J. Am. Chem. Soc. 75, 5704 (1953)

73) "Handbook of Biochemistry" H.A. Sober (ed.) CRC (1968)

74) C. Tanford; "Physical Chemistry of Macromolecules" Wiley (1961)

75) H. Edelhoch; J. Biol.Chem. 235, 1326 (1960)

76) J.M. Junge, E.A. Stein, H. Neurath, E.H. Fischer; J. Biol. Chem 234, 556 (1959)

77) R.J. Hill, W. Konigsberg, G. Guiclotti, L.C. Craig; J. Biol.Chem. 237, 1549 (1962)

78) E. Margoliash, J.R. Kimmel, R.L. Hill, W.R. Schmidt; J. Biol. Chem. 237, 2148 (1962)

79) F.W. Putman (ed.) "The Plasma Proteins" p 143 Academic (1960)

80) A.T. Chadwick; D. Phil Thesis, Oxford (1978)

81) L.G. Longsworth; J. Am.Chem.Soc. 75, 5705 (1953)

82) J.T. Edward; J. Chem.Ed. 47, 261 (1970)

83) D.E. Bidstrup, C.J. Geankoplis; J. Chem. Eng. Data. 8, 170 (1973)

84) C.R. Wilke, P. Chang; A.I. Ch. E.J., 1, 264 (1955)

85) F. Perrin; J. Phys. Radium; 7, 1 (1936)

86) D.C. Johnson, S. Bruckenstein; J. Electrochem. Soc. 117, 460 (1970)

87) M.L. Hitchman, W.J. Albery; Electrochimica Acta 17, 787 (1972)

88) J.E. O'Reilley; Anal. Chem. 47, 1077 (1975)

89) "Handbook of Biochemistry"